Beneficiation of Rare Earth Minerals from Niobec Ore: Froth Flotation

Eileen Ross L. Espiritu

Doctor of Philosophy

Department of Mining and Materials Engineering

McGill University
Montreal, Quebec
May 2018

A thesis submitted to McGill University in partial fulfilment of the requirements of the degree of Doctor of Philosophy

Dedication

To my beloved mom and siblings.
Whose love and support made me where I am today.

To my dearest best friend and partner in life, Kelvin.
Whose affection, love and encouragements made it possible
for me to finish this work.

Abstract

Rare earth elements are the key components of the emerging green technologies such as wind turbines, hybrid vehicles and storage batteries. The expected increase in demand for rare earths and the export quota restriction that was imposed by China (the largest producer of rare earths) in 2008, have alarmed the rest-of-the-world consumers of rare earth elements. By 2025, the following rare earth elements: lanthanum, neodymium, praseodymium, dysprosium, and terbium, are likely to be in short supply. This global demand can only be met with constant development of new mines outside of China. A number of advanced research projects outside China can be found in Canada. Among the projects in Canada, Niobec rare earth project of Magris Resources Inc. is found to contain the largest resource of rare earth elements with 1058.6 million tonnes at 1.73% total rare earth oxide (TREO). This corresponds to 18 million tonnes of TREO, which is almost half of China's rare earth elements reserve (43 million tonnes TREO). Detailed characterization conducted through Quantitative Evaluation of Minerals by Scanning Electron Microscopy (QEMSCAN) reveals that the main rare earth minerals in the ore sample were monazite (1.43%) and bastnäsite/synchisite (1.96%), while the main gangue is dolomite (50%). The fine grain sizes (-20 μm) of the rare earth minerals makes froth flotation the most applicable beneficiation technique for separation. However, literature regarding rare earth mineral flotation is very limited.

To process the rare earth ore, fundamental properties of the pure minerals (monazite, bastnäsite and dolomite) are first understood through surface characterization (*e.g.*, ATR-FTIR and XPS), thermodynamic calculations (speciation diagrams), electrophoretic measurements (*i.e.*, zeta potential measurements) and single-mineral microflotation tests using three different rare earth mineral collectors: benzohydroxamate, sodium oleate and organic phosphoric acid. These fundamental investigations enabled further understanding of the mineral – reagent interactions and offered possible collector adsorption mechanisms. Benzohydroxamate proved to be the most selective, while sodium oleate and organic phosphoric acid demonstrated strong affinity to the gangue. Several dolomite depressants were then investigated in the presence of these two strong collectors. Polymeric-type depressants (especially carboxymethylcellulose) showed promising depressing ability towards dolomite. However, the performance of these depressants is better with sodium oleate than with organic phosphoric acid, indicating a high influence of collector's chemistry on their depressing ability. Since single-mineral flotation does not consider the mineral's solubility, the effect of dissolved mineral species (in the presence of benzohydroxamate and sodium oleate) was also explored through the mentioned techniques, complemented with molecular modeling based on density functional theory (DFT). XPS analyses indicated that Ca^{2+}, $CaCO_3/MgCO_3$ or HCO_3^- from dissolved dolomite could be present at the rare earth mineral surface, providing new sites for collector adsorption. DFT-based molecular modeling found useful in validating the experimental results, provided a deeper understanding of the mineral−collector interaction and presented possible conformation of adsorbed species or collectors on the surface of the minerals. The DFT simulations were also able to provide explanation to phenomena that could not be explained with experimental observations alone.

The insights acquired through fundamental investigations and the knowledge of the mineralogy of the Niobec rare earth ore provided guidance in the processing of the ore. The observed concentration of rare earth elements in the fine (-20 μm) fraction led to a decision to split the processing of the ore into two routes. This does not only prevent overgrinding of the -20 μm particles, but also achieves a more efficient grinding of the +20 μm particles. Although the work focuses on the feasibility of using the specially designed column cell in processing the fines, the coarse (+20 μm) fraction is also processed using a conventional bench-scale flotation cell. It was presented that significant enrichment and recovery of the rare earth elements can be achieved even with only one stage of rougher flotation in both the column and the conventional cell, which was typically obtained through several stages of cleaning or scavenging stages. An improvement in the column cell parameters (physical aspect) and further investigations regarding the reagent scheme (chemistry aspect) are suggested for future work.

Résumé

Les terres rares sont les éléments clés des technologies vertes émergentes telles que les éoliennes, les véhicules hybrides et les batteries d'accumulateurs. L'augmentation attendue de la demande en terres rares et la restriction des quotas d'exportation imposée par la Chine (le plus grand producteur de terres rares) en 2008 ont alarmé les consommateurs du reste du monde d'éléments de terres rares. D'ici 2025, les éléments des terres rares suivants: lanthane, néodyme, praséodyme, dysprosium et terbium, seront très rares. Cette demande mondiale ne peut être satisfaite qu'avec le développement constant de nouvelles mines en dehors de la Chine. Un certain nombre de projets de recherche avancée en dehors de la Chine peuvent être trouvés au Canada. Parmi les projets au Canada, le projet Niobec des terres rares de Magris Resources Inc. contient la plus grande ressource d'éléments de terres rares avec 1058,6 millions de tonnes à 1,73% d'oxyde de terres rares totaux (OTRT). Cela correspond à 18 millions de tonnes d'OTRT, soit près de la moitié de la réserve d'éléments de terres rares de la Chine (43 millions de tonnes d'OTRT). La caractérisation détaillée réalisée par QEMSCAN révèle que les principaux minéraux des terres rares dans l'échantillon sont la monazite (1,43%) et la bastnäsite / synchisite (1,96%), tandis que la gangue principale est la dolomite (50%). Les granulométries fines (<20 µm) des minéraux des terres rares font de la flottation par mousse la technique d'enrichissement la plus applicable pour la séparation. Cependant, la littérature concernant la flottation des minéraux des terres rares est très limité.

Pour traiter le minerai de terres rares, les propriétés fondamentales des minéraux purs (monazite, bastnäsite et dolomite) sont d'abord comprises par la caractérisation de surface (p.ex., ATR-FTIR et XPS), calculs thermodynamiques (diagrammes de spéciation), mesures électrophorétiques (c.-à-d., mesures du potentiel zêta) et test de microflottation mono-minérale en utilisant trois différents collecteurs de minéraux de terres rares, le benzohydroxamate, l'oléate de sodium et l'acide phosphorique organique. Ces investigations fondamentales ont permis de mieux comprendre les interactions minéral – réactif et ont offert des mécanismes d 'adsorption collecteurs possibles. Le benzohydroxamate s'est révélé être le plus sélectif, tandis que l'oléate de sodium et l'acide phosphorique organique ont montré une

forte affinité pour la gangue. Plusieurs dépresseurs de dolomite ont ensuite été étudiés en présence de ces deux collecteurs forts. Les dépresseurs de type polymérique (en particulier la carboxyméthylcellulose) présentaient une capacité déprimante prometteuse vis-à-vis de la dolomite. Cependant, la performance de ces dépresseurs est meilleure avec l'oléate de sodium qu'avec l'acide phosphorique organique, ce qui indique une forte influence de la chimie du collecteur sur leur capacité à déprimer. Puisque la flottation mono-minérale ne tient pas compte de la solubilité du minéral, l'effet des espèces minérales dissoutes (en présence de benzohydroxamate et d'oléate de sodium) a également été étudié par les techniques mentionnées, complétées par une modélisation moléculaire basé sur la théorie fonctionnelle de la densité (DFT). Les analyses XPS ont indiqué que Ca^{2+}, $CaCO_3/MgCO_3$ ou HCO_3^- provenant de la dolomite dissoute pourraient être présents à la surface des minéraux des terres rares, fournissant de nouveaux sites pour l'adsorption des collecteurs. La modélisation moléculaire basée sur la DFT s'est avérée utile pour valider les résultats expérimentaux, a permis une compréhension plus approfondie de l'interaction minérale et a montré une éventuelle conformation des espèces adsorbées ou des collecteurs à la surface des minéraux. Les simulations DFT ont également permis de fournir des explications sur des phénomènes qui ne pouvaient pas être expliqués par des observations expérimentales uniquement.

Les connaissances acquises grâce à des études fondamentales et la connaissance de la minéralogie du minerai de terres rares Niobec ont fourni des conseils pour le traitement du minerai. La concentration observée d'éléments des terres rares dans la fraction fine (-20 µm) du minerai a conduit à la décision de scinder le traitement du minerai en deux voies. Cela empêche non seulement le surgrémentage des particules de -20 µm, mais permet également un broyage plus efficace des particules de +20 µm. Bien que le travail se concentre sur la faisabilité de l'utilisation de la cellule de colonne spécialement conçue dans le traitement des fines, la fraction grossière (+20 µm) est également traitée en utilisant une cellule de flottation classique à l'échelle du laboratoire. Il a été présenté que l'enrichissement et la récupération significatifs des éléments de terres rares peuvent être réalisés même avec une seule étape de flottation plus grossière dans la colonne et la cellule conventionnelle, qui était typiquement obtenue par plusieurs étapes de nettoyage ou de balayage. Une amélioration des paramètres des cellules de la colonne (aspect physique) et d'autres investigations concernant le schéma de réactif (aspect chimie) sont suggérées pour les travaux futurs.

Acknowledgements

This thesis would not have been possible without the guidance and help of several individuals who in one way or another contributed and extended their valuable assistance in the preparation and completion of this study.

First of all, I would like to express my sincerest gratitude to my supervisor, Prof. Kristian Waters for taking me on this project. I am grateful to the invaluable guidance and support he has given me throughout the course of this research. He deserves acknowledgement for working overtime to review and submit my manuscripts for publications. I am very grateful for his insightful comments and suggestions that helped me improve my research outputs. Without his generosity and commitment, it would not be possible for me to finish this work.

I am very lucky to be part of the McGill Mineral Processing Group who are always ready to lend their help whenever I need it. I would like to thank Dr. Pengbo Chu, Mr. Mark Lepage, Mr. Hao Ma, Mr. Sungjae Moon, Ms. Jabun Mita, Dr. Shiva Mohammadi-Jam, Dr. Aysan Molaei, Mr. Ravi Multani, Dr. Yue Tan, Mr. Luis Vinnett, Mr. Percy Zambrano, and Mr. Meng Zhou for the productive discussions regarding my research. I would also like to thank Mr. Christopher Marion for his time and effort in helping me conduct exploratory magnetic and gravity separation experiments. I also would like to thank Dr. Ozan Kökkılıç and Dr. Cesar Gomez for offering their expertise in DOE and column flotation, respectively. I also appreciate the things Mr. Ronghao Li has done for me during my doctoral studies including the help for figuring laboratory set-up and other research-related stuffs. I would like to thank Ms. Martha Araceli Elizondo-Alvarez for helping me in my adsorption tests and for being a really good friend. Special mention to Mr. Ray Langlois for providing valuable suggestions on how to do things faster and more efficient. I would not be able to finish my experiments without his kindness and assistance.

Mr. Gilberto Rodrigues da Silva deserves special acknowledgement for being a great colleague and a friend. He became my go-to whenever I am stuck in an experiment, or whenever I could not figure out why experiments don't go as expected. I have learned a lot from our exchanges of ideas. I am very thankful for his invaluable suggestions and assistance; and for his friendship during my doctoral studies.

I would also like to thank Niobec rare earth project team composed of Prof. Jamal Chaouki, Prof. Louis Fradette, Dr. Mohammad Latifi, Mr. Adrian Carillo Garcia, Mr. Rahi Avazpour and Ms. Maryam Abdollahi of Ecole Polytechnic de Montreal; Prof. Claude Bazin, Prof. Faiçal Larachi, Mr. Keven Turgeon and Mr. Dariush Azizi of Laval University; and Mr. Dominic Downey of Niobec. Special thanks to Mr. Keven Turgeon for prioritizing my samples sent for XRF analysis. I would also like to acknowledge Mr. Jean-Francois Boulanger, Mr. Keven Turgeon and Prof. Bazin for sharing the QEMSCAN results of the Niobec ore. I also would like to specially thank Prof. Larachi for sparing some of his time in reviewing some of my manuscripts and providing insightful comments and suggestions. I would also like to give my special thanks to my friend, Dariush, for all his help and encouraging words during my doctoral studies.

I am also grateful to the people at the department who helped me during the course of my studies. I am grateful to Ms. Shiva Naseri for assisting in the ATR-FTIR experiments and to Prof. Showan Nazhat for letting me use the ATR-FTIR equipment at no cost. I would like to thank the laboratory technicians and postdocs who have been very kind and helpful to me Ms. Monique Riendeau, Ms. Aleksandra Djuric, Dr. Lihong Shang, Dr. Sriraman Rajagopalan, Dr. Mehdi Sanjari and Dr. Florence Paray. I would also like to thank Ms. Barbara Hanley for her kindness, patience and commitment to her work making it easier for me to finish my doctoral studies.

I would like to acknowledge Natural Sciences and Engineering Research Council of Canada (NSERC) and Niobec, a Magris Resources Company for funding this research through the Collaborative Research and Development Program (CRDPJ 453164-13). I am also grateful to the financial support provided by McGill University through the McGill Engineering Doctoral Award, including Hatch Fellowship in Engineering, Shahbaz Mavaddat Fellowship, Graduate Excellence Award and Mineral Processing Award.

I am grateful to my Master's thesis supervisor, Dr. Herman D. Mendoza, for inspiring me to pursue a higher degree of learning and for his encouraging words whenever I feel the burden of my doctoral studies. I am also grateful to my family and close friends for their moral and professional support, for their heartening words and love. I am deeply thankful for my mom for being my source of inspiration, and for her support in all my aspirations ever since I was a child.

Finally, I would like to express my deepest gratitude to my dearest Kelvin for all the encouragements, support and love. Thank you for cheering me up when everything seems impossible. Thank you for your understanding and patience when I have to work overtime to finish this research work. I could never find enough words to truly express how grateful I am to you and to everyone who has helped me towards the finishing of this dissertation.

Contribution of Authors

All the experiments including (but not limited to) material preparations, material characterization, flotation, data collection and analyses were designed and conducted by the candidate. All the manuscripts are co-authored by **Prof. Kristian E. Waters** in his capacity as research supervisor. He provided guidance throughout the whole research project, reviewed the manuscripts and contributed to the general layout and discussions. **Prof. Faiçal Larachi** reviewed the manuscripts involving molecular modeling (Publications 3 and 4) and provided insightful comments and suggestions to improve the discussions. **Mr. Dariush Azizi** conducted the molecular modeling simulations and helped a lot in the interpretation of the results (Publications 3 and 4). **Mr. Ronghao Li** contributed to the zeta potential measurements involving dolomite depressants (Publication 2). **Mr. Gilberto R. da Silva** contributed to the zeta potential measurements involving the dolomite supernatant (Publications 3 and 4); and helped in X-ray Photoelectron Spectroscopy (XPS) (Publication 3 and 4). **Ms. Shiva Naseri** provided guidance and training in using the ATR-FTIR equipment (Publications 2 and 3). **Mr. Ray Langlois** helped in setting up the specially-designed column cell (Publication 5). **Dr. Ozan Kökkılıç** offered his experties on statistical design of experiments (Publication 5). **Dr. Cesar Gomez** provided suggestions on improving the set-up and imparted his insightful comments and knowledge about column cell (Publication 5).

Contents

List of Tables

List of Figures

Nomenclature

Abbreviations

ANOVA	Analysis of Variance
ATR	Attenuated total reflectance
BBD	Box-Behnken design
CCD	Central composite design
CHA	Concentric hemispherical analyzer
DFT	Density Functional Theory
DNP	Double numerical plus polarization
EDL	Electrical double layer
FTIR	Fourier-transform infrared
FWHM	Full width at half-maximum
GGA	Generalized gradient approximation
HREE	Heavy rare earth element
ICP-OES	Inductively Coupled Plasma Optical Emission Spectrometry
IEP	Isoelectric point
IR	Infrared
LREE	Light rare earth elements
PDI	Potential determining ion

PZC	Point of zero charge
RE	Rare earth
ROW	Rest of the world
SB	Single-beam
SCF	Self-consistent field
SG	Specific gravity
SPA	Styrene phosphonic acid
TREO	Total rare earth oxide
UV	Ultraviolet
XPS	X-ray Photoelectron Spectroscopy

Chemical abbreviations

BHA	Benzohydroxamate
CMC	Carboxymethylcellulose
EDTA	Ethylenediaminetetraacetic acid
F1682	Flotinor 1682
F8920	Florrea 8920
HA	Hydroxamic acid
NaOl	Sodium oleate

Constants

c	Velocity of light, 3×10^{8} m$\cdot$s^{-1}
e	Elementary charge, $1.60217662 \times 10^{-19}$ C
g	Gravitational acceleration, 9.8 m$\cdot$s^{-2}
h	Planck constant, 6.626×10^{-34} J$\cdot$s
k	Boltzmann constant, 1.381×10^{-23} m^{2}kg s^{-2} K^{-1}

ε_0	Electric permittivity of vacuum, 8.85×10^{-12} F·m^{-1}
π	Pi, 3.14159...

Greek Symbols

χ	Magnetic susceptibility
δ	Optical retardation, m
$\Delta\alpha$	Acceptance angle
ε_{rs}	Relative permittivity of the electrolyte solution
η	Dynamic viscosity, kg·m^{-1}·s^{-1}
γ_{LA}	Liquid - air interfacial tension, N·m^{-1}
γ_{SA}	Solid - air interfacial tension, N·m^{-1}
γ_{SL}	Solid - liquid interfacial tension, N·m^{-1}
κ^{-1}	Debye length, m
λ	Wavelength, m
μ	Fluid viscosity, kg·m^{-1}·s^{-1}
ν	Frequency, Hz
$\bar{\nu}$	Wave number, m^{-1}
ν_e	Electrophoretic velocity, m·s^{-1}
ν_T	Terminal velocity, m·s^{-1}
ψ^0	Surface potential, V
ρ_f or ρ_0	Density of the fluid, kg·m^{-3}
ρ_s	Density of the solid, kg·m^{-3}
θ	Contact angle or scattering angle
ζ	Zeta potential, V

Roman Symbols

A	Absorbance, %
a	Particle radius, m
CC	Concentration criterion
C_d	Drag coefficient
d	Particle diameter, m
D_{50}	Average particle size, µm
E	Applied electric field, V
E_B	Electronic binding energy, eV
E_K	Kinetic energy, J
F	Magnetic force, N
F80	80% passing size of a circuit feed, µm
H	Magnetic field intensity, $A{\cdot}m^{-1}$
m_1, m_2	Mass, g
n	Refractive index
n_i	Number of concentration of ion I
p	Static pressure, $N{\cdot}m^{-2}$
$p\mathrm{CO}_2$	Partial pressure of CO_2, atm
pKa	Acid dissociation constant
P80	80% passing size of a circuit product, µm
T	Thermodynamic temperature, K
$\%T$	Transmittance
U	Flow speed, $m{\cdot}s^{-1}$
U_{mol}	Energy of isolated molecule, J

U_{ads}	Adsorption energy, J
U_s	Energy of pure surface, J
u_e	Electrophoretic mobility, m s^{-1} V^{-1}
w	Slid width, m
W_D	Doppler shift, Hz
z_i	Charge number of ion I

Chapter 1

Introduction

Rare earth (RE) elements (*i.e.* yttrium and the lanthanoids [1.1]) have gained a lot of interest due to their important applications [1.2]. They are found in daily items such as cellphones, computers and televisions [1.3]. They are also used as fluid cracking catalysts in petroleum refining, additive to glass and as alloying elements to other metals to improve their physical properties [1.4]. The emergence of green technologies such as LEDs, batteries, hybrid motors and wind turbines [1.5], which require RE elements, will continue to increase the demand for RE elements [1.6]. It was projected that the demand for RE elements will increase between now and 2025 [1.7]. Currently, China is the biggest producer of RE oxides, amounting to 83% of the world's total annual production [1.8]. In 2008, China started imposing restriction on export quota in RE production affecting the global supply [1.9–1.11]. Although export quota restrictions have been lifted last May 2015 due to complaints from Australia, Japan, and the U.S. [1.12], the Rest-of-the-World (ROW) consumers are still apprehensive about the status of the RE market. With the forecasts of RE production and demand, the following RE elements: La, Nd, Pr, Dy, and Tb, are highly to be in short supply by 2025 [1.7]. This global demand can only be met with constant development of new mines outside of China. Among the Advanced Projects outside China, many are located in Canada [1.13, 1.14]; one of them is the Niobec RE project of Magris Resources Inc. which has been found to contain the largest resource of RE elements with 1058.6 million tonnes at 1.73% total RE oxide (TREO) [1.14]. This corresponds to 18.3 million tonnes of TREO, which is almost half of China's RE elements reserve (∼43 million tonnes TREO) [1.15]. Thus, there is a great potential for Canada to be competitive in the RE industry because of its large deposit of RE minerals [1.16]. However, there are some challenges with regards to RE processing. RE elements often occur in complex deposits [1.17], and are not often found concentrated [1.18], thus, not economically exploitable. Similarities of properties of RE minerals with the associated gangue minerals makes their separation difficult [1.19]. In addition, due to more than a decade of China's monopoly on the RE industry, there is a limited expertise in the field outside of China [1.10]. In order to develop economically viable projects, additional research studies are required to develop processing technologies suitable for the complex mineralogy of rare earths.

Due to the fine-grained nature of the RE minerals found in the Niobec ore, froth flotation appears to be the most applicable beneficiation method of RE minerals recovery [1.20]. Froth flotation is the process that takes advantage of the hydrophobicity of the minerals [1.21]. Separation is achieved by the introduction of bubbles in an agitated tank or a column. The hydrophilic minerals will remain in the solution, while the hydrophobic minerals will attach to the rising bubbles. The hydrophobicity differences of the valuable and gangue minerals can be enhanced by the addition of reagents such as collectors and modifiers. Collectors make the mineral hydrophobic (or more hydrophobic); while modifiers alter the surface chemistry of the minerals, which aims to improve or minimize collector adsorption. The adsorption of the reagents are govern by various parameters including mineral surface charge, mineral solubility and surface complexation, collector speciation in solution, mineral – reagent interaction, *etc.* [1.22]. The flotation efficiency are not only dictated by the effective adsorption of the reagents, but also by bubble stability and bubble – mineral interaction [1.21]. That is why froth flotation, which is a three-phase system, is regarded as a complex process [1.19]. Unfortunately, the available literature regarding RE flotation is limited, requiring researchers to fill this gap in scientific knowledge to achieve an efficient method of processing RE ores.

1.1 Objectives of the study

The main goal of this study was to selectively recover the RE minerals from the Niobec ore using flotation. In order to recover the RE minerals from the ore, the physico-chemical properties of the pure RE minerals and the primary gangue minerals must be first understood. This can be achieved if the following are satisfied:

a. Determine the zeta potential (estimate of the surface charge) of the pure minerals in the presence and absence of collectors;
b. Investigate the effect of different collectors and depressants on the floatability of the pure minerals; and
c. Understand the possible mineral - reagent interaction through surface characterization and density functional theory (DFT) based molecular modeling.

By relating the flotation behavior with electrokinetic zeta potential investigations and surface characterizations, possible adsorption mechanisms will be proposed. DFT-based simulations will validate some of these proposed mechanisms and possible conformations of some of the reagents at the surface of the minerals will be presented. In addition, fundamental knowledge obtained through pure mineral studies will be utilised to propose a viable Niobec ore flotation process.

1.2 Scope and limitations of the study

The study involved grinding studies and investigated other concentration methods prior to flotation. However, the focus of the study is flotation. Several minerals are present in the ore, but only the main RE minerals (monazite and bastnäsite) and the main gangue (dolomite) were investigated. Fundamental studies (*i.e.*, zeta potential measurements, surface characterization and microflotation) were conducted on single pure minerals, not on a mixture. In the bench-scale ore flotation, although the coarse fraction is processsed, the focus of the investigation is on the fine particle flotation. The chemical aspect (*e.g.*, reagent dosage, pH, temperature) of the process was paid more attention than the physical aspect (*e.g.*, air flowrate, gas holdup, cell diameter). Statistical design of experiment was employed mainly to determine the effect of the independent variables on the response (grade and recovery), and the possible interaction effects between the variables, but not to optimise the process.

1.3 Thesis structure

This thesis is a collection of five manuscripts prepared by the candidate according to the guidelines for a manuscript-based dissertation published by the Graduate and Postdoctoral Studies office of McGill University. Two manuscripts (Chapters 3 and 5) have already been published; one manuscript (Chapter 6) has been accepted for publication; one manuscript (Chapter 5) has been submitted to the Journal of Advanced Powder Technology; while the last one (Chapter 7) is to be presented at the Hi-Tech Metals Conference (part of Minerals Engineering International conference series).

This thesis is comprised of eight chapters and eight appendices.

Chapter 1 includes a general introduction, main and specific objectives, scope and structure of the thesis.

Chapter 2 provides a literature review on rare earth minerals and rare earth processing. It also presents briefly the fundamental operations in mineral processing, focused on froth flotation. A more detailed review on mineral - solution equilibria of dolomite, monazite and bastnäsite; and general collector adsorption mechanisms of carboxylates, hydroxamates and organic phosphoric acid are also provided.

Chapter 3 presents the surface chemistry and flotation behavior of bastnäsite, monazite and dolomite in the presence of benzohydroxamate, sodium oleate and Flotinor 1682 (a commercial phosphoric acid ester collector). This work is a more detailed version of previous work presented in Appendix A, which is an exploratory test. Based on the findings of this detailed work, possible collector adsorption mechanisms were proposed and possible flotation routes have been suggested. This work has been published as a journal article as follows:

Publication 1: Espiritu, E. R. L., Naseri, S. & Waters, K. E. (2018). Surface chemistry and flotation behavior of dolomite, monazite and bastnäsite in the presence of benzohydroxamate, sodium oleate and phosphoric acid ester collectors. *Colloids and Surfaces A: Physicochemical and Engineering Aspects, 546*, 254-265.

Chapter 4 details the investigation of several dolomite depressants such as citric acid, sodium carbonate, carboxymethylcellulose, starch, lignosulfonate and biopolymer. As Chapter 3 presents that sodium oleate and Flotinor 1682 were not as selective as benzohdroxamate and were able to float dolomite (gangue), this work then focuses on the possible depression of dolomite using sodium oleate and Flotinor 1682 as collectors.

Publication 2: Espiritu, E. R. L., Ronghao, L. & Waters, K. E. (2018). Depressing of dolomite in the presence of sodium oleate and phosphoric acid ester collectors. (Submitted to the Journal of Advanced Powder Technology).

In Chapters 5 and 6, the effect of dissolved mineral species on the flotation of dolomite, monazite and bastnäsite in the presence of benzohydroxamate and sodium oleate are presented, respectively. Since previous work indicated that efficient separation could be achieved with the use of benzohydroxamate (Chapter 3) and sodium oleate (Chapter 4), only these two collectors were investigated further in these Chapters. These research works have been published/submitted as following journal articles:

Publication 3: Espiritu, E. R. L., da Silva, G. R., Azizi, D., Larachi, F., & Waters, K. E. (2018). The effect of dissolved mineral species on bastnäsite, monazite and dolomite flotation using benzohydroxamate collector. *Colloids and Surfaces A: Physicochemical and Engineering*

Aspects, 539, 319-334.

Publication 4: Espiritu, E. R. L., da Silva, G. R., Azizi, D., Larachi, F., & Waters, K. E. (2018). Flotation behavior and electronic simulations of rare earth minerals in the presence of dolomite supernatant using sodium oleate collector. (Accepted and currently in press in the Journal of Rare Earths).

Chapter 7 presents the separate processing of the fine (-20 µm) and coarse (+20 µm) fractions of Niobec rare earth ore. The work focuses on exploring the feasibility of using an specially designed column cell for the processing of the fine fraction. The work investigates the effect of pH, collector, collector dosages, conditioning time, *etc.* on the rare earth elements grade and recovery.

Publication 5: Espiritu, E. R. L., Kökkılıç, O., Langlois, R., Gomez, C. & Waters, K. E. (2018). An exploratory investigation of alternative approach in processing rare earth ore using an specially designed column flotation. (To be presented at Hi-Tech Metals 2018).

Chapter 8 concludes the dissertation, proposes avenues for future research and presents the contributions of this thesis to original knowledge.

Appendix A includes the exploratory investigations of the different collectors on the flotation of monazite and dolomite. This work has been published as a journal article: Espiritu, E. R. L., & Waters, K. E. (2018). Flotation studies of monazite and dolomite. *Minerals Engineering, 116,* 101-106.

Appendix B includes the attenuated total reflectance Fourier-transform infrared (ATR-FTIR) spectra of the minerals conditioned with benzohydroxamate (Chapter 3).

Appendix C includes the determination of acid dissociation constants (pKa) of Flotinor 1682 by titration (Chapter 3).

Appendix D includes the investigation of the effect of carbonate ions on the electrophoretic properties of dolomite, monazite and bastnäsite. This work has been published in a conference proceeding: Espiritu, E. R. L., da Silva, G. R., & Waters, K. E. (2016). The effect of carbonate ions on the electrokinetic properties of bastnäsite, monazite and dolomite, in *XVIII International Mineral Processing Congress*, Quebec City, Canada.

Appendix E includes the speciation diagrams of the minerals (Chapter 5).

Appendix F and G include the statistical *t*-test results of the changes of zeta potential values of the minerals in the presence of benzohydroxamate (Chapter 5) and sodium oleate (Chapter 6), respectively.

Appendix H include the mineralogy results shared by the Department of Mining, Metallurgical and Materials Engineering of Laval University (Quebec, Canada), from the mineralogical study of the Niobec ore conducted by SGS (Lakefield, Canada).

References

[1.1] Henderson, P. General geochemical properties and abundances of the rare earth elements. In Henderson, P., Editor, *Developments in Geochemistry*, volume 2, pages 1–32. Elsevier, 1984.

[1.2] Fernandez, V. Rare-earth elements market: A historical and financial perspective. *Resources Policy*, 53(Supplement C):26–45, 2017.

[1.3] Mancheri, N. A. World trade in rare earths, Chinese export restrictions, and implications. *Resources Policy*, 46(Part 2):262–271, 2015.

[1.4] Goonan, T. G. Rare Earth Elements – End Use and Recyclability. Report Scientific Investigations Report 2011-5094, US Geological Survey, 2011.

[1.5] Clark II, W. W. and Cooke, G. Emerging Green Industrial Revolution Technologies. In Clark II, W. W. and Cooke, G., Editors, *The Green Industrial Revolution*, pages 173–190. Butterworth-Heinemann, Boston, 2015.

[1.6] Matamec. Matamec Management Discussion and Analysis. Report, 2017.

[1.7] Castilloux, R. Rare Earth Market Outlook: Supply, Demand, and Pricing from 2016 through 2025. Report, 2016.

[1.8] Gambogi, J. Rare earths. Report, US Geological Survey, 2017.

[1.9] Hong, F. Rare Earth: Production, Trade and Demand. *Journal of Iron and Steel Research, International*, 2006.

[1.10] Kingsnorth, D. Meeting the Challenges of Supply this Decade. www.eesi.org-files-kingsnorth_031111.pdf, 2011. Accessed Nov. 07, 2014.

[1.11] Tse, P.-K. China's rare-earth industry. Report, US Department of the Interior, US Geological Survey Reston, 2011.

[1.12] World Trade Organization. China – Measures Related to the Exportation of Rare Earths, Tungsten and Molybdenum. https://www.wto.org/english/tratop_e/dispu_e/cases_e/1pagesum_e/ds431sum_e.pdf, 2015.

[1.13] Canadian Rare Earth Elements Network. Submission to the House of Commons Standing Committee on Finance Pre-Budget Consultations 2014. Report, 2014.

[1.14] Hatch, G. TMR Advanced Rare-Earth Projects Index. Report, Technology Metals Research, 2015.

[1.15] Chen, Z. Global rare earth resources and scenarios of future rare earth industry. *Journal of Rare Earths*, 29(1):1–6, 2011.

[1.16] Kremnidas, T. Canada's Rare Earth Deposits Can Offer A Substantial Competitive Advantage. Report, The Canadian Chamber of Commerce, 2012.

[1.17] Golev, A., Scott, M., Erskine, P. D., Ali, S. H., and Ballantyne, G. R. Rare earths supply chains: Current status, constraints and opportunities. *Resources Policy*, 41:52–59, 2014.

[1.18] Haskin, L. and Paster, T. Geochemistry and mineralogy of the rare earths. In Gschneidner, K. and Eyring, L., Editors, *Handbook on the Physics and Chemistry of Rare Earths: Non-metallic compounds I, Vol. 3*. North-Holland Publishing Company, New York, 1979.

[1.19] Bulatovic, S. M. Flotation of REO Minerals. In Bulatovic, S. M., Editor, *Handbook of Flotation Reagents: Chemistry, Theory and Practice*, pages 151–173. Elsevier, Amsterdam, 2010.

[1.20] Jordens, A., Cheng, Y. P., and Waters, K. E. A review of the beneficiation of rare earth element bearing minerals. *Minerals Engineering*, 41:97–114, 2013.

[1.21] Wills, B. A. and Finch, J. A. Froth Flotation. In Finch, J. A. and Wills, B. A., Editors, *Wills' Mineral Processing Technology*, pages 265–380. Butterworth-Heinemann, Boston, 8th edition, 2016.

[1.22] Leja, J. *Surface Chemistry of Froth Flotation*. Springer US, New York, 1982.

Chapter 2

Rare earth mineral processing

Due to their unique chemical properties, RE elements have become vital to many high-technology applications. Bastnäsite and monazite are the primary sources of RE elements. However, due to the similarities of the properties of these minerals with their associated gangue, RE ore processing becomes challenging. This chapter will briefly discuss some of the properties of RE elements, the occurrence of RE elements in minerals, the challenges of separating these minerals from the ore and the current mineral processing techniques being applied.

2.1 Rare earth elements

The RE elements consist of scandium (Sc), yttrium (Y) and the lanthanoids [2.1]. In geochemistry, only yttrium and the lanthanoids are considered as RE elements [2.2], since scandium's properties are sufficiently different from these elements [2.3]. RE elements are further divided into subgroups - the cerium and the yttrium groups [2.4, 2.5], or the light and heavy RE elements [2.2], respectively. The light RE elements consist of lanthanum to europium [2.2, 2.4, 2.5], while the heavy RE elements consist of gadolinium to lutetium and yttrium [2.5].

The term “rare” is a historical misnomer [2.6, 2.7]. One reason for coining the term “rare” arose from the fact that during their time of discovery, separating them from their constituent rare earths is considerably difficult [2.8, 2.9]. In addition, during the 19th century, the minerals on which they were originally separated from were in fact rare [2.7, 2.8]. Despite the name, RE elements are not particularly rare. Abundances of some RE elements are comparable to molybdenum, tin, tungsten, arsenic and bromide (abundances in between 1 to 10 μg/g); and to cobalt, nickel, copper and zinc (abundances in between 15 to 100 μg/g) [2.10]. Most of the aforementioned elements are major industrial metals with global production greater than or equal to 30,000 MT per year [2.11]. However, RE elements do not occur naturally in pure form, and are found dispersed in most rock-forming processes [2.4]. Among the ~200 RE minerals [2.12], only a few justify economic exploitation [2.5, 2.13].

2.1.1 Geochemical properties

Due to their similar chemical properties, RE elements usually occur together in nature [2.14]. This phenomenon is attributed primarily to their electronic configurations. Only the inner energy level ($4f$ subshell) is being affected by the change in the number of electrons; the outer shell (energy level > 4) remains the same for all the elements. Because of this phenomenon, the electrons of the $4f$ subshell do not substantially take part in chemical interactions, thus leading to similarities in the chemical behaviour of the RE elements [2.2, 2.15]. The electronic configuration has been accounted for the +3 state of the elements, their ionic size, and coordination polyhedra.

Because RE elements are highly electropositive [2.8, 2.14], they tend to form trivalent ions, giving them the ionic state M^{3+} [2.8, 2.9, 2.16, 2.17]. The oxidation states of the RE elements are influenced by the stability of the f^0 (empty), f^7 (half-filled) and f^{14} (filled) configurations [2.14]. This is a result of a stable configuration of the noble gases (*e.g.*, Y^{3+}, La^{3+}), a half-filled (*e.g.*, Gd^{3+}) or a filled (*e.g.*, Lu^{3+}) f configuration. Others that form a M^{2+} (*e.g.*, Eu^{2+} and Yb^{2+}) and M^{4+} states (*e.g.*, Ce^{4+} and Tb^{4+}) are results of the stability of f^7 and f^{14}, and f^0 and f^7, respectively [2.14].

RE elements also take a variety of coordination polyhedra because of their large coordination numbers, which range from 6 - 12, or higher [2.2]. Light RE elements tend to occupy larger sites with a coordination number 7 to 11, while heavy RE elements tend to occupy the relatively smaller sites with coordination number between 6 and 9 [2.12]. This is dependent on the ionic size, where larger ions will likely occupy the larger sites. Based on the data compiled by Shannon and Prewitt [2.18], trivalent RE elements have large ionic sizes (approximately 1Å). Thus, unless the "substituted cation" is also large, RE elements cannot participate in substitution into minerals because of their large ionic sizes [2.2]. It is worth noting that their size is comparable to the ionic sizes of cations such as Na^+, Ca^{2+}, Th^{4+} and U^{4+}, but smaller than Ba^{2+}, K^+, Cs^+ and Rb^+. The differences and similarities of the ionic sizes is one of the reasons why RE elements occur rarely with rock-forming elements such as Si, Al, K, and Mg [2.4, 2.19] while commonly found associated with Na^+, Ca^{2+}, Th^{4+}, U^{4+} and Mn^{2+} [2.2, 2.12].

2.1.2 Basic geology of rare earth elements

Primary RE deposits are found in igneous rocks, where mineralization is either hydrothermal or magmatic, while secondary RE ores are formed as product of weathering and sedimentation [2.19–2.21]. RE minerals (any minerals which contains RE elements as essential component [2.22]) are being concentrated into ore deposits by three natural processes [2.3]. The following are the general classification of RE deposits based from the description given by Haskin and Paster [2.3]:

Placer deposit. A deposit formed by the natural concentration of heavy and weathering resistant minerals due to the effect of gravity. Initially, these minerals are diluted in the host rock but eventually concentrated as the host rock is being weathered. Then, these resistant minerals are carried downslope by water and accumulate and concentrate into placer [2.23].

Pegmatites. Pegmatite, a very coarse grained igneous rock [2.24], is formed during the final stage of magmatic crystallization. During the initial stage of crystallization, significant amount of dissolved water and volatiles (*e.g.*, chlorine, fluorine and carbon dioxide) are present in the magma [2.25]. In this stage, high-temperature-mineral forming ions are being depleted [2.26] as they crystallize into minerals. Since RE ions do not take part in crystallization of the common rock forming ions as discussed in Section 2.1.1, they tend to concentrate in the final liquid.

Alkali rock complexes. RE minerals tend to concentrate in magma that yields "highly alkali basalts and related materials" such as carbonatites [2.3]. The mechanism of concentration involves cooling of the magma beneath the surface and believed to be subjected to fractional crystallization, magma convection and hydrothermal processes only [2.27]. Formation of these rocks is not well understood due to its complexity, but the concentration process is believed to be similar to that of pegmatites where the ions (in this case, the RE ions) that are not suited to the coordination polyhedra of the common rock-forming minerals are being enriched in remaining liquid [2.24].

Long *et al.* [2.24] reported that RE elements are predominantly associated with igneous rocks. Igneous rocks cover a wide range, but regarding the RE elements, the most important are carbonatites and peralkaline rocks [2.28]. An igneous rock, as suggested by International Union of Geological Sciences (IUGS) system of igneous rock classification, is termed carbonatites if it contains more than 50% modal carbonates [2.19, 2.29, 2.30]. Moreover, igneous (or even with unascertained origin), metasomatic and hydrothermal rocks with less than 50% modal carbonates are considered to be related to carbonatites [2.19]. The primary RE element-bearing minerals found in carbonatitic deposits, which are enriched with light RE elements, are phosphate (monazite); fluorocarbonates (bastnäsite, synchysite and parasite); and hydrated carbonate (ancylite) [2.31]. Peralkaline, on the other hand, is a term coined for alkaline rocks in which the combined amount of Na_2O and K_2O is greater than the amount of Al_2O_3 [2.28, 2.29]. The RE deposits related to peralkaline intrusions are enriched with heavy RE elements. The RE minerals associated with these type of deposit are apatite, eudialyte, loparite, gittinsite, xenotime, gadolinite, monazite, bastnäsite, kainosite, mosandrite, britholite, allanite, fergusonite, and zircon [2.32].

2.1.3 Primary sources of rare earth elements

Despite the large number of RE element bearing minerals (approximately 200 [2.12]), only a few justify economic exploitation. Table 2.1 shows some of the currently exploited minerals as sources of RE elements. Among these RE minerals, the major sources of light RE elements are bastnäsite and monazite, and the main source of heavy RE elements is xenotime [2.5, 2.13, 2.21, 2.33, 2.34]. Bastnäsite is a fluorocarbonate mineral with the general formula $REE(CO_3)F$, where RE element is primarily La or Ce, possibly mixed with other light RE elements. It occurs mainly as finely disseminated or phenocryst in carbonatites [2.5]. Monazite is a phosphate mineral of light RE elements and thorium. It is present in small quantities in acidic igneous rocks or in metamorphic rocks; and because it is resistant to weathering, it concentrates mostly into placer deposits. Gupta and Krishnamurthy [2.5] mentioned that considering economic aspects, the most significant source of monazite is "beach placers and associated dune sand deposits". Xenotime is quite similar to monazite in terms of mineral type. It is also a phosphate mineral of RE and thorium, but it contains mostly Y (up to 63% Y_2O_3) and other heavy RE elements. It is mainly found concentrated in placer sand deposits (with monazite) and in cassiterite ores [2.35].

2.2 Rare earth deposit

Most of the RE productions come from deposits associated with carbonatites, such as the Mountain Pass deposit in California (USA) and the Bayan Obo deposit in Inner Mongolia (China) [2.28].

Table 2.1 – Principal sources of RE elements [2.19, 2.35].

Mineral	Chemical formula	Weight % REO
Light RE elements		
Bastnäsite	$REE(CO_3)F$	53 - 79
Monazite	$(REE,Th)PO_4$	38 - 71
Cerite	$(Ce,La,Ca)_9Fe^{3+}(SiO_4)[(SiO_3)(OH)](OH)_3$	50 - 70
Loparite-*Ce*	$(Ce,Na,Ca)(Ti,Nb)O_3$	31- 33
Heavy RE elements		
Xenotime	$(Y,REE)PO_4$	43 - 65
Gadolinite	$REE_2FeBe_2Si_2O_{10}$	45 - 54
Euxenite	$REE(Nb,Ta)TiO_6$	15 - 35

2.2.1 Mountain Pass and Bayan Obo deposits

From late 1880's to mid-1990's, monazite from placer deposit was the most important source of RE elements, until Mountain Pass (a carbonatite deposit), containing significant amounts of bastnäsite, was discovered in the 1950's [2.36, 2.37]. This deposit initially had 3.3 million metric tons with 7.7% TREO [2.14], and from 1965 to 1995, this deposit satisfied the world's RE consumption [2.38]. However, due to environmental concerns and the decline of RE prices [2.37, 2.38], eventually Mountain Pass ceased operation in 1998 and its mining operation in 2002 [2.39, 2.40]. The low RE prices was driven by China, a major competitor of the U.S. in terms of RE production. Bayan Obo, located in Inner Mongolia (China), is the largest known RE deposit (800 million metric tons, 6% TREO), but was known first to be the largest iron deposit in the world [2.14]. Although mining commenced in 1957, RE production started only in 1980 [2.14]. China's strategic plan to increase its production and to give special attention on the research and development of RE's [2.41], has resulted in their emergence as the major producer of RE.

For the past few decades, China has dominated the RE industry. When they started restricting export quotas, the world's RE supply was affected, and threatened the Rest-of-the-World (ROW) consumers of RE elements. The ROW has subsequently been searching for alternative sources of RE elements outside of China.

2.2.2 Niobec deposit

Currently, a number of the Advanced Projects outside China can be found in Canada. Among these projects, the Niobec project of Magris Resources Inc. has been found to contain the largest resource of RE elements with 1058.6 million tonnes at 1.73% TREO [2.42]. This corresponds to 18.3 million tonnes of TREO, which is almost half of China's RE element reserve (43 million tonnes TREO) [2.43]. Thus, there is a great potential for Canada to be competitive in the RE industry because of its large deposit of RE minerals [2.41].

The Niobec RE deposit is part of St. Honoré Carbonatite Complex and is adjacent to the current Niobec Mine in Quebec. Based from the characterization of 22 drill samples from the deposit, the samples contain gangue such as carbonates (73%), silicates, sulphides, oxides and barite. The primary RE minerals present in the ore are monazite (Ce,La,Nd,Th)PO_4, with an average grade of 1.2% and bastnäsite (Ce,La,Sm,Nd)(CO_3)F, with an average grade of 1% [2.44]. The characterization was done on size fractions +150 µm, -150/+38 µm and -38 µm. It was found that liberation increases significantly from +150 µm to -38 µm, suggesting that current particle size range is not suitable for physical processing. Monazite is found to have better liberation values and better exposure (surface area exposed) than bastnäsite (approximately half of the mineral mass is <30% exposed). Thus, to increase liberation and surface exposure, further grinding must be carried out. Preliminary testwork involving gravity separation, magnetic separation, flotation and attrition scrubbing showed a REO recovery of 58 - 70% in a 25 - 40% mass pull, respectively. Considering the physical processing and an additional leaching process, an average TREO recovery of 58% was estimated [2.45].

2.3 Typical concentration methods

The primary RE minerals are usually associated with the following gangue minerals: fluorite, siderite, barite, calcite, dolomite, ankerite, quartz, pyrite and iron oxides [2.46–2.50] as shown in Table 2.2. Beneficiation processes that were reported to successfully recover the RE minerals are gravity separation, magnetic separation, electrostatic separation and froth flotation [2.13, 2.14, 2.33, 2.51].

Table 2.2 – Specific gravities and magnetic properties of minerals.

Mineral	Specific gravity [2.52]	Magnetic property [2.53]	Electrical property [2.54–2.56]
Bastnäsite	5.12	Paramagnetic	Nonconductor**
Monazite	5.26	Paramagnetic	Nonconductor*
Ankerite	2.86	Paramagnetic	*Information not available*
Siderite	3.94	Paramagnetic	Semiconductor*, Nonconductor**
Hematite	5.18	Ferromagnetic	Semiconductor*
Magnetite	5.08	Ferromagnetic	Semiconductor*
Fluorite	3.17	Diamagnetic	Dielectrics**
Barite	4.48	Diamagnetic	Nonconductor**
Calcite	2.71	Diamagnetic	Dielectrics*
Dolomite	2.88	Diamagnetic	Semiconductor*
Quartz	2.65	Diamagnetic	Dielectrics**
Pyrite	4.99	Diamagnetic	Semiconductor*

*Classified based on electrical property. Dielectrics are poor conductors or insulator [2.54, 2.56]
**Classified based characteristics in electrostatic separation process. Nonconductors are those pinned to electrostatic (high-tension) separation surface [2.55]

2.3.1 Magnetic separation

In mineral beneficiation, the most essential parameter that dictates the magnetic separation is the "magnetic force acting upon the particle" [2.57]. The force acting on the particle when applied with magnetic field is proportional to the field intensity H and field gradient dH/dl by a constant χ which is known as the magnetic susceptibility [2.58, 2.59] as expressed in Equation 2.1. Table 2.2 clearly shows differences of magnetic properties of the minerals, as such magnetic separation could be considered. Magnetic separation exploits the differences of magnetic susceptibility of minerals [2.60, 2.61] to effect concentration of valuable minerals. It is defined as the degree of magnetization of a certain mineral/material in response to an applied magnetic field [2.62].

$$F = \chi H \frac{dH}{dl} \tag{2.1}$$

In general, minerals can be classified into three groups depending on their response to the applied magnetic field. They can be paramagnetic, diamagnetic or of a ferromagnetic type [2.59]. Paramagnetic and ferromagnetic minerals are both attracted along the lines of magnetic field [2.59, 2.63], however, ferromagnetic minerals are much more susceptible to magnetic force than paramagnetic [2.59]. Diamagnetic minerals, on the other hand, are repelled along the lines of magnetic field [2.59, 2.63]. Although magnetic susceptibility of the particles is to be considered to determine suitability of magnetic separation, another important factor is the size of materials [2.61, 2.64].

2.3.2 Electrostatic separation

This type of separation utilizes the differences in electrical conductivities of the different minerals in the ore. When a particle is subjected to an electrostatic charge, it behaves depending on its conductivity [2.65]. In the early 1900's, Crook [2.65] performed various experiments that led to the following conclusions: (1) Good conductors are more affected by an external electrostatic force than poor conductors; (2) When particles are electrified and are placed near a non-charged particle, they exert an attraction force that is dependent on their susceptibility to conductivity; (3) The differences of conductivity are more pronounced than differences in densities in terms of its response to attraction forces; (4) Moisture affects conductivity such that a poor conductor can be converted to a good conductor, as such humidity control is essential.

Minerals can be classified as conducting and nonconducting [2.66], while the separators are classified based on their charging methods [2.67] - induction, corona and triboelectricity [2.68]. Corona charging happens when one or more electrodes ionizes the gas around them due to high voltage used, charging nearby particles [2.69]. Another mechanism of charging, induction, is observed when an uncharged particle adopts the field polarity of the applied electric field. Tribo- or frictional charging, on the other hand, happens when particles make contact; when they do, a transfer of charge occurs, making the particles acquire opposite electric charges depending on their dielectric properties [2.70].

2.3.3 Gravity separation

The minerals commonly found in RE deposits exhibit significant diffferences in specific gravities (See Table 2.2). One method of concentrating the ore is to take advantage of the differences of densities between the valuable and gangue minerals [2.51]. To determine the suitability of this method, the factor being considered is the concentration criterion as given by Equation 2.2, where SG is the specific gravity [2.71].

$$\text{Concentration Criterion (CC)} = \frac{\text{SG of heavy mineral - SG of fluid}}{\text{SG of light mineral - SG of fluid}} \tag{2.2}$$

However, the effectiveness of separation is not only dependent on this criteria but also with the particle size. Taggart and Behre [2.72] summarized the suitability of gravity separation for a given CC in relation to particle size.

Table 2.3 – Concentration criterion guide for gravity separation

Concentration criterion	Suitability to gravity separation
$CC > 2.5$	easy down to 75 µm
$1.75 < CC < 2.5$	possible down to 150 µm
$1.5 < CC < 1.75$	possible down to 1.7 mm
$1.25 < CC < 1.5$	possible down to 6.35 mm
$CC < 1.25$	impossible at any size

Considering both the particle size and density, another factor that will determine the separability of minerals is its settling rate. Depending on the particle size, the terminal settling velocity of a particle can be estimated using the Stoke's law (Equation 2.3) or Newton's (Equation 2.4) [2.73], where d is the particle diameter, ρ_s and ρ_f is the density of solid and fluid respectively, C_d is the drag coefficient, μ is the fluid viscosity and g is the gravitational acceleration.

$$\nu_T = \frac{g(\rho_s - \rho_f)d^2}{18\mu} \tag{2.3}$$

$$\nu_T = \sqrt{\frac{4g(\rho_s - \rho_f)d}{3C_d\rho_f}} \tag{2.4}$$

Various gravity separators are classified based on the mechanism of dispersing the particles such that they can move freely and be separated from other particles due to their differences in settling rates [2.71].

1. *Jigging.* In jigging, the particles attain a stratification due to a repeated pulsation of liquid through the bed. When a liquid is pulsated through the bed, the bed expands and contracts. As it contracts, it results to stratification on the basis of settling rate of each particle (see Figure 2.1).

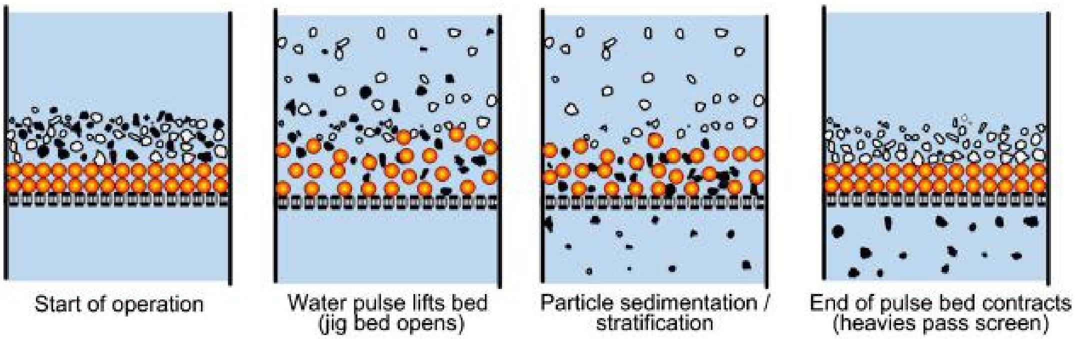

Figure 2.1 – The separation of heavies from lights in a jig [2.73]. Reprinted with permission from Elsevier.

2. *Shaking concentrators.* In a shaking concentrator, the particles are being separated because of a horizontal shaking motion. The common example of a shaking concentrator is a shaking table (see Figure 2.2). The shaking motion expands the bed and causes a differential motion, achieving a stratification of particles. The motion depends on different types of tables but the common among them is that the forward motion is slow as compared to the direction perpendicular to the particle movement. The separation is affected by action of the flowing water film and stratification of the particles by settling.

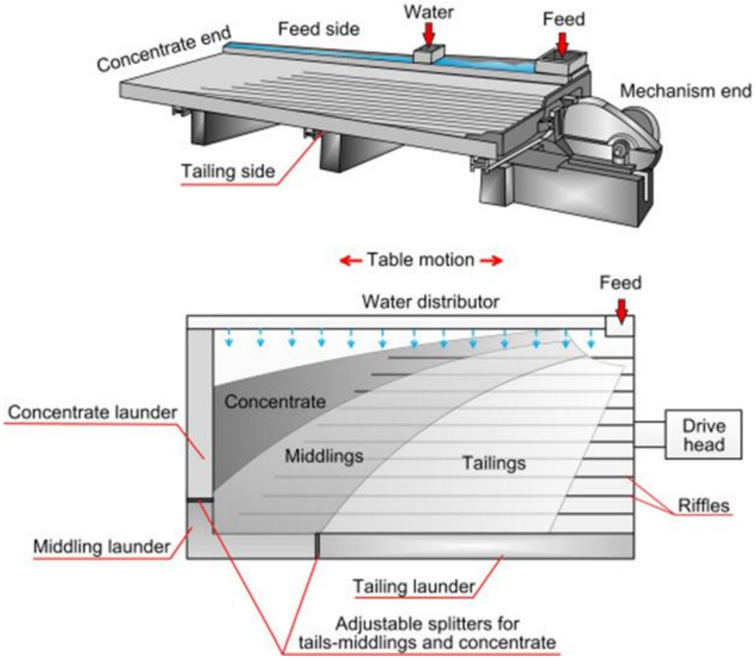

Figure 2.2 – Schematic diagram of a shaking table [2.73]. Reprinted with permission from Elsevier.

3. *Flowing film concentrators.* Using this method, the particle segregation is attained by letting a slurry flow down an inclined surface. The separation is again governed by

the differences of the settling rates of the particles. As the slurry moves down the slope, the slow-settling light particles are being carried further down the slope while the heavy particles tend to settle early. The most commonly used concentrators of this type are spiral concentrators (*e.g.*, Humphrey spiral), and centrifugal separators (*e.g.*, Knelson and Falcon concentrators). An example of a centrifugal concentrator is shown in Figure 2.3.

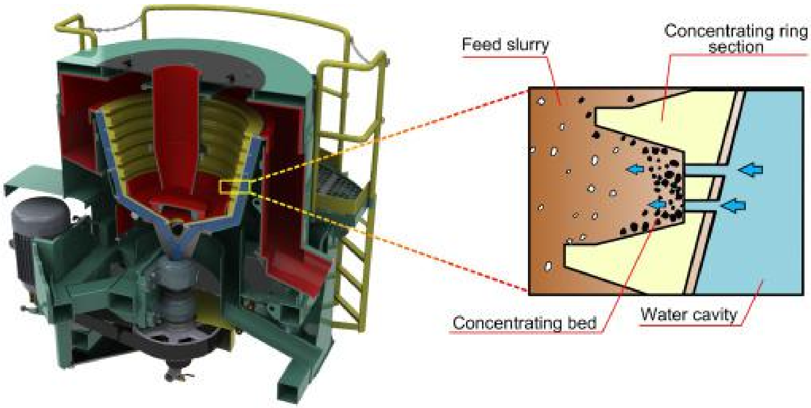

Figure 2.3 – Diagram of a Knelson concentrator [2.73]. Reprinted with permission from Elsevier.

Another type of gravity (density) separation is *dense media separation*. Basically, it uses a medium with density in between the densities of the valuable and gangue minerals. This type is also called sink-float separation as the light minerals will float, while the heavy minerals will sink [2.74]. The advantage of this gravity method is having a sharp separation with high separation efficiency, however, it is only applicable to coarse materials (>4mm) as the fine particles take too long to settle [2.74].

2.4 Froth flotation

Effective separation of RE minerals from gangue is rarely achieved with purely physical separation methods due to the fine liberation size. Thus, froth flotation is still currently the most widely investigated beneficiation process for processing RE minerals [2.75]. The basis of this separation technique is to take advantage of differences in the hydrophobicity of the minerals [2.71]. Bubbles, which are introduced to a slurry in an agitated tank or a column (shown in Figure 2.4, act as the medium of separation. The hydrophobic particles will attach to the bubbles, while the hydrophilic will remain in suspension. The bubbles carry the attached particles on top of the suspension forming a froth layer, which can be collected in the launder as concentrate.

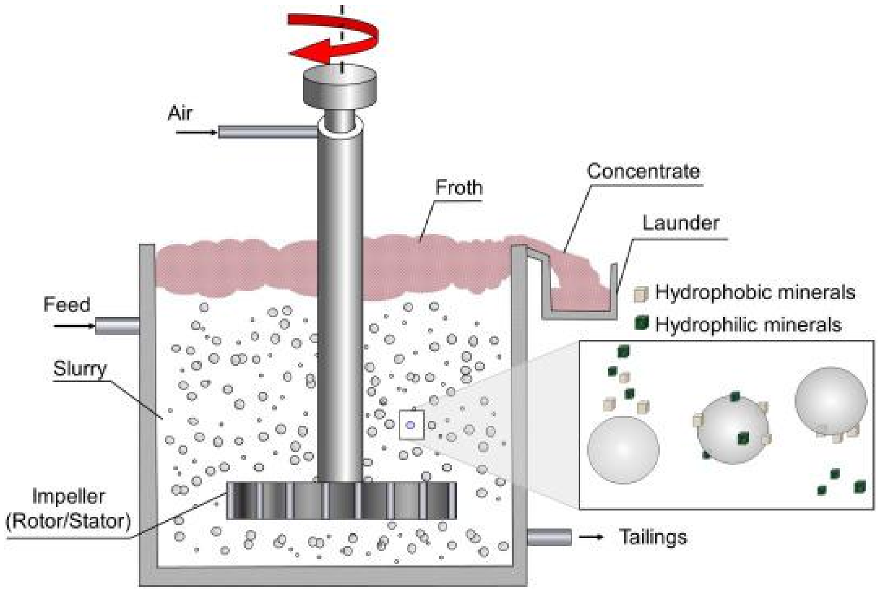

Figure 2.4 – Schematic diagram of a flotation machine [2.73]. Reprinted with permission from Elsevier.

In this process, when water, the stable bubble and the mineral particle become in contact, an equilibrium is established. The interfacial tensions between their surfaces find an equilibrium state which is described by the contact angle (θ) as shown in Figure 2.5 [2.71]. At equilibrium, the interfacial tension between the solid and the air (γ_{SA}) can be given by the Young's equation (Equation 2.5), where θ is the contact angle, and γ_{LA} and γ_{SL} are the liquid - air, solid - liquid interfacial tensions, respectively. The contact angle is a physical indicator of the hydrophobicity of a mineral. When its value is greater than 90°, the particle is categorized as hydrophobic, on the other hand, when its value is less than 90°, it is considered as hydrophilic [2.71].

$$\gamma_{SA} = \gamma_{SL} + \gamma_{LA} \cos\theta \tag{2.5}$$

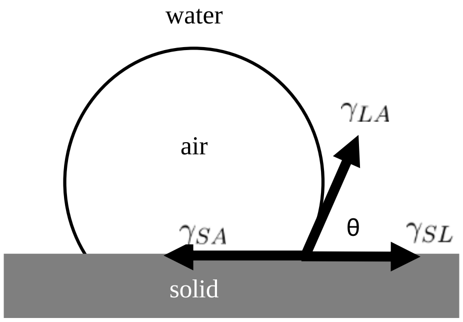

Figure 2.5 – The balance of the interfacial tensions in a flotation system.

2.4.1 Flotation reagents

The contact angle, thus the hydrophobicity of a mineral, can be modified using various reagents [2.71]. These reagents can be classified based on their functions.

Collectors

Collectors are organic chemical with a polar head and a nonpolar hydrocarbon tail. Collectors selectively adsorb onto the surface of a mineral [2.76] such that the nonpolar part is oriented to the water phase and the polar part toward the mineral phase [2.71, 2.77], rendering the mineral surface hydrophobic [2.77].

Considering RE mineral recovery, oxhydryl collectors such as carboxylates, phosphoric acid esters and hydroxamates have been the focus of flotation studies due to their effectiveness [2.78, 2.79]. These oxhydryl collectors have two oxygen atoms available for bonding [2.63] as seen in Figure 2.6.

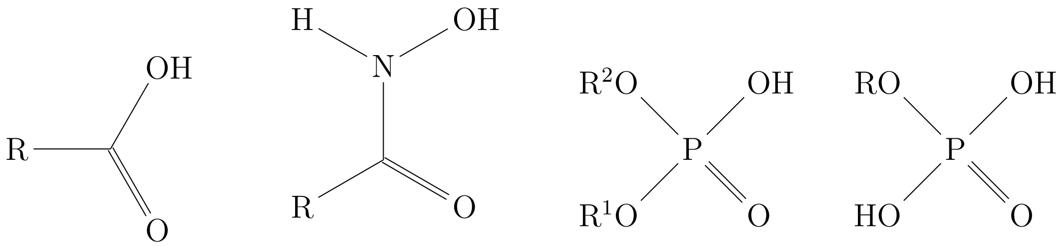

(a) Carboxylate **(b)** Hydroxamate **(c)** Phosphoric acid ester

Figure 2.6 – Structure of different collectors in RE mineral flotation: a) carboxylate, b) hydroxamate, and c) phosphoric acid esters.

Carboxylates, which include fatty acids, oleates and tall oils, are the most widely used industrial collector due to their popularity (most researched) and not because of high performance [2.77]. They are considered strong collectors, but have poor selectivity towards RE minerals [2.80]. Based on various flotation studies, hydroxamates are more selective than the carboxylates [2.78, 2.79, 2.81, 2.82]. This is due to its formation of more stable chelates with RE metals cations than with alkaline earth metal cations [2.83]. Another family of collectors that has been investigated includes organic phosphoric acids, but these are relatively new in RE mineral flotation [2.84]. These collectors were investigated in the RE mineral flotation at Weishan county, Shandong province in China. They are worth investigating as research indicates RE oxide recovery of 60% at 20% grade [2.84]. Further discussion of these collectors is provided in Section 2.5.3.

Frothers

Frothers have typically the same structure as collectors, consisting of a polar group and a hydrocarbon group [2.85]. Frothers adsorb at the air - water interface [2.71] such that the polar head is oriented towards the water phase, while the hydrocarbon tail is oriented towards the air phase [2.85]. Accordingly, the effectiveness of a frother is dependent on its ability to adsorb on the air-water interface [2.80]. Frothers can be classified as soluble or partially soluble [2.86] based on their solubility in water; and acidic, neutral or basic based on their behavior at different pH conditions [2.85]. Acidic frothers (*e.g.*, phenols and alkyl-lauryl sulfonates) are only effective in acidic pH, basic frothers (*e.g.*, pyridine base), on the other hand, are used for flotation of base metal ores [2.85]. The most widely used frothers are alcohols (*e.g.*, pine oil and methyl isobutyl carbinol) and polyglycols (*e.g.*, Dowfroth 250 and F150) due to their neutral nature [2.85, 2.87].

Modifiers

The principal function of the modifier is to alter the action of the collector on the mineral surface [2.80]. Modifiers play a significant role in flotation as it makes possible the selective adsorption of collectors on the target mineral (Bulatovic, 2007e). They can be classified as pH modifiers, activators and depressants [2.71, 2.80]. The same modifier may function as pH modifier, activator or depressant under different flotation conditions [2.88]. Activators and depressants both alter the surface of the mineral: activators enhance the adsorption of collector; while depressant inhibit the adsorption of collectors onto the mineral surface [2.80].

2.4.2 Flotation machines

2.4.2.1 Small-scale tests

Small-scale tests are usually conducted to evaluate the floatability of a pure mineral (typically 1 g) in a microflotation cell.

Modified Partridge-Smith cell. The cell was first introduced by Partridge and Smith [2.89]. The cell (see Figure 2.7a), which is made of glass, has a silicate frit at the bottom where the air can be introduced. It also has a launder that receives the froth at the top, which can be collected through scraping. The flotation volume of the cell is approximately 60 mL. A magnetic stirring bar can be employed to ensure that the minerals remain in suspension.

Modified Hallimond tube. This cell was first introduced by Hallimond [2.90]. In the original design, the bottom part was constricted and does not have mechanism for suspension agitation [2.91]. In the modified version (see Figure 2.7b), the flotation cell volume is approximately 170 mL. The cell, also made of glass, has three parts. The lower part has a silicate frit at the bottom, the middle part connects the lower part and the upper part, and the upper part is where the concentrate can be collected. A magnetic stirring bar can be employed to ensure that the minerals remain in suspension. Unlike the modified Partridge-Smith cell, the modified Hallimond cell does not need scraping to collect the floated particles. The hydrophobic particles attached to the bubbles, can be collected through floated particles outlet as the bubble rises and bursts at the froth layer.

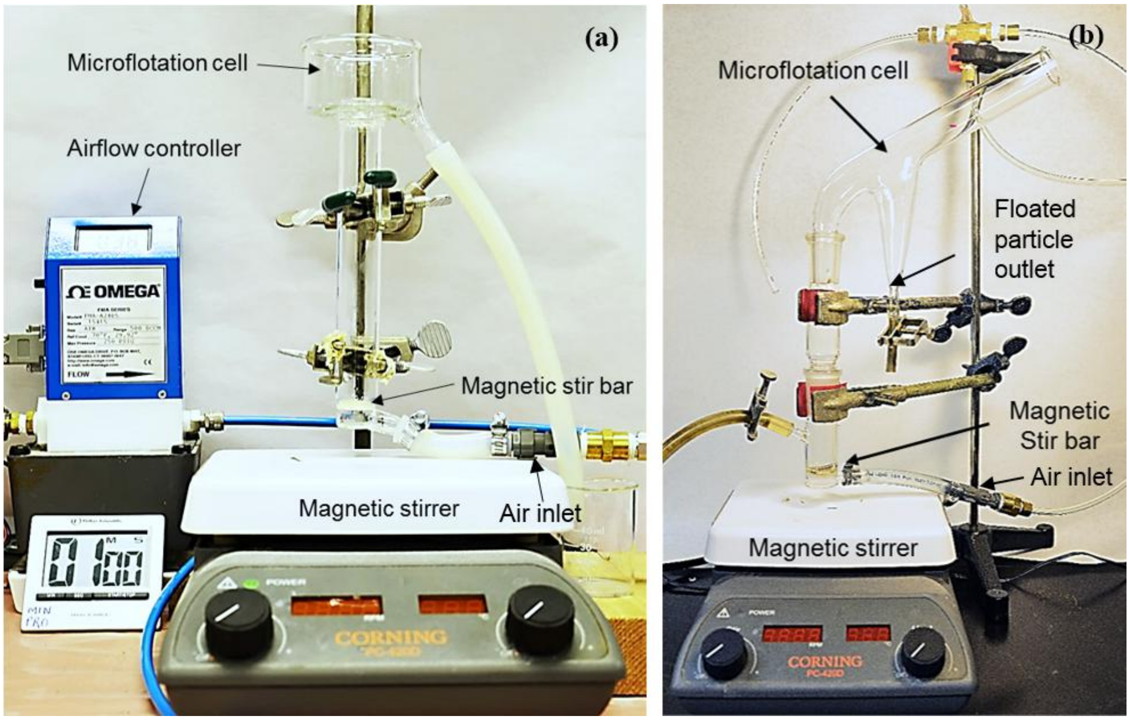

Figure 2.7 – Actual microflotation set-up of (a) modified Partridge-Smith cell; and (b) modified Hallimond tube.

2.4.2.2 Laboratory scale tests

Laboratory flotation testwork is conducted typically with 500 g, 1000 g or 2000 g samples in a batch flotation cell [2.80]. An example of which is the Denver cell, a mechanical flotation machine which simulates the conventional industrial mechanical cell set-up. The air is introduced through the hollow tube which is connected to the impeller. The mechanical impeller which agitates the pulp also disperses the incoming air as bubbles into the pulp.

The actual set up and the schematic of air dispersion is shown in Figure 2.8.

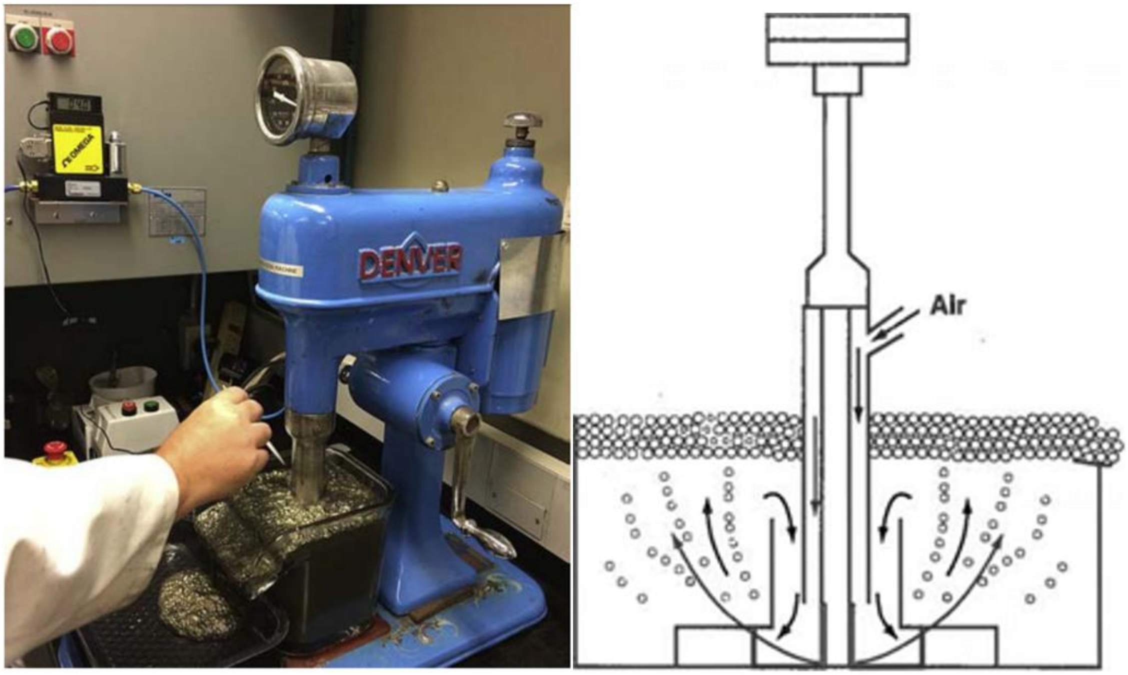

Figure 2.8 – Actual set-up of a Denver cell [2.80] (left) and air dispersion in a Denver cell [2.92] (right). Reprinted with permission from Elsevier.

2.4.2.3 Industrial set up

Several flotation machines have been developed which can be categorized mainly into mechanical, column and reactor/separator flotation machine [2.80].

Mechanical cells are distinguished by a mechanical impeller which agitates the pulp, keeping it in suspension. The air is introduced through the hallow shaft connected to the impeller [2.93]. The formation of flotation bubbles is proposed to be due to cavitation formed at the edge of the impeller blades, which are being sheared into smaller bubbles as the blade rotates [2.93].

Column cells have been proposed as a better alternative to conventional mechanical cells due to improved recovery (especially of fine particles), higher grade, lower capital and operating cost, and low space requirement [2.80, 2.94]. In the column cell, bubbles are formed by passing compressed air through a bubble generator, which can be installed internally or externally [2.94]. Internal spargers are not preferred due to possible wear and plugging of ore particles. SlamJet® (internal jetting sparger) is an improved version of these internal spargers with the added wear protection, air flowrate control and shut-off mechanism. As for external spargers, CISA/Microcel$^{\text{TM}}$ mixes slurry (from the column) and air through an in-line contactor. This mechanism breaks the air into smaller bubbles at the same time mixes them with the particles. Another way of introducing air is by using a cavitation tube (CavTube$^{\text{TM}}$), in which fine bubbles are produced due to cavitation [2.80]. Cavitation is defined by Ross [2.95] as the rupture of a liquid or of a liquid-surface interface caused by a local static pressure. One way to produce cavitation is by dynamic effects of liquid flows, hence the term hydrodynamic cavitation. A dimensionless parameter, K, was defined to measure the condition of a flow relevant to cavitation. This parameter was derived from the relationship between static pressure (p) and flow speed (U), which follows the Bernoulli's equation:

$$p + \rho_0 g z + \frac{1}{2}\rho_0 U^2 = \text{constant} \tag{2.6}$$

which states that a pressure drop due to flow is proportional to the product of density and square of flow speed. The dimensionless parameter, K, can be derived by dividing the available static pressure, $p_0 - p_v$, by the dynamic pressure of the flow.

$$K = \frac{p_0 - p_v}{\frac{1}{2}\rho_0 U^2} \tag{2.7}$$

This parameter indicates whether a cavitation is likely to occur (higher number) or not (lower number). A critical cavitation index or inception cavitation index was also defined as the value/s that borders the occurrence of cavitation or non-occurrence. For further information about cavitation, the readers are referred to Ross [2.95].

Another type of flotation machine is the **reactor/separator machines**. These machines differentiate the bubble-particle mixing region (reactor) and the bubble-particle aggregates separation (from the slurry) region (separator). The most well known version is the Jameson cell (Figure 2.9) which was developed by Mount Isa Mines Ltd and University of Newcastle in Australia. It is referred as a column machine; however, due to the mechanism of bubble-particle mixing and separation from the slurry, it was also considered a reactor/separator type machine. The mode of air introduction in Jameson cell is by plunging a jet of slurry through a downcomer. The high-pressure jet entrains the air in the atmosphere and the impact with the liquid shears the air into fine bubbles [2.80].

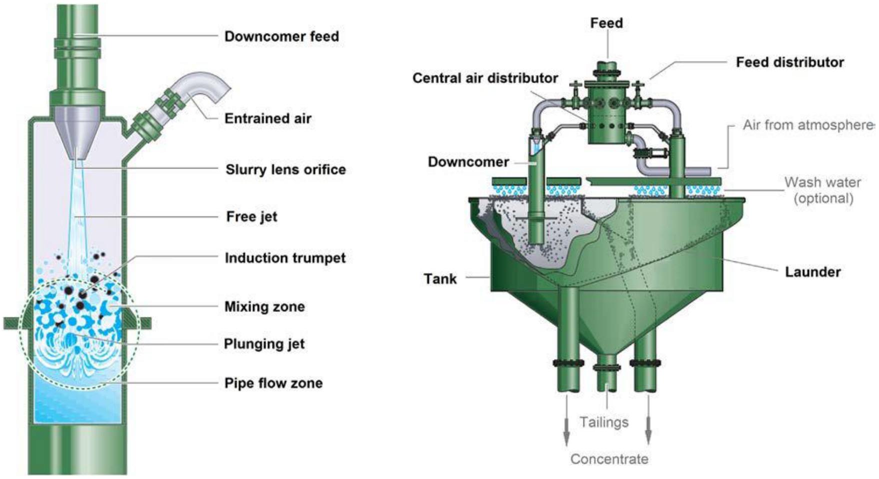

Figure 2.9 – Principles of operation of the Jameson cell [2.80]. Reprinted with permission from Elsevier.

2.5 Surface chemistry

"The process of froth flotation is an outstanding example of applied surface chemistry" [2.96]. The physical and chemical phenomena occurring at the interfaces (solid-liquid, liquid-gas, solid-gas) govern flotation performance.

2.5.1 Mineral - solution equilibria and surface complexation

RE minerals and common associated gangue minerals such as calcite are slightly soluble minerals [2.97, 2.98]. Heterogenous systems such as flotation, which involves slightly soluble minerals, are regarded as being complex systems [2.99]. The constituent ions from the sparingly soluble minerals could be dissolved in the solution and species / complexes could be formed or precipitate at the minerals' surface, hence could affect their flotation behavior [2.79, 2.100, 2.101]. In this section, the mineral-solution equilibria and the possible surface complexes/precipitates of the main RE minerals and gangue present in Niobec ore will be discussed. It should be noted that although bastnäsite and monazite could have other RE elements present in their structure, only cerium or lanthanum will be considered in the following discussion to avoid redundancy, since other RE elements tend to form similar species as that of cerium or lanthanum.

2.5.1.1 Dolomite

It has been suggested that when a carbonate is placed in contact with water, two primary hydration sites will occur: (1) hydroxylated cation sites ($>MeOH^0$); and (2) protonated mineral anion sites ($>CO_3H^0$), where Me represents the mineral cation and > represents the mineral lattice. The formation of these surface complexes was speculated by Van Cappellen *et al.* [2.102] and the presence was confirmed by Stipp and Hochella [2.103] through spectroscopic studies.

It has also been proposed that the dissolution of dolomite consists of two consecutive steps in three parallel reactions: (1st) the reaction of $CaCO_3$ components with the H^+, $H_2CO_3^o$ and H_2O in solution; and (2nd) the interaction of the $MgCO_3$ with the H^+, $H_2CO_3^o$ and H_2O species in solution. The breakdown of $MgCO_3$ component, the rate limiting step, is a half order reaction dependent on H^+, $H_2CO_3^*$ and H_2O, where $H_2CO_3^*$ represents $CO_{2(aq)}$ + $H_2CO_3^o$. This shows that the $CaCO_3$ components of dolomite dissolve faster than $MgCO_3$ components which results to initially Mg-rich dolomite surface [2.104].

The possible speciation of dolomite in solution was also studied. The equilibrium equations for dolomite – water – CO_2 system are presented below. The equilibrium constants are based on the Gibbs free energy of the species at standard conditions (25 °C, 1 atm) [2.105].

$$\mathrm{MgCO_{3(s)} \rightleftharpoons MgCO_{3(aq)}} \qquad \mathrm{pK_1} = 4.51 \tag{2.8}$$
$$\mathrm{MgCO_{3(aq)} \rightleftharpoons Mg^{2+} + CO_3^{2-}} \qquad \mathrm{pK_2} = 3.40 \tag{2.9}$$
$$\mathrm{CO_3^{2-} + H_2O \rightleftharpoons HCO_3^- + OH^-} \qquad \mathrm{pK_3} = 3.67 \tag{2.10}$$
$$\mathrm{HCO_3^- + H_2O \rightleftharpoons H_2CO_3 + OH^-} \qquad \mathrm{pK_4} = 7.62 \tag{2.11}$$
$$\mathrm{H_2CO_3 \rightleftharpoons CO_2(g) + H_2O} \qquad \mathrm{pK_5} = -1.43 \tag{2.12}$$
$$\mathrm{Mg^{2+} + HCO_3^- \rightleftharpoons MgHCO_3^+} \qquad \mathrm{pK_6} = -1.16 \tag{2.13}$$
$$\mathrm{MgHCO_3^+ \rightleftharpoons H^+ + MgCO_{3(aq)}} \qquad \mathrm{pK_7} = 8.09 \tag{2.14}$$
$$\mathrm{Mg^{2+} + OH^- \rightleftharpoons MgOH^+} \qquad \mathrm{pK_8} = -2.57 \tag{2.15}$$
$$\mathrm{MgOH^+ + OH^- \rightleftharpoons Mg(OH)_{2(s)}} \qquad \mathrm{pK_9} = -8.48 \tag{2.16}$$
$$\mathrm{MgOH^+ + OH^- \rightleftharpoons Mg(OH)_{2(aq)}} \qquad \mathrm{pK_{10}} = -5.81 \tag{2.17}$$
$$\mathrm{Mg(OH)_{2(aq)} \rightleftharpoons Mg(OH)_{2(s)}} \qquad \mathrm{pK_{11}} = -2.67 \tag{2.18}$$
$$\mathrm{CaMg(CO_3)_2 \rightleftharpoons Ca^{2+} + Mg^{2+} + 2\,CO_3^{2-}} \qquad \mathrm{pK_{12}} = 19.35 \tag{2.19}$$
$$\mathrm{Ca^{2+} + HCO_3^- \rightleftharpoons CaHCO3^+} \qquad \mathrm{pK_{13}} = -0.87 \tag{2.20}$$
$$\mathrm{CaHCO_3^+ \rightleftharpoons CaCO_{3(aq)} + H^+} \qquad \mathrm{pK_{14}} = 7.99 \tag{2.21}$$
$$\mathrm{Ca^{2+} + OH^- \rightleftharpoons CaOH^+} \qquad \mathrm{pK_{15}} = -1.30 \tag{2.22}$$
$$\mathrm{CaOH^+ + OH^- \rightleftharpoons Ca(OH)_{2(aq)}} \qquad \mathrm{pK_{16}} = 1.30 \tag{2.23}$$
$$\mathrm{Ca(OH)_{2(aq)} \rightleftharpoons Ca(OH)_{2(s)}} \qquad \mathrm{pK_{17}} = -5.10 \tag{2.24}$$

Speciation of dolomite was calculated and is presented as the log of α as a function of pH (Figure 2.10), where α is the concentration of the species divided by the total concentration of the ionic species. For a sparingly soluble mineral, M_nX_m, the total concentrations of cation and anion, C_{TM} and C_{TX}, are expressed as follows [2.106], thus $\alpha_{Mg^{2+}} = [Mg^{2+}]/C_{TMg^{2+}} = [Mg^{2+}]/[Mg^{2+}] + [MgOH^{+}] + [Mg(OH)_2]$, and so on.

$$C_{TM} = [M^{m+}] + [MOH^{+m-1}] + [M(OH)_2^{+m-2}] + ... \tag{2.25}$$

$$C_{TX} = [X^{n-}] + [HX^{-n+1}] + [H_2X^{-n+2}] + ... \tag{2.26}$$

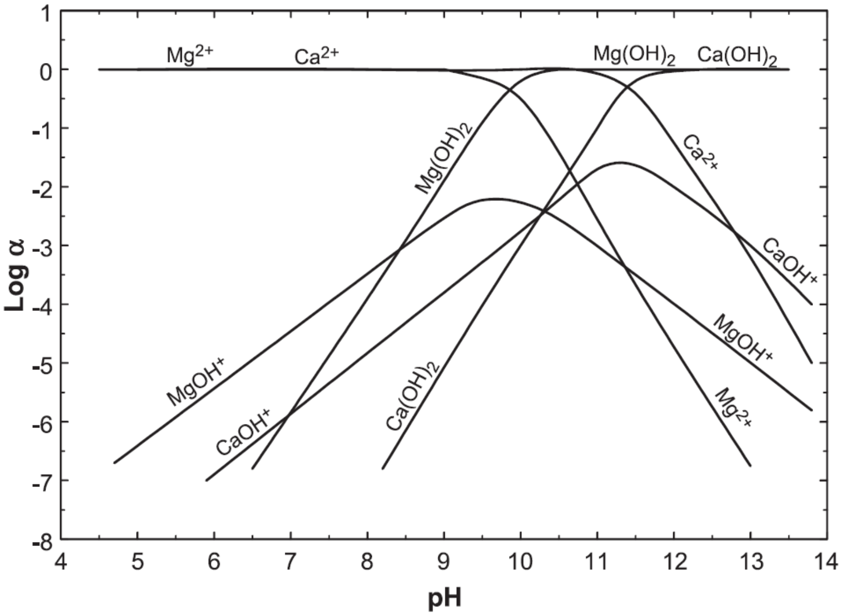

Figure 2.10 – Species distribution constants as a function of pH in dolomite solution [2.106]. Reprinted with permission from Elsevier.

2.5.1.2 Bastnäsite

Herrera - Urbina *et al.* [2.107] calculated the bastnäsite - solution equilibria to understand the complex chemistry of the mineral in solution. Mass balance equations were presented in Equations 2.27 - 2.44, in which the first consideration is that bastnäsite is the only solid species. However, as bastnäsite becomes highly soluble at acidic and basic conditions, equations involving coexistence of solid cerium fluoride and solid cerium hydroxide with bastnäsite and the complete dissolution of bastnäsite were also considered.

Figure 2.11 shows the speciation of 0.05 wt. % initial bastnäsite in solution closed to the atmosphere. It shows the amount of free Ce^{3+}, F^{-}, CO_3^{2-} and the solid species present in the solution. The solubility of these solid species in equilibrium was also calculated considering a 0.05 wt. % initial bastnäsite (Figure 2.12). For further understanding of the bastnäsite - solution equilibria, the readers are referred to Herrera - Urbina *et al.* [2.107].

Cerium species

$$Ce^{3+} + H_2O \rightleftharpoons Ce(OH)^{2+} + H^+ \qquad \log {}^*\beta_1 = -8.1 \tag{2.27}$$

$$Ce^{3+} + 2\ H_2O \rightleftharpoons Ce(OH)_2^+ + 2\ H^+ \qquad \log {}^*\beta_2 = -16.3 \tag{2.28}$$

$$Ce^{3+} + 3\ H_2O \rightleftharpoons Ce(OH)_3^0 + 3\ H^+ \qquad \log {}^*\beta_3 = -26.0 \tag{2.29}$$

$$Ce^{3+} + 4\ H_2O \rightleftharpoons Ce(OH)_4^- + 4\ H^+ \qquad \log {}^*\beta_4 = -38.0 \tag{2.30}$$

$$3\ Ce^{3+} + 5\ H_2O \rightleftharpoons Ce_3(OH)_5^{4+} + 5\ H^+ \qquad \log {}^*\beta_5 = -32.8 \tag{2.31}$$

$$Ce^{3+} + F^- \rightleftharpoons CeF^{2+} + 3\ H^+ \qquad \log \beta_1 = 3.86 \tag{2.32}$$

$$Ce^{3+} + 2\ F^- \rightleftharpoons CeF_2^+ + 3\ H^+ \qquad \log \beta_2 = 7.3 \tag{2.33}$$

$$Ce^{3+} + CO_3^{2-} \rightleftharpoons CeCO_3^+ \qquad \log \beta_1 = 7.56 \tag{2.34}$$

$$Ce^{3+} + 2\ CO_3^{2-} \rightleftharpoons Ce(CO_3)^{2-} \qquad \log \beta_1 = 12.19 \tag{2.35}$$

$$Ce^{3+} + HCO_3^- \rightleftharpoons CeHCO_3^{2+} \qquad \log \beta_{HCO_3} = 2.42 \tag{2.36}$$

Fluoride species

$$F^- + H^+ \rightleftharpoons HF \qquad \log K_1 = 3.176 \tag{2.37}$$

$$HF + F^- \rightleftharpoons HF_2^- \qquad \log K_2 = 0.591 \tag{2.38}$$

Carbonate species

$$CO_{2(g)} + H_2O \rightleftharpoons H_2CO_3^* \qquad \log K = -1.46 \tag{2.39}$$

$$H_2CO_3^* \rightleftharpoons HCO_3^- + H^+ \qquad \log K_1 = 10.35 \tag{2.40}$$

$$HCO_3^- \rightleftharpoons CO_3^{2-} + H^+ \qquad \log K_2 = 6.35 \tag{2.41}$$

Carbonate species

$$CeFCO_{3(s)} \rightleftharpoons Ce^{3+} + F^- + CO_3^{2-} \qquad K_{sp} = 10^{-16} \tag{2.42}$$

$$CeF_{3(s)} \rightleftharpoons Ce^{3+} + 3\ F^- \qquad K_{sp} = 8 \times 10^{-16} \tag{2.43}$$

$$Ce(OH)_{3(s)} + 3\ H^+ \rightleftharpoons Ce^{3+} + 3\ H_2O \qquad \log {}^*K_{s_0} = 20.1 \tag{2.44}$$

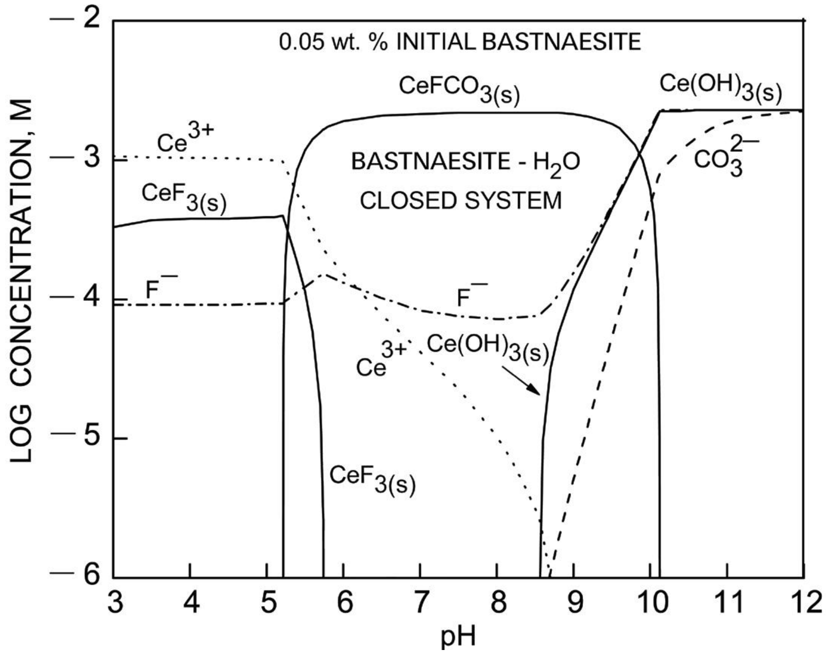

Figure 2.11 – Speciation diagram of 0.05 wt. % initial bastnäsite in aqueous solution closed to the atmosphere [2.107]. Reproduced with permission from Society of Mining, Metallurgy and Exploration, Inc.

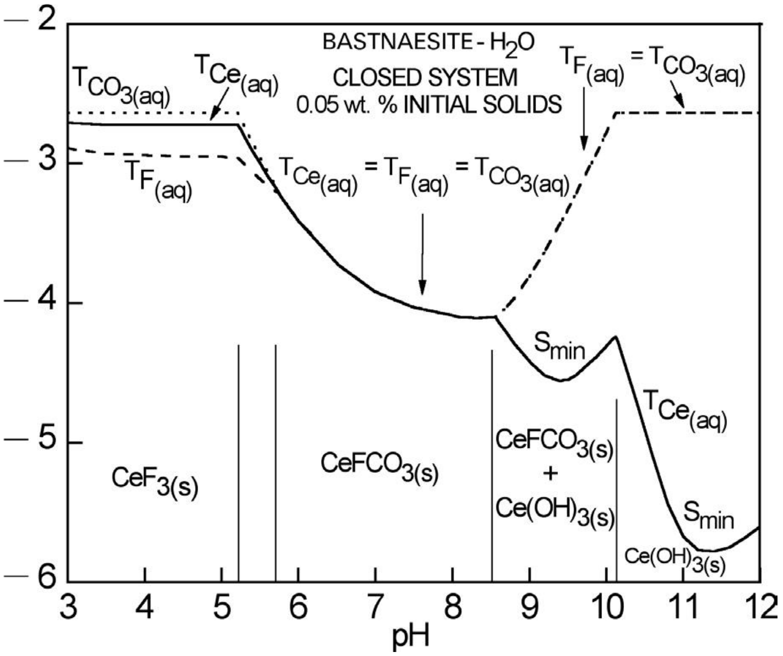

Figure 2.12 – The equilibrium concentration of total aqueous cerium, fluoride and carbonate species for 0.05 wt. % initial bastnäsite in aqueous solution closed to the atmosphere as a function of pH [2.107]. Reproduced with permission from Society of Mining, Metallurgy and Exploration, Inc.

2.5.1.3 Monazite

Several researchers have studied the surface complexation of monazite (in the form of $LaPO_4$) in solution [2.108]. It has been shown that two reactive sites could be formed when monazite is in solution: the phosphate sites ($>P(OH)_2$) and the lanthanum sites ($>La(OH)_2$).

The speciation of monazite in solution is shown in Figure 2.13 [2.109]. The diagram was constructed using CHEMIX [2.110], a program developed by the Commonwealth Scientific and Industrial Research Organization (CSIRO, Australia). The free energy data of monazite used in the calculation is readily available in the CHEMIX database [2.109]. The figure indicates that monazite in the form of $CePO_4$ could have dissolved cerium species, such as Ce^{3+}, $CeOH^{2+}$, $Ce(OH)_2^+$ and $Ce(OH)_4^-$ depending on the pH.

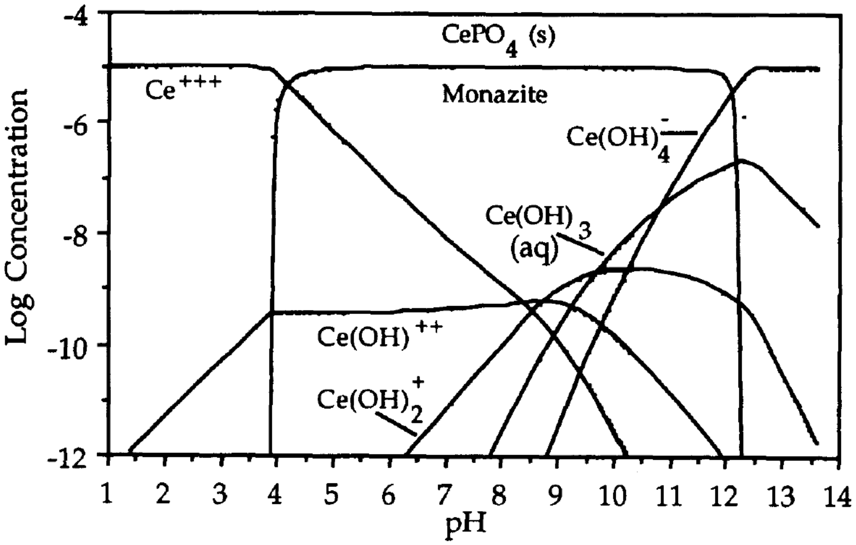

Figure 2.13 – Speciation diagram of monazite at 10^{-5} total solution concentration [2.109]. Reprinted with permission from Elsevier.

2.5.2 Electrokinetic properties

When a mineral particle is submerged in a liquid, it may be electrically charged in various ways [2.111, 2.112] depending on the nature of the particle and the medium. These can be ionization of surface groups, preferential dissolution of ions and ion adsorption to the surface [2.112]. When the particle is charged, ions of opposite charge will attach to the surface [2.113]. Ions in the solution are either classified as surface ions or potential-determining ions (PDI), indifferent and specifically adsorbed ions [2.114]. Surface ions or PDI are those ions responsible for the surface charge [2.113]. These ions define the potential difference between the solid and the liquid. Sometimes, they are part of the adsorbent (minerals being adsorbed on) or they are H^+ or OH^- in the case of most of the oxides. Indifferent ions adsorb due to Coulombic force where the mechanism of adsorption is based on electrostatic forces, such that particles with opposite charges will attract each other. Specifically adsorbed ions adsorb not only because of the Coulombic force but also with other forces such as Van der Waals, π-electron exchange and complexation [2.114]. When these ions adsorb onto the surface of the mineral, they cause an unequal distribution of ions in the solution. This unequal distribution of ions leads to the formation of the electrical double layer (EDL). Electrical double layer contains the stationary layer (the Stern layer) and the diffuse layer as shown in Figure 2.14. The unequal distribution of charges around the particle forms an electrical potential as a function of distance [2.114]. The surface potential (surface charge) is denoted by ψ^0 while the zeta potential (the potential at the shear plane) is denoted by ζ. The point of zero charge (PZC) is the pH at which the average surface charge density at the surface is zero [2.114]. This is commonly measured by titration method [2.114]. The isoelectric point (IEP), on the other hand, is the pH at which the zeta potential is zero (Lyklema, 1991). This is normally determined by measuring the electrokinetic properties of the particles [2.113, 2.114] which will be discussed in Section 2.5.4.1.

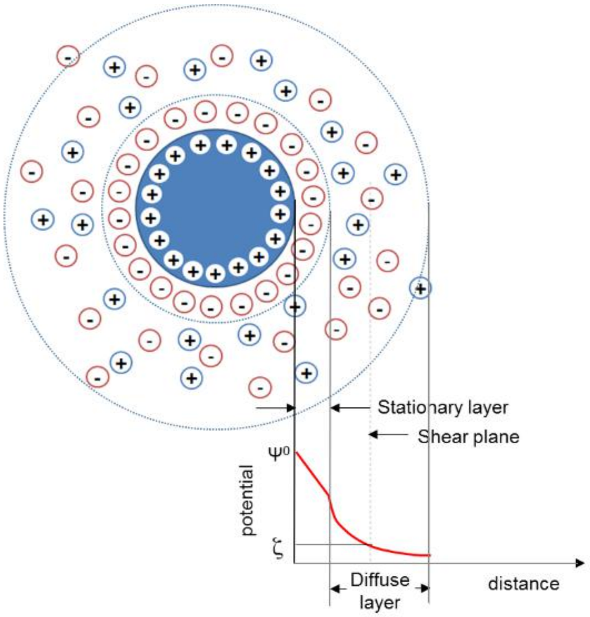

Figure 2.14 – Gouy-Chapman-Stern model of the electrical double layer.

Salt-type minerals, such as monazite and xenotime, are expected to have their lattice ions to be the potential-determining ions [2.79, 2.115, 2.116]. It was observed that for salt-type minerals, there is a wide discrepancy in measured IEP values, as shown in Tables 2.4 and 2.5. These may be accounted for by several factors such as the "compositional differences" of the minerals used, presence of impurities, the variation in sample preparation and most importantly, the slight solubility of the minerals in aqueous solution [2.79].

Table 2.4 – Summary of isoelectric point of monazite-*Ce*

IEP	References
5.5	Viswanathan *et al.* [2.117]
5.5	Abeidu [2.118]
1.1 - 3.2, 6.1, 6.4, 9	Huout *et al.* [2.81]
3.4	Harada *et al.* [2.119]
3.1, 5.1, 5.5, 6.8	Luo and Chen [2.120]
5.0	Pavez and Peres [2.121]
5.2	Cheng *et al.* [2.109]
5.3	Pavez *et al.* [2.122]
4.7	Ren *et al.* [2.123]
7.0	Cheng [2.124]

Table 2.5 – Summary of isoelectric point of bastnäsite-*Ce*

IEP	Origin	References
9.5	Synthesis	Pradip [2.115]
5.3	Mountain Pass	Smith and Steiner [2.125]
6.8	Mountain Pass	Huout *et al.* [2.81]
7.2	Mountain Pass	Huout *et al.* [2.81]
4.6	Mountain Pass	Smith and Shonnard [2.97]
7.0	Bayan Obo	Luo and Chen [2.120]
4.9	Pocos de Caldas	Pavez *et al.* [2.122]
7.8	Haoniuping mine	Ren *et al.* [2.123]
8.0	Maoniuping mine	Ren *et al.* [2.126]

2.5.3 Collector adsorption mechanism

The mechanisms of collector adsorption are physical adsorption and chemisorption [2.76]. If the adsorption involves forces such as electrostatic (coulombic forces) or hydrophobic bonding, it is considered physical adsorption; however, if it involves covalent bonding, then it is chemisorption [2.98]. Fuerstenau and Herrera-Urbina [2.127] summarized the reactions involved in flotation of sparingly soluble salt minerals as follows, and some examples of flotation system are also given:

a. Physical adsorption of collector ions in the double layer: Somasundaran [2.128] reported that adsorption of oleate on calcite below the IEP involves physical adsorption.
b. Chemisorption in the Stern plane: Chemisorption was defined by Chander and Fuerstenau [2.129] as the "interaction with the surface without movement of metal atoms from their lattice sites". Based from the study conducted by Hu and Xu [2.130], it appeared that adsorption of α-benzol amino benzyl phosphoric acid on fluorite, calcite and scheelite is due to chemisorption.
c. Surface formation of a more insoluble compound: Amankonah and Somasundaran [2.131] observed the formation of calcite on apatite or apatite on calcite surface.
d. Chemisorption on hydrolyzed metal sites: Pradip and Fuerstenau [2.116] explained that one possible mechanism of hydroxamate adsorption onto barite, calcite and bastnäsite involves formation of cation hydroxyl complexes on the surface of the minerals. These complexes provide sites for hydroxamate adsorption.
e. Surface reaction, dissolution of mineral and precipitation of metal-collector salt
f. Autoactivation through surface dissolution, cation hydrolysis, and readsorption of hydrolyzed ion

Other than chemisorption, Chander and Fuerstenau [2.129] also described surface precipitation and bulk precipitation as possible metal ion – reagent reactions. Surface precipitation happens when the reagent interacts with the surface "through movement of metal atoms from their lattice sites", while bulk precipitation of the metal reagent salts occurs when the dissolved lattice ions forms an insoluble compound with the collector away from the surface of the mineral [2.129]. For salt-type minerals, these two reactions may be more common than chemisorption [2.116].

The knowledge of the zeta potential and IEP will bring about further understanding of the mechanisms of collector adsorption. For example, Cheng *et al.* [2.109] explained the adsorption mechanism of sodium oleate onto the surface of monazite and xenotime minerals using the concept of IEP and the obtained flotation recoveries. The adsorption mechanisms of the typical collectors used in RE mineral flotation will be discussed in the following sections.

2.5.3.1 Carboxylates

Sodium oleate, a carboxylate, is a widely used flotation collector. Chemical equilibria for oleate solutions is given below [2.132]. Species distribution diagram as a function of pH is presented in Figure 2.15, where the total oleate concentration is 3 × 10^{-5} M. In the figure, it is presented that: (1) the maximum in the activity of acid soap ($RCOOH{\cdot}RCOO^-$) occurs at pH around 7.8; (2) precipitation of neutral oleic acid (RCOOH) occurs at pH 7.8; and (3) activities of the ionic monomer and the ionic dimer increase up to pH 7.8 and remain constant above this value [2.132].

$$RCOOH_{(l)} \rightleftharpoons RCOOH_{(aq)} \qquad pK_{sol} = 7.6 \tag{2.45}$$

$$RCOOH \rightleftharpoons RCOOH^- + H^+ \qquad pKa = 4.95 \tag{2.46}$$

$$2\ RCOO^- \rightleftharpoons (RCOO)_2^{2-} \qquad pK_D = -4.0 \tag{2.47}$$

$$RCOO^- + RCOOH \rightleftharpoons (RCOO)_2H^- \qquad pK_{AD} = -4.95 \tag{2.48}$$

$$Na^+ + (RCOO)_2H^- \rightleftharpoons (RCOO)_2HNa \qquad pK_{SAS} = -9.35 \tag{2.49}$$

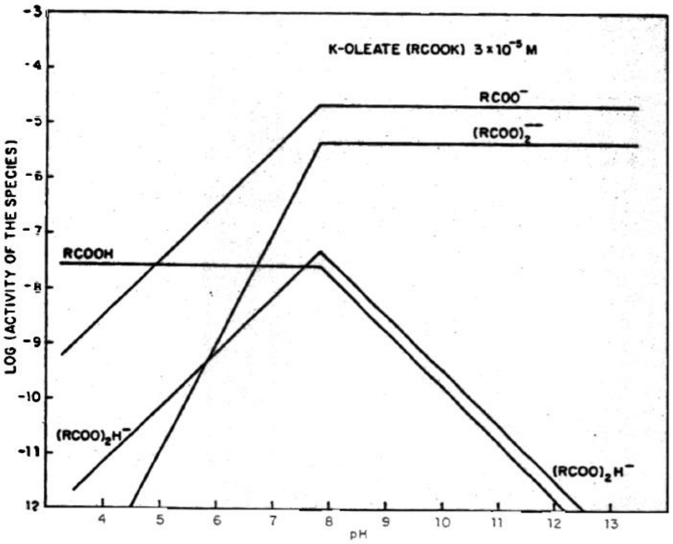

Figure 2.15 – Oleate species distribution diagram as a function of pH (total oleate concentration = 3 × 10^{-5} M) [2.132]. Reproduced with permission of Springer US.

For carbonate minerals such as dolomite, it has been suggested that the mechanism of adsorption of the collector at pH below the mineral's IEP is by hydrogen bonding between the oleic acid molecules (RCOOH) and the H_2CO_3 sites at the mineral surface [2.133]. It could also be a "physical coating of the oleic acid" on the mineral surface [2.134]. At pH above the mineral's IEP, the suggested mechanism of adsorption is chemisorption [2.135] through oleate interaction with the surface forming CO_3^{2-} ions and $Me(OOCR)_2$ (Me being the metal cation).

In the case of monazite, Cheng *et al.* [2.109] found that the maximum recovery (pH 8.5 - 9) correlates well with the maximum concentration of $La(OH)^{2+}$ and $Ce(OH)^{2+}$. Since their obtained pzc of monazite is around 5.3, the monazite surface is negatively charged at the pH where maximum recovery occurs. As such, it has been suggested that at this pH range, dissociated oleate ($RCOO^-$) interacts with monazite through chemisorption Cheng *et al.* [2.109]. Further discussion on the mineral - sodium oleate interaction will be presented in Chapters 3 and 6.

2.5.3.2 Hydroxamates

Hydroxamic acids occur in two tautomeric forms [2.136]:

(1) Hydroxyamide (2) Hydroxyoxime,

Hydroxyamide has only one replaceable hydrogen atom, while hydroxyoxime has two replaceable oxygen. Infrared (IR) and ultraviolet (UV) spectral studies have shown that the tautomer that forms metal complexes is the hydroxyamide and not the hydroxyoxime [2.137]. The complexes are formed by the replacement of the hydrogen atom with a metal ion and the formation of a coordinate bond with the carbonyl oxygen as shown below [2.83].

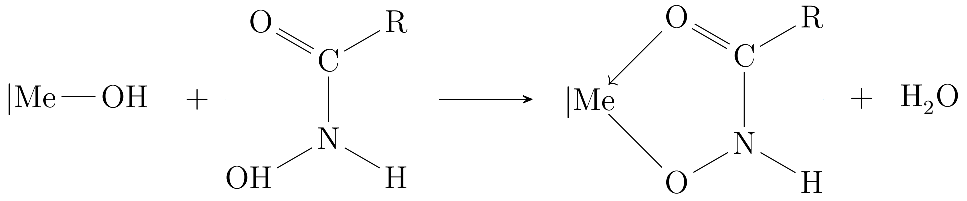

The strength of the complexes formed by hydroxamic acids depend upon the metal cation position in the periodic table. The weakest are those with alkaline-earth metal, while those with transition elements (Nb, Ti, V, Mn, Zr, Hf, Ta) have more stability. Strong complexes are also formed with RE elements and aluminum due to their high positive charge [2.83, 2.116]. Due to this difference in the strength of metal complexes, hydroxamates have better selectivity for RE minerals than gangue which has alkaline-earth metal [2.116].

It has been reported that most of the hydroxamic acids dissociate between pH 7 - 9 (acid dissociation constant or pKa) [2.137]. Fuerstenau and Pradip [2.83] mentioned that since most of the flotation with octyl hydroxamate (pKa = 9.55) occurs at pH below 9.55, it was suggested that the undissociated form of hydroxamic acid is the active collector species for those systems. It has been suggested that hydroxamic acid adsorbs onto the mineral surface in multilayer [2.83], as such, at higher pH (pH > pKa), hydroxamate ions will experience electrostatic repulsion leading to a decrease in flotation [2.138]. The mechanism of mineral interaction with chelating agent such as hydroxamates, which were proposed by Fuerstenau and Pradip [2.139] are schematically presented in Figure 2.16. In the following schematics, HA could represent the undissociated hydroxamic acid, while A^- could represent the dissociated form of the hydroxamic acid.

Chemisorption (Surface chelation)

$$\mathrm{M^{+n}| + A^- \longrightarrow M^{+n}|A^-}$$
$$\mathrm{M^{+n}| + HA \longrightarrow M^{+n}|A^- + H^+}$$

Bulk chelation

$$\mathrm{M^{+n} + xA^- \longrightarrow [MA_x]^{(n-x)+}}$$
$$\mathrm{M^{+n} + nA^- \longrightarrow [MA_n]}$$

Adsorption with surface chelation / reaction

$$\mathrm{M^{+n}| + A^- \longrightarrow \square|[MA]^{(n-1)+}}$$
$$\mathrm{M^{+n}| + HA \longrightarrow \square|[MA]^{(n-1)+} + H^+}$$
$$\mathrm{M^{+n}| + xOH^- \longrightarrow \square|[M(OH)_x]^{(n-x)+}}$$
$$\mathrm{M^{+n}| + xHCO_3^- \longrightarrow \square|[M(HCO_3)_x]^{(n-x)+}}$$

Surface chelation / reaction through adsorbed hydroxy complexes

$$\mathrm{\square|[M(OH)_x]^{(n-x)+} + yA^- \longrightarrow \square|[MA_y]^{(n-y)+} + xOH^-}$$
$$\mathrm{\square|[M(OH)_x]^{(n-x)+} + yHA \longrightarrow \square|[MA_y]^{(n-y)+} + xH_2O + (y-x)H^+}$$
$$\mathrm{\square|[M(OH)_x]^{(n-x)+} + (n-x)OH^- \longrightarrow \square|[M(OH)_n]}$$

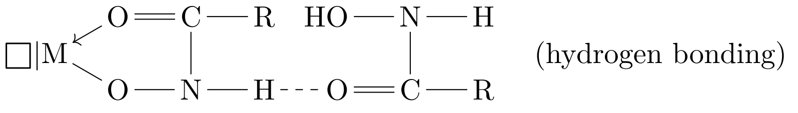
(hydrogen bonding)

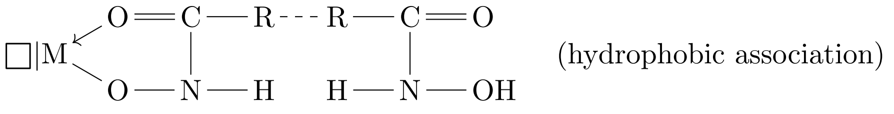
(hydrophobic association)

Figure 2.16 – The mechanism of mineral interaction with chelating agent [2.139]

2.5.3.3 Organic phosphoric acid

Organic phosphoric acid was used to successfully float RE minerals [2.84], however, literature regarding its adsorption mechanism is limited. In this section, the adsorption mechanism of organic phosphoric acid and some organophosphorus will be discussed.

Almost all organic phosphoric acids are moderately strong acids; they mostly dissociate at acidic pH [2.140]. Hu and Xu [2.130] studied the interaction of amino phosphoric acid with calcium-containing minerals. The dissociation constants of the collector they investigated was 6.68 (pKa_1) and 9.86 (pKa_2). Spectroscopic studies indicated that the collector forms a complex through coordinate bond between -P=O (collector) and Ca (on the mineral surface); and binding of -P-O (collector) with Ca (on the mineral surface) forming a ring closure. It also seemed that hydrogen bond occurs between the collector and the mineral (see Figure 2.17). Due to the pKa values found and the flotation behavior, Hu and Xu [2.130] suggested that the monovalent anion form of the collector is the main binding species.

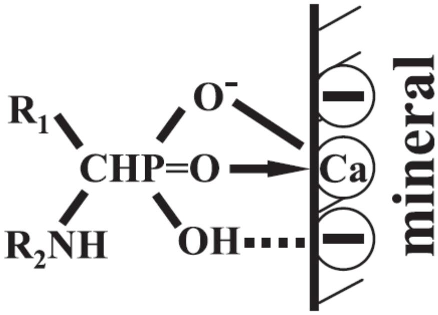

Figure 2.17 – Schematic diagram of interaction between amphoteric collector and calcium mineral (covalent bonds are shown in solid lines, coordination bond in arrow and hydrogen bonding in dotted line) [2.130]. Reprinted with permission from Elsevier.

Several studies suggested different adsorption mechanism of styrene phosphonic acid (SPA) on cassiterite surface. Fourier transform infrared spectroscopy (FTIR) [2.141] and molecular modeling [2.142] were used to identify which of the surface complexes (monodentate, bidentate, binuclear or bridging) are formed on cassiterite surface. Kuys and Roberts [2.141] suggested based from their FTIR studies that monoanion of SPA adsorbed on cassiterite hydroxy species through a slow ion exchange and chemisorption process, followed by a rapid bidentate complex (rather than binuclear) as shown in Figure 2.18. However, Gong *et al.* [2.142] found through molecular modeling that binuclear complex is the final structure (as it is the most stable structure) of the SPA – cassiterite complex (Figure 2.19), and that bidentate complex could just be an intermediate product during the adsorption process.

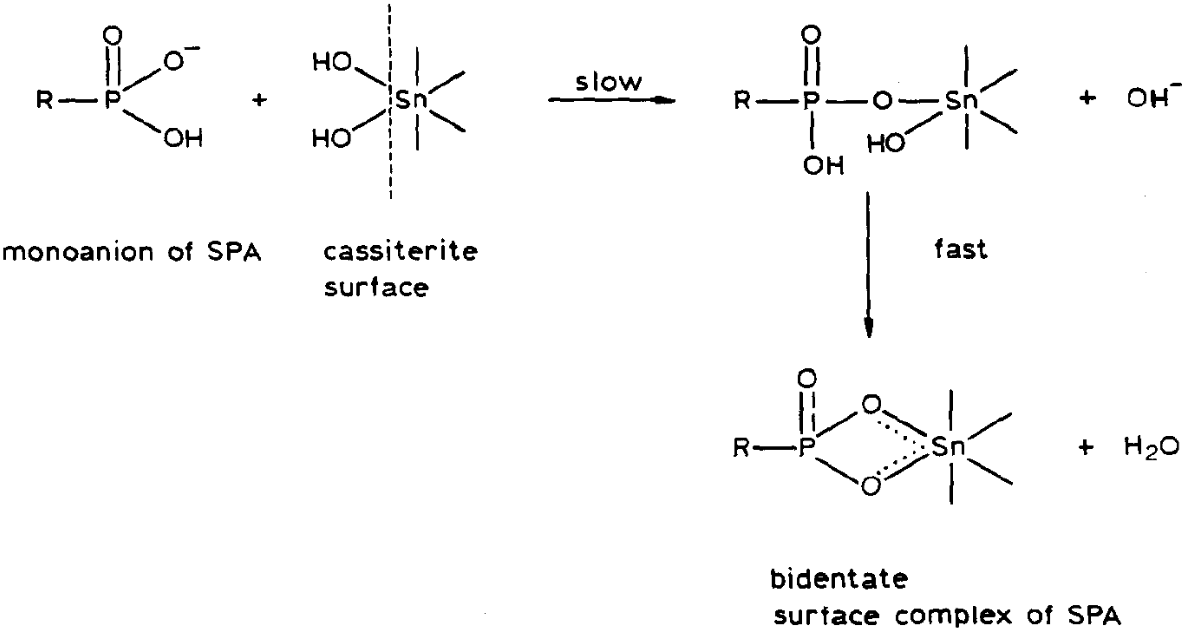

Figure 2.18 – The proposed step-by-step process during the adsorption of SPA on cassiterite surface [2.141]. Reprinted with permission from Elsevier.

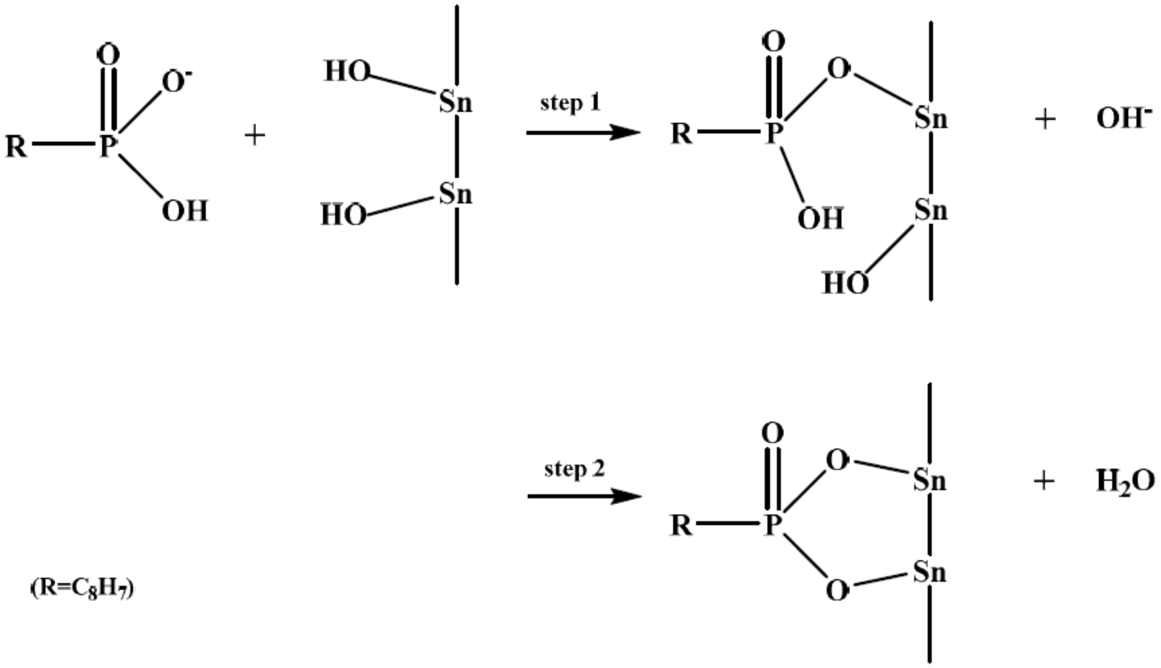

Figure 2.19 – The proposed adsorption mechanism of SPA on cassiterite [2.142]. Reprinted with permission from Elsevier.

2.5.4 Electrophoresis and surface characterization techniques

To understand the adsorption mechanism of the surfactants (*e.g.*, collectors or depressants) on the mineral surface, techniques involving electrokinetic potential measurement and surface characterization are necessary. In this section, the techniques employed in this work will be discussed.

2.5.4.1 Electrophoretic zeta potential measurements

As discussed in Section 2.5.2, minerals may become electrically charged when they are placed in water. For sparingly soluble in water, the surface charge is due to surface formation and hydrolysis of lattice ions which is a consequence of hydration and dissolution of lattice ions [2.106]. These ions in the solution will reorient in the solution to electroneuralize the mineral's surface charge, forming the electrical double layer (EDL). The unequal distribution of charges around the particle forms an electrical potential as a function of distance [2.114]. The surface potential (surface charge), ψ^0, can be estimated through zeta potential (the potential at the shear plane), ζ, measurement. It must be noted that zeta potential cannot be determined directly, but through measuring the electrokinetic properties of the particles [2.113, 2.114].

Electrokinetic effects are phenomena that are observed when one of the phases (solid or liquid) is caused to move tangentially past the second phase [2.111]. The four distinct electrokinetic phenomena are: electrophoresis, electro-osmosis, streaming potential and sedimentation potential. It has been mentioned that "all electrokinetic effects originate from two generic phenomena: electro-osmotic flow and convective electric surface current within EDL" [2.143]. Smoluchowski derived a general equation for nonconducting solids for these generic phenomena, which could be extended to other specific electrokinetic effects. The Smoluchowski theory is valid for any shape of a particle or pores inside a solid, if the (local) curvature radius a largely exceeds the Debye length κ^{-1}($\kappa a \gg$1), which can be expressed in Equation 2.50, where

$$\kappa = \left\{ \frac{\sum_{i=1}^{N} e^2 z_i^2 n_i}{\varepsilon_{rs}\varepsilon_0 kT} \right\}^{1/2} \tag{2.50}$$

e is the elementary charge, z_i, n_i is the charge number and number of concentration of ion I (the solution contains N ionic species), ε_{rs} is the relative permittivity of the electrolyte solution, ε_0 is the electric permittivity of vacuum, k is the Boltzmann constant and T the thermodynamic temperature. The four electrokinetic phenomena are being taken advantage to measure the zeta potential, but among them, the utmost interest remains in electrophoresis because it can be utilised for materials throughout the whole colloid size range [2.111].

Since the EDL is assumed to be very thin compared to the particle radius, hydrodynamic and electric field are parallel for a large κa. For electrophoresis, where the "movement of a charged surface relative to stationary liquid by an applied electric field E" [2.112] as shown in Figure 2.20, it can be expressed that the particle velocity ν_e with respect to the medium at rest is:

$$\nu_e = \frac{\varepsilon_{rs}\varepsilon_0\zeta}{\eta}E \tag{2.51}$$

where η is the dynamic viscosity of the liquid, and the electrophoretic mobility, u_e, is

$$u_e = \frac{\varepsilon_{rs}\varepsilon_0\zeta}{\eta} \tag{2.52}$$

It can be seen from the equation that zeta potential is directly proportional to the electrophoretic mobility u_e.

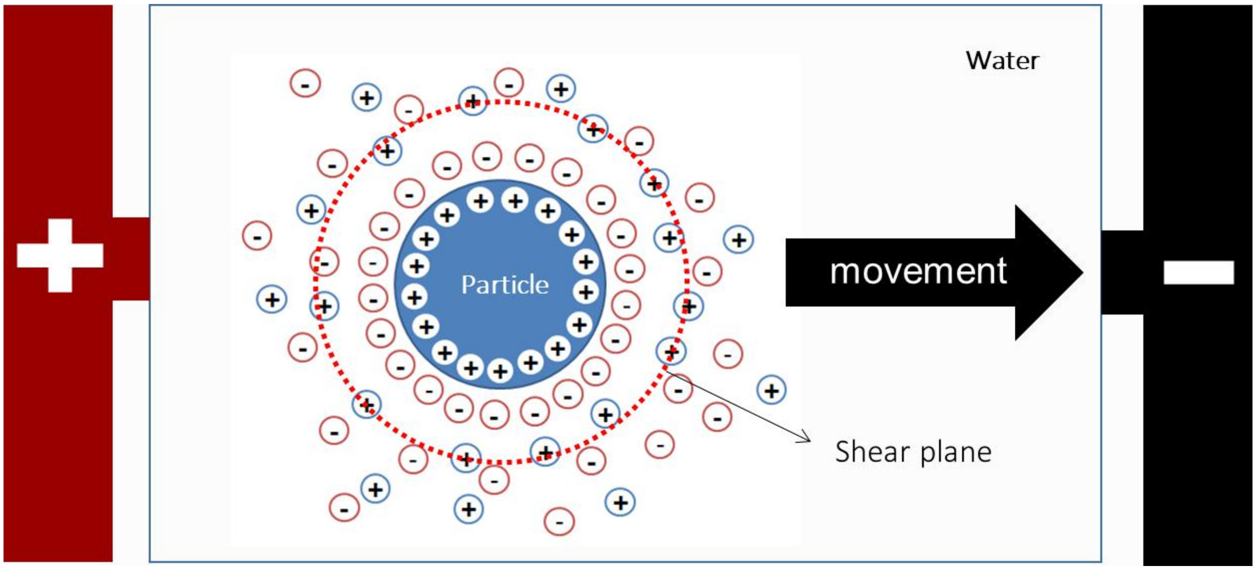

Figure 2.20 – Illustration of a charged particle moving in aqueous solution under an applied electric field.

In this work, electrophoretic light scattering (ELS) technique was used to determine the zeta potential by measuring the electrophoretic mobility. This technique is based on the combination of electrophoresis and laser Doppler shift spectroscopy [2.144]. In a typical light scattering experiment (Figure 2.21), a laser light with incident vector k_0 is scattered by particles at all angles. The photodetector (positioned at an angle with respect to the incident light) collects some of the scattered light with wave vector k_s. The phase of the scattered light radiated from its surface is defined by the position of the particles, while the intensity correlates with the sum of all the scattered light incident. Since the particles experience Brownian movement and directed movement (electrophoresis), the particles constantly shift their position and the phases of the light scattering waves change with time resulting to intensity fluctuations. The Doppler model can be used to interpret the intensity fluctuations. For a monochromatic laser light that can be characterized by a single frequency, w_0 ($\sim$1014 Hz), the scattered light will have a frequency that is shifted relative to w_0, which is proportional to the velocity of the particle. The frequency shift (referred as Doppler shift) W_D is given by:

$$W_D = K \times V/2\pi \tag{2.53}$$

where the particle's velocity vector is V, the scattering vector K is equal to $|k_0$ - $k_s|$, and the magnitude of K is $(4\pi n/\lambda)\ \sin(\theta/2)$. n is the refractive index of the solution, λ is the vacuum wavelength of the incident laser light and θ is the scattering angle. The Doppler shift frequency W_D of the scattered light due to an application of electric field to a cell suspension can be related to electrophoretic mobility u_e through Equations 2.54 and 2.55, below:

$$W_D = (2nu_eE/\lambda)\ \sin(\theta/2)\ \cos(\theta/2) \tag{2.54}$$

$$= (2nu_eE/\lambda)\ \sin\ \theta \tag{2.55}$$

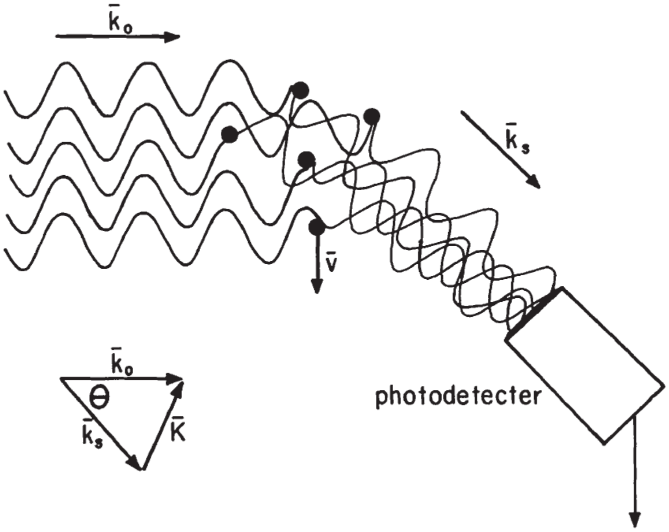

Figure 2.21 – Schematic of a typical laser light scattering experiment. The incident light is given by wave vector k_0, the scattered light by k_s, the scattering wave vector by K and the scattering angle θ [2.144]. Reprinted with permission from Springer Nature.

"To measure the Doppler frequencies, the scattered light is mixed with a portion of the incident reference beam at the surface of a photodetector located at a predetermined angle. The photodetector is a square-law device; *i.e.,* the photosensitive element in the photodetector detects light intensity which is proportional to the square of the sum of the electric fields illuminating the surface. Therefore, the output signal from the photo detector contains information about the modulation frequencies (or intensity fluctuations described earlier) which correspond to the rapidly oscillating optical field" [2.144].

2.5.4.2 Attenuated total reflectance Fourier-transform infrared spectroscopy

The attenuated total reflectance (ATR) technique allows quick sampling while Fourier-transform infrared (FTIR) technique allows fast and stable collection of IR spectra [2.145].

Basic principles of infrared spectroscopy

Infrared (IR) spectroscopy is a characterization method which deals with the interaction between molecules and infrared radiation. IR is an electromagnetic radiation with longer wavelengths than those of visible light (see Figure 2.22). IR spectra are obtained by passing an IR radiation through a sample, and determining the fraction of the adsorbed incident radiation [2.146]. The amount of adsorbed radiation correlates to molecular vibrations [2.147]. Molecular vibrations associated with infrared spectroscopy can be represented in terms of quantized discrete energy levels ($E_0, E_1, E_2,$ *etc.*). Each atom in a molecule or a system must exist in one of these levels, thus in a molecule there will be a distribution of the atoms in various energy levels. A quantum of energy (or photon) is either emitted or absorbed, when a molecule is radiated, which can be represented by the following:

$$\Delta E = h\nu \tag{2.56}$$

where h is the Planck constant ($h = 6.626 \times 10^{-34}$ J s) and ν is the frequency. Thus, the frequency of emission or absorption for a transition between energy states E_0 and E_1 can be represented as:

$$\nu = (E_1 - E_0)/h \tag{2.57}$$

where ν can be related to the wave number, $\bar{\nu}$ through the equation $\bar{\nu} = \nu/c$ (c = velocity of light = 3×10^8 m s^{-1}). The frequency (which can be represented as the wave number) at which molecular bonds vibrate is distinctive of the type of bonds, hence functional groups [2.146].

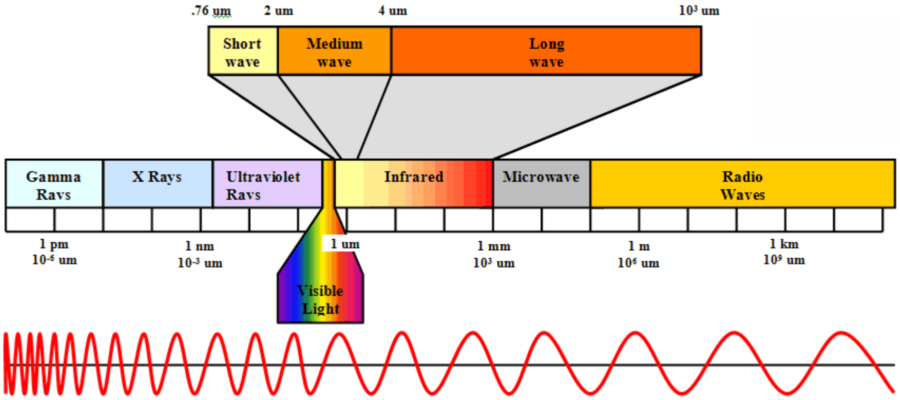

Figure 2.22 – Regions of the electromagnetic spectrum [2.148].

In order for a molecule to absorb infrared radiations, there should be a net change in the dipole moment during the vibration. It should be noted that a molecule can only absorb radiation when its fundamental mode of vibration is of the same frequency as the incoming IR radiation. For groups/molecules with polar bonds (permanent dipole), strong IR absorptions will be observed. In the mid-infrared region (4,000 - 1,000 cm^{-1}), vibrations involving bond-length changes (stretching vibrations) and involving bond angles changes (δ - in plane bending vibrations, π - out of plane bending vibrations) could be observed. The system could be modeled by a simple harmonic oscillator [2.149], such that the fundamental vibration frequency follows Hooke's law which can be expressed as:

$$\bar{\nu} = \frac{1}{2\pi c}\sqrt{\frac{k}{\mu}} \tag{2.58}$$

where $\bar{\nu}$ is the fundamental vibration frequency (wave number), k is the force constant, and μ the reduced mass, $m_1 m_2/(m_1 + m_2)$, where m_1 and m_2 are the component masses for the chemical bond under consideration [2.146].

Attenuated total reflectance

The ATR technique utilizes the phenomenon of internal reflection [2.150]. The refraction of light passing through a sample can be expressed by Snell's Law where it states that the ratio of the refractive indeces (n_1, n_2) of the medium is equal to the ratio of the sines of the angle of transmitted (θ_t) and incident light (θ_i) [2.145] as shown in Equation 2.59.

$$\frac{n_1}{n_2} = \frac{\sin\theta_t}{\sin\theta_i} \tag{2.59}$$

Internal reflection (attenuated total reflection) can occur when the angle of the refracted beam (θ_t) is larger than the angle of incidence (θ_i). This can be controlled by using a medium 2 with refractive index smaller than that of medium 1 [2.145]. Piketech [2.151] explained that when an IR beam is directed into a crystal (*e.g.,* ZnSe or diamond) with relatively higher refractive index, the internally reflected IR beam creates an evanescent wave (see Figure 2.23). Some of the energy of the evanescent wave is absorbed by the sample and the reflected IR beam is return to the detector.

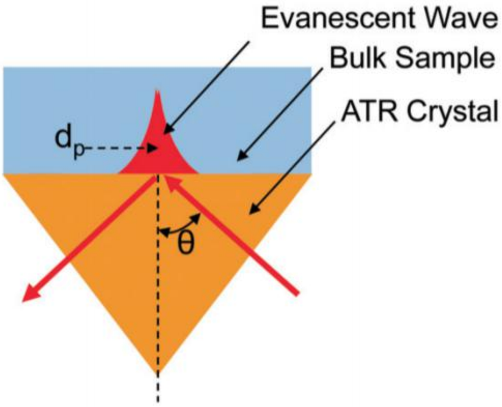

Figure 2.23 – Graphical representation of a single reflection ATR [2.151].

Fourier-transform infrared spectroscopy

In this study, Fourier-transform infrared (FTIR) type spectrometer was employed, which measures interferograms with an interferometer (optical device) based on Michelson interferometer shown in Figure 2.24. Markovich and Pidgeon [2.152] described that the process in the Michelson interferometer during an infrared scan involves the following steps in sequence: (1) the beam splitter divides the light from the IR source in two beams, (2) the movable mirror changes the path of one of the beam, (3) the two beams are recombined to create optical interference, and (4) the IR light is passed through the sample for single-beam spectrum. The optical path difference for the moving mirror (with displacement x) can be expressed as $|2(\mathrm{OM} - \mathrm{OF})|$, also referred to as optical retardation δ.

As the mirror moves through a cycle, the high intensity incident IR beam is regulated into a beam of varying intensity. Thus, the output of the interferometer is a single-beam of light with oscillating intensity as shown in Figure 2.25 which is plotted against mirror movement x or $I(\delta)$ as a function of optical retardation δ. Modern FTIR spectrometers have mirrors moving at a constant velocity with signal intensity $I(\delta)$ oscillating during each $1/2\lambda$ of optical retardation δ. The signal intensity can be expressed as

$$I(\delta) = 0.5I(\bar{\nu})\cos(2\pi\delta/\lambda) \tag{2.60}$$

$$= 0.5I(\bar{\nu})\cos(2\pi\bar{v}\delta) \tag{2.61}$$

where $I(\bar{\nu})$ is the IR source intensity, δ is the optical path difference $|2(\mathrm{OM} - \mathrm{OF})|$, λ is the wavelength of light and $1/\lambda$ is $\bar{\nu}$. Considering the instrument variables, optical retardation t seconds after zero path difference (ZPD, where OM = OF) equal to $2Vt$ and optical retardation being equal to twice the distance of mirror movement ($2x$), the equation can be rewritten as

$$I(t) = B(\bar{\nu})\cos(2\pi\bar{\nu}2Vt) \tag{2.62}$$

This equation is equivalent to the amplitude equation of a cosine wave,

$$A(t) = A_0\cos(2\pi ft) \tag{2.63}$$

where $A(t) = I(t)$, $A_0 = B(\bar{\nu})$, $f = 2V\bar{\nu}$ and V is the velocity of the movable mirror in centimeters.

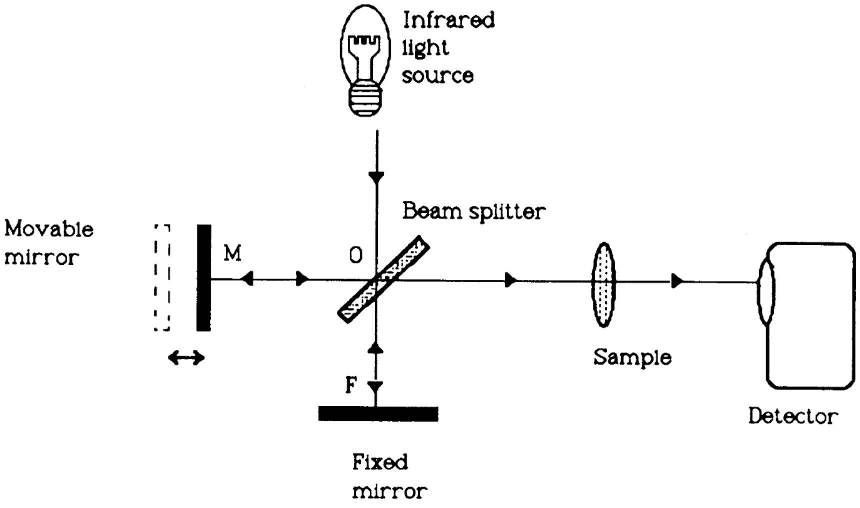

Figure 2.24 – Essential components of a Michelson interferometer [2.152]. Reprinted with permission from Springer Nature.

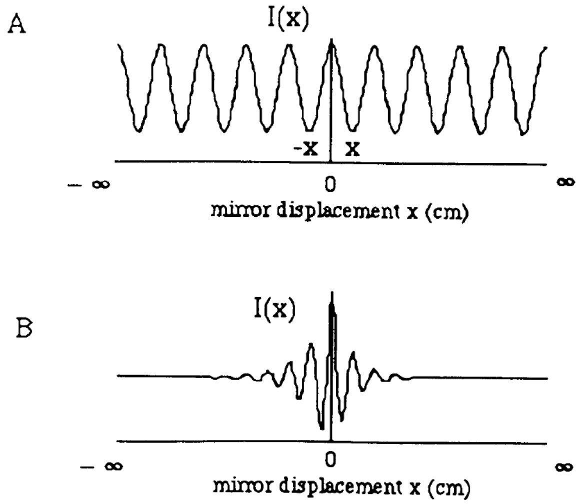

Figure 2.25 – Output from Michelson interferometer as a function of mirror displacement x from (a) monochromatic IR source and (b) polychromatic IR source [2.152]. Reprinted with permission from Springer Nature.

The $I(t)$ equation can also be express as a function of mirror displacement x as,

$$I(x) = \sum_{i=0}^{k} B(\bar{\nu}_i)\cos(2\pi\bar{\nu}_i x) \tag{2.64}$$

$$I(x) = \int_{\bar{\nu}=0}^{\bar{\nu}=\infty} B(\bar{\nu})\cos(2\pi\bar{\nu}x)d\bar{\nu} \text{ (integral form)} \tag{2.65}$$

However, since $I(x)$ is the experimentally measured variable, the desired spectral information $B(\bar{\nu})$ can be obtained from this interferogram using the cosine Fourier transform which can be expressed as:

$$B(\bar{\nu}) = \int_{x=-\infty}^{x=\infty} I(x)\cos(2\pi\bar{\nu}x)dx \tag{2.66}$$

for a finite mirror displacement. To consider a finite mirror displacement, a function $D_g(x)$ is introduced which has the value 1 when $|x| \leq |L|$ and 0 when $|x| > |L|$ (L being the maximum displacement). This allows the integral to maintain the limits that approach infinity which is a requirement for Fourier transformation. The single-beam (SB) spectrum that runs from 4000 to 400 cm^{-1} wave number ($\bar{\nu}$) can then be expressed as:

$$\text{SB} = \int_{\bar{\nu}=400}^{\bar{\nu}=4000} \int_{x=-\infty}^{x=\infty} I(x)D_g(x)\cos(2\pi\bar{\nu}x)d\bar{\nu}dx \tag{2.67}$$

which calculates the intensity of light $B(\bar{\nu})$, for $\bar{\nu}$ from 4000 to 400 cm^{-1} and x from $-L$ to

L cm. The percentage of transmitted light through the sample can be calculated by:

$$\%T(\bar{\nu}) = \frac{\mathrm{SB}_{\mathrm{sample}}}{\mathrm{SB}_{\mathrm{background}}} \times 100 \tag{2.68}$$

where $\mathrm{SB}_{\mathrm{sample}}$ is the single-beam spectrum obtained with the sample in the light path and $\mathrm{SB}_{\mathrm{background}}$ is the single-beam spectrum without the sample in the light path. The absorbance spectrum $A(\bar{\nu})$ can be derived from $\%T(\bar{\nu})$ by:

$$A(\bar{\nu}) = -\log\left(\frac{\%T(\bar{\nu})}{100}\right) \tag{2.69}$$

2.5.4.3 X-ray photoelectron spectroscopy (XPS)

X-ray photoelectron spectroscopy (XPS) is similar to IR spectroscopy, but as name implies, instead of an IR beam, XPS utilizes X-rays. When an X-ray with energy $h\nu$ hits a sample, it can eject a photoelectron from the sample's surface with a binding energy EB (see Figure 2.26). The kinetic energy of the ejected photoelectron can be expressed as

$$E_K = h\nu - E_B - \Phi_s \tag{2.70}$$

where E_K is the kinetic energy, and Φ_s is a small (almost constant) work-function term. Since the electronic binding energy is a unique property of an element, the measurement of photoelectron kinetic energy gives the information of the element/s. The changes in the chemical environment of an atom can also be detected in the measured E_K, reflecting the chemical information [2.153].

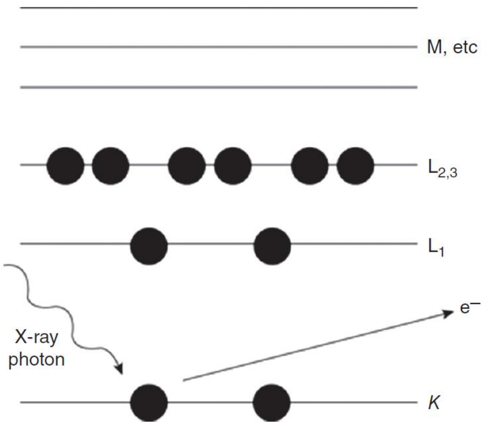

Figure 2.26 – Schematic diagram of X-ray photoelectron spectroscopy process [2.154]. Reproduced with permission. © John Wiley and Sons.

Typical configuration in an XPS spectrometer is shown in Figure 2.27. X-rays are produce from the Al anode by electron bombardment (electron kinetic energies are higher than produced X-ray energies). The monochromator focuses the produced X-rays to the sample; it also removes satellites and Bremsstrahlung background to achieve higher resolution. The ejected electrons from the sample will be confined in the energy analyzer [2.154].

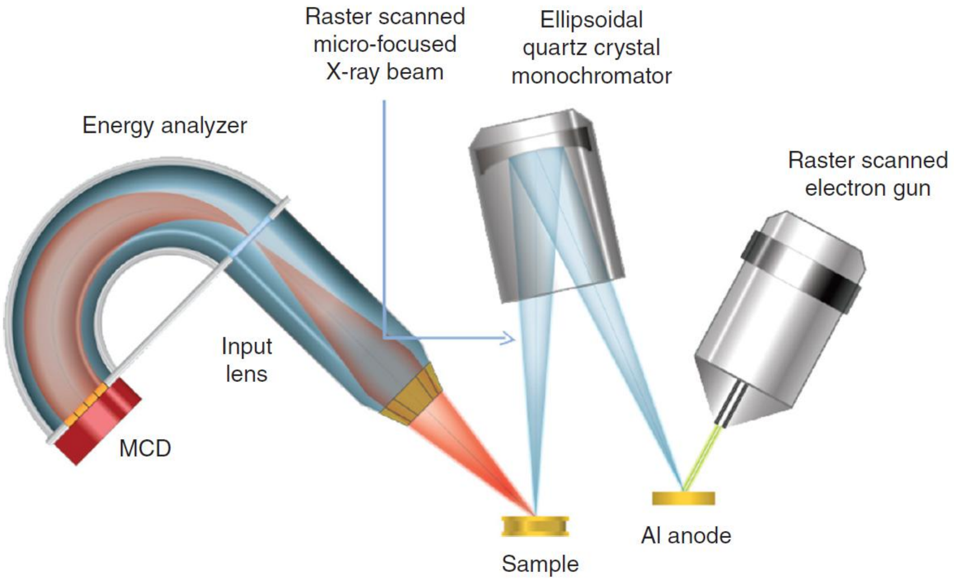

Figure 2.27 – Typical configuration in an XPS spectrometer [2.154]. Reproduced with permission. © Physical Electronics, Inc.

When electrons are injected following the equipotential surface R_0 inside the energy analyzer, in this case, a concentric hemispherical analyzer (CHA) as shown in Figure 2.28, with an acceptance angle $\Delta\alpha$ and a slit width w, then the relative energy resolution can be given by:

$$\frac{\Delta E}{E_K} = \left(\frac{w}{2R_0}\right) + \left(\frac{\delta\alpha^2}{4}\right) \tag{2.71}$$

where ΔE is the absolute energy resolution that is the full width at half-maximum intensity (FWHM) of a chosen peak and E_K is the kinetic energy at the peak position. The measured kinetic energy can be used to determine the binding energy E_B which is a "characteristic for each energy level and can be used to determine the element from which the electron originated" [2.154].

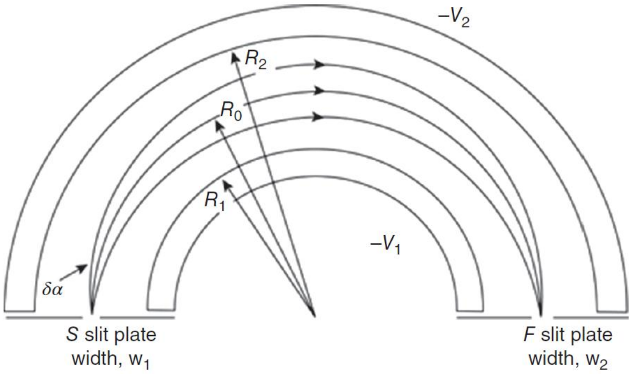

Figure 2.28 – Concentric hemispherical analyzer (energy analyzer) [2.154]. Reproduced with permission. © John Wiley and Sons.

2.5.5 Molecular modeling based on density functional theory

The previously discussed surface characterization methods which aid in elucidating the possible adsorption mechanism of the reagents (collector or depressant) on the mineral surface are rarely conducted in situ, as such the measurements obtained could have some discrepancies from actual scenario. In this regard, atomically-resolved computer simulations such as Density Functional Theory (DFT) simulations could strengthen the inferences from these experimental results. DFT simulations could contribute further understandings of the mineral flotation behavior in the presence of supernatant that cannot be directly achieved by experiments.

The basic definition of molecular modeling is "anything that requires the use of a computer to paint, describe, or evaluate any aspect of the properties of the structure of a molecule" [2.155]. Most methods available in molecular modeling are based on the energetics models of the system, and includes density functional. Density functional theory (DFT) states that the electron density $\rho(r)$, which can be expressed as a wave function, uniquely determines the total energy of the system. For the conceptual basis and mathematics of DFT, the readers are referred to Capelle [2.156]. In molecular modeling, the atoms in molecules are considered as rubber balls with varying sizes (atom sizes) connected by springs with varying length (or bond), which has a potential energy:

$$E_{\text{total}} = E_{\text{valence}} + E_{\text{crossterm}} + E_{\text{nonbond}} \tag{2.72}$$

expressed as the sum of the energy of the valence interactions (*e.g.*, bond-stretching, angle-bending, dihedral-angle torsion, inversion of out-of-plane interactions), cross-terms (bond or angle distortions) and nonbond interactions (*e.g.*, van der Waals and electrostatic) [2.157]. Any deviations from equilibrium resulting in an increase in total energy of the system are dealt with by various energy minimization techniques (*e.g.*, steepest descent, Newton - Raphson methods, conjugate gradient) to obtain the most stable configuration of the molecule. The readers are referred to Rai [2.157] for basic descriptions of these methods.

For solids, the basis of simulation is the Born model of solids, which states that the total interaction between the atoms in a crystal yields the lattice energy of the crystal. The lattice energy is given by:

$$U(r_{ij}) = \sum_{ij}^{/} \frac{q_i q_j}{r_{ij}} + \sum_{ij}^{/} \Phi_{ij}(r_{ij}) + \sum_{ijk} \Phi_{ijk}(r_{ijk}) + ... \tag{2.73}$$

where the first term corresponds to long range electrostatic interactions, the second and the third terms correspond to short-range two body and many-body interactions, respectively. The slash above the summation indicate that the interaction where $i = j$ is not considered. This equation is sufficient to describe an ionic solid, however for systems which involves covalent bonding, additional terms are required to evaluate the total interaction energy (lattice energy) [2.157].

To calculate surface and bulk block energies, static lattice energy minimizations are used. “The crystal is regarded as a series of charged planes parallel to the surface and periodic in two dimensions” [2.157]. For energy minimization, the ions (surface ions) of Region I are relaxed, while the ions (bulk ions) in Region II are fixed (see Figure 2.29). The block energy E can be expressed as $E_I + E_{II}$, where E_I and E_{II} is the total energy of the ions in Region I and Region II, respectively. The energy of the surface block E_S and bulk block E_B, which can be expressed as interaction energies, are required to calculate the surface energy of the crystal face.

$$E_S = E'_{I-II} + E'_{I-I} + E'_{II-I} + E'_{II-II} \tag{2.74}$$

$$E_B = E''_{I-II} + E''_{I-I} + E''_{II-I} + E''_{II-II} \tag{2.75}$$

The term E'_{I-I} is the interaction energy between the ions in Region I, and so on. The surface energy of the crystal faces can be then represented as:

$$\lambda = \frac{(E_S - E_B)}{\text{AREA}} \tag{2.76}$$

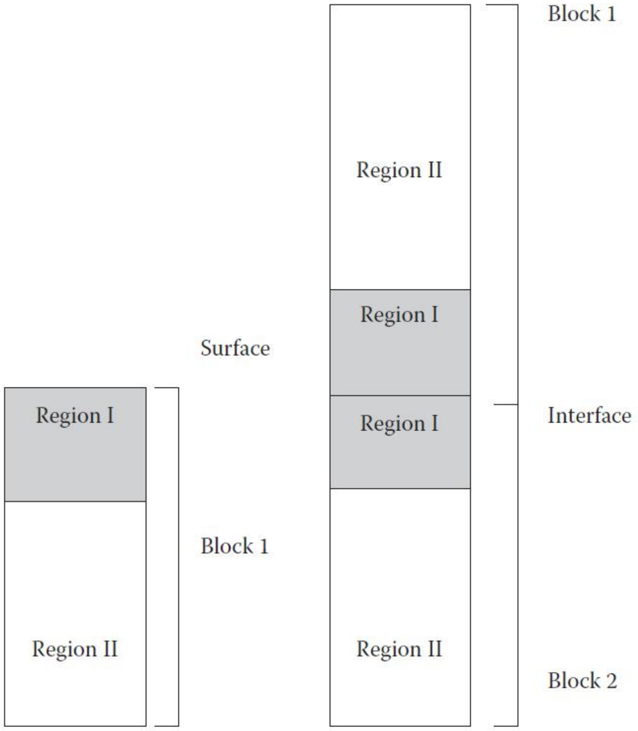

Figure 2.29 – Schematic representation of the two-region approach used for (a) surfaces and (b) interfaces [2.157]. Reprinted with permission from Taylor and Francis.

The adsorption energy (*e.g.*, collector on a mineral surface) can be calculated by considering the energy of the pure surface (U_s), the isolated adsorbed molecule (U_mol) and the energy of the covered surface (U_def) as shown in Equation 2.77. In Chapters 5 and 6, the adsorption energy is also referred to as interaction energy.

$$U_\mathrm{ads} = U_\mathrm{def} - (U_\mathrm{s} + U_\mathrm{mol}) \tag{2.77}$$

For further understanding on the utilisation of molecular modeling in mineral surface reactions in flotation, the readers are referred to the works of Rai [2.157], Rai and Pradip [2.158] and Pradip and Rai [2.159].

2.6 Rare earth processing

Physical separation methods such as gravity, magnetic and electrostatic separation are commonly employed to recover RE minerals from placer deposits, while flotation is utilized for recovery of RE minerals from igneous and hydrothermal deposits [2.160].

2.6.1 Monazite

Gravity separation is the most commonly used concentration method in beneficiation of monazite from mineral sands [2.14]. However, it is unusual that efficient separation will be achieved by just using gravity separation techniques. A study conducted at the Nuclear Fuel Cycle Research School in Tehran using a Humphrey spiral, upgraded a 2650 ppm Iranian monazite ore to 6050 ppm with 57% recovery [2.161]. This improvement in grade is relatively low. Typically, for a low grade ore (heavy mineral content <20%), bulk concentration of the heavy minerals is necessary to obtain a more concentrated product [2.81]. This is then treated using another process such as magnetic separation, electromagnetic separation and flotation to concentrate the desired minerals [2.14]. A combination of magnetic and gravity separation was able to successfully recover monazite from Manavalakurchi beach sand in India with about 97% recovery and 90% distribution [2.162]. Occassionally, a much more complex process is needed to achieve a good quality monazite concentrate. A final concentrate with 97% monazite (76.8% recovery) was obtained by processing Egyptian black sands from Abu Khashaba beach area at the Mediterranean coast using a combination of gravity (Wifley shaking table), magnetic (cross-belts, high-intensity induced roll, high-intensity lift type) and electrostatic (roll-type high tension) separators [2.163].

For finely disseminated monazite, flotation is considered the ideal method of beneficiation [2.109, 2.164–2.167]. Various flotation studies have focused on recovering monazite from placer deposit which usually contain heavy minerals such as ilmenite, magnetite, rutile and zircon. In terms of flotation behavior, monazite has similar characteristics to the associated heavy minerals [2.79]. Because of this, activators and depressants play an important role in monazite flotation. Cuthbertson [2.168] floated monazite from heavy minerals (wolframite, rutile and cassiterite) conditioned with starch, and using a cationic amine collector at acidic pH. The addition of starch made the separation of monazite from gangue minerals more efficient [2.168]. Other research studies aiming to purify ilmenite concentrate with minor amount of monazite were also conducted by Singh Sidhu *et al.* [2.166], Viswanathan *et al.* [2.167] and Somney [2.169] using amine collector or oleic acid. Monazite flotation, using high molecular weight sulfonates as collector with sodium oxalate as activator, was proven successful by Farah and Fayed [2.170]. This activator was also used together with oleic acid by Salatic [2.171]. Blazy and Houot [2.172], on the other hand, studied monazite flotation at basic pH using high molecular weight sulfonates with CO_3^- as activator. A comparison of different collectors was conducted by Abeidu [2.118]. Anionic collectors (oleic acid and sodium dodecyl sulphate), a cationic collector (dodecylaminium chloride) with sodium sulphide were used in the flotation of monazite from zircon. In terms of selectivity, oleic acid was the most selective, followed by dodecylaminium chloride, then by sodium dodecyl sulphate. The sodium sulphide worked as an activator for monazite by displacing lattice sites by S^{2-} and SH^{-} (product of dissociation of sodium sulfide in aqueous solution) [2.118]. These sites are where the oleate and oleic acid molecules attached to. In the early 90's, Pavez *et al.* [2.121, 2.122, 2.165, 2.173] conducted comparative flotation studies of monazite, rutile and zircon using oleate, pure hydroxamate and commercial hydroxamate. It was found that both oleate and a commercial hydroxamate displayed selectivity towards monazite using sodium metasilicate as gangue depressant [2.165]. Pavez and Peres [2.121] also investigated the effect of conditioning temperature as previous research studies. Pradip and Fuerstenau [2.82] suggested that adsorption of fatty acids onto RE mineral is stronger at elevated temperature, and hydroxamate is more selective at higher temperature. However, in their study, the floatability of monazite appears unaffected by an increase in conditioning temperature while the floatability of zircon and rutile are observed to be greatly affected.

2.6.2 Bastnäsite

In most cases, concentration methods such as magnetic separation [2.75, 2.174, 2.175] and gravity separation [2.160, 2.175] are used as preconcentration method in bastnäsite recovery prior to flotation [2.174, 2.176]. Typically, magnetic separation is used when the ore contains a significant amount of iron oxides (*e.g.*, Bayan Obo deposit in China) [2.14, 2.174]. Similar to monazite, beneficiation of bastnäsite is considered impossible without the aid of flotation due to occurrence of a "very fine to extremely fine grained" texture [2.14, 2.174]. Numerous research studies have investigated the use of different collectors and depressants to recover bastnäsite over a wide range of pH conditions (pH 5 - 10) [2.79]. Collectors include various types such as carboxylic acid (*e.g.*, fatty acids, oleate, tall oil, O-phthalic acid) [2.63, 2.79, 2.122, 2.177, 2.178], alkyl phosphoric and phosphonic acid (*e.g.*, alkyl phosphate ester P538, styrene phosphonic acid) [2.79], hydroxamates [2.63, 2.81, 2.82, 2.84, 2.116, 2.122, 2.126, 2.179–2.182] and sometimes a mixture of reagents [2.183]. Wide variations in pH conditions and reagents use in bastnäsite flotation is mainly due to ore variability. Flotation, in general, is heavily dependent on the composition and origin of the ore. For example, a bastnäsite from a carbonatite deposit may be recovered using a fatty acid collector, while those from pegmatite deposit can be recovered using tall oil modified with petroleum sulphonate collector [2.78]. Bastnäsite in barite-fluorite ores may not be recovered using the collectors mentioned. In some cases, preflotation of barite and fluorite is necessary to improve the recovery of bastnäsite [2.78].

Two of the largest bastnäsite deposits are in Mountain Pass Mine in California and

Bayan Obo Mine in China [2.14, 2.28, 2.81]. Both mineral deposits are associated with carbonatites with primary gangue minerals such as barite, calcite, celestite and quartz [2.14]. One of the first type of collector used in RE mineral flotation was carboxylic acid (*e.g.*, fatty acids, oleates, tall oil) [2.84]. In the early processing of the Molycorp plant (Mountain Pass, USA), distilled tail oil was used as a collector [2.82]. Since the gangue minerals behave similarly to the RE minerals in a flotation system, depressants were necessary [2.82, 2.184]. These includes sodium fluosilicate, ammonium lignin sulfonate and sodium carbonate [2.82]. Sodium carbonate produces carbonate ions in solution, which is also the potential determining ion of bastnäsite and most of the gangue minerals associated with it [2.97, 2.100]. Smith *et al.* [2.97] and Fuerstenau *et al.* [2.100] studied the effect of carbonate ions in the bastnäsite-calcite-barite system. Interestingly, the former found that sodium carbonate has little effect on the zeta potential of bastnäsite [2.97], while the latter found that bastnäsite was the most sensitive to addition of sodium carbonate among the three minerals [2.100]. Different conditioning times were used (2 hrs and 24 hrs), which may be the reason for the differences in the results obtained. As conditioning time appears to be a factor to consider in RE flotation, conditioning temperature is another. Since chemisorption is believed to be the mechanism of adsorption of carboxylic acid collectors onto the mineral surface, the conditioning temperature in the Mountain Pass process was elevated to enhance collector adsorption [2.82]. It was found that the collecting power of fatty acid was improved, however, it is still not selective towards RE minerals. This led to the search for a more selective collector. One such collector that was found selective was an organic phosphoric acid collector [2.81, 2.84]. It was shown to be effective in the RE flotation of Weishan deposit in China [2.84], however, the literature regarding this collector is relatively scarce. Another type of collector that has been gaining a lot of interests is the hydroxamate due to its selectivity. Flotation studies conducted by Pradip and Fuerstenau were the first to indicate that hydroxamates are more selective than carboxylate collectors in terms of RE flotation [2.115, 2.116, 2.139, 2.185–2.187]. Since then, a number of studies have been conducted on bastnäsite flotation with hydroxamate [2.81, 2.84, 2.122, 2.126, 2.179, 2.180, 2.188]. As discussed in Section 2.5.3, the improved selectivity of hydroxamate was due to formation of a more stable complexes with RE's than with alkali earths metal cations [2.83].

In terms of flotation performance, formation of complexes is not only the reaction that needs to be considered. It was stated in Section 2.5.1 that the minerals have certain degree of solubility, leading to huge differences in measured IEP (Section 2.5.2). In Section 2.5.3, possible mechanisms of collector adsorption on mineral surface have been shown to be highly affected by minerals' solubility (thus surface speciation) and collector's pKa. D.

Fuerstenau *et al.* [2.100], M. Fuerstenau [2.83, 2.86] and Pradip *et al.* [2.82] provide a good backgorund on the effect of conditioning time, conditioning temperature, solubility of the minerals, pKa of the collector and adsorption selectivity in the performance of RE flotation.

References

[2.1] Connelly, N., Hartshorn, R., Damhus, T., and Hutton, A. *Nomenclature of Inorganic Chemistry: IUPAC recommendations 2005.* Royal Society of Chemistry Publishing and International Union of Pure Applied Chemistry (IUPAC), King's Lynn, Norfolk, UK, 2005.

[2.2] Henderson, P. General geochemical properties and abundances of the rare earth elements. In Henderson, P., Editor, *Developments in Geochemistry*, volume 2, pages 1–32. Elsevier, 1984.

[2.3] Haskin, L. and Paster, T. Geochemistry and mineralogy of the rare earths. In Gschneidner, K. and Eyring, L., Editors, *Handbook on the Physics and Chemistry of Rare Earths: Non-metallic compounds I, Vol. 3.* North-Holland Publishing Company, New York, 1979.

[2.4] Clark, A. M. Mineralogy of the rare earth elements. In Henderson, P., Editor, *Developments in Geochemistry*, volume 2, pages 33–61. Elsevier, 1984.

[2.5] Gupta, C. and Krishnamurthy, N. Extractive metallurgy of rare earths. *International Materials Reviews*, 37(5):52, 1992.

[2.6] Hurst, C. China's rare earth elements industry: What can the west learn? Report, Institute for the Analysis of Global Security Washington DC, 2010.

[2.7] Lusty, P. and Walters, A. Rare earth elements. Report, British Geological Survey, 2010.

[2.8] Greenwood, N. N. and Earnshaw, A. The Lanthanide Elements (Z = 58 - 71). In *Chemistry of the Elements.* Elsevier, 2nd edition, 1997.

[2.9] Greenwood, N. N. and Earnshaw, A. Scandium, Yttrium, Lanthanum and Actinium. In *Chemistry of the Elements.* Elsevier, 2nd edition, 1997.

[2.10] Tse, P.-K. *China's rare-earth industry.* US Department of the Interior, US Geological Survey Reston, 2011.

[2.11] Haxel, G., Hendrick, J. B., and Orris, G. J. Rare Earth Elements - Critical Resources for High Technology. Report Fact Sheet 087-02, US Geological Survey, 2002.

[2.12] Kanazawa, Y. and Kamitani, M. Rare earth minerals and resources in the world. *Journal of Alloys and Compounds*, 408–412:1339–1343, 2006.

[2.13] Zheng, Z. and Greedan, J. E. Rare earth elements and materials. In Meyers, R., Editor, *Encyclopedia of Physical Science and Technology*, pages 1–22. Academic Press, New York, 3rd edition, 2003.

[2.14] Gupta, C. and Krishnamurthy, N. *Extractive Metallurgy of Rare Earths.* CRC Press, Boca Raton, Florida, 2005.

[2.15] Moeller, T. *The Chemistry of the Lanthanides.* Reinhold Pub. Corp., New York, 1963.

[2.16] Miyawaki, P. and Nakai, I. Crystal chemical aspects of rare earth minerals. In Jones, A., Wall, F., and Williams, T., Editors, *Rare Earth Minerals: Chemistry, Origin and Ore Deposits*, pages 21–40. Chapman Hall, Boundary Row, London, 1996.

[2.17] Rossotti, H. *Diverse Atoms: Profiles of the Chemical Elements.* Oxford University Press, 1998.

[2.18] Shannon, R. D. and Prewitt, C. T. Effective ionic radii in oxides and fluorides. *Acta Crystallographica Section B*, 25(5):925–946, 1969.

[2.19] Linnen, R. L., Samson, I. M., Williams-Jones, A. E., and Chakhmouradian, A. R. Geochemistry of the Rare-Earth Element, Nb, Ta, Hf, and Zr Deposits. In Holland, H. and Turekian, K., Editors, *Treatise on Geochemistry*, pages 543–568. Elsevier, Oxford, 2nd edition, 2014.

[2.20] Golev, A., Scott, M., Erskine, P. D., Ali, S. H., and Ballantyne, G. R. Rare earths supply chains: Current status, constraints and opportunities. *Resources Policy*, 41(Supplement C):52–59, 2014.

[2.21] Kamitani, M. Rare earth resources and the problems. In Siribumrungsukha, B., Arrykul, S., Sanguansai, P., Pungrassami, T., Sikong, L., and Kooptarnond, K., Editors, *International Conference on Rare Earth Minerals and Minerals for Electronic Uses*, volume 70-72, pages 181–191, Switzerland, 1991. Trans Tech Publications.

[2.22] Levinson, A. A. A System of Nomeclature for Rare-Earth Minerals. *The American Mineralogist*, 51:152, 1966.

[2.23] Encyclopedia Britannica. Placer deposit. www.britannica.com/EBchecked/topic/462598/placer-deposit, 2015. Accessed April 23, 2015.

[2.24] Long, K., Van Gosen, B., Foley, N., and Cordier, D. The principal rare earth elements deposits of the United States - A summary of domestic deposits and a global perspective. Report, US Geological Survey, 2010.

[2.25] King, H. Pegmatite. http://geology.com/rocks/pegmatite.shtml, 2015. Accessed April 20, 2015.

[2.26] Hurlbut, C. S., Klein, C., and Dana, J. D. *Manual of Mineralogy (after James D. Dana)*. Wiley, New York, 1977.

[2.27] Farla, R. The Skaergaard Layered Intrusion, East Greenland: The mechanisms of the formation of layering and the trend of differentiation revisited. Technical Report, Utrecht University, 2004.

[2.28] Verplanck, P. L. and Van Gosen, B. S. Carbonatite and alkaline intrusion-related rare earth element deposits - a deposit model. Report Open-File Report 2011–1256, US Geological Survey, 2011.

[2.29] Maitre, R. L. *Igneous Rocks: A Classification and Glossary of Terms*. Cambridge University Press, New York, 2nd edition, 2005.

[2.30] Streckeisen, A. Classification and nomenclature of volcanic rocks, lamprophyres, carbonatites and melilitic rocks IUGS Subcommission on the Systematics of Igneous Rocks. *Geologische Rundschau*, 69(1):194–207, 1980.

[2.31] Zaitsev, A. N., Wall, F., and Le Bas, M. J. REE-Sr-Ba minerals from the Khibina carbonatites, Kola Peninsula, Russia; their mineralogy, paragenesis and evolution. *Mineralogical Magazine*, 62(2):225–250, 1998.

[2.32] Verplanck, P. L., Van Gosen, B. S., Seal, R. R., and McCafferty, A. E. A deposit model for carbonatite and peralkaline intrusion-related rare earth element deposits. Report Scientific Investigations Report 2010-5070-J, US Geological Survey, 2014.

[2.33] Jordens, A., Cheng, Y. P., and Waters, K. E. A review of the beneficiation of rare earth element bearing minerals. *Minerals Engineering*, 41:97–114, 2013.

[2.34] Takeda, O., Uda, T., and Okabe, T. H. Rare earth, titanium group metals, and reactive metals production. In Seetharaman, S., Editor, *Treatise on Process Metallurgy*, pages 995–1069. Elsevier, Boston, 2014.

[2.35] Bünzli, J.-C. G. Lanthanides. In *Kirk-Othmer Encyclopedia of Chemical Technology*. John Wiley & Sons, Inc., New York, 2014.

[2.36] Olson, J. C., Shawe, D. R., Pray, L. C., and Sharp, W. N. Rare-earth mineral deposits of the Mountain Pass District, San Bernardino County, California. *Science*, 119(3088):325, 1954.

[2.37] Castor, S. B. Rare earth resources of North America. In *SME Annual Meeting, February 25, 1991 - February 28, 1991*. Society of Mining Engineers of AIME, 1991.

[2.38] Hellman, P. L. and Duncan, R. K. Evaluation of rare earth element deposits. *Transactions of the Institutions of Mining and Metallurgy, Section B: Applied Earth Science*, 123(2):107–117, 2014.

[2.39] Hedrick, J. B. Rare earths. Report, US Geological Survey Minerals Yearbook, 1999.

[2.40] Hedrick, J. B. Rare earths. Report, US Geological Survey Minerals Yearbook, 2003.

[2.41] Kremnidas, T. Canada's Rare Earth Deposits Can Offer A Substantial Competitive Advantage. Report, The Canadian Chamber of Commerce, 2012.

[2.42] Hatch, G. TMR Advanced Rare-Earth Projects Index. Report, Technology Metals Research, 2015.

[2.43] Chen, Z. Global rare earth resources and scenarios of future rare earth industry. *Journal of Rare Earths*, 29(1):1–6, 2011.

[2.44] SGS. The mineralogical characteristics of twenty-two drill core samples from a REE carbonatite deposit, adjacent to the Niobec Mine, Quebec. Technical Report, 2012.

[2.45] Grenier, L. and Tremblay, J.-F. IAMGOLD NI 43-101 Technical report: Surface diamond drilling exploration program for rare earth elements (Niobec mine property). Report, 2013.

[2.46] Bolonin, A. V., Nikiforov, A. V., Lykhin, D. A., and Sugorakova, A. M. The Chailag-Khem fluorite-barium-strontium rare earth carbonatite occurrence, the Western Sayan Range, Russia. *Geology of Ore Deposits*, 51(1):17–32, 2009.

[2.47] Lykhin, D. A. and Yarmolyuk, V. V. Magmatism and formation conditions of the Urma helvite-bertrandite deposit, West Transbaikal berillium province. *Geology of Ore Deposits*, 56(4):281–301, 2014.

[2.48] Nikiforov, A. V., Ozturk, H., Altuncu, S., and Lebedev, V. A. Kizilcaoren ore-bearing complex with carbonatites (northwestern Anatolia, Turkey): Formation time and mineralogy of rocks. *Geology of Ore Deposits*, 56(1):35–60, 2014.

[2.49] Sal'nikova, E. B., Yakovleva, S. Z., Nikiforov, A. V., Kotov, A. B., Yarmolyuk, V. V., Anisimova, I. V., Sugorakova, A. M., and Plotkina, Y. V. Bastnaesite: A promising U-Pb geochronological tool. *Doklady Earth Sciences*, 430(1):134–136, 2010.

[2.50] Xie, Y., Hou, Z., Yin, S., Dominy, S. C., Xu, J., Tian, S., and Xu, W. Continuous carbonatitic melt-fluid evolution of a REE mineralization system: Evidence from inclusions in the Maoniuping REE Deposit, Western Sichuan, China. *Ore Geology Reviews*, 36(1-3):90–105, 2009.

[2.51] Thompson, W., Lombard, A., Santiago, E., and Singh, A. Mineralogical studies in assisting beneficiation of rare earth element minerals from carbonatite deposits. In Broekmans, M., Editor, *Proceedings of the 10th International Congress for Applied Mineralogy (ICAM)*, pages 665–672. Springer Berlin Heidelberg, 2012.

[2.52] Crain, E. R. Crain's Petrophysical Handbook. www.spec2000.net/05-mineralprops.htm, 2001. Accessed July 10, 2015.

[2.53] Rosenblum, S. and Brownfield, I. K. Magnetic susceptibilities of minerals. Report, US Geological Survey, 2000.

[2.54] Mason, T. O., Maximov, B. A., Gorbatov, G. A., Cervelle, B., and Jin-Kai, X. Electrical properties of minerals. In Marfunin, A. S., Editor, *Advanced Mineralogy: Volume 1 Composition, Structure, and Properties of Mineral Matter: Concepts, Results, and Problems*, pages 395–411. Springer Berlin Heidelberg, Berlin, Heidelberg, 1994.

[2.55] Gupta, C. *Chemical Metallurgy : Principles and Practice*. Wiley-VCH Verlag GmbH & Co. KGaA, Weinheim, Germany, 2003.

[2.56] Telford, W. M., Geldart, L. P., and Sheriff, R. E. *Applied Geophysics*. Cambridge University Press, Cambridge, England, 1990.

[2.57] Gerber, R. Magnetic separation. In Gerber, R., Wright, C. D., and Asti, G., Editors, *Applied Magnetism*, volume 253 of *NATO ASI Series*, pages 165–220. Springer Netherlands, 1994.

[2.58] Golosov, S. I., Klyarovskii, V. M., Molchanov, V. I., and Tsibulichuk, V. M. Recovery of weakly magnetic minerals from the fine-grained material of weathered rocks by bulk magnetic separation. *Soviet Mining*, 4(2):165–168, 1968.

[2.59] Wills, B. A. and Finch, J. A. Magnetic and electrical separation. In Finch, J. A. and Wills, B. A., Editors, *Wills' Mineral Processing Technology*, pages 381–407. Butterworth-Heinemann, Boston, 8th edition, 2016.

[2.60] Allen, N. R. The concept of magnetic mineral separation by particle rotation. *Magnetic and Electrical Separation*, 11:33–50, 2002.

[2.61] Gill, C. B. Magnetic separation. In *Materials Beneficiation*, Materials Research and Engineering, pages 128–140. Springer New York, 1991.

[2.62] Buschow, K. H. J. and deBoer, F. R. Some basic concepts and units. In *Physics of Magnetism and Magnetic Materials*, pages 75–83. Springer US, 2003.

[2.63] Jordens, A., Sheridan, R. S., Rowson, N. A., and Waters, K. E. Processing a rare earth mineral deposit using gravity and magnetic separation. *Minerals Engineering*, 62:9–18, 2014.

[2.64] Cohen, H. E. Magnetic separation. In Wills, B. A. and Barley, R. W., Editors, *Mineral Processing at a Crossroads*, volume 117 of *NATO ASI Series*, pages 287–315. Springer Netherlands, 1986.

[2.65] Crook, T. The electrostatic separation of minerals. *Mineralogical Magazine*, 15(70):260–264, 1909.

[2.66] Fraas, F. Electrostatic separation of high-conductivity minerals. Report, U.S. Bureau of Mines, 1964.

[2.67] Higashiyama, Y. and Asano, K. Recent progress in electrostatic separation technology. *Particulate Science and Technology*, 16(1):77–90, 1998.

[2.68] Kelly, E. G. and Spottiswood, D. J. The theory of electrostatic separations: A review Part I. Fundamentals. *Minerals Engineering*, 2(1):33–46, 1989.

[2.69] Kelly, E. G. and Spottiswood, D. J. The theory of electrostatic separations. A review. Part II. Particle charging. *Mining Engineering*, 2(2):193–205, 1989.

[2.70] Lindley, K. S. and Rowson, N. A. Charging mechanisms for particles prior to electrostatic separation. *Magnetic and Electrical Separation*, 8(2):101–113, 1997.

[2.71] Gupta, A. and Yan, D. S. Gravity separation. In Gupta, A. and Yan, D. S., Editors, *Mineral Processing Design and Operation*, pages 494–554. Elsevier Science, Amsterdam, 2006.

[2.72] Taggart, A. and Behre, H. *Handbook of Mineral Dressing, Ores and Industrial Minerals*. J. Wiley & Sons, Inc., 1945.

[2.73] Wills, B. A. and Finch, J. A. Gravity concentration. In Finch, J. A. and Wills, B. A., Editors, *Wills' Mineral Processing Technology*, pages 223–244. Butterworth-Heinemann, Boston, 8th edition, 2016.

[2.74] Wills, B. A. and Finch, J. A. Dense medium separation (DMS). In Finch, J. A. and Wills, B. A., Editors, *Wills' Mineral Processing Technology*. Butterworth-Heinemann, Boston, 8th edition, 2016.

[2.75] Yang, X., Satur, J. V., Sanematsu, K., Laukkanen, J., and Saastamoinen, T. Beneficiation studies of a complex REE ore. *Minerals Engineering*, 71:55–64, 2015.

[2.76] Bulatovic, S. M. Classification of Flotation Reagents. In Bulatovic, S. M., Editor, *Handbook of Flotation Reagents*, pages 1–3. Elsevier, Amsterdam, 2007.

[2.77] Bulatovic, S. M. Collectors. In Bulatovic, S. M., Editor, *Handbook of Flotation Reagents*, pages 5–40. Elsevier, Amsterdam, 2007.

[2.78] Bulatovic, S. M. Flotation of REO Minerals. In Bulatovic, S. M., Editor, *Handbook of Flotation Reagents: Chemistry, Theory and Practice*, pages 151–173. Elsevier, Amsterdam, 2010.

[2.79] Zhang, X., Du, H., Wang, X., and Miller, J. D. Surface chemistry considerations in the flotation of rare-earth and other semisoluble salt minerals. *Minerals and Metallurgical Processing*, 30(1):24–37, 2013.

[2.80] Wills, B. A. and Finch, J. A. Froth Flotation. In Finch, J. A. and Wills, B. A., Editors, *Wills' Mineral Processing Technology*, pages 265–380. Butterworth-Heinemann, Boston, 8th edition, 2016.

[2.81] Houot, R., Cuif, J.-P., Mottot, Y., and Samana, J.-C. Recovery of rare earth mineral, with emphasis on flotation process. In *International Conference on Rare Earth Minerals and Minerals for Electronic Uses*, volume 70-72, pages 301–324. Trans Tech Publications, 1991.

[2.82] Pradip, P. and Fuerstenau, D. Design and development of novel flotation reagents for the beneficiation of Mountain Pass rare-earth ore. *Minerals and Metallurgical Processing*, 30(1):1–9, 2013.

[2.83] Fuerstenau, M. Chelating Agents as Flotation Collectors. In Miller, J., Young, C., Kellar, J., and Free, M., Editors, *Innovations in Natural Resource Processing: Proceedings of the Jan. D. Miller Symposium*. 2005.

[2.84] Ren, J., Wang, W., Luo, J., Zhou, G., and Tang, F. Progress of flotation reagents of rare earth minerals in China. *Journal of Rare Earths*, 21(1):1–8, 2003.

[2.85] Bulatovic, S. M. Frothers. In Bulatovic, S. M., Editor, *Handbook of Flotation Reagents*, pages 43–51. Elsevier, Amsterdam, 2007.

[2.86] Fuerstenau, M., Jameson, G. J., and Yoon, R.-H. *Froth flotation: A century of innovation*. Society for Mining, Metallurgy, and Exploration, Colorado, USA, 2007.

[2.87] Pearse, M. J. An overview of the use of chemical reagents in mineral processing. *Minerals Engineering*, 18(2):139–149, 2005.

[2.88] Bulatovic, S. M. Modifying Reagents. In Bulatovic, S. M., Editor, *Handbook of Flotation Reagents*, pages 53–79. Elsevier, Amsterdam, 2007.

[2.89] Partridge, A. and Smith, G. Small-sample flotation testing: a new cell. *Transactions of the Institution of Mining and Metallurgy, Section C*, 80:C199, 1971.

[2.90] Hallimond, A. Laboratory apparatus for flotation tests. *Mineralogical Magazine*, 70:87–91, 1944.

[2.91] Rao, S. R. *Surface Chemistry of Froth Flotation*, volume 1. Springer, New York, 2nd edition, 2004.

[2.92] Michaud, D. D-R Denver Float Cell. www.911metallurgist.com/blog/flotation-machines/d-r-denver-float-cell, 2015.

[2.93] Crozier, R. D. and Klimpel, R. R. Frothers: Plant Practice. *Mineral Processing and Extractive Metallurgy Review*, 5(1-4):257–279, 1989.

[2.94] Sastri, S. Column flotation: theory and practice. In *Workshop on Froth Flotation: Recent Trends*, RRL Bhubaneswar, 1998.

[2.95] Ross, D. Cavitation. In *Mechanics of Underwater Noise*, pages 202–252. Pergamon, New York, 1976.

[2.96] Leja, J. Flotation Surfactants. In *Surface Chemistry of Froth Flotation*, pages 205–339. Springer US, 1982.

[2.97] Smith, R. and Shonnard, D. Electrokinetic study of the role of modifying agents in flotation of salt-type minerals. *AIChE Journal*, 32(5):865–868, 1986.

[2.98] Somasundaran, P. and Moudgil, B. *Reagents in Mineral Technology.* Marcel Dekker, Inc., New York, 1987.

[2.99] Bulatovic, S. M. Adsorption mechanism of flotation collectors. In Bulatovic, S. M., Editor, *Handbook of Flotation Reagents*, pages 125–152. Elsevier, Amsterdam, 2007.

[2.100] Fuerstenau, D., Pradip, P., and Herrera-Urbina, R. The surface chemistry of bastnaesite, barite and calcite in aqueous carbonate solutions. *Colloids and Surfaces*, 68(1–2):95–102, 1992.

[2.101] Zhang, W., Honaker, R. Q., and Groppo, J. G. Flotation of monazite in the presence of calcite part I: Calcium ion effects on the adsorption of hydroxamic acid. *Minerals Engineering*, 100:40–48, 2017.

[2.102] Van Cappellen, P., Charlet, L., Stumm, W., and Wersin, P. A surface complexation model of the carbonate mineral-aqueous solution interface. *Geochimica et Cosmochimica Acta*, 57(15):3505–3518, 1993.

[2.103] Stipp, S. L. and Hochella, M. F. Structure and bonding environments at the calcite surface as observed with X-ray photoelectron spectroscopy (XPS) and low energy electron diffraction (LEED). *Geochimica et Cosmochimica Acta*, 55(6):1723–1736, 1991.

[2.104] Busenberg, E. and Plummer, L. N. The kinetics of dissolution of dolomite in CO_2-H_2O systems at 1.5 to 65 °C and 0 to 1 atm $p\mathrm{CO}_2$. *American Journal of Science*, 282(1):45–78, 1982.

[2.105] Predali, J. J. and Cases, J. M. Zeta potential of magnesian carbonates in inorganic electrolytes. *Journal of Colloid and Interface Science*, 45(3):449–458, 1973.

[2.106] Chen, G. and Tao, D. Effect of solution chemistry on flotability of magnesite and dolomite. *International Journal of Mineral Processing*, 74(1–4):343–357, 2004.

[2.107] Herrera-Urbina, R., Pradip, P., and Fuerstenau, D. Electrophoretic mobility and computations of solid-aqueous solution equilibria for the bastnaesite-H_2O system. *Minerals and Metallurgical Processing*, 30(1):18–23, 2013.

[2.108] Ordoñez-Regil, E., Drot, R., and Simoni, E. Surface complexation modeling of uranium(VI) sorbed onto lanthanum monophosphate. *Journal of Colloid and Interface Science*, 263(2):391–399, 2003.

[2.109] Cheng, T. W., Holtham, P. N., and Tran, T. Froth flotation of monazite and xenotime. *Minerals Engineering*, 6(4):341–351, 1993.

[2.110] Turnbull, A. and Wadsley, M. W. *CSIRO-Monash Thermochemistry System: Version 1.0*. Monash University, 1992.

[2.111] Hunter, R. J. *Zeta Potential in Colloid Science*. Academic Press, Inc., San Diego, CA, 1981.

[2.112] Shaw, D. J. and Costello, B. *Introduction to Colloid and Surface Chemistry*. Elsevier, Oxford, 1993.

[2.113] Delgado, À. V. *Interfacial Electrokinetics and Electrophoresis*. Marcel Dekker, Inc., New York, 2002.

[2.114] Lyklema, J. Nomeclature, Symbols, Definitions and Measurements for Electrified Interfaces in Aqueous Dispersions of Solids. *Pure and Applied Chemistry*, 63(6):12, 1991.

[2.115] Pradip, P. *The Surface Properties and Flotation of Rare-earth Minerals*. PhD Thesis, University of California, Berkeley., 1981.

[2.116] Pradip, P. and Fuerstenau, D. The adsorption of hydroxamate on semi-soluble minerals. Part I: Adsorption on barite, calcite and bastnaesite. *Colloids and Surfaces*, 8(2):103–119, 1983.

[2.117] Viswanathan, K. V., Shukla, S. K., and Majumdar, K. K. Adsorption of long chain electrolytes at the solid-liquid interface. Part 1 - The adsorption of monazite-water system. *Transactions of the Indian Institute of Metals*, 23(2):6–10, 1970.

[2.118] Abeidu, A. M. The separation of monazite from zircon by flotation. *Journal of the Less Common Metals*, 29(2):113–119, 1972.

[2.119] Harada, T., Owada, S., Takiuchi, T., and Kurita, M. A flotation study for effective separation of the heavy mineral sands. In *XVIII International Mineral Processing Congress*, volume 4, page 10, 1993.

[2.120] Luo, J. and Chen, X. Research into the recovery of high-grade rare-earth concentrate from Baotou Complex Iron Ores, China. *Mineral Processing and Extractive Metallurgy*, pages 663–675, 1984.

[2.121] Pavez, O. and Peres, A. Flotation of monazite-zircon-rutile with sodium oleate and hydroxamates. In *XVIII International Mineral Processing Congress*, volume 4, pages 1007–1012, 1993.

[2.122] Pavez, O., Brandao, P. R. G., and Peres, A. E. C. Adsorption of oleate and octylhydroxamate on to rare-earths minerals. *Minerals Engineering*, 9(3):357–366, 1996.

[2.123] Ren, J., Song, S., Lopez-Valdivieso, A., and Lu, S. Selective flotation of bastnaesite from monazite in rare earth concentrates using potassium alum as depressant. *International Journal of Mineral Processing*, 59(3):237–245, 2000.

[2.124] Cheng, T. W. Point of zero charge of monazite and xenotime. *Minerals Engineering*, 13(1):105–109, 2000.

[2.125] Smith, R. and Steiner, S. D. Autoactivation in anionic flotation of bastnaesite. *Institution of Chemical Engineers Symposium Series*, 1980.

[2.126] Ren, J., Lu, S., Song, S., and Niu, J. A new collector for rare earth mineral flotation. *Minerals Engineering*, 10(12):1395–1404, 1997.

[2.127] Fuerstenau, D. and Herrera-Urbina, R. Flotation fundamentals. In Somasundaran, P. and Moudgil, B., Editors, *Reagents in Mineral Technology*, pages 1–38. Marcel Dekker, Inc., New York, 1987.

[2.128] Somasundaran, P. Adsorption of starch and oleate and interaction between them on calcite in aqueous solutions. *Journal of Colloid and Interface Science*, 31(4):557–565, 1969.

[2.129] Chander, S. and Fuerstenau, D. Electrochemical reaction control of contact angles on copper and synthetic chalcocite in aqueous potassium diethyldithiophosphate solutions. *International Journal of Mineral Processing*, 2(4):333–352, 1975.

[2.130] Hu, Y. and Xu, Z. Interactions of amphoteric amino phosphoric acids with calcium-containing minerals and selective flotation. *International Journal of Mineral Processing*, 72(1–4):87–94, 2003.

[2.131] Amankonah, J. O. and Somasundaran, P. Effects of dissolved mineral species on the electrokinetic behavior of calcite and apatite. *Colloids and Surfaces*, 15:335–353, 1985.

[2.132] Somasundaran, P. and Ananthapadmanabhan, K. Solution chemistry of surfactants and the role of it in adsorption and froth flotation in mineral-water systems. *Solution Chemistry of Surfactants*, 2:17–38, 1979.

[2.133] Predali, J. J. Flotation of carbonates with salts of fatty acids: role of pH and the alkyl chain. *Transactions of the Institution of Mining and Metallurgy*, 78:C140–C147, 1969.

[2.134] Moudgil, B. and Chanchani, R. Selective flotation of dolomite from apatite using sodium oleate as the collector. In *SME-AIME Annual Meeting*, 1983.

[2.135] Fuerstenau, M. and Miller, J. D. The role of the hydrocarbon chain in anionic flotation of calcite. *Transactions of the AIME*, 238(2):153–160, 1967.

[2.136] Yale, H. L. The hydroxamic acids. *Chemical Reviews*, 33(3):209–256, 1943.

[2.137] Chatterjee, B. Donor properties of hydroxamic acids. *Coordination Chemistry Reviews*, 26(3):281–303, 1978.

[2.138] Fuerstenau, D. and Pradip, P. Zeta potentials in the flotation of oxide and silicate minerals. *Advances in Colloid and Interface Science*, 114–115:9–26, 2005.

[2.139] Fuerstenau, D. and Pradip, P. Mineral flotation with hydroxamate collectors. In Jones, M. J. and Oblatt, R., Editors, *Reagents in the Minerals Industry*, pages 161–168. The Institution of Mining and Metallurgy, 1984.

[2.140] Quin, L. D. *A Guide to Organophosphorus Chemistry*. John Wiley & Sons, New York, 2000.

[2.141] Kuys, K. J. and Roberts, N. K. In situ investigation of the adsorption of styrene phosphonic acid on cassiterite by FTIR-ATR spectroscopy. *Colloids and Surfaces*, 24(1):1–17, 1987.

[2.142] Gong, G., Han, Y., Liu, J., Zhu, Y., Li, Y., and Yuan, S. In situ investigation of the adsorption of styrene phosphonic acid on cassiterite (110) surface by molecular modeling. *Minerals*, 7(10):181, 2017.

[2.143] Delgado, À. V., González-Caballero, F., Hunter, R. J., Koopal, L. K., and Lyklema, J. Measurement and interpretation of electrokinetic phenomena. *Journal of Colloid and Interface Science*, 309(2):194–224, 2007.

[2.144] Josefowicz, J. Y. Electrophoretic light scattering and its application to the study of cells. In Catsimpoolas, N., Editor, *Methods of Cell Separation*, pages 67–91. Springer US, Boston, MA, 1979.

[2.145] Ramer, G. and Lendl, B. Attenuated total reflection Fourier transform infrared spectroscopy. In *Encyclopedia of Analytical Chemistry.* John Wiley & Sons, Ltd, 2006.

[2.146] Stuart, B. *Infrared Spectroscopy: Fundamental and Applications.* John Wiley & Sons, Ltd, Chichester, UK, 2004.

[2.147] Siesler, H. W., Ozaki, Y., Kawata, S., and Heise, H. M. *Near-Infrared Spectroscopy: Principles, Instruments, Applications.* John Wiley & Sons, 2008.

[2.148] Protherm. Infrared basics. https://www.pro-therm.com/infrared_basics.php, 2005. Accessed March 1, 2018.

[2.149] Berthomieu, C. and Hienerwadel, R. Fourier transform infrared (FTIR) spectroscopy. *Photosynthesis Research*, 101(2):157–170, 2009.

[2.150] Coates, J. Interpretation of infrared spectra, a practical approach. *Encyclopedia of Analytical Chemistry*, 2000.

[2.151] Piketech. ATR - Theory and applications. http://mmrc.caltech.edu/FTIR/Pike/Intro%20to%20ATR.pdf, 2016.

[2.152] Markovich, R. J. and Pidgeon, C. Introduction to fourier transform infrared spectroscopy and applications in the pharmaceutical sciences. *Pharmaceutical Research*, 8(6):663–675, 1991.

[2.153] Bubert, H., Rivière, J. C., and Werner, W. S. M. X-Ray Photoelectron Spectroscopy (XPS). In *Surface and Thin Film Analysis*, pages 7–41. Wiley-VCH Verlag GmbH & Co. KGaA, 2011.

[2.154] Hofmann, S. Surface and interface analysis. In *Kirk-Othmer Encyclopedia of Chemical Technology*. John Wiley & Sons, Inc., 2000.

[2.155] Pensak, D. A. Molecular modelling: scientific and technological boundaries. *Pure and Applied Chemistry*, 61(3):601–603, 1989.

[2.156] Capelle, K. A bird's-eye view of density-functional theory. *arXiv preprint cond-mat/0211443*, 2002.

[2.157] Rai, B. *Molecular Modeling for the Design of Novel Performance Chemicals and Materials*. CRC Press, New York, 2012.

[2.158] Rai, B. and Pradip. Design of highly selective industrial performance chemicals: a molecular modelling approach. *Molecular Simulation*, 34(10-15):1209–1214, 2008.

[2.159] Pradip and Rai, B. Molecular modeling and rational design of flotation reagents. *International Journal of Mineral Processing*, 72(1–4):95–110, 2003.

[2.160] Özbayoğlu, Gülhan and Ümit Atalay, M. Beneficiation of bastnaesite by a multi-gravity separator. *Journal of Alloys and Compounds*, 303–304:520–523, 2000.

[2.161] Khanchi, A. R., Sedighi, H., Ansar, S., and Fasihi, J. Preconcentration of rare earth elements from Iranian monazite ore by spiral separator using multi-response optimization method. *International Journal of Mining Science and Technology*, 24(1):117–121, 2014.

[2.162] Peravadhanulu, A., Prasad Rao, P., Mathur, G., and Altekar, V. Beneficiation of beach sands. In *Monograph on Ores and Minerals of India - Beneficiation and Agglomeration Techniques for Industrial and Economic Exploitation*, pages 272–275. GSI, New Delhi, Janshedpur, 1979.

[2.163] Moustafa, M. I. and Abdelfattah, N. A. Physical and chemical beneficiation of the Egyptian beach monazite. *Resource Geology*, 60(3):288–299, 2010.

[2.164] Pai, K. M. and Mallikarjunan, R. Flotation of beach sand minerals. *Mineralogical Magazine*, 112(4):242–243, 1965.

[2.165] Pavez, O. and Peres, A. Effect of sodium metasilicate and sodium sulphide on the floatability of monazite-zircon-rutile with oleate and hydroxamates. *Minerals Engineering*, 6(1):69–78, 1993.

[2.166] Singh Sidhu, G. and Oberbillig, E. Monazite flotation. *Mining Congress Journal*, 45(8):82–83, 1959.

[2.167] Viswanathan, K. V., Madhavan, T. R., and Majumdar, K. K. Selective flotation of beach sand monazite. *Mining Magazine*, 113(1):17192123, 1965.

[2.168] Cuthbertson, R. E. Froth flotation of monazite from heavy gravity minerals. Patent, 1952.

[2.169] Somney, J. Y. Recovery of Economic Minerals from Kerala Sands. *Journal of Mines Metals and Fuels*, page 8, 1960.

[2.170] Farah, M. and Fayed, L. Activation par l'oxalate dans la flottation des sables a monazite a l'aide des sulfonates lourds. In *Congress International de la preparation des minerais*, 1963.

[2.171] Salatic, D. Floatability of monazite and zircon related to electrochemical changes on their surfaces. *Transactions of the Institution of Mining and Metallurgy*, pages C231–237, 1967.

[2.172] Blazy, P. and Houot, R. Procédé de préparation par flottation de minéraux lourds. *Brevet CNRS*, (66):689, 1966.

[2.173] Pavez, O. and Peres, A. Bench scale flotation of a Brazilian monazite ore. *Minerals Engineering*, 7(12):1561–1564, 1994.

[2.174] Li, L. Z. and Yang, X. China's rare earth ore deposits and beneficiation techniques. In *ERES2014: 1st European Rare Earth Resources Conference*, 2014.

[2.175] Smith, W. L. and Cisney, E. A. Bastnaesite, accessory mineral in redstone granite from Westerly, Rhode Island. *American Mineralogist*, 41(1-2):76–81, 1956.

[2.176] Baroch, C. J. *Processing of California bastnasite ore.* PhD Thesis, Iowa State University., 1958.

[2.177] Qiu, X., He, X., Rao, J., Tang, Y., Luo, C., and Zhang, J. Flotation mechanism of sodium oleate on bastnaesite. *Xiyou Jinshu/Chinese Journal of Rare Metals*, 37(3):422–428, 2013.

[2.178] Wang, C.-H., Qiu, X.-Y., Hu, Z., and Tong, X. Study on the flotation mechanism of bastnaesite by sodium oleate. *Chinese Rare Earths*, 34(6):24–30, 2013.

[2.179] Assis, S. M., Montenegro, L. C. M., and Peres, A. E. C. Utilisation of hydroxamates in minerals froth flotation. *Minerals Engineering*, 9(1):103–114, 1996.

[2.180] Cui, J., Hope, G. A., and Buckley, A. N. Spectroscopic investigation of the interaction of hydroxamate with bastnaesite (cerium) and rare earth oxides. *Minerals Engineering*, 36-38:91–99, 2012.

[2.181] Jiake, L. and Xiangyong, C. Selective flotation of rare-earth minerals from fluorite, barite and calcite. In Guangxian, X. and Jimei, X., Editors, *New Frontiers in Rare Earth Science and Applications*, pages 67–70. Academic Press, 1985.

[2.182] Zhang, X., Du, H., Wang, X., and Miller, J. D. Surface chemistry aspects of bastnaesite flotation with octyl hydroxamate. *International Journal of Mineral Processing*, 133:29–38, 2014.

[2.183] Jianzhong, C., Yunbing, H., and Liping, C. Flotation separation on rare earth minerals and gangues. *Journal of Rare Earths*, 25 (Special Issue):62–66, 2007.

[2.184] Marinakis, K. and Shergold, H. The mechanism of fatty acid adsorption in the presence of fluorite, calcite and barite. *International Journal of Mineral Processing*, 14(3):161–176, 1985.

[2.185] Fuerstenau, D., Khan, L. A., Raghavan, S., and Pradip, P. Alternate reagent scheme for the flotation of Mountain Pass rare-earth ore. In *XIV International Mineral Processing Congress: Worldwide Industrial Application of Mineral Processing Technology*. CIM, 1983.

[2.186] Pradip, P. and Fuerstenau, D. Adsorption of hydroxamate collectors on semisoluble minerals Part II: Effect of temperature on adsorption. *Colloids and Surfaces*, 15:137–146, 1985.

[2.187] Pradip, P. and Fuerstenau, D. The role of inorganic and organic reagents in the flotation separation of rare-earth ores. *International Journal of Mineral Processing*, 32(1–2):1–22, 1991.

[2.188] Li, F., Wang, J., and Zeng, X. A process on the recovery of RE minerals with a chelating collector. *Rare Earths: Extraction, Preparation and Applications*, pages 71–79, 1989.

Chapter 3

Flotation behavior of dolomite, monazite and bastnäsite

This chapter presents a detailed investigation of the flotation behavior of dolomite, monazite and bastnäsite in the presence of benzohydroxamate, sodium oleate and organic phosphoric acid collectors. Previous exploratory tests (Appendix A) revealed that these collectors could be potential collectors for RE minerals, as such further investigations through microflotation, zeta potential measurements and ATR-FTIR studies considering wider pH range values and various collector concentrations are presented in this chapter.

Abstract

Carboxylates, hydroxamates and organic phosphoric acids are typical collectors used for rare earth mineral flotation. Carboxylates are not selective, while hydroxamates, though selective, require high concentrations to recover a significant amount of rare earth minerals. Other collectors such as organic phosphoric acids, which showed promising rare earth minerals collecting potential, have recently been explored. However, the mechanism of organic phosphoric acid adsorption on the surface of rare earth minerals has not been very well investigated. In this study, zeta potential measurements were conducted to study the surface property of dolomite, monazite and bastnäsite in the presence of benzohydroxamate (hydroxamate), sodium oleate (carboxylate) and Flotinor 1682 (phosphoric acid ester). These measurements, complemented with ATR-FTIR spectroscopy, evaluated the adsorption of the collectors at the surface of the minerals. The adsorption of the collectors was found to be highly influenced by the mineral cations present at the mineral/solution interface and in the solution. Possible adsorption mechanisms are proposed and discussed; some of which agree with those presented in the literature, while others provided different perspective. Although

benzohydroxamate was the most selective, potential flotation processes to recover rare earth minerals using sodium oleate and Flotinor 1682 were also suggested.

3.1 Introduction

Rare earth (RE) elements are the elements yttrium (Y) and the lanthanides [3.1], which could be further divided into light and heavy RE elements [3.2]. Due to their unique chemical properties, RE elements are useful in high technology applications [3.3]. The emergence of green technologies requiring RE elements have continue to increase the demand of RE elements [3.4]. It has been projected that by 2025, there will be a supply shortage of some RE elements, which can only be met with constant development of new mines outside of China [3.5]. A number of the exploited deposits are located in Canada and among these projects, the Niobec project of Magris Resources Inc. is found to contain the largest resource of RE elements with 1058.6 million tonnes at 1.73% total RE oxide (TREO) [3.6]. This corresponds to 18.3 million tonnes of TREO, which is almost half of China's RE element reserve (43 million tonnes TREO) [3.7]. The Niobec RE deposit is adjacent to the existing niobium mine in Quebec and drill sample characterization revealed that the deposit contains bastnäsite and monazite (primary sources of light RE elements [3.8]), while the gangue is mostly carbonates such as dolomite. Ore characterization also indicated that the deposit has fine RE minerals' liberation size, flotation is thus an applicable method for recovering these RE minerals [3.9].

Some of the most common collectors for RE minerals are hydroxamates, carboxylates and organic phosphoric acids. In RE mineral flotation, carboxylate, such as fatty acids and sodium oleate, is the most widely used collector [3.10]. However, this type of collectors also adsorbed to gangue minerals such as dolomite, which is typically associated with RE minerals, making them float as well [3.11]. The use of carboxylate would then require dolomite depressants to make flotation efficient [3.12]. This has led to investigations into more selective collectors, such as hydroxamates. The selectivity of this form of collector is attributed to its formation of more stable chelates with RE metal cations than with alkaline earth cations [3.13]. The limited studies on the use of hydroxamates have shown good recovery of bastnäsite and monazite at basic pH conditions [3.14, 3.15]. However, it requires sufficiently large quantity to recover significant amount of RE minerals [Appendix A, 3.15, 3.16]. Another type of collector that is recently being investigated is the organic phosphoric acid. It has been used in the RE flotation at Weishan county, Shandong province in China and showed promising grade and recovery [3.17]. Recent work also suggests the potential collecting ability of Flotinor 1682 (commercial organic phosphoric acid) at certain pH conditions (Appendix A). The adsorption of carboxylate and hydroxamate on RE minerals has already been studied and possible adsorption mechanisms have already been presented. However, the mechanism of organic phosphoric acid adsorption on the surface of RE minerals has not been very well investigated.

In this work, the effect of these collectors on the flotation recovery of pure bastnäsite, monazite and dolomite were investigated. Zeta potential measurements and attenuated total reflectance Fourier transform infrared (ATR-FTIR) spectroscopy provided insights on the collector adsorption at the surface of the minerals. Possible adsorption mechanisms of the collectors on the mineral surface, as well as possible flotation routes to recover RE minerals are presented.

3.2 Materials and methods

3.2.1 Material

Dolomite from Sterling Hill Mine (New Jersey) was purchased from Ward's Science (USA). Dolomite is a carbonate mineral with the formula $CaMg(CO_3)_2$. Monazite, a RE phosphate mineral ($REPO_4$) from Eureka Farm 99 (Namibia) was purchased from Mineralogical Research Company (USA). Bastnäsite, a RE fluorocarbonate ($REFCO_3$), was provided by African Rare Earths (Pty.) Ltd. (South Africa). Although the RE minerals contain several RE elements (mostly light RE elements) in their structure such as La, Ce, Nd, *etc.*, the following discussions will consider only Ce to avoid redundancy, as these elements behave similarly.

The potassium chloride that was used as supporting electrolyte was purchased from Sigma-Aldrich (Canada); the hydrochloric acid and the potassium hydroxide that were used as pH modifiers were obtained from Fisher Scientific (Canada). Benzohydroxamate was obtained from Sigma-Aldrich (Canada); sodium oleate was purchased from Fisher Scientific (Canada); and Flotinor 1682, a commercial organic phosphoric acid collector, was obtained from Clariant (Canada). F150, the frother that was used, was provided by Flottec (Canada). The general structure of these collectors is presented in Figure 3.1. Benzohydroxamate is a chelating reagent with a bidentate group, HO–N–C=O [3.18], while sodium oleate has the functional group $-COO^-$ as seen in Figure 3.1. Although the presented structure of the organic phosphoric acid is not the actual structure of Flotinor 1682, the structure presented follows the general organic phosphoric acid, $ROPO_3H_2$ [3.19], in this case, $R = CH_3$.

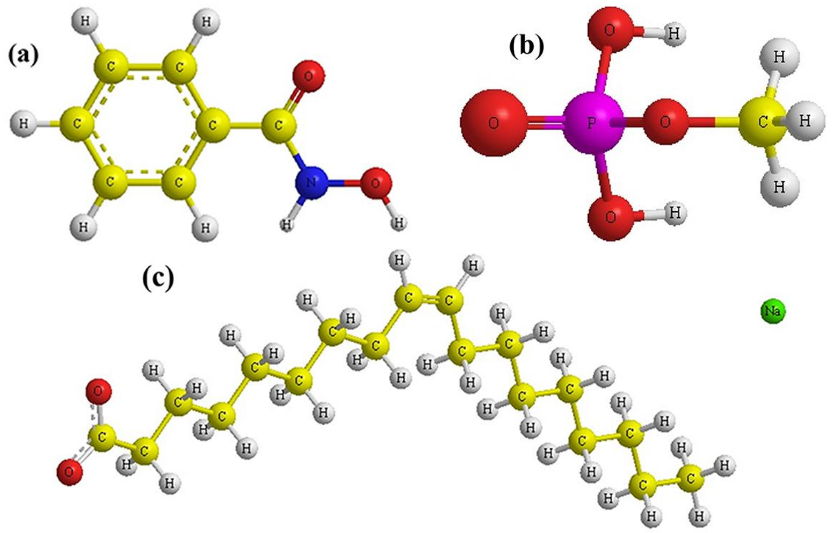

Figure 3.1 – Collector structure of (a) benzohydroxamate (*cis*); (b) organic phosphoric acid (not the actual structure of Flotinor 1682); and (c) sodium oleate.

3.2.2 Mineral characterization

The minerals were characterized using an X-ray Diffractometer using Bruker D8 Discovery X-Ray Diffractometer (Cobalt source: Co Kα, $\lambda = 1.79$ Å) to identify the purity of the samples.

The elemental analysis was conducted using Inductively Coupled Plasma Optical Emission Spectrometry (ICP-OES). Samples of 0.1 g were digested at 95 °C for 6 hours using aqua regia and was analyzed using Thermo Scientific 6000 Series Spectrometer (Thermo Fisher Scientific Inc., USA).

3.2.3 Zeta potential measurements

To obtain a particle size smaller than 10 μm for zeta potential measurements, mineral samples were pulverized in a Planetary Monomill, Pulverisette 6 (Fritsch, Germany). A D_{50} of 2.3 μm for dolomite, monazite and bastnäsite was measured using Horiba Laser Scattering Particle Size Distribution Analyzer LA-920 (ATS Scientific Inc., Canada). A solution of 1×10^{-3} M NaCl was used as the indifferent background electrolyte for all the measurements. The solutions were pH adjusted using hydrochloric acid and potassium hydroxide prior to addition of the mineral particles. Prior to measurement, the 100 mg/L mineral suspension was ultrasonicated for 180 s to ensure particle dispersion. Electromobility measurements were taken using a NanoBrook 90Plus Zeta Particle Size Analyzer (Brookhaven Instruments, USA). These measurements were converted to zeta potential using Smoluchowski's approximation [3.20].

3.2.4 ATR-FTIR spectroscopy

Attenuated total reflectance Fourier transform infrared (ATR-FTIR) spectroscopy were conducted with the bare mineral samples and the samples conditioned with the collectors using PerkinElmer Spectrum 400 (Perkin Elmer, USA). The samples were washed 3 times with pH adjusted deionised water, then dried in a vacuum oven at ambient temperature prior to the measurements being taken. The IR transmittance spectra were obtained by passing 32 scans, between 4000 and 650 cm^{-1}, with a resolution of 4 cm^{-1}. The obtained spectra were baseline corrected and were normalized to the total surface area under the transmittance bands using PerkinElmer Spectrum software (Perkin Elmer, USA).

3.2.5 Microflotation tests

Microflotation tests were conducted using a modified Hallimond tube. The flotation cell volume is approximately 170 mL. The cell, made of glass, has three parts – the lower part has a silicate frit at the bottom; the extensor part connects the lower part and the upper part; and the upper part is where the floated fractions can be collected.

One (1) gram of mineral sample, with a particle size range -106+38 μm, was placed in a beaker with 30 mL distilled water (adjusted to desired pH) and a magnetic stirring bar was employed to ensure that the mineral particles remained in suspension. The pH of the suspension was adjusted (by addition of diluted HCl and/or KOH) prior to addition of the collector. The pH was maintained during the 5-minute conditioning. The suspension was then transferred to the cell and was next added with 140 mL of pH adjusted water. Air was introduced through the cell at a flowrate of 40 mL/min. Flotation was conducted for 1 minute. The floated and non-floated fractions were collected, filtered, dried and weighed to calculate the recovery.

3.3 Results

3.3.1 Mineral characterization

X-ray diffractogram (Figure 3.2) shows that the minerals do not present other significant peaks, show that the minerals do not present significant peaks other than those expected, suggesting that the samples are relatively pure. For monazite, minor amounts of calcite were observed as shown in the diffractogram. This result correlated well with the ICP-OES elemental analysis as presented in Table 3.1.

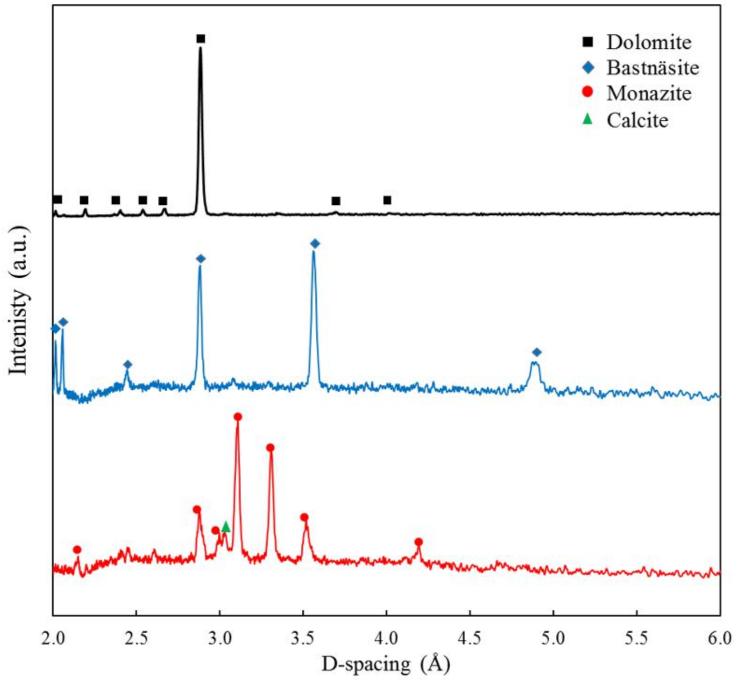

Figure 3.2 – X-ray diffractograms of dolomite, monazite and bastnäsite (Source: Co Kα, λ= 1.79 Å).

Table 3.1 – Elemental analysis (in wt %) of the mineral samples.

Minerals	**Al**	**Ca**	**Ce**	**Fe**	**La**	**Mg**	**Nd**	**P**
Dolomite	0.05	20.99	-	0.423	-	13.194	-	-
Monazite	0.48	1.10	8.00	0.405	4.64	0.041	5.41	10.24
Bastnäsite	0.202	0.31	13.55	0.292	13.44	0.014	6.92	0.43

3.3.2 Zeta potential

Zeta potential measurements of the minerals in the presence of 1×10^{-3} KCl demonstrate different IEPs for the 3 minerals (Figure 3.3a). The obtained IEP for dolomite, monazite and bastnäsite occur at around pH 5, pH 7 and pH 8, respectively. The obtained IEP values for monazite [3.21–3.23] and bastnäsite [3.16, 3.23, 3.24] agree with those reported in the literature. However, the IEP obtained for dolomite is slightly lower than reported in the literature [3.25–3.27]. This discrepancy could be due to differences in the mineral solubility, Ca/Mg content, and different sources of the mineral. Zeta potential of the minerals were also measured in the presence of different collectors – benzohydroxamate (BHA), sodium oleate (NaOl) and Flotinor 1682 (F1682). Figures 3.3b, 3.3c and 3.3d present the zeta potential of dolomite, monazite and bastnäsite, respectively. The zeta potential values of dolomite did not change significantly when conditioned with BHA. For monazite, the zeta potential has been changed substantially, especially at basic pH values. The IEP also shifted from ∼ pH 7 to ∼ pH 6. This trend was also observed for bastnäsite conditioned with BHA, where a marked change in zeta potential values was observed at basic pH values, and a shift in IEP from pH 8 to between pH 7 and 8. The presence of NaOl also significantly reduced the zeta potential of monazite and shifted the IEP from pH 7 to 4.5. For dolomite and bastnäsite, it can be seen the NaOl has also moved the zeta potential to more negative values. The same behavior with F1682-conditioned minerals, where a change of zeta potential to more negative values, was also observed.

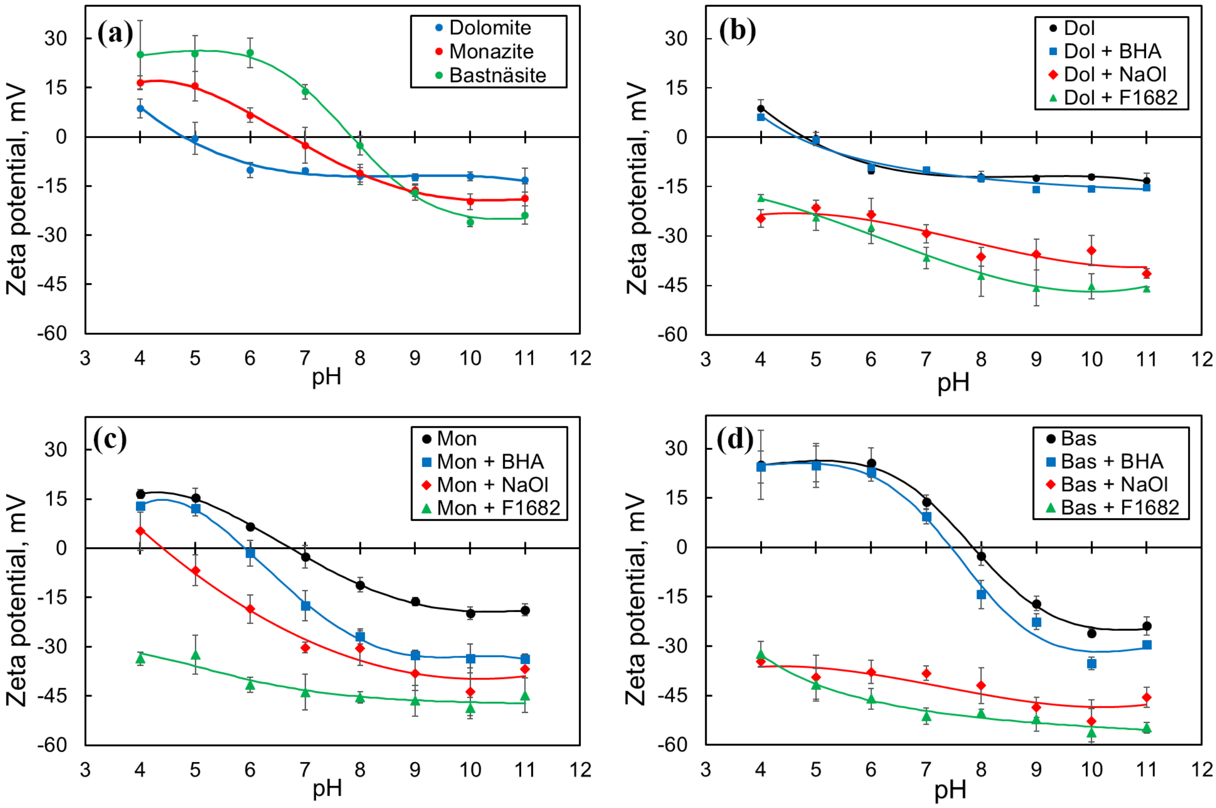

Figure 3.3 – Zeta potential of (a) the minerals in the presence of 1 × 10^{-3} M KCl; (b) dolomite; (c) monazite and (d) bastnäsite in the presence of different collectors.

3.3.3 ATR-FTIR spectra

The adsorption of the collectors (benzohydroxamate, sodium oleate and Flotinor 1682) on the surface of the minerals were also investigated using ATR-FTIR. The spectra of the collectors, the bare minerals, and the minerals conditioned with the collectors at different pH conditions were presented for comparison.

3.3.3.1 ATR-FTIR spectra in the presence of benzohydroxamate

The characteristic peaks are consistent with the spectra presented by Hadži and Prevoršek [3.28] and Al-Saadi [3.29]. The peaks at 1650 cm^{-1} and 1623 cm^{-1} could be assigned to C=O stretching from the amide group of BHA [3.29–3.32]. The shoulder at 1585 cm^{-1} and peak at 1490 cm^{-1} could be due to aromatic ring stretch [3.30]. The peak at 1623 cm^{-1}, 1490 cm^{-1} and the rest of the bands between 1605 cm^{-1} and 1315 cm^{-1} could be assigned to C–H in-plane bending [3.29]. The broad peak at 1560 cm^{-1} could be due to N–H bending and C–N stretching [3.32]. The doublets 1330 and 1315 cm^{-1} could also be attributed to O–H in-plane bending [3.28].

The spectra of the minerals conditioned with BHA is difficult to resolve which could be due to small amount of adsorbed BHA. Other researchers have encountered the same issue [3.33]. Therefore, the presented spectra are the difference of minerals conditioned with BHA and bare mineral surface; and are normalized within the range presented. The ATR-FTIR spectra of the dolomite, monazite and bastnäsite conditioned with BHA at different pH conditions are presented in Figure 3.4, 3.5, and 3.6, respectively. The spectra are presented as the difference between the bare mineral and mineral conditioned with BHA for easier analysis of collector adsorption. The spectrum of dolomite at pH 9 (Figure 3.4a) presents the exact characteristic peaks of BHA, which could indicate residual BHA not removed by washing. For monazite (Figure 3.4b), the presence of a new peak at 1605 cm^{-1} could be due to the formation of RE-hydroxamate [3.34]. This, along with the shifting of other BHA characteristic peaks, manifests chemical adsorption [3.35]. The occurrence of new band at 1265 cm^{-1} was assigned to C–N stretching and N–H bending [3.31], which indicate that these groups could be involved in the chemical reaction between BHA and monazite surface. Bastnäsite spectra (Figure 3.4c), also present the peak at around 1610 cm^{-1}, which is attributed to the presence of RE-hydroxamate [3.34]. The presence of the band at 1570 cm^{-1}, which was assigned to C–N stretching and N–H bending [3.31], supported the finding with BHA-conditioned monazite that these groups could be involved in the RE-hydroxamate interaction. The summary of the peaks assignment is presented in Table 3.2.

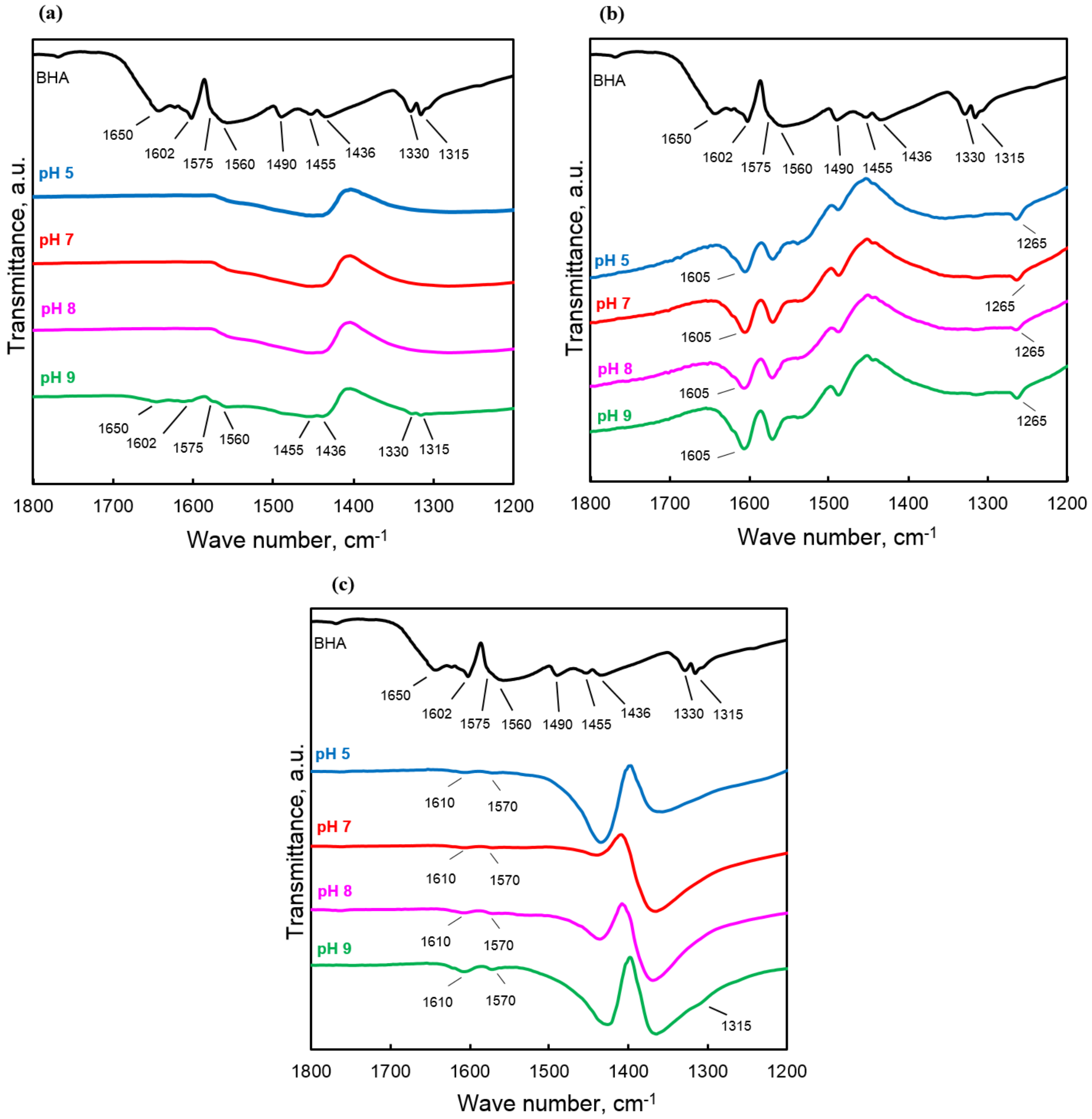

Figure 3.4 – ATR-FTIR spectra of BHA, and the difference between the spectra of the bare and the BHA-conditioned (a) dolomite, (b) monazite and (c) bastnäsite at different pH conditions.

Table 3.2 – Infrared bands of benzohydroxamate collector.

Wave number (cm^{-1})	Assignment
1650	C=O stretching, N–H in-plane bending
1623	C=O stretching, C–H in-plane bending
1602	C–H in-plane bending
1575	Aromatic ring stretching
1560	C–H in-plane bending, N–H bending and C–N stretching
1490	Aromatic ring stretching, C–H in-plane bending
1330	C–H in-plane bending, O–H in-plane bending
1315	C–H in-plane bending, O–H in-plane bending
1265	N–H bending and C–N stretching

3.3.3.2 ATR-FTIR spectra in the presence of sodium oleate

The characteristic bands of sodium oleate presented (Figure 3.5) at these ranges are similar to those reported in the literature [3.36–3.38]. The band at 3290 cm^{-1} is assigned to carboxylic O-H stretching [3.32]. The peaks 2920 cm^{-1} and 2850 cm^{-1} could be assigned to methylene (–CH_2–) C–H asymmetric and symmetric stretching, respectively [3.30, 3.38]; while, the higher peaks 2960 cm^{-1} and 2935 cm^{-1} could be attributed to methyl (–CH_3) C–H asymmetric stretching mode [3.30]. The transmittance band at 1559 cm^{-1} corresponds to asymmetric carboxylate stretching, while the region 1500 - 1400 cm^{-1} could be attributed to symmetric carboxylate vibrations [3.36]. The observed peaks at 1460 and 1445 cm^{-1} may be assigned to –CH_2– bending vibration, while the lower peak number, 1425 cm^{-1}, could be assigned to –COO^- stretching [3.36].

The peaks in the region 1500 - 1400 cm^{-1} were not observed in the spectra of dolomite conditioned with NaOl (Figure 3.5a), which may be due to the intense dolomite band masking these peaks at this region. The peaks between 2960 - 2850 cm^{-1} of dolomite conditioned with NaOl at the pH investigated correspond well with the characteristic peaks of NaOl, suggesting that NaOl has been adsorbed at the surface of dolomite. The peak at 1594 cm^{-1} is attributed to the asymmetric carboxylate stretching due to the formation of Mg-oleate at the surface [3.39]. It can also be observed that peaks 1575 and 1540 cm^{-1} appeared on the surface of dolomite conditioned with the collector. These peaks are attributed to the asymmetric carboxylate stretching vibration due to the presence of Ca-oleate from bulk precipitation [3.36, 3.38]. It can be seen that the intensity of these peaks becomes weaker as pH increases. Another band, 1710 cm^{-1}, appeared when dolomite was conditioned with NaOl at pH 5, which corresponds to C=O stretching vibration of carboxylic acid dimer [3.36–3.38]. The presence of the bands at 1170 - 1093 cm^{-1} may be due to CO_3^{2-} stretching vibration [3.40, 3.41] attributed to the presence of newly precipitated carbonate species.

The C–H stretching bands corresponding to sodium oleate were also observed on the NaOl- conditioned monazite samples (Figure 3.5b), indicating collector adsorption. As the conditioning pH increases, the intensity of these peaks become weaker. The same band at 1710 cm^{-1} for monazite conditioned at pH 5 and 7 was detected, which is attributed to the adsorption of carboxylic acid dimer [3.36, 3.38]. The peaks at 1465 cm^{-1} and 1412/1405 cm^{-1} were assigned to $–CH_2–$ symmetric bending vibration and $–COO^-$ symmetric stretching, respectively [3.36]. The shift of the peaks 1460 cm^{-1} (to 1465 cm^{-1}) and 1425 cm^{-1} (to 1412/1405 cm^{-1}) could indicate chemical nature of the interaction [3.32]. The appearance of the bands at 1550 and 1545 cm^{-1} is ascribed to the presence of RE-oleate at the surface [3.15], which also suggests chemical interaction.

Similar to dolomite, the peaks in the region 1500 - 1400 cm^{-1} were not observed in the spectra of bastnäsite (Figure 3.5c) which could be due to the intense bastnäsite band masking these peaks. The C–H stretching bands corresponding to NaOl was observed, indicative of the adsorption of the collector. The peak at around 1710 cm^{-1}, which was assigned to carboxylic acid dimer, was also observed on the NaOl-conditioned bastnäsite at pH 5 and 7. The strong peak of bastnäsite at around 1410 cm^{-1}, corresponding to CO_3^{2-} stretching vibrations [3.32, 3.40], was observed to be broader as the peak corresponding to NaOl becomes sharper (sharpest at pH 5). This indicates presence of more NaOl at the mineral surface, covering the bastnäsite surface (less surface exposure), hence a broader CO_3^{2-} band. The summary of the peaks assignment is presented in Table 3.3.

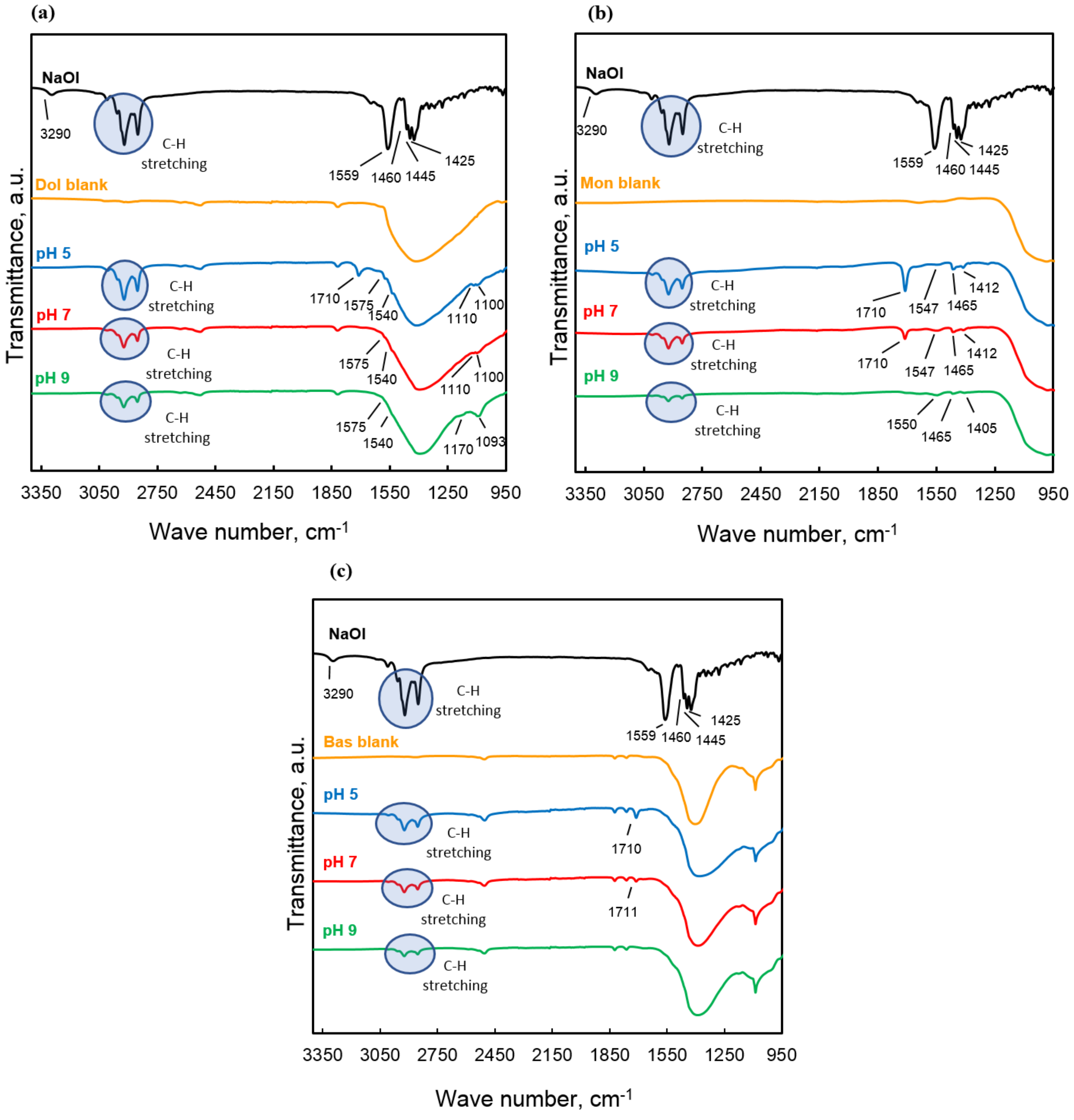

Figure 3.5 – ATR-FTIR spectra of NaOl, untreated (blank) and NaOl-conditioned (a) dolomite, (b) monazite and (c) bastnäsite at different pH conditions.

Table 3.3 – Infrared bands assigned to sodium oleate and metal-oleate species.

Wave number (cm^{-1})	Assignment
3290	Carboxylic O–H stretching
2960, 2935	C–H asymmetric stretching (–CH_3)
2920, 2850	C–H asymmetric/symmetric stretching (–CH_2–)
1710	Carboxylic acid dimer C=O stretching vibration
1597	Mg-oleate carboxylate asymmetric stretching
1575, 1540	Ca-oleate carboxylate asymmetric stretching
1559	Sodium oleate carboxylate asymmetric stretching
1550 - 1547	RE-oleate carboxylate asymmetric stretching
1460 - 1445	C–H bending vibration (–CH_2–)
1425 - 1405	Carboxylate asymmetric stretching (–CH_2–)
1170 - 1093	CO_3^{2-} stretching vibrations

3.3.3.3 ATR-FTIR spectra in the presence of Flotinor 1682

The ATR-FTIR spectra of the minerals conditioned with Flotinor 1682 (F1682) are presented in (Figure 3.6). The spectra were displayed from 2700 - 3100 cm^{-1} since the attempt to resolve the bands at 650 - 1900 cm^{-1} is rather difficult, which could be due to small amount of adsorbed collector and the masking of the characteristic peaks by the mineral bands at this range. The spectra were normalized within the range mentioned for easier comparison. The band at 2956 cm^{-1} could be assigned to methyl (–CH_3) C–H asymmetric stretching mode [3.30]. While the bands at 2926 cm^{-1} and 2870 cm^{-1} could be due to methylene (–CH_2–) C–H asymmetric and symmetric stretching, respectively [3.30]. The presence of these peaks at the surface of F1682-conditioned minerals indicate the existence of the said collector at the surface of the minerals. The shift of the characteristic peaks of F1682 such as 2956 and 2926 cm^{-1} could indicate a chemical nature of the interaction [3.32].

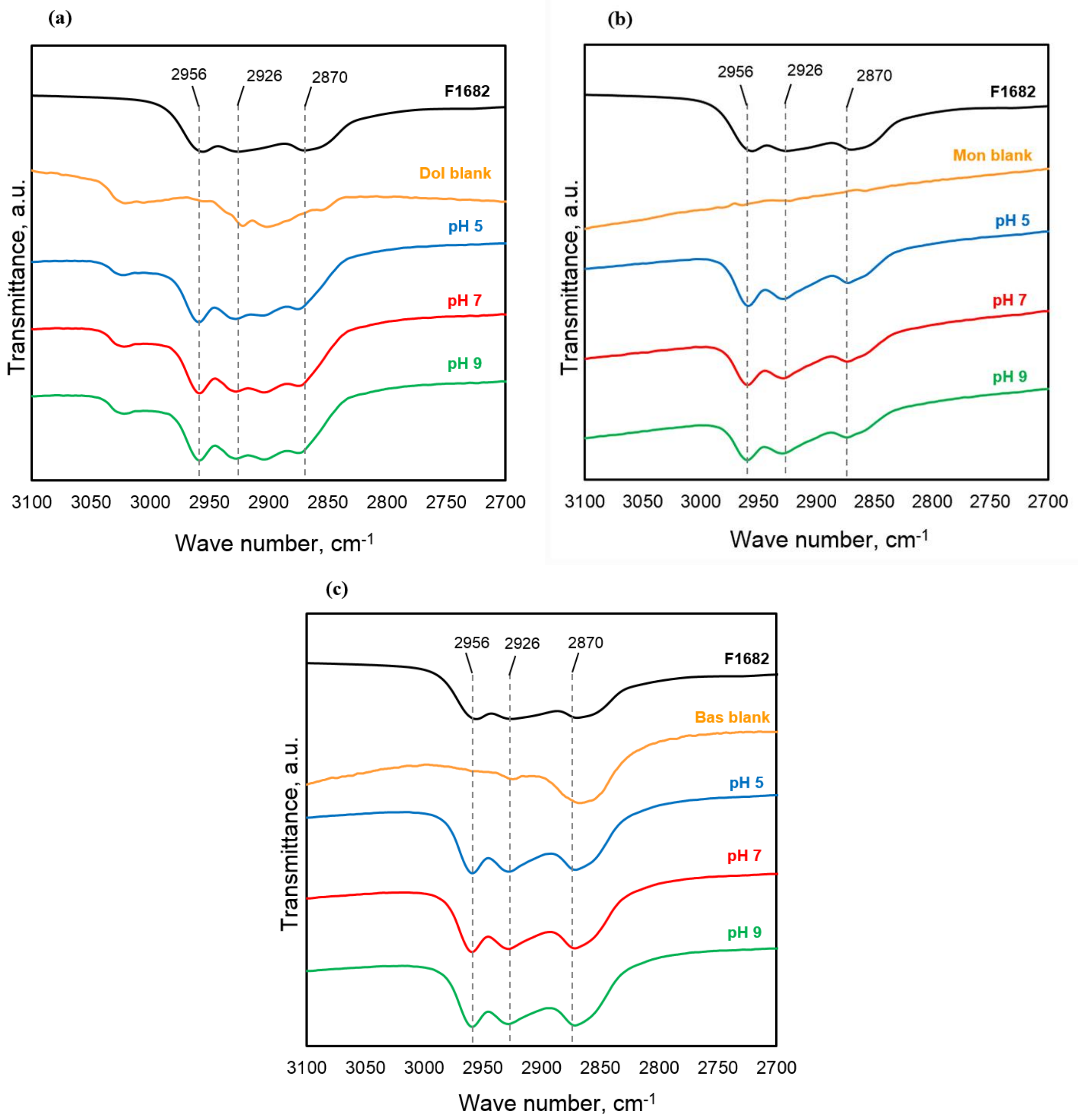

Figure 3.6 – ATR-FTIR spectra of F1682, untreated (blank) and F1682-conditioned (a) dolomite, (b) monazite and (c) bastnäsite at different pH conditions.

3.3.4 Flotation

Microflotation of the minerals in the presence of different concentrations of the benzohydroxamate, sodium oleate and Flotinor 1682 are presented in Figures 3.7a, 3.7b and 3.7c, respectively. The error bars represent 95% confidence interval; the fitted curves are inserted for enhanced visualisation and do not necessarily imply a model. It should be emphasized that the legend in Figure 3.7a-1, applies to Figure 3.7a-2 and Figure 3.7a-3; the legend in Figure 3.7b-3, applies to Figure 3.7b-1 and Figure 3.7b-2; and the legend in Figure 3.7c-1, applies to Figure 3.7c-2 and Figure 3.7c-2, respectively.

The presence of 170 mg/L and 250 mg/L BHA collector did not seem to affect dolomite's recovery (Figure 3.7a-1). However, when 330 mg/L BHA was used, the floatability increased slightly at certain pH values. For monazite, the highest recovery occurred in between pH 7 and 9 for the BHA concentrations investigated (Figure 3.7a-2). This is consistent with the findings of Cheng *et al.* [3.14]. The maximum recovery of bastnäsite can be found in between pH 8 and 10 (Figure 3.7a-3), which is similar to the results presented by Pavez *et al.* [3.15].

Sodium oleate collector seems to have higher collecting power than BHA as seen from the results presented in Figure 3.7b. Only 10 mg/L (or 3.3×10^{-5}M) of NaOl collector ($\ll$ 330 mg/L or 1.9×10^{-3}M BHA) yielded to a maximum of 99%, 99% and 98% recovery for dolomite, monazite and bastnäsite, respectively. It can be observed that the general trend in dolomite's recovery is decreasing with increasing pH condition, then starts to increase again at pH 11 (Figure 3.7b-1). This trend is similar to the work of Moudgil and Chanchani [3.42]. The recovery of monazite with NaOl collector has a maximum in pH between 5 and 8 (Figure 3.7b-2), which agrees with that presented in the literature [3.43]. The trend of bastnäsite's recovery (Figure 3.7b-3) is quite similar to that of monazite's, however, bastnäsite showed remarkable floatability at pH 4 as well as pH 8, compared to monazite.

In the presence of 5 mg/L Flotinor 1682, dolomite (Figure 3.7c-1) exhibits a relatively high degree of floatability at pH 4 to 8. Similar behavior was observed for flotation of bastnäsite using the same collector dosage (Figure 3.7c-2). By increasing the concentration to 7.5 mg/L and 10 mg/L, the recovery of dolomite and bastnäsite have significantly increased. For dolomite, a plateau was observed from pH 4 to pH 7, then a gradual decrease as pH increases further. For bastnäsite, the recovery plateaus from pH 4 to 9, then decreases abruptly at pH 10 and 11. Monazite flotation (Figure 3.7c-3) in the presence of 5 mg/L F1682 has already presented satisfactory recovery at pH 4 to 7, then diminishes at higher pH values. Increasing the collector concentration to 7.5 mg/L yielded the same monazite recovery at pH 4 to 7, and substantially improved the recovery at higher pH values. Increasing further the concentration resulted in almost 100% recovery at all pH values investigated.

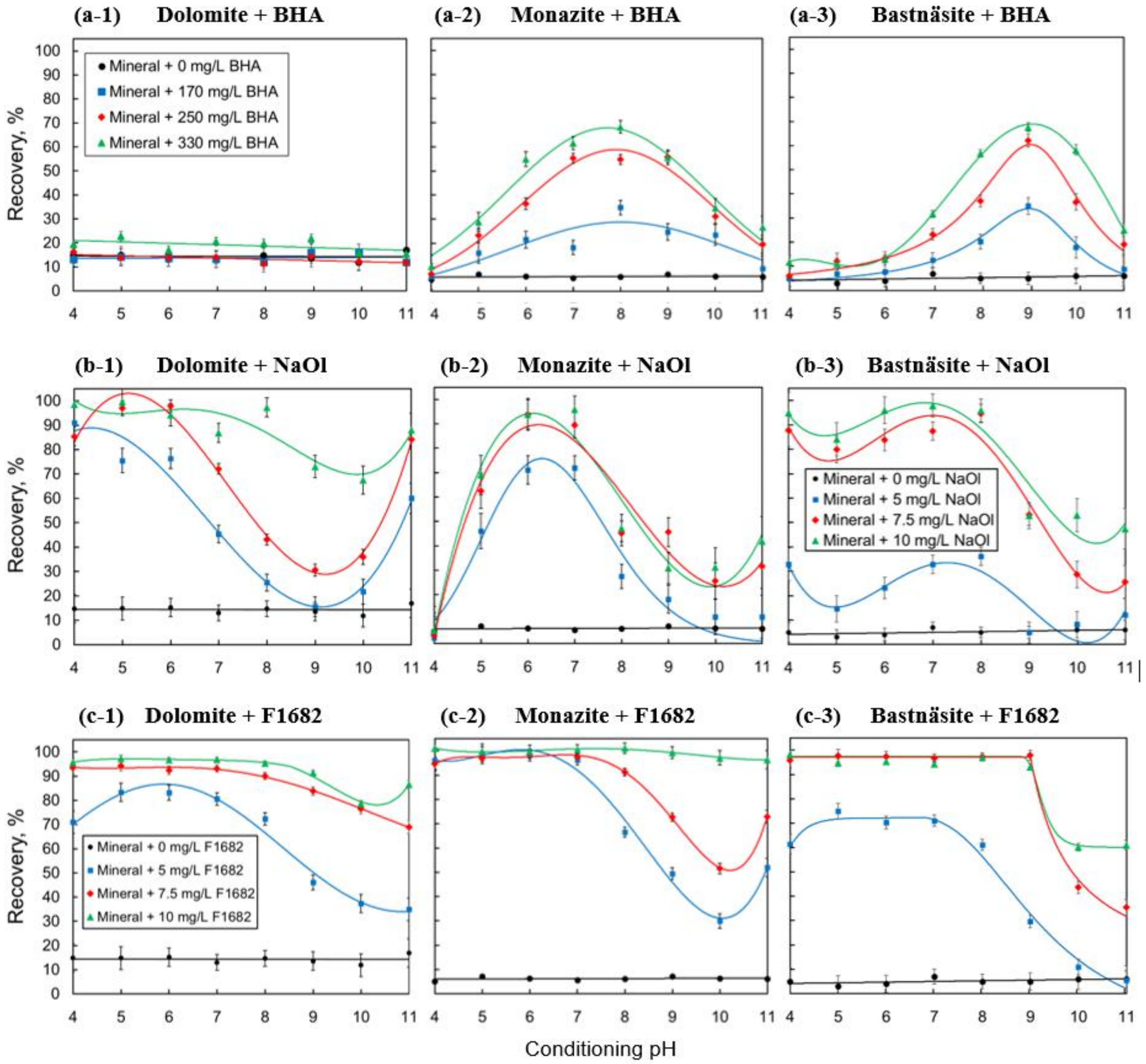

Figure 3.7 – Flotation of (1) dolomite, (2) monazite and (3) bastnäsite in the presence of (a) BHA, (b) NaOl and (c) F1682, respectively, as a function of conditioning pH.

3.4 Discussion

The adsorption of different collectors and the floatability of the dolomite, monazite and bastnäsite in the presence of these collectors at different pH conditions were investigated.

Different IEPs for each mineral were obtained from the zeta potential measurements in the presence of 1 × 10^{-3} M KCl. The IEP obtained for dolomite, which is around pH 5, is slightly lower than what was reported in the literature [3.25–3.27]. The discrepancy of the measured IEP could be due to differences in the mineral solubility, Ca/Mg content, and different sources of the deposit. The IEPs of monazite and bastnäsite occur at around pH 7 and 8, respectively. These values agree with the reported values for monazite [3.21–3.23] and bastnäsite [3.16, 3.23, 3.24], respectively.

3.4.1 Benzohydroxamate

The zeta potential changes in the absence or presence of BHA indicate the preferential adsorption of this collector to RE minerals over dolomite (Figure 3.3). This is corroborated by the flotation results (Figure 3.7a-1) which show that dolomite did not float significantly even with the presence of 330 mg/L BHA; while the RE minerals showed a maximum of 68% recovery using the same collector concentration (Figures 3.7a-2 and 3.7a-3). Since BHA has a bidentate group, HO–N–C=O, which is suitable for the formation of metal complexes [3.13], it is then classified as a chelating agent [3.18]. Thus, this behavior could be attributed to the different strengths of chelates formed when BHA interacts with the metal cations (RE metal - BHA > alkaline earth metal - BHA chelate) [3.13]. This was validated by ATR-FTIR spectra (Figure 3.4) showing the appearance of new peaks at 1605 and 1610 cm^{-1}, which was ascribed to complexation of BHA with metals from the mineral surface [3.30]. It was also observed that monazite and bastnäsite adsorbed significant amount of BHA at around the IEP and at pH above their IEP. Although the ATR-FTIR spectra of monazite (Figure 3.4b) do not present clearly this behavior, ATR-FTIR spectra (Figure 3.4c) of the BHA-conditioned bastnäsite can confirm this observation, which indicates that the adsorption of BHA occurs preferentially at pH 8 and 9. Flotation results also agree with these findings, which show that using 330 mg/L, monazite has significant recovery between pH 6 to 9, while bastnäsite has significant recovery between 7 to 11. This could be attributed to the dissociation of BHA occurring at around pH 8.8 (pKa)[3.44]. At pH above this value, dissociated BHA will be more dominant than molecular BHA. Since the chelation of BHA with the metal cation (from RE mineral) happens by the substitution of H^{+} by Ce^{3+} [3.45], the presence of more dissociated form of BHA would be more desirable for mineral – collector interaction. This behavior could also be due to the hydroxylation of RE cation (*e.g.*, Ce^{3+}) at these pH conditions (Figure 3.8). It is believed that the hydroxylated RE cations on the surface provides adsorption sites for BHA [3.46]. It can be observed that the flotation of monazite (see Figure 3.7b) corresponds well with the amount of $Ce(OH)^{2+}$ that can be formed when the mineral is in solution (see Figure 3.8), which also agrees with that in the literature [3.14]; while bastnäsite recovery (see Figure 3.7c) corresponds well with the amount of $Ce(OH)^{2+}$ and $Ce(OH)_2^+$.

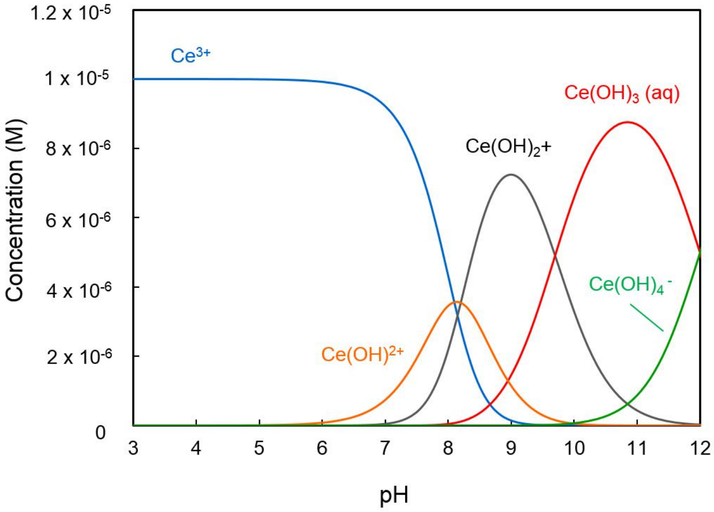

Figure 3.8 – Speciation of Ce^{3+} in aqueous solution (Ce^{3+} total concentration = 1×10^{-5} M).

3.4.2 Sodium oleate

NaOl has the form RCOONa, which can occur dominantly as $RCOO^-$ and $(RCOO)_2^{2-}$ at pH approximately above 4.95 and pH above 7, respectively. It can also exist as $H(OOCR)_2^-$ with a maximum at around pH 7.5 [3.47]. The presence of NaOl has made significant changes to the zeta potential of minerals, even at pH conditions where the minerals are negatively charged. It is reported at pH below the minerals' IEP, NaOl could adsorbed onto the minerals by physisorption [3.42, 3.48, 3.49]. This was also suggested by the ATR-FTIR spectra which shows the presence of oleate as a dimer at the IEP and lower pH. The formation of the dimer (RCOOH--HOOCR), which interacts with the mineral surface through physical adsorption, is attributed to strong intermolecular hydrogen bonding of the carboxylic acid [3.32]. At pH above the mineral's IEP, where the minerals are negatively charged, it can be deduced that negatively charged forms of NaOl adsorb onto the minerals through chemisorption. It has been proposed that metal cation (Me^{n+}) reacts with either $RCOO^-$ or $(RCOO)_2^{2-}$ forming $Me(OOCR)_n$ at the surface, rendering the minerals hydrophobic [3.49, 3.50]. For dolomite, it was suggested that $CaCO_3$ component dissolves faster than $MgCO_3$ component [3.51], suggesting that dolomite surface will be richer with Mg^{2+}, while the solution will be dominated by Ca^{2+}. From the speciation diagram (Figure 3.9), it can be seen that the amount of

Mg^{2+} corresponds well with the dolomite recovery in the presence of 5 and 7.5 mg/L NaOl (Figure 3.7b-1). It could also be presumed that some of the NaOl is being consumed by the dissolved Ca^{2+} forming $Ca(OOCR)_{2(s)}$ in the solution, which could adsorb back onto the dolomite surface as suggested by ATR-FTIR, thus rendering the surface hydrophobic. At a certain point, the bulk precipitated $Ca(OOCR)_2$ appears to prefer to remain in the solution rather than adsorb back to the surface, decreasing dolomite's floatability. As the pH increases further, the available Ca^{2+} decreases, leaving the $RCOO^-$ free to adsorb onto dolomite surface. Also, it could be inferred that formation of $Mg(OH)_2$ and $Ca(OH)_2$, which could adsorb at the surface of dolomite, plays an important role in the improvement of the recovery at pH 10 and 11. It has been proposed that $RCOO^-$ could replace one of the OH^- of $Mg(OH)_2$ and $Ca(OH)_2$, yielding hydrophobic Mg(OH)OOCR and Ca(OH)OOCR, respectively [3.52]. As the concentration of NaOl is increased to 10 mg/L, the significant decrease in the recovery was only observed after pH 9, which could be attributed to more available $RCOO^-$ for adsorption. So even with the formation of Ca-oleate in the solution, there are still enough oleate available (relative to Ca^{2+}) to be adsorbed onto the dolomite surface.

Monazite flotation with NaOl have a maximum recovery at pH between 5 and 8, which is consistent with the work of Pavez and Peres [3.43]. Similar work was conducted by Cheng *et al.* [3.14], which shows a maximum monazite recovery at pH between 3 and 10. It was noted that the amount of $Ce(OH)^{2+}$ corresponds well with the amount of monazite recovered. In this work, it appears that monazite recovery could be influenced by the presence of hydroxylated form of Ce^{3+}, but it is more likely that the recovery can be mostly attributed to the amount of Ce^{3+} (Figure 3.8) except at pH 4 and 5. At these pH conditions, the zeta potential curves suggested the adsorption of oleate dimer (physisorption) and the formation of Ce-oleate (chemisorption) on the surface of monazite. The observed increase in the recovery from pH 4 to 6 could then be due to the increase of the amount of $RCOO^-$, $(RCOO)_2^{2-}$ or $H(OOCR)_2^-$ in the solution and their electrostatic adsorption onto the monazite surface. Considering the flotation results, it would appear that at pH 4, the molecular form of NaOl is not significant in the monazite−NaOl interaction. If it does, then there should be a significant floatability even at pH 4; however, that is not the case. In contrast to monazite flotation, bastnäsite has a significant recovery at pH 4, which could be explained by physical adsorption of RCOOH and $H(OOCR)_2^-$ on the mineral's surface [3.49]. However, the floatability at pH 5 to 8, however, corresponds well with the amount of $RCOO^-$, $(RCOO)_2^{2-}$ and $H(OOCR)_2^-$ in the solution. It also appears that the amount of Ce^{3+} and $Ce(OH)^{2+}$ could have influence this behavior, similar to that of monazite.

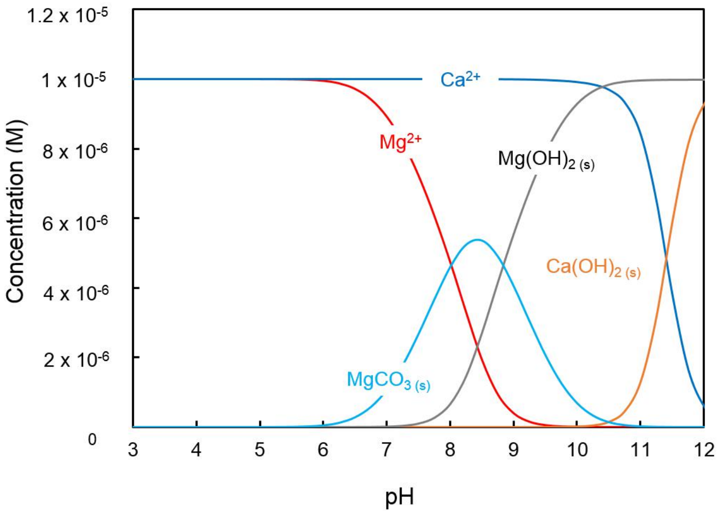

Figure 3.9 – Speciation of Ca^{2+} and Mg^{2+} in aqueous solution (Ca^{2+} total concentration = Mg^{2+} total concentration = 1×10^{-5} M).

3.4.3 Flotinor 1682

Flotinor 1682 (F1682) also present promising collecting capability with the 3 minerals being investigated. The actual structure of Flotinor 1682, a commercial phosphoric acid ester collector, is unknown. For this, a general and simple form of phosphoric acid ester, $ROPO_3H_2$, will be used in explaining the mechanism of collector adsorption. Figure 3.10 is presented for the graphical representation which could aid in some of the reactions that will be described. Zeta potential changes showed significant adsorption of F1682 onto the minerals' surface whether they are positively- or negatively-charged, indicating that adsorption could be driven by electrostatic forces or chemical bonding, respectively. However, ATR-FTIR spectra of F1682-conditioned minerals presented a slight shift of the F1682 characteristic peaks, suggesting a chemical nature of the interaction even at pH 5 (pH below the IEP of monazite and bastnäsite). Since phosphoric acid ester dissociates in the acidic pH condition, at pH below the minerals' IEP, monovalent collector anion ($ROPO_3H^-$) could be initially adsorbing electrostatically (see Figure 3.10a) followed by chemisorption (see Figure 3.10b). It is proposed that this species (and its family, phosphonic acid) can form a bidentate complex (see Figure 3.10c) with the metal cation, which is believed to be a stepwise process [3.53, 3.54]. It has been proposed that the $ROPO_3H^-$ anion initially adsorb onto the minerals through chemisorption (P–O forms covalent bond with the metal cation), followed by the dissociation of H^+. The second P–O from the collector forms coordinate bond with the same metal cation [3.53, 3.54]. It was also suggested that the bidentate complex could be formed even without the second dissociation of H^+, created by the covalent bond formed by P–O with the metal cation, and the coordinate bond from by P=O with the same metal cation [3.55]. As mentioned previously, the zeta potential and ATR-FTIR confirms the chemical nature of the interaction of F1682 with the minerals; however, they could not distinguish whether the complex structure formed agrees with the former or the latter. Other authors proposed that even the bidentate complex is just an intermediate product during the adsorption, and will eventually convert to binuclear complex [3.56] (see Figure 3.10d). In the presence of 5 mg/L F1682, it can be seen that dolomite and bastnäsite have similar behavior, where the floatability is maximum at around pH 5, followed by significant decrease after pH 8. Considering the $pKa_1 = 2.65$ and $pKa_2 = 5.21$ of F1682, which were determined in this work (see Appendix C), it is more likely that the reason for the maximum floatability at around pH 5 is the product of the second dissociation ($ROPO_3^{2-}$) of F1682, contrary to what was found by Hu and Xu [3.55] and Quin [3.19]. It could then be proposed that at pH 5 to 8, $ROPO_3^{2-}$ is the main species that adsorb onto the mineral surface forming either bidentate or binuclear complex, while the floatability at pH 4 could be due to the adsorption of $ROPO_3H^-$. The gradual decrease from pH 5 to 8 is highly due to the decrease in the amount of metal cations on the surface of dolomite and bastnäsite. Since the metal cations (Mg^{2+} and Ce^{3+}) start to decrease significantly from pH 7, the floatability at pH 8 could then be attributed to the presence of metal-hydroxy complex at the surface. When the collector approached these hydroxy complexes, they will interact initially by ion exchange (electron from O replaces OH^- of the hydroxy complex), then will be followed by the process of forming bidentate complex [3.54]. For monazite, when 5 and 7.5 mg/L F1682 were used, the high recovery at pH 4 was maintained until pH 7, then started decreasing as pH was increased further (slight increase at pH 11). This behavior corresponds well with the amount of Ce^{3+} as presented in the speciation diagram. However, when the concentration was increased further to 10 mg/L used, the floatability of monazite becomes independent of the amount of Ce^{3+} and pH.

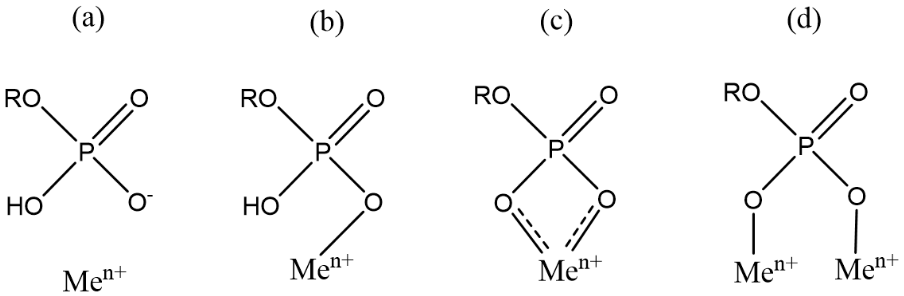

Figure 3.10 – Schematic of the collector (a) approaching the metal cation at mineral surface; (b) forming covalent bond with the metal cation; (c) forming bidentate complex and (d) forming binuclear complex.

3.4.4 Comparison of the 3 collectors

Based on the data obtained, BHA is the most selective of the 3 collectors investigated; this is attributed to the difference in the strength of the chelates that it can form with RE minerals and with dolomite [3.13]. NaOl and F1682 could also have some selectivity at certain pH values, but are both stronger collectors, compared to BHA, and these collectors also have an affinity to dolomite (gangue). The selectivity of the collectors could be explained by the polarity of O atoms involved in the collector – mineral interactions. Since the N atom from N–O of BHA is more electronegative than the C atom in C–O of NaOl, the O atom in N–O will be lesser negatively charged than O atom in C–O. In parallel, the C atom in C–O of NaOl is more electronegative than P atom in P–O of F1682, making O atom in P–O the most negatively charged. The negative charge of O atom reflects its electron cloud, thus the O atoms carrying the most electrons will be the most reactive, thus nonselective.

3.5 Conclusions

This work provides deeper understanding of the flotation behavior and adsorption mechanisms which will assist in developing effective RE mineral flotation schemes. The 3 collectors investigated form surface precipitates, rendering the minerals hydrophobic. Since the minerals are sparingly soluble in water, the adsorption of the collectors was found to be highly influenced by the presence of cations in solution. NaOl forms metal-oleate precipitates, which explains the floatability of the minerals with NaOl is mostly dependent on the amount of metal cations that are exposed at the surface of the minerals. BHA and F1682 have similar mechanisms of adsorption, which is the formation of surface complex either with the metal cation or the hydroxylated cation. Some of the proposed adsorption mechanisms agree with the mechanisms presented in the literature, however, this paper also presented additional and different perspective based on the results of this work.

The flotation performance correlates with the collectors' pKa values. It was observed that BHA performed better at around neutral to basic pH conditions, while F1682 and NaOl performed well between acidic to neutral pH. Although BHA could be the most effective collector among the 3, the differences in floatability between the RE minerals and dolomite using NaOl and F1682 could also be exploited to obtain some selectivity. Some process route to recover RE minerals in a mixed mineral flotation that could also be explored are:

1. Bulk flotation of bastnäsite and dolomite at pH 4 using 7.5 mg/L NaOl, leaving the monazite in the tailings. Followed by a selective flotation of bastnäsite by increasing

the pH of the concentrate slurry to around pH 8, leaving dolomite in the second tailings.

2. A reverse flotation of dolomite at pH 11 using 10 mg/L NaOl.
3. Flotation of both monazite and bastnäsite at pH around 6 or 7 using 7.5 mg/L NaOl in the presence of dolomite depressant such as carboxymethyl cellulose (CMC), ligno sulfonate, starch, *etc.*
4. Flotation of both monazite and bastnäsite at pH between 5 and 7 using 5 mg/L F1682 or at between pH 4 and 7 using 7.5 mg/L in the presence of dolomite depressant such as carboxymethyl cellulose (CMC), ligno sulfonate, starch, *etc.*

References

[3.1] Henderson, P. *General Geochemical Properties and Abundances of the Rare Earth Elements*, volume 2, pages 1–32. Elsevier, 1984.

[3.2] Gupta, C. and Krishnamurthy, N. Extractive metallurgy of rare earths. *International Materials Reviews*, 37(5):52, 1992.

[3.3] Fernandez, V. Rare-earth elements market: A historical and financial perspective. *Resources Policy*, 53(Supplement C):26–45, 2017.

[3.4] Matamec. Matamec Management Discussion and Analysis. Report, 2017.

[3.5] Castilloux, R. Rare Earth Market Outlook: Supply, Demand, and Pricing from 2016 through 2025. Adamas Intelligence, 2016.

[3.6] Hatch, G. TMR Advanced Rare-Earth Projects Index. Report, Technology Metals Research, 2015.

[3.7] Chen, Z. Global rare earth resources and scenarios of future rare earth industry. *Journal of Rare Earths*, 29(1):1–6, 2011.

[3.8] Jordens, A., Cheng, Y. P., and Waters, K. E. A review of the beneficiation of rare earth element bearing minerals. *Minerals Engineering*, 41:97–114, 2013.

[3.9] Bulatovic, S. M. Flotation of REO Minerals. In Bulatovic, S. M., Editor, *Handbook of Flotation Reagents: Chemistry, Theory and Practice*, pages 151–173. Elsevier, Amsterdam, 2010.

[3.10] Bulatovic, S. M. Collectors. In Bulatovic, S. M., Editor, *Handbook of Flotation Reagents*, pages 5–40. Elsevier, Amsterdam, 2007.

[3.11] Wills, B. A. and Finch, J. A. Froth Flotation. In Finch, J. A. and Wills, B. A., Editors, *Wills' Mineral Processing Technology*, pages 265–380. Butterworth-Heinemann, Boston, 8th edition, 2016.

[3.12] Zheng, X. and Smith, R. W. Dolomite depressants in the flotation of apatite and collophane from dolomite. *Minerals Engineering*, 10(5):537–545, 1997.

[3.13] Fuerstenau, M. Chelating Agents as Flotation Collectors. In Miller, J., Young, C., Kellar, J., and Free, M., Editors, *Innovations in Natural Resource Processing: Proceedings of the Jan. D. Miller Symposium*. 2005.

[3.14] Cheng, T. W., Holtham, P. N., and Tran, T. Froth flotation of monazite and xenotime. *Minerals Engineering*, 6(4):341–351, 1993.

[3.15] Pavez, O., Brandao, P. R. G., and Peres, A. E. C. Adsorption of oleate and octylhydroxamate on to rare-earths minerals. *Minerals Engineering*, 9(3), 1996.

[3.16] Jordens, A., Marion, C., Kuzmina, O., and Waters, K. E. Surface chemistry considerations in the flotation of bastnäsite. *Minerals Engineering*, 66–68:119–129, 2014.

[3.17] Ren, J., Wang, W., Luo, J., Zhou, G., and Tang, F. Progress of flotation reagents of rare earth minerals in China. *Journal of Rare Earths*, 21(1):1–8, 2003.

[3.18] Somasundaran, P. and Nagaraj, D. Chemistry and applications of chelating agents in flotation and flocculation. In *Reagents in the Minerals Industry*, pages 209–219. IMM London, 1984.

[3.19] Quin, L. D. *A Guide to Organophosphorus Chemistry*. John Wiley & Sons, New York, 2000.

[3.20] Delgado, À. V. *Interfacial Electrokinetics and Electrophoresis*. Marcel Dekker, Inc., New York, 2002.

[3.21] Cheng, T. W. Point of zero charge of monazite and xenotime. *Minerals Engineering*, 13(1):105–109, 2000.

[3.22] Harada, T., Owada, S., Takiuchi, T., and Kurita, M. A flotation study for effective separation of the heavy mineral sands. In *XVIII International Mineral Processing Congress*, volume 4, page 10, 1993.

[3.23] Houot, R., Cuif, J.-P., Mottot, Y., and Samana, J.-C. Recovery of rare earth mineral, with emphasis on flotation process. In *International Conference on Rare Earth Minerals and Minerals for Electronic Uses*, volume 70-72, pages 301–324. Trans Tech Publications, 1991.

[3.24] Luo, J. and Chen, X. Research into the recovery of high-grade rare-earth concentrate from Baotou Complex Iron Ores, China. *Mineral Processing and Extractive Metallurgy*, pages 663–675, 1984.

[3.25] Chen, G. and Tao, D. Effect of solution chemistry on flotability of magnesite and dolomite. *International Journal of Mineral Processing*, 74(1–4):343–357, 2004.

[3.26] Gallios, G. P. and Matis, K. A. *Flotation of Salt-Type Minerals*, pages 357–382. Springer Netherlands, Dordrecht, 1992.

[3.27] Predali, J. J. and Cases, J. M. Zeta potential of magnesian carbonates in inorganic electrolytes. *Journal of Colloid and Interface Science*, 45(3):449–458, 1973.

[3.28] Hadži, D. and Prevoršek, D. Infra-red absorption bands associated with the NH group—III: Hydroxamic acids and derivatives. *Spectrochimica Acta*, 10(1):38–51, 1957.

[3.29] Al-Saadi, A. A. Conformational analysis and vibrational assignments of benzohydroxamic acid and benzohydrazide. *Journal of Molecular Structure*, 1023(Supplement C):115–122, 2012.

[3.30] Coates, J. Interpretation of infrared spectra, a practical approach. *Encyclopedia of Analytical Chemistry*, 2000.

[3.31] Hope, G. A., Woods, R., Buckley, A. N., White, J. M., and McLean, J. Spectroscopic characterisation of n-octanohydroxamic acid and potassium hydrogen n-octanohydroxamate. *Inorganica Chimica Acta*, 363(5):935–943, 2010.

[3.32] Stuart, B. *Infrared Spectroscopy: Fundamental and Applications.* John Wiley & Sons, Ltd, Chichester, UK, 2004.

[3.33] Li, M., Gao, K., Zhang, D., Duan, H., Ma, L., and Huang, L. The influence of temperature on rare earth flotation with naphthyl hydroxamic acid. *Journal of Rare Earths*, 2017.

[3.34] Cui, J., Hope, G. A., and Buckley, A. N. Spectroscopic investigation of the interaction of hydroxamate with bastnaesite (cerium) and rare earth oxides. *Minerals Engineering*, 36:91–99, 2012.

[3.35] Zhang, W., Honaker, R. Q., and Groppo, J. G. Flotation of monazite in the presence of calcite part I: Calcium ion effects on the adsorption of hydroxamic acid. *Minerals Engineering*, 100:40–48, 2017.

[3.36] Gong, W., Parentich, A., Little, L., and Warren, L. Adsorption of oleate on apatite studied by diffuse reflectance infrared Fourier transform spectroscopy. *Langmuir*, 8(1):118–124, 1992.

[3.37] Ince, D., Johnston, C., and Moudgil, B. Fourier transform infrared spectroscopic study of adsorption of oleic acid/oleate on surfaces of apatite and dolomite. *Langmuir*, 7(7):1453–1457, 1991.

[3.38] Labidi, N. S. and Iddou, A. Adsorption of oleic acid on quartz/water interface. *J. Saudi Chem. Soc*, 11(2):221–234, 2007.

[3.39] Brandąo, P. R. G. *Adsorption of oleate on magnesite and its influence on flotation.* PhD Thesis, University of British Columbia, 1982.

[3.40] Botha, A. and Strydom, C. A. DTA and FT-IR analysis of the rehydration of basic magnesium carbonate. *Journal of Thermal Analysis and Calorimetry*, 71(3):987–996, 2003.

[3.41] Koroleva, L. F., Larionov, L., and Gorbunova, N. Biomaterial based on doped calcium carbonate-phosphate for active osteogenesis. *Journal of Biomaterials and Nanobiotechnology*, 3(2):226, 2012.

[3.42] Moudgil, B. and Chanchani, R. Selective flotation of dolomite from apatite using sodium oleate as the collector. In *SME-AIME Annual Meeting*, 1983.

[3.43] Pavez, O. and Peres, A. Flotation of monazite-zircon-rutile with sodium oleate and hydroxamates. In *XVIII International Mineral Processing Congress*, volume 4, pages 1007–1012, 1993.

[3.44] Bonnitcha, P. D., Kim, B. J., Hocking, R. K., Clegg, J. K., Turner, P., Neville, S. M., and Hambley, T. W. Cobalt complexes with tripodal ligands: implications for the design of drug chaperones. *Dalton Transactions*, 41(37):11293–11304, 2012.

[3.45] Agrawal, Y. Hydroxamic acids and their metal complexes. *Russian Chemical Reviews*, 48(10):948, 1979.

[3.46] Pradip, P. and Fuerstenau, D. The adsorption of hydroxamate on semi-soluble minerals. Part I: Adsorption on barite, calcite and bastnaesite. *Colloids and Surfaces*, 8(2):103–119, 1983.

[3.47] Somasundaran, P. and Ananthapadmanabhan, K. Solution chemistry of surfactants and the role of it in adsorption and froth flotation in mineral-water systems. *Solution Chemistry of Surfactants*, 2:17–38, 1979.

[3.48] Predali, J. J. Flotation of carbonates with salts of fatty acids: role of pH and the alkyl chain. *Transactions of the Institution of Mining and Metallurgy*, 78:C140–C147, 1969.

[3.49] Wang, C.-H., Qiu, X.-Y., Hu, Z., and Tong, X. Study on the flotation mechanism of bastnaesite by sodium oleate. *Chinese Rare Earths*, 34(6):24–30, 2013.

[3.50] Fuerstenau, M. and Miller, J. D. The role of the hydrocarbon chain in anionic flotation of calcite. *Transactions of the AIME*, 238(2):153–160, 1967.

[3.51] Busenberg, E. and Plummer, L. N. The kinetics of dissolution of dolomite in CO_2-H_2O systems at 1.5 to 65 °C and 0 to 1 atm $p\mathrm{CO}_2$. *American Journal of Science*, 282(1):45–78, 1982.

[3.52] Paterson, J. G. *The adsorption of sodium oleate on metal hydroxide.* PhD Thesis, McGill University, 1970.

[3.53] Das, B. and Naik, P. K. Electrokinetics, adsorption and floatation studies of sphalerite using DI (2-ethyl hexyl) phosphoric acid. *Canadian Metallurgical Quarterly*, 43(3):355–362, 2004.

[3.54] Kuys, K. J. and Roberts, N. K. In situ investigation of the adsorption of styrene phosphonic acid on cassiterite by FTIR-ATR spectroscopy. *Colloids and Surfaces*, 24(1):1–17, 1987.

[3.55] Hu, Y. and Xu, Z. Interactions of amphoteric amino phosphoric acids with calcium-containing minerals and selective flotation. *International Journal of Mineral Processing*, 72(1–4):87–94, 2003.

[3.56] Gong, G., Han, Y., Liu, J., Zhu, Y., Li, Y., and Yuan, S. In situ investigation of the adsorption of styrene phosphonic acid on cassiterite (110) surface by molecular modeling. *Minerals*, 7(10):181, 2017.

Chapter 4

Dolomite depressants

This chapter details the investigation of several dolomite depressants such as citric acid, sodium carbonate, carboxymethylcellulose, starch, lignosulfonate and biopolymer. As Chapter 3 presents that sodium oleate and Flotinor 1682 were not as selective as benzohdroxamate and were able to float dolomite (gangue), this work then focuses on the possible depression of dolomite using sodium oleate and Flotinor 1682 as collectors.

Abstract

Hydroxamates are currently the most promising rare earth mineral collector due to their selectivity for these minerals; however, they are costly and require significant volume to recover sufficient rare earth minerals. Carboxylate (such as sodium oleate) and organic phosphoric acid collectors are a more economical alternative; however, their low selectivity is a challenge. In this regard, additional reagents to depress associated carbonatite gangue minerals such as calcite and dolomite are required. In this study, the effect of various depressants including sodium carbonate, citric acid, starch, carboxymethylcellulose, lignosulfonates and F-100 on dolomite flotation were investigated through single-mineral microflotation. Zeta potential measurements and ATR-FTIR spectroscopy were also conducted to elucidate the depressant behavior. Several depressants, mostly polymeric type, were found to have superior depressing ability than others. The effect of carboxymethylcellulose, which presented the best dolomite depressing power, with rare earth minerals (*e.g.,* monazite and bastnäsite) were also investigated. The findings indicated that a balance between depressant and collector concentration must be achieved to obtain an acceptable selectivity. Moreover, the effectiveness of the depressant is found to be highly dependent on the collector's chemistry.

4.1 Introduction

Flotation of rare earth (RE) minerals such as bastnäsite and monazite is possible using carboxylate, phosphoric acid, and hydroxamate collectors. Among them, the most promising are hydroxamates, as they are the most selective due to their formation of strong chelates with RE cations over the typical gangue cations. Researchers have thus started exploring these type of collectors, however, they are costly and require significant dosage to be effective [4.1]. The use of carboxylic and phosphoric acid collectors has also been a challenge due to the collectors' low selectivity (see Chapter 3), with the addition of modifiers required for effective separation. Most of the RE minerals come from deposits associated with carbonatites [4.2]; typical modifiers that are used to depress these carbonate gangue such as calcite and dolomite include sodium carbonate, starch and carboxymethylcellulose [4.3].

Electrokinetic studies revealed that sodium carbonate species affect the zeta potential of barite and calcite more than bastnäsite [4.4], making it a potential depressant for these gangue minerals. However, others found that at a certain sodium carbonate concentration, bastnäsite is more affected than calcite and barite, depressing the RE mineral instead [4.5]. Recent work also reported that sodium carbonate affected the electrokinetic properties of dolomite, monazite and bastnäsite differently at different pH conditions, which was suggested to indicate different flotation responses (see Chapter 3).

The use of citric acid as a depressant is due to its ability to form weak complexes with metal cations such as Ca, Mg, Fe, and Cu, *etc.* [4.3, 4.6], making it a potential candidate for dolomite depression. In addition, this reagent was recently used to reduce the depression of RE minerals caused by Al ions present in solution [4.6]. Lignosulfonate is another type of depressant that has been investigated with gangue minerals associated with RE minerals such as barite and calcite [4.4, 4.5].

Starch is a popular polymer depressant of calcite and dolomite in phosphate flotation. Flotation of calcite and dolomite with sodium oleate has been shown to decrease significantly in the presence of starch [4.7–4.9]. Carboxymethyl cellulose (CMC), another polymer depressant which is made from reed and rice straw, has also been investigated as a depressant for calcium-bearing, magnesium-bearing minerals and RE minerals [4.3]. It was found that CMC preferentially depresses calcite and fluorite and works as a depressant for dolomite too [4.3, 4.10]. Biopolymers are also of interest in clay depression during copper-gold flotation [4.11, 4.12]. It was found that a lignosulfonate-based biopolymer, Pionera

F-100, improved the copper flotation recovery by reducing the effects of the clay minerals present in the pulp. Pionera (USA) mentioned that this specific type of biopolymer is applicable to calcite and barite depression [4.13].

In this work, potential dolomite depressants such as citric acid, lignosulfonate and a lignosulfonate-based biopolymer as well as those that have already been proven to work with either calcite or dolomite (or both) such as sodium carbonate, starch and CMC are investigated in the presence of NaOl and F1682 as collectors. The performance of each depressant is evaluated through flotation tests at pH 6 and 7. These conditions were chosen based from the detailed flotation studies of dolomite with sodium oleate and organic phosphoric acid presented recently (see Chapter 3). The flotation results are elucidated through zeta potential measurements and attenuated total reflectance Fourier transform infrared (ATR-FTIR) spectroscopy.

4.2 Materials and methods

4.2.1 Materials

Dolomite from Sterling Hill Mine (New Jersey, USA) was purchased from Ward's Science (USA). Monazite from Eureka Farm 99 (Namibia) was purchased from Mineralogical Research Company (USA). Bastnäsite was provided by African Rare Earths (Pty.) Ltd. (South Africa). These minerals are relatively pure as shown from previous characterization test (see Chapter 3). The purity of the samples obtained from Rietveld analysis were at least 95%.

The potassium chloride that was used as a supporting electrolyte was purchased from Sigma-Aldrich (Canada); the hydrochloric acid and the potassium hydroxide that were used as pH modifiers were obtained from Fisher Scientific (Canada).

Sodium oleate was purchased from Fisher Scientific (Canada); and Flotinor 1682, a commercial organic phosphoric acid collector, was obtained from Clariant (Canada). The depressants' information is as follows:

- Anhydrous sodium carbonate, Na_2CO_3, was obtained from Fisher Scientific (Canada).
- Anhydrous citric acid, $C_6H_8O_7$, was purchased from Acros (USA).
- Soluble starch (density of 1.0384 g/cm^3) was provided by Fisher Scientific (Canada).

- CMC (sodium salt), a completely water-soluble polymer (not an ion exchanger) has a high viscosity of 1500 - 3000 cps if prepared at 1% aqueous solution at 25 °C. This reagent was purchased from Sigma Chemical Company (USA). The information on MW was not presented, only the viscosity.
- The lignosulfonate (sodium salt) used, which was obtained from Sigma-Aldrich (Canada), has a weight average molecular weight (MW) of ~52,000 and a number average molecular weight (MN) of ~7,000.
- Pionera F-100, a lignosulfonate-based biopolymer, was provided by Pionera (USA).

4.2.2 Zeta potential measurements

The minerals' particle size (D_{50}) of 2.3 μm was determined using a Horiba Laser Scattering Particle Size Distribution Analyzer LA-920 (ATS Scientific Inc., Canada). The zeta potential measurements were conducted using a NanoBrook 90Plus Zeta Particle Size Analyzer (Brookhaven Instruments, USA). One (1) mg of each mineral was placed in a 20-mL glass container. Five (5) mL of pH-preadjusted depressant solution was added to the sample. The pH was adjusted by the addition of HCl and KOH. The suspension was ultrasonicated for 30 s to ensure particle dispersion and was allowed to condition for another 30 s prior to further addition of 5 mL pH-preadjusted 1×10^{-3} M KCl background electrolyte or collector solution. The mineral suspension was then conditioned for a further 60 s before the zeta potential was measured.

4.2.3 ATR-FTIR spectroscopy

Attenuated total reflectance Fourier transform infrared (ATR-FTIR) spectroscopy was conducted with the original dolomite samples and those conditioned with the depressants, using a PerkinElmer Spectrum 400 (Perkin Elmer, USA). The samples were washed 3 times with pH adjusted deionised water, then dried in a vacuum oven at ambient temperature prior to measurements being taken. The IR transmittance spectra were obtained by passing 32 scans, between 4000 and 650 cm^{-1}, with a resolution of 4 cm^{-1}. The obtained spectra were baseline corrected and were normalized to the total surface area under the transmittance bands using PerkinElmer Spectrum software (Perkin Elmer, USA).

4.2.4 Microflotation

Dolomite, monazite and bastnäsite samples used in flotation tests, with a particle size range -106+38 μm, have BET surface areas equal to 0.05 m^2/g, 0.15 m^2/g and 0.11 m^2/g, respectively. The tests were conducted using a modified Hallimond tube, with a volume of approximately 170 mL. The glass cell has three parts - the lower part has a silicate frit at the bottom; the extensor part connects the lower part and the upper part; and the upper part is where the floated fractions can be collected. One (1) gram of mineral sample was placed in a beaker with 30 mL deionised water (adjusted to desired pH). The suspension was agitated using a magnetic stirrer to ensure that the mineral particles are properly mixed and remained suspended. The pH of the suspension was adjusted prior to addition of the depressant and was maintained during the 2-minute conditioning period. Collector was then added, and the suspension was conditioned for an additional 5 minutes. It was then transferred to the cell and 140 mL of pH adjusted water was added. Air was introduced through the cell at a flowrate of 40 mL/min. Flotation was conducted for 1 minute with the floated and non-floated fractions were collected, filtered, dried and weighed to calculate the recovery.

4.3 Results

4.3.1 Zeta potential

The zeta potential of dolomite in the presence of different depressants (Figure 4.1) was measured at pH 6 and pH 7 using NaOl and F1682 as collectors. The error bars represent 95% confidence interval. For values where the error bars overlap, Student's *t*-test was carried out to determine whether the difference was significant or not.

The zeta potential of dolomite conditioned with sodium carbonate is presented in Figure 4.1a. It can be observed that addition of sodium carbonate has increased the zeta potential of dolomite (blank) at pH 6 and 7. The addition of collectors (both NaOl and F1682) onto the carbonate-conditioned dolomite made the zeta potential more negative, indicating that the collectors still adsorb onto the dolomite surface even in the presence of sodium carbonate. It can be seen that at pH 6 the zeta potential of dolomite conditioned with only NaOl is comparable to that conditioned with sodium carbonate prior to addition of NaOl (labeled as Depressant + NaOl). Conversely, at pH 7, the zeta potential of dolomite with depressant and NaOl is less negative than that of only NaOl.

Citric acid made the zeta potential of dolomite more negative at pH 6 and 7 (Figure

4.1b). The addition of NaOl or F1682 to the depressant-conditioned dolomite made the zeta potential more negative. However, this is not the case when NaOl was added at pH 6 to the depressant-conditioned dolomite, where the zeta potential was maintained. The presence of collectors affected the zeta potential of virgin dolomite and depressant-conditioned dolomite differently. However, at pH 7, the addition of F1682 is similar for both virgin and depressant-conditioned dolomite.

In the presence of starch (Figure 4.1c), the zeta potential of dolomite at pH 6 increased, but was not affected at pH 7. It can also be observed that the addition of NaOl to the starch-conditioned dolomite did not affect its zeta potential, but the addition of F1682 did for both pH 6 and 7. For the cases with F1682, the zeta potential corresponding to depressant + F1682 is similar to the zeta potential when dolomite was added with only F1682. This could indicate that the zeta potential observed was mainly due to the zeta potential of dolomite with F1682 but not the depressant.

In Figure 4.1d, the presence of CMC reduced the zeta potential of dolomite. The addition of both collectors at pH 6 and 7 did not affect the zeta potential of dolomite. The same behavior was observed with lignosulfonate (Figure 4.1e) and F-100 (Figure 4.1f). For these 3 depressants, the zeta potential difference when NaOl is added onto bare dolomite and depressant-conditioned dolomite is statistically significant. However, in the case of F1682, this is only observed at pH 6 and not at pH 7.

The use of CMC in flotation (discussed in Section 4.3.3) revealed that CMC has the best depressing effect considering the concentration and pH investigated. Therefore, further zeta potential measurements to explore whether monazite and bastnäsite could also be affected by this depressant were conducted and are presented in Figure 4.2. The zeta potential of monazite (Figure 4.2a) became negative in the presence of CMC at pH 6 and 7. When the CMC-conditioned monazite was added with NaOl (labeled CMC + NaOl), the zeta potential became less negative, both at pH 6 and 7. When it was added with F1682 (labeled CMC + F1682), the zeta potential became more negative at pH 6 and was maintained at pH 7. The presence of CMC has also made the zeta potential of bastnäsite negative (Figure 4.2b). It can be observed that the addition of NaOl (labeled CMC + NaOl) did not change the zeta potential of the CMC-conditioned bastnäsite, however, the addition of F1682 (labeled CMC + F1682) made the zeta potential more negative. This may indicate that CMC also adsorb on the surfaces on monazite and bastnäsite. The decrease in the zeta potential after addition of F1682 to the CMC-conditioned monazite (only at pH 6) and bastnäsite may also indicate that F1682 could still adsorb on the surface of these minerals.

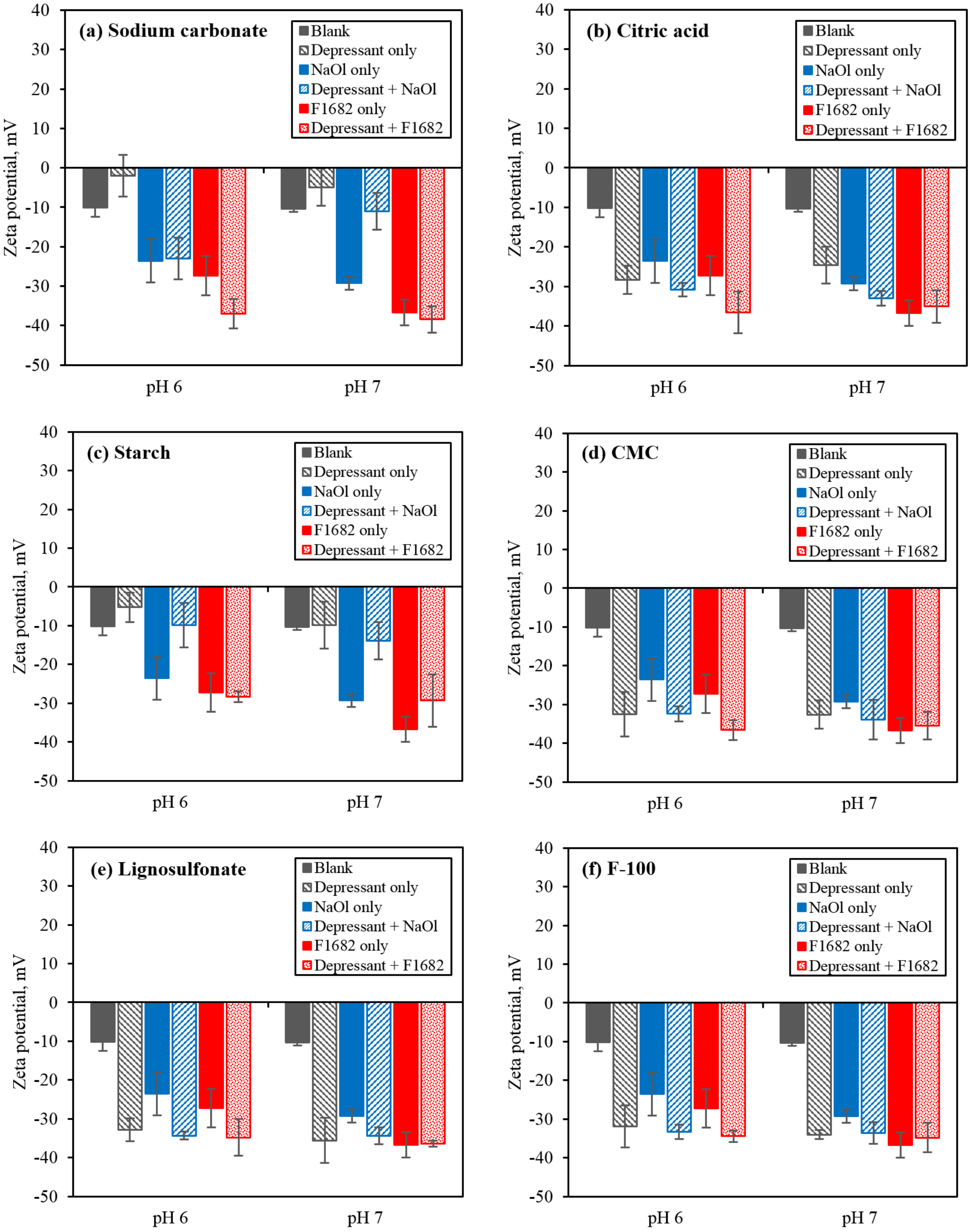

Figure 4.1 – Zeta potential of dolomite in the presence of depressants and collectors (NaOl and F1682) at pH 6 and 7.

For CMC-conditioned monazite, the increase in the zeta potential after addition of NaOl might also indicate NaOl adsorption given that the zeta potential measured is between that of CMC-conditioned and NaOl-conditioned monazite. However, no logical inference can be drawn regarding NaOl adsorption on bastnäsite from only the zeta potential considering the measurements with NaOl only, CMC only and CMC + NaOl, since the three of them have the same values.

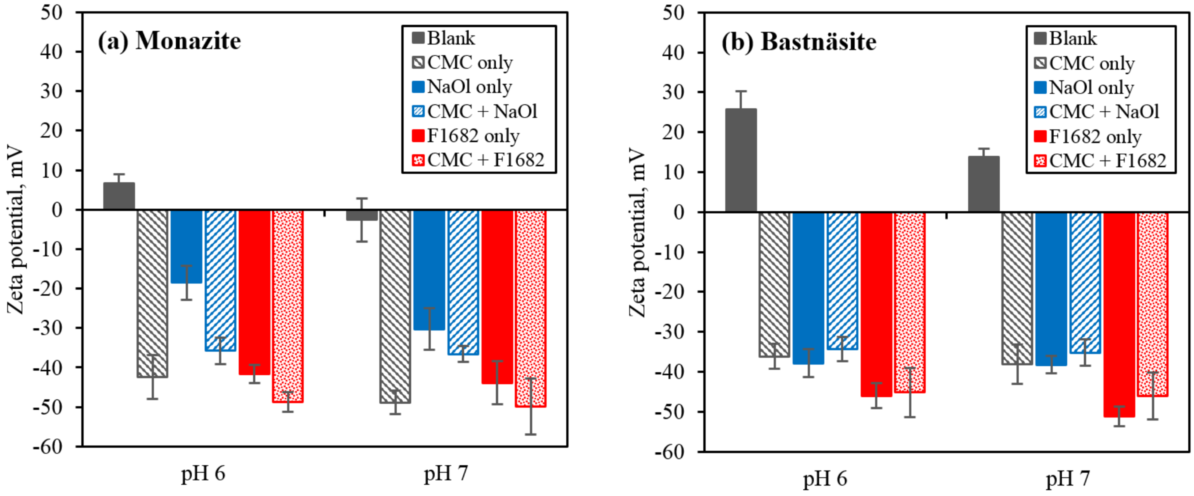

Figure 4.2 – Zeta potential of (a) monazite and (b) bastnäsite in the presence of CMC and collectors (NaOl and F1682) at pH 6 and 7.

4.3.2 ATR-FTIR spectroscopy

The structure of each depressant with the exception of F-100 is presented in Figure 4.3 to guide the reader when discussing the peaks. The ATR-FTIR spectra of the solid depressants (1), the original dolomite mineral (2), the dolomite conditioned with the depressant at pH 6 (3) and pH 7 (4) are presented in Figure 4.4. Most of the spectra of the depressant-conditioned dolomite is difficult to resolve, which could be due to small amount of adsorbed depressant and the masking of the depressant peaks by the dolomite peaks. As such, the difference between depressant-conditioned dolomite spectra and the original dolomite spectra is also presented. For these cases, the spectra are normalized within the range presented to identify the peaks clearer. Since the purpose of the ATR-FTIR spectroscopy in this study was to identify possible adsorption of the depressant at the surface of dolomite, only the important peaks which could be involved in the adsorption process will be defined. Dolomite characteristic peaks located at 1416 cm^{-1} and 876 cm^{-1} are assigned to asymmetric CO_3 stretching and deformation, respectively [4.14].

The sodium carbonate (Figure 4.4a) bands at 1423 cm^{-1} and 878 cm^{-1} can be assigned to asymmetric CO_3 stretching and deformation, respectively [4.14, 4.15]. The difference of the spectra between the depressant-conditioned dolomite presented bands at 1373 cm^{-1} (pH 6), 1382 cm^{-1} (pH 7) and 873 cm^{-1}, which could be due to the formation of new carbonate species at the surface of conditioned dolomite (see Chapter 5).

The ATR-FTIR of aqueous citric acid presented by Siriwardane [4.16] consists of the characteristic bands at pH 5.5 and 7.5: 1570 cm^{-1}, 1391 cm^{-1} (asymmetric and symmetric carboxylate stretching, respectively) and 1280 cm^{-1} (coupled carboxylate stretching and bending). In the ATR-FTIR of solid citric acid (Figure 4.4b), bands occurred at 1740 cm^{-1} and 1684 cm^{-1}, which could be assigned to C=O stretching [4.16]. There are also bands at 1590 cm^{-1} and 1389 cm^{-1} which are attributed to asymmetric and symmetric carboxylate stretching. The band at 1293 cm^{-1} could be due to coupled carboxylate stretching and bending. In the spectra of depressant-conditioned dolomite, 1293 cm^{-1} could be masked by the carbonate peak. The band at 1590 cm^{-1} is weakly observed. The other 2 bands are not distinct which could be due to a small amount of citric acid present at the surface.

Solid starch (Figure 4.4c) presented bands at 1150 cm^{-1} which could be due to C–O, C–C and C–O–H stretching. The band at 1077 and 995 cm^{-1} could be attributed to C–O–H bending [4.17]. These characteristic peaks are also present in the starch-conditioned dolomite, indicating depressant adsorption.

CMC (Figure 4.4d) presented bands at 1587 cm^{-1}, 1406 cm^{-1}, 1050 cm^{-1} corresponding to carboxyl (C=O stretching), methyl (C–H stretching) and hydroxyl (C–O symmetric stretching) functional groups [4.18, 4.19]. The bands at 1587 cm^{-1} and 1050 cm^{-1} were observed on the CMC-conditioned dolomite at pH 6 and 7.

The bands at 1595 cm^{-1}, 1510 cm^{-1}, and 1454 cm^{-1} presented by sodium lignosulfonate (Figure 4.4e) are assigned to C=C benzene ring vibration. The band at 1421 cm^{-1} could be attributed to C–H in plane deformation with aromatic ring stretching. The peaks at 1167 cm^{-1} and 1142 cm^{-1} are assigned to asymmetric and symmetric SO_2 vibrations, respectively. The band at 1035 cm^{-1} corresponds to C–O vibration of aliphatic OH [4.20].

The bands of F-100 (Figure 4.4f) are quite similar to those of lignosulfonate (Figure 4.4e). The peaks at 1591 cm^{-1}, 1510 cm^{-1}, and 1451 cm^{-1} are also assigned to C=C benzene ring vibration. The peak at 1419 cm^{-1} could be due to C–H in plane deformation with aromatic ring stretching. The peaks at 1183 cm^{-1} and 1135 cm^{-1}, which are slightly shifted compared to those of lignosulfonate, can be assigned to asymmetric and symmetric SO_2 vibrations, respectively. The band at 1036 cm^{-1} is assigned to C–O vibration of aliphatic OH.

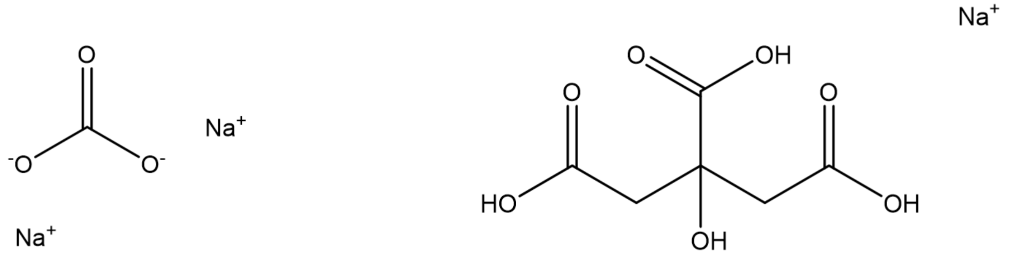

Sodium carbonate Citric acid

Starch Carboxymethylcellulose

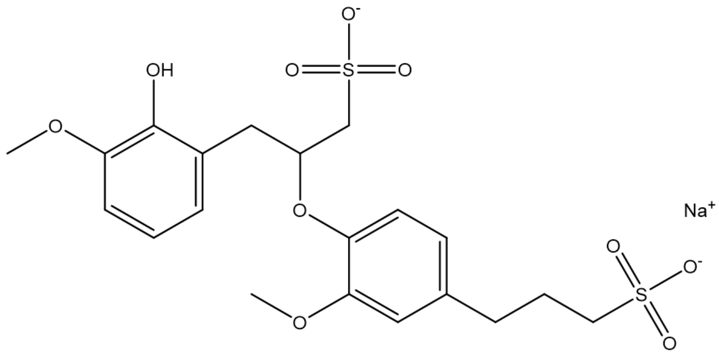

Sodium lignosulfonate

Figure 4.3 – Structure of different depressants.

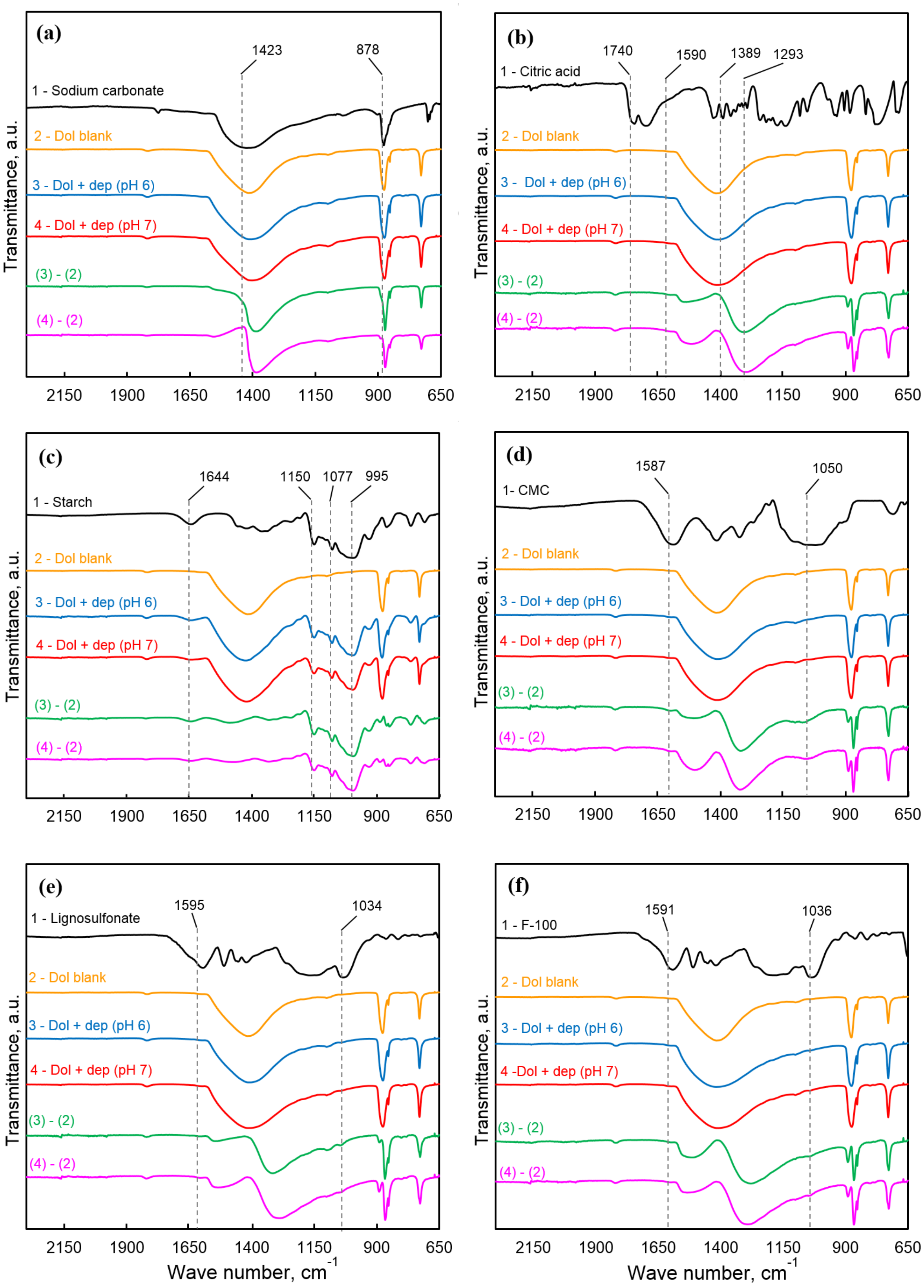

Figure 4.4 – ATR-FTIR spectra of (1) the depressants, (2) original dolomite surface; depressant-conditioned dolomite at (3) pH 6 and (4) pH 7; the difference of (3) and (2), and (4) and (2). The depressants include: (a) sodium carbonate, (b) citric acid, (c) starch, (d) CMC, (e) lignosulfonate and (f) F-100.

4.3.3 Microflotation

4.3.3.1 Different depressants

The collector concentration used, which was initially 7.5 mg/L for NaOl and F1682, was considered based on the result presented in a previous work (see Chapter 3). However, most of the depressants (even at higher concentrations) did not appear to work with 7.5 mg/L F1682. As such, the concentration of F1682 was decreased to 6 mg/L. Flotation of dolomite with different depressants using NaOl and F1682 are presented in Figures 4.5 and 4.6, respectively. Fitted curves are shown for visual presentation and do not imply predictive model. Error bars represent 95% confidence interval.

Figure 4.5 shows that CMC, lignosulfonate and F-100 have depressed dolomite significantly. CMC has depressed a maximum of 95% and 93% dolomite at pH 6 and 7, respectively. Lignosulfonate also performed quite well with 76% and 83% of dolomite depressed at pH 6 and 7, respectively. F-100 was also able to reduce the recovery at pH 6 from 94% to 41%, and at pH 7 from 68% to 11%, which reflects to 57% and 84% depression, respectively.

There is also a certain level of dolomite depression observed with starch, sodium carbonate and citric acid. Starch was able to reduce dolomite recovery from 94% to 40% and 68% to 45% at pH 6 and 7, respectively. Citric acid did not affect the recovery at pH 6, but it has decrease the recovery at pH 7 from 68% to 40%. In the presence of sodium carbonate, minimal reduction was observed with only a maximum of 18%.

For the flotation of dolomite with F1682 (Figure 4.6), CMC, lignosulfonate and F-100 have also presented good depressing capability. It can be seen that CMC was able to depress 70% and 79% of dolomite, while lignosulfonate reduced the recovery about 65% and 53% at pH 6 and pH 7, respectively. F-100 has also reduced dolomite's recovery from 93% to 53% and from 96% to 42% at pH 6 and 7, respectively. In addition to the list, citric acid was also able to lessen dolomite recovery significantly from 93% to 48% and from 96% to 35% at pH 6 and 7, respectively. It can be observed that sodium carbonate and starch have minimal depressing effect on dolomite.

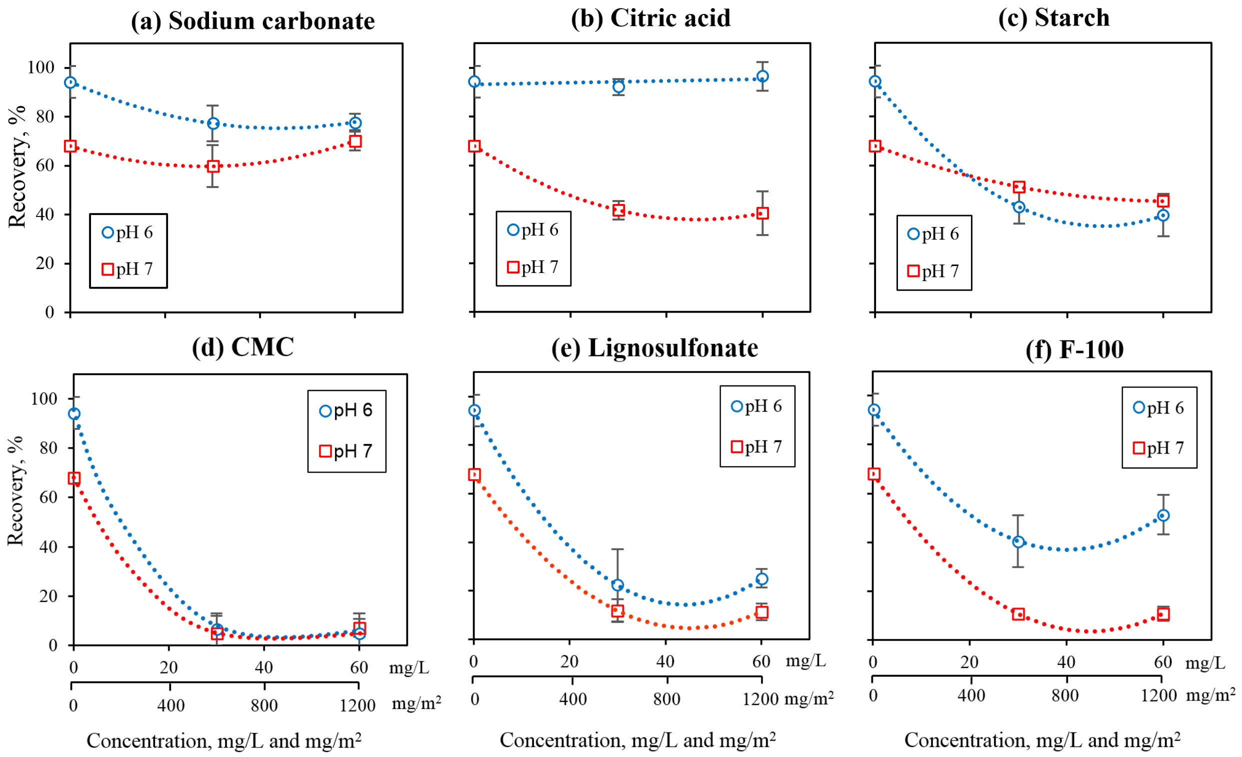

Figure 4.5 – Flotation recovery of dolomite in the presence of different depressants with 7.5 mg/L NaOl as collector.

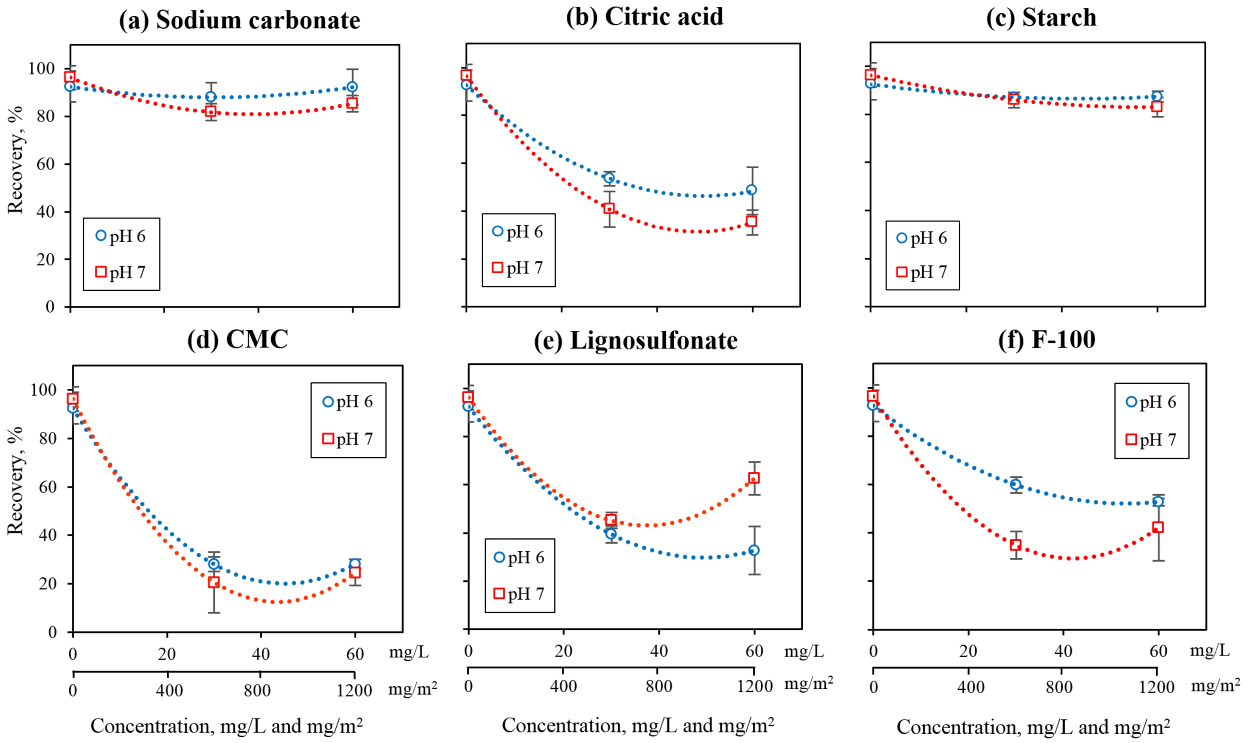

Figure 4.6 – Flotation recovery of dolomite in the presence of different depressants with 6 mg/L F1682 as collector.

4.3.3.2 Varying CMC concentrations

In both the cases (NaOl and F1682) presented, the best depressant for dolomite is CMC. Further tests considering lower CMC concentrations were conducted in the presence of different collector concentrations; the results thereof are presented in Figures 4.7 and 4.8. The results showed that there is a concentration where the depressing effect of CMC is reduced significantly. In the presence of 7.5 mg/L NaOl (Figure 4.7a), lowering the CMC concentration from 10 to 5 mg/L (or 200 to 100 mg/m^2) CMC has slightly increased dolomite recovery from 6.5% (pH 6) and 4.5% (pH 7) to 16%. Further decreasing the concentration to 2.5 mg/L (or 50 mg/m^2) has further increased dolomite recovery to 44% and 24% at pH 6 and 7, respectively. When a higher concentration of NaOl was used (Figure 4.7b), the recovery curves of dolomite have shifted slightly higher.

In the presence of 6 mg/L F1682 (Figure 4.8a), the lowest dolomite recovery (20%) was observed at pH 7 with 30 mg/L (or 600 mg/m^2) CMC. Decreasing the amount of CMC increases dolomite recovery. It can also be observed that increasing the F1682 concentration to 7.5 mg/L has moved the recovery curves slightly upward (Figure 4.8b), similar to that observed with NaOl. It can be seen in Figure 4.8b that at CMC concentrations between 5 and 20 mg/L (or 100 and 400 mg/m^2), dolomite recovery decreases gradually. However when the concentration was increased to 30 mg/L (or 600 mg/m^2), the recovery dropped sharply.

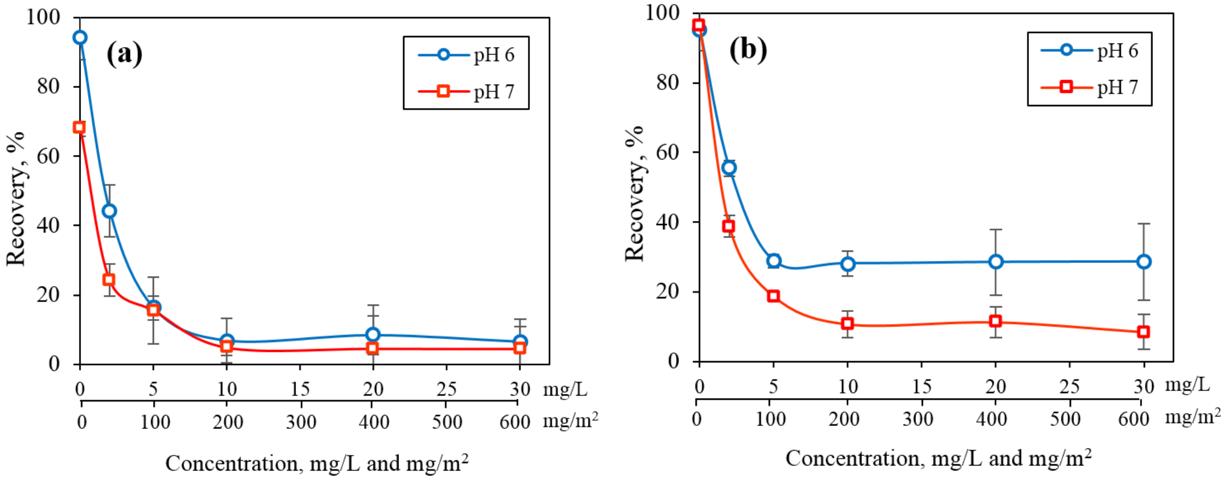

Figure 4.7 – Flotation recovery of dolomite in the presence of different CMC concentrations with (a) 7.5 mg/L and (b) 10 mg/L NaOl.

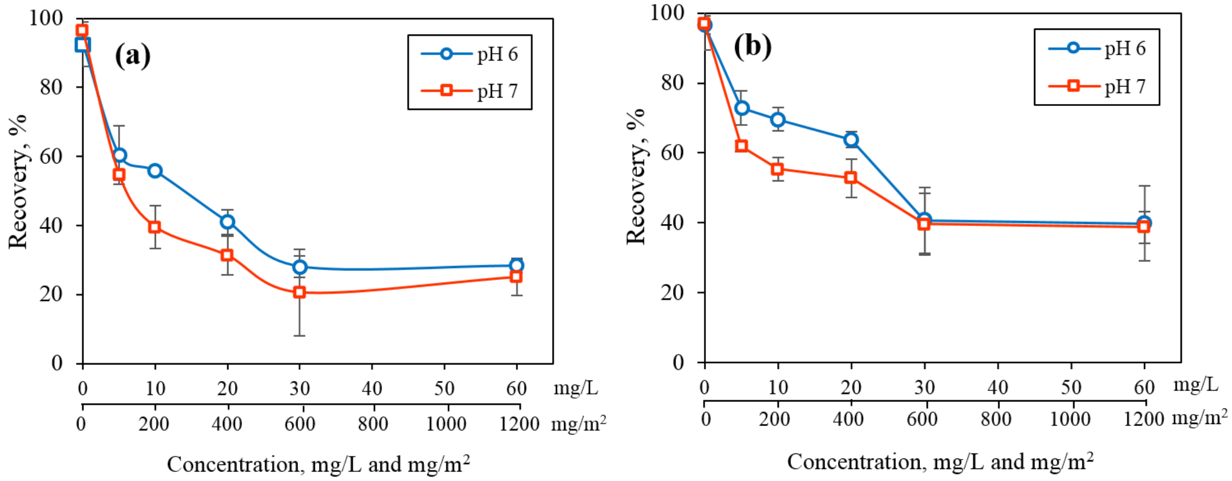

Figure 4.8 – Flotation recovery of dolomite in the presence of different CMC concentrations with (a) 6 mg/L and (b) 7.5 mg/L F1682.

4.3.3.3 Depressing effect of CMC on monazite and bastnäsite

Although it was shown that CMC could successfully depress dolomite, it is important to ascertain whether this depressant would affect the RE minerals, monazite and bastnäsite. The chosen ranges of CMC concentration to test with the RE minerals are 0 - 5 mg/L for NaOl and 0 - 10 mg/L for F1682. These concentrations were normalized to the surface area of the minerals (with a unit of mg/m^2) to compare directly the effect of CMC concentrations on the mineral's flotation.

With 6 mg/L of NaOl (Figure 4.9a), the presence of 13.8 mg/m^2 CMC (or 2 mg/L CMC) can depress 10 - 15% monazite and 18 mg/m^2 CMC (or 2 mg/L CMC) can depress 30% bastnäsite (pH 7). Although an increase in CMC concentration improved the depressing action of CMC with dolomite, it also negatively affected the recovery of the RE minerals. By increasing the NaOl concentration to 7.5 mg/L (Figure 4.9b), the depression of the RE minerals was reduced, however dolomite recovery increased. The same trend for F1682 was observed when the concentration was increased (Figure 4.9d). Using this collector, the amount of recovered RE minerals is comparable at pH 6 and 7. In Figure 4.9c, it can be seen that bastnäsite is more affected by CMC than monazite in the presence of 6 mg/L F1682.

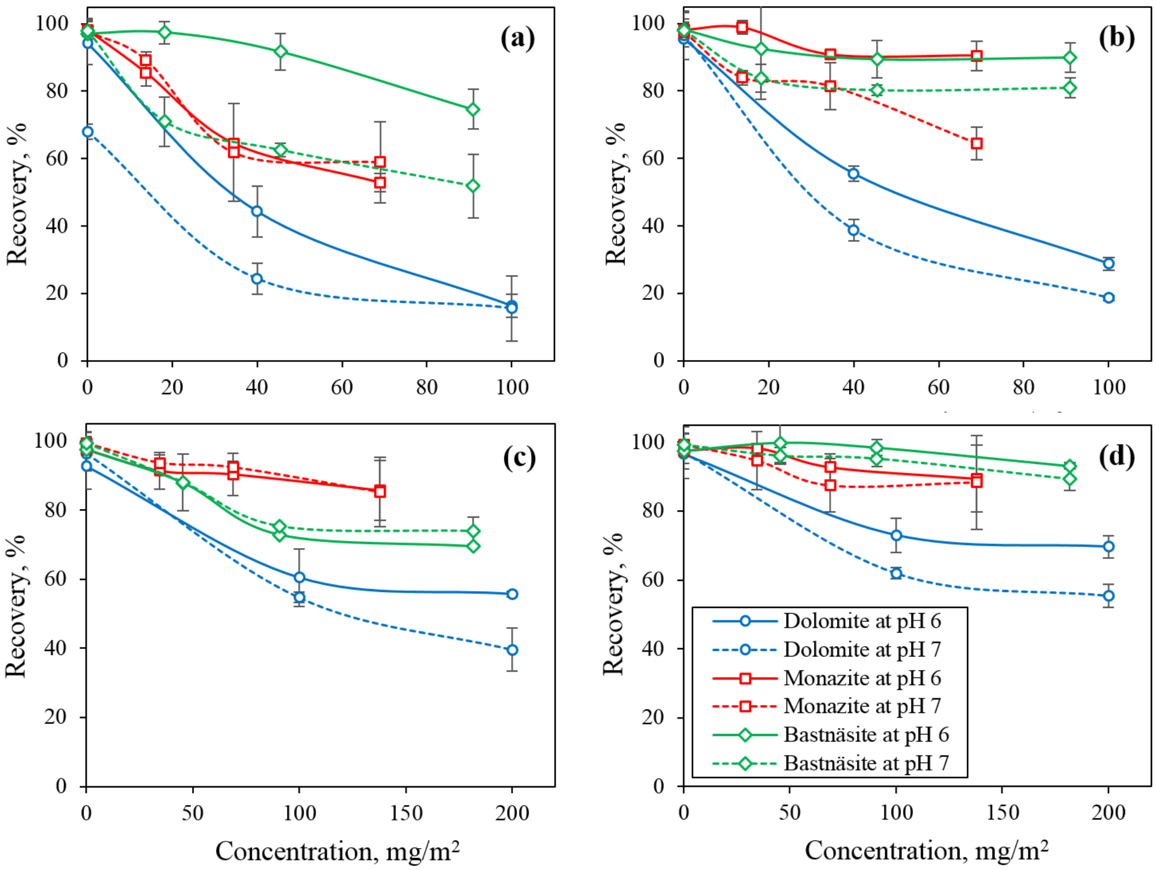

Figure 4.9 – Flotation recovery of dolomite, monazite and bastnäsite in the presence of different CMC concentrations with (a) 7.5 mg/L NaOl, (b) 10 mg/L NaOl, (c) 6 mg/L F1682 and (d) 7.5 mg/L F1682.

4.4 Discussion

4.4.1 Different depressants on dolomite

4.4.1.1 Sodium carbonate

It can be observed that at pH 6 and 7, sodium carbonate was able to increase the zeta potential of dolomite (see Figure 4.1a). It can be argued that this could be due to the presence of Na^+ in the solution, which could be compressing the electrical double layer (EDL), hence making the zeta potential less negative. However, a recent study proposed that the effect could be more attributed to the carbonate species in the solution (see Appendix D). The adsorption of CO_3^{2-} could form surface complexes and precipitates at the surface of dolomite. The surface complexes were suggested to be lowering the zeta potential of dolomite (see Chapter 5). ATR-FTIR spectra (Figure 4.4a) presented bands corresponding to residual carbonate peaks that could be due to the formation of new species at the surface of dolomite. These species could hinder collector adsorption as seen in the flotation results, where a minor amount of dolomite was depressed at pH 6 in the presence of 7.5 mg/L NaOl (Figure 4.5a) and at pH 7 in the presence of 6 mg/L F1682 (Figure 4.6a).

4.4.1.2 Citric acid

The pKa of citric acid, a tricarboxylic acid, are as follows: $pKa_1 = 3.13$, $pKa_2 = 4.76$ and $pKa_3 = 6.40$ [4.16]. This means that citric acid occurs mainly as $HCit^{2-}$ and Cit^{3-} at pH 6 and 7, respectively. From the zeta potential results (Figure 4.1b), it can be seen that citric acid makes the zeta potential of dolomite more negative at both pH values investigated. Since dolomite surface is negatively charged, zeta potential changes after adsorption of negatively charged citric acid species indicate that they adsorb onto dolomite through chemical reactions. It has been suggested that citric acid can form chelates with Ca and Mg through the carboxylate functional group [4.3]. ATR-FTIR spectra (Figure 4.4b) showed weak carboxylate stretching band suggesting small amount of adsorbed citric acid on the surface or that the complex could be easily removed by washing attributed to its weak chelating ability [4.3]. The adsorption of citric acid could hinder the collector adsorption as seen in the flotation results, which show that citric acid was able to depress a significant amount of dolomite in the presence of NaOl (except at pH 6) and F1682 (Figures 4.5b and 4.6b, respectively). The deviation at pH 6 in the presence of NaOl was reflected in the zeta potential results (Figure 1b) which shows that the difference between citric acid + collector and citric acid only is not significant at this pH value using NaOl as collector. Since citric acid mainly occurs as $HCit^{2-}$ at pH 6, and carboxylates (RCOOH) are capable of strong intermolecular hydrogen bonding [4.21], it is believed that the undissociated carboxylate group of citric acid may have interacted with NaOl ($RCOO^-$) rendering dolomite hydrophobic. The electrostatic repulsion between the undissociated carboxylate group of citric acid (RCOOH) and dissociated NaOl ($RCOO^-$) is almost completely absent, making this interaction possible [4.22].

4.4.1.3 Starch and CMC

Starch and CMC have the same structure except that the R's in starch are H, while R's in CMC are either H or carboxyl. Both were able to depress dolomite, but CMC showed better performance than starch in the presence of either NaOl (Figure 4.5) or F1682 (Figure 4.6). Starch did not significantly change the zeta potential of dolomite at pH 6 and 7; addition of NaOl to the starch-conditioned dolomite did not affect the zeta potential either (Figure 4.1c). However, the addition of F1682 has made the zeta potential of starch-conditioned dolomite more negative indicating collector adsorption (Figure 4.1c). These correlate with the flotation results which show dolomite depression in the presence of starch and NaOl (Figure 4.5c), and dolomite flotation in the presence of F1682 (Figure 4.6c). Even with the presence of starch at the surface of dolomite, which was confirmed by the ATR-FTIR spectroscopy (Figure 4.4c), F1682 appears to still be adsorbing at the surface. The adsorption of starch on dolomite has been reported to be due to the interaction of OH functional groups of starch with Ca and Mg sites forming a metal-starch complex at the surface [4.7]. The adsorption is said to be governed by steric compatibility of the OH (from starch) and metal cation (from dolomite surface). Since OH groups lie along the starch structure at distances d_n (n=1,2,3. . .), while Ca or Mg occurs at a specific orientation, there will be some metal cation – OH that will not be paired [4.7]. This could indicate that there are still patches at the surface not covered by starch where collector could adsorb. Since F1682 is a strong collector, it could still float a significant amount of dolomite.

The CMC depressed a significant amount of dolomite in the presence of both NaOl (Figure 4.5d) and F1682 (Figure 4.6d). This indicates that CMC has hindered collector adsorption. The zeta potential of dolomite became more negative after conditioning with CMC (see Figure 4.1d), suggesting that depressant has adsorbed on dolomite surface through chemical interaction. This was also confirmed by ATR-FTIR spectra of the CMC-conditioned dolomite (Figure 4.4d) which presented bands corresponding to C=O and C–O of carboxylate groups. The excellent depressing ability of CMC is attributed to its abundant carboxylate groups and high molecular weight [4.3]. It has been mentioned that the carboxylate groups could interact with the metal cations present on the dolomite surface forming metal – CMC complexes [4.10].

4.4.1.4 Lignosulfonate and F-100

ATR-FTIR spectroscopy showed that lignosulfonate (Figure 4.4e) and F-100 (Figure 4.4f) have similar spectra, confirming F-100 to be a lignosulfonate-based biopolymer. The two will then be referred together as lignosulfonates in the following discussion. Lignosulfonates presented good depressing power as can be observed from the flotation results (Figures 4.5 and 4.6). Zeta potential results showed that both depressants made the zeta potential of dolomite more negative (Figures 4.1e and 4.1f). It appears that the adsorption of these lignosulfonates on negatively charged dolomite is through chemical interaction. The actual mechanism is not yet understood, since several functional groups are present in lignosulfonate such as aliphatic, aromatic, sulfonic, carboxylic and hydroxyl. ATR-FTIR spectra did not present very useful information, except that the bands corresponding to aromatic ring and aliphatic OH group are present after conditioning dolomite with lignosulfonates (see Figures 4.4e and 4.4f). Although significant adsorption of the lignosulfonates onto dolomite was indicated by flotation and zeta potential results (Figures 4.1e and 4.1f), the weakly surface-active lignosulfonates could have been easily washed off, consequently showing weak characteristic bands on depressant-conditioned dolomite spectra.

It can be observed from the flotation results at pH 6 that lignosulfonate performs better than F-100 in the presence of NaOl (Figure 4.5) and F1682 (Figure 4.6). It could be presumed that this has something to do with the amount of adsorbed reagent at dolomite surface, however, zeta potential (Figure 4.1) showed no significant difference between conditioning with lignosulfonate and with F-100. Although the information regarding F-100 is not available, it could be that the different performance of the 2 lignosulfonates might be due to their differences in molecular weight. Higher molecular weights would be more favorable to depressant-mineral interaction because this indicates more active depressant sites are available to interact with dolomite surface.

In general, all the depressants performed better at pH 7 than 6 which could be due to the presence of less cations (Ca and Mg) on the surface of dolomite at this pH. Given the same amount of depressant used at pH 6 and 7, more active sites on dolomite at pH 6 would mean there could be some excess sites not interacted by the depressant. As such, collector can still adsorb consequently floating some dolomite. It was also observed that these depressants worked better with NaOl than F1682. The mechanism of F1682 adsorption on depressant-conditioned dolomite has not been really explored as the investigation of these depressants with F1682 is very limited in the open literature. At pH 6 and 7, F1682 (with a general structure of $ROPO_3H_2$) could occur as $ROPO_3H^-$ and $ROPO_3^{2-}$ in solution (see Chapter 3). Although $ROPO_3H^-$ is negatively charged, it could still adsorb on depressant-conditioned dolomite as presented by the zeta potential results. It could then be presumed that the H atom from $ROPO_3H^-$ interacts with the O atom from the collector, replacing the H atom that was dissociated from the depressants. Another explanation could be that F1682 is a strong (less selective) enough collector that it can still interact with the Ca and Mg that was not paired with the active functional groups from the depressants. Previous study indicated that F1682 is a less selective collector than NaOl, which was attributed to the charges of their O atoms involved in the collector-mineral interaction (see Chapter 3).

4.4.2 CMC - collector concentration on dolomite

Due to the performance of CMC, further tests were conducted with different concentrations of the depressant. It can be observed that there is a CMC concentration where dolomite depression becomes constant (Figures 4.7 and 4.8). The critical CMC concentration (steepest part of the curve) when NaOl was used occurs between 3 and 4 mg/L (Figure 4.7). Even though the same critical concentration was estimated for both NaOl concentration used, the lowest dolomite recovery obtained were 6.5% (pH 6) and 4.5% (pH 7) in the presence of 7.5 mg/L NaOl (Figure 4.7a); while 28% (pH 6) and 8.4% (pH 7) using 10 mg/L NaOl (Figure 4.7b). This observation indicates that addition of further NaOl could have detrimental effect to dolomite depression. It should be emphasized that carboxyl group (–COOH) of CMC, which is also present in NaOl structure, ionizes to form –COO$^-$ [4.23]. This can be represented by the following equation:

$$-\mathrm{CH_2}-\mathrm{COOH} \rightleftharpoons -\mathrm{CH_2}-\mathrm{COO}^- + \mathrm{H}^+ \quad K_i = [\mathrm{H}^+][-\mathrm{CH_2}-\mathrm{COO}^-] \tag{4.1}$$

where K_i represents the ionization constant. It has been reported that full ionization occurs above pH 6 [4.23, 4.24]; however, further increasing NaOl (RCOO$^-$) at pH 6 and 7 could have affected the ionization leading the reaction backward instead of forward. The reduction of dissociated carboxyl groups of CMC consequently reduces the CMC active sites, hence the possible CMC – dolomite interaction, which could also result to more uninteracted Ca and Mg on dolomite surface. Combined with the reduced CMC active sites, dissociated NaOl (RCOO$^-$) could possibly interacted with undissociated carboxyl groups of CMC through hydrogen bonding, providing a certain level of hydrophobicity to the CMC-conditioned dolomite. It is also possible that NaOl interacts with the Ca and Mg on dolomite.

The critical CMC concentration (between 10 and 30 mg/L) and the minimum dolomite recovery (20%) in the presence of 6 mg/L F1682 (Figure 4.8a) are significantly higher than those with NaOl. The possible reason for this has already been explained in the previous section. It was also observed that in the presence of 7.5 mg/L F1682 (Figure 4.8b), dolomite recovery seemed to be unchanged between 10 and 20 mg/L CMC, until it started to reduce significantly at higher concentration. This flotation behavior of CMC-conditioned dolomite in the presence of 7.5 mg/L F1682 as a function of CMC concentration presents an unusual trend which seems to show 2 different critical CMC concentration. If this is solely due to the changes in the adsorption of CMC, then the same trend should have been present in the flotation curve of dolomite using NaOl collector. This suggests that F1682 has a big influence in this behavior. Recall that at these pH conditions, F1682 occurs mainly as

$ROPO_3H^-$ and $ROPO_3^{2-}$. It seems that at CMC concentration above 20 mg/L, the repulsion between the highly negative CMC and the negatively charged F1682 becomes strong enough to keep the collector from adsorbing.

4.4.3 CMC with RE minerals

Zeta potential results showed that CMC (Figure 4.2) could reduce the zeta potential of monazite and bastnäsite to highly negative values, similar to that of dolomite. However, flotation results (Figure 4.9) showed that CMC preferably depressed dolomite over bastnäsite and monazite, using either NaOl or F1682. Due to the abundant carboxylate groups of CMC, which are deprotonated at pH 6 and 7, adsorption of CMC could make the mineral surface highly negative. Zeta potential results indicate that CMC could be adsorbed at the surface of either dolomite or RE minerals; however, flotation results suggest that CMC seemed to preferentially interact with Ca and Mg than RE cations. Although this is the case, it has been suggested that the presence of Ca or Mg on mineral surface does not always imply that the depressant would work. It was mentioned that the interaction of polymeric depressant with minerals is highly governed by stereochemistry other than conventional chemistry. Since the functional groups lie along some distances d_n (n=1,2,3...) as explained earlier, the compatibility of these functional groups with the crystallographic location of the cations on the mineral surface will affect the depressant – mineral interaction. It was also presented that Ca and Mg on dolomite surface are more exposed than RE cation on monazite surface (see Chapter 5); in addition, RE cations on bastnäsite or monazite surface are more scarce than Ca and Mg on dolomite surfaces. These scenarios could have some influence on the varying depressing power of CMC on each of these minerals. At higher depressant concentrations, monazite and bastnäsite became affected by CMC. It could be explained by the interaction of previously unmatched RE cation with the extra CMC added, hindering collector adsorption.

4.5 Conclusions

Several depressants, mostly polymeric, were found to have better depressing ability. This was attributed to these depressants' high molecular volume and abundant active functional groups. Among these, CMC performs the best at depressing dolomite in the presence of NaOl or F1682. It was found that the depressing power varies by pH, collector type, collector dosage and depressant dosage. This observation indicates that a balance between collector dosage and depressant dosage is important to depress the target mineral as much as possible, at the same time avoid depressing significant amount of the valuable mineral.

The results also indicated that depressant performance is highly affected by the type of collector. When a reagent presents a superior depressing ability when used with NaOl, it does not imply it would also work (with the same efficiency) with other collectors, as the other collectors could also interact with the depressant depending on its chemistry, diminishing its depressing ability.

Performance and proposed adsorption mechanisms of different depressants with NaOl and F1682 (organic phosphoric acid) were presented in this work. Still, adsorption of lignosulfonates is still not quite clear due to the presence of various functional groups in their structure. In addition, suggested mechanism of F1682 adsorption on depressant-conditioned minerals was described. Further investigations, including molecular modeling, should be conducted to verify these mechanisms.

References

[4.1] Jordens, A., Sheridan, R. S., Rowson, N. A., and Waters, K. E. Processing a rare earth mineral deposit using gravity and magnetic separation. *Minerals Engineering*, 62:9–18, 2014.

[4.2] Verplanck, P. L. and Van Gosen, B. S. Carbonatite and alkaline intrusion-related rare earth element deposits - a deposit model. Report Open-File Report 2011–1256, US Geological Survey, 2011.

[4.3] Zheng, X. and Smith, R. W. Dolomite depressants in the flotation of apatite and collophane from dolomite. *Minerals Engineering*, 10(5):537–545, 1997.

[4.4] Smith, R. and Shonnard, D. Electrokinetic study of the role of modifying agents in flotation of salt-type minerals. *AIChE Journal*, 32(5):865–868, 1986.

[4.5] Pradip, P. and Fuerstenau, D. The role of inorganic and organic reagents in the flotation separation of rare-earth ores. *International Journal of Mineral Processing*, 32(1–2):1–22, 1991.

[4.6] Xia, L., Hart, B., and Douglas, K. The role of citric acid in the flotation separation of rare earth from the silicates. *Minerals Engineering*, 74:123–129, 2015.

[4.7] Leal Filho, L. S., Seidl, P. R., Correia, J. C. G., and Cerqueira, L. C. K. Molecular modelling of reagents for flotation processes. *Minerals Engineering*, 13(14):1495–1503, 2000.

[4.8] Leal Filho, L. S., Martins, M., and Horta, D. Concentration of igneous phosphate ores via froth flotation - challenges and developments. In *XXV International Mineral Processing Congress*, pages 63–75, 2010.

[4.9] Somasundaran, P. Adsorption of starch and oleate and interaction between them on calcite in aqueous solutions. *Journal of Colloid and Interface Science*, 31(4):557–565, 1969.

[4.10] Turrer, H. D. G. and Peres, A. E. C. Investigation on alternative depressants for iron ore flotation. *Minerals Engineering*, 23(11–13):1066–1069, 2010.

[4.11] Seaman, D., Lauten, R., Kluck, G., and Stoitis, N. Usage of anionic dispersants to reduce the impact of clay particles in flotation of copper and gold at the telfer mine. In *Proceedings 11th AusIMM Mill Operators' Conference*, page 207, 2012.

[4.12] Wang, Y., Lauten, R. A., and Peng, Y. The effect of biopolymer dispersants on copper flotation in the presence of kaolinite. *Minerals Engineering*, 96-97:123–129, 2016.

[4.13] Pionera. PIONERA BioPolymers product portfolio. http://pionera.com/Products/Product-Portfolio, 2018.

[4.14] Gunasekaran, S., Anbalagan, G., and Pandi, S. Raman and infrared spectra of carbonates of calcite structure. *Journal of Raman Spectroscopy*, 37(9):892–899, 2006.

[4.15] Joshi, S., Kalyanasundaram, S., and Balasubramanian, V. Quantitative analysis of sodium carbonate and sodium bicarbonate in solid mixtures using Fourier transform infrared spectroscopy (FT-IR). *Applied spectroscopy*, 67(8):841–845, 2013.

[4.16] Siriwardane, I. W. *Adsorption of citric acid on cerium oxide nanoparticles (nanoceria): effects of pH, surface charge and aggregation.* MS Thesis, The University of Iowa, 2012.

[4.17] Warren, F. J., Gidley, M. J., and Flanagan, B. M. Infrared spectroscopy as a tool to characterise starch ordered structure – a joint FTIR–ATR, NMR, XRD and DSC study. *Carbohydrate Polymers*, 139:35–42, 2016.

[4.18] Saputra, A. H., Qadhayna, L., and Pitaloka, A. B. Synthesis and characterization of carboxymethyl cellulose (CMC) from water hyacinth using ethanol-isobutyl alcohol mixture as the solvents. *International Journal of Chemical Engineering and Applications*, 5(1):36, 2014.

[4.19] Tufan, M., Uraz, E., Tosun, C., and Gercel, H. Synthesis and characterization of carboxymethyl cellulose film from pistachio shells. *International Journal of Advances in Science, Engineering and Technology*, 4(1):153–155, 2016.

[4.20] Lima, R. B., Raza, R., Qin, H., Li, J., Lindström, M. E., and Zhu, B. Direct lignin fuel cell for power generation. *RSC Advances*, 3(15):5083–5089, 2013.

[4.21] Stuart, B. *Infrared Spectroscopy: Fundamental and Applications.* John Wiley & Sons, Ltd, Chichester, UK, 2004.

[4.22] Ananthapadmanabhan, K. P. and Somasundaran, P. Acid-soap formation in aqueous oleate solutions. *Journal of Colloid and Interface Science*, 122(1):104–109, 1988.

[4.23] López-Valdivieso, A., Lozano-Ledesma, L. A., Robledo-Cabrera, A., and Orozco-Navarro, O. A. Carboxymethylcellulose (CMC) as PbS depressant in the processing of Pb-Cu bulk concentrates. Adsorption and floatability studies. *Minerals Engineering*, 112:77–83, 2017.

[4.24] Cuba-Chiem, L. T., Huynh, L., Ralston, J., and Beattie, D. A. In situ particle film ATR-FTIR studies of CMC adsorption on talc: The effect of ionic strength and multivalent metal ions. *Minerals Engineering*, 21(12):1013–1019, 2008.

Chapter 5

The effect of dissolved mineral species on mineral – benzohydroxamate interaction

The rare earth minerals and dolomite are sparingly soluble in water, which means that constituent ions may be dissolved in solution. In this chapter, the effect of the dissolved mineral species on the flotation of dolomite, monazite and bastnäsite in the presence of benzohydroxamate is presented. Since Chapter 3 indicated that efficient separation could be achieved with the use of benzohydroxamate, this collector was investigated further in this chapter.

Abstract

Flotation is the most commonly used beneficiation method for RE ores. Due to the dissolution characteristics of the RE minerals and the gangue minerals, they may behave similarly in a flotation system. Previous work has shown that dissolved mineral species from gangue could precipitate/adsorb at the mineral surface affecting the minerals' flotation behavior. In this work, the effect of dolomite supernatant on the surface of bastnäsite, monazite and dolomite is presented. Zeta potential measurements, complemented with flotation tests, were conducted with and without the presence of the supernatant using benzohydroxamate as the collector. XPS results confirmed the surface speciation, and DFT simulations detail the possible mineral – collector, mineral – precipitated species and precipitated species – collector interactions. The results show that carbonate precipitates and Ca^{2+} from the supernatant could adsorb onto the mineral surface through covalent bonding, both affecting the zeta potential and reducing collector adsorption. Another important finding of this study is the potential loss of the collector in the solution due to complexation with ions from the supernatant. These findings confirmed that an effective rare earth mineral separation through

flotation does not rely solely on the strength of collector – mineral interaction, but rather is highly dependent on the chemistry of the flotation solution. Taking advantage or controlling the surface reactions, should be the key to having a more efficient and cost-effective flotation process. Different measures have been proposed to reverse/reduce the detrimental effects of the dolomite supernatant to RE mineral flotation.

5.1 Introduction

Main sources of rare earth (RE) elements, such as bastnäsite (a RE fluorocarbonate) and monazite (a RE phosphate), are typically associated with carbonate minerals such as calcite and dolomite. These RE minerals occur naturally disseminated in the ore body [5.1], requiring fine liberation sizes thus making flotation to be the most common beneficiation process [5.2, 5.3]. Among the RE collectors, hydroxamate-type collectors have caught the attention of the researchers due to its selectivity towards RE minerals. It is suggested that hydroxamate collectors form stronger chelate with RE metals than metals from gangue minerals [5.4]. It is proposed that hydroxamates interact with either RE-hydroxylated species at the surface or with the RE-hydroxylated species in the solution then adsorb at the mineral surface, rendering the mineral hydrophobic [5.5]. However, this scenario is not straightforward because of the natural solubility of both the RE and associated carbonate minerals in solution.

The RE minerals and the associated gangue are considered salt-type minerals [5.6], which means that they have relatively higher solubilities than most minerals, but lower than salt minerals [5.7]. Since they are sparingly soluble in water, constituent ions that are dissolved may influence other mineral surfaces. Flotation studies involving single mineral flotation do not often take into account the effect of the dissolved mineral species from the gangue minerals, as such further research involving constituent ions is encouraged (Appendix A). RE flotation studies [5.8, 5.9] concerning semi-soluble gangue minerals have noted that dissolved species could precipitate/adsorb at the surface of RE minerals affecting their flotation behavior. Although there have been several attempts to study the effect of dissolved mineral species from typical carbonate gangue minerals in mineral flotation [5.9–5.12], few studies concern RE flotation and mostly are relating to calcite, but not to dolomite. Also, very few research works with regards to RE flotation have considered using a solution with the dissolved carbonate mineral species (gangue supernatant) as the flotation medium. Espiritu *et al.* (Appendix D) have studied the effect of the dolomite (gangue) supernatant on the surface property of the RE minerals such as bastnäsite and monazite. It was found that dolomite supernatant could potentially affect bastnäsite and monazite flotation due to the changes of their surface properties when exposed to the solution.

The surface complexation model of carbonate minerals have been presented in detail by Van Cappellen *et al.* [5.13]. It is suggested that upon in contact of carbonate in water, two primary hydration sites will occur: (1) hydroxylated cation sites ($>MeOH^0$) and (2) protonated anion sites ($>CO_3H^0$), where > represents mineral lattice and Me the mineral cation. For monazite, two surface sites are also present: (1) phosphate sites ($>P(OH)_2$) and (2) hydrated RE sites ($>RE(OH)_2$) [5.14]. These surface sites provides interaction sites for other metal cations and anions in the solution [5.13, 5.14].

Some of the calcium and magnesium from dolomite could dissolve out in the solution; they could occur in different species which could interact with the mineral surface leading to surface precipitation and/or adsorption [5.13, 5.15]. To be able to study the effect of dissolved dolomite species on bastnäsite, monazite and dolomite, zeta potential, hydrophobicity and interactions at molecular scale were investigated with the presence of benzohydroxamate, a common RE mineral collector. These were conducted using electrophoretic measurements, flotation tests and quantum mechanical simulations based on density functional theory (DFT). For reference on zeta potential, flotation and DFT simulations, readers are referred to Fuerstenau and Pradip [5.16], Wills and Finch [5.17] and Rai [5.18], respectively.

5.2 Materials and methods

5.2.1 Material

Bastnäsite was obtained from African Rare Earths (Pty.) Ltd. (South Africa). Monazite (Eureka Farm 99, Namibia) was acquired from Mineralogical Research Company (USA). Dolomite (Sterling Hill Mine, New Jersey) was purchased from Ward's Science (USA).

Sodium chloride (supporting electrolyte); hydrochloric acid and potassium hydroxide that were used as pH modifiers were obtained from Fisher Scientific (Canada). Benzohydroxamic acid was obtained from Sigma-Aldrich (Canada), F150 (a common frother) was obtained from Flottec (Canada).

The dolomite supernatant was prepared by placing 75 g of dolomite with particle size -106+38 μm in 1500 mL distilled water. The suspension was mixed for 8 hours at elevated temperature of 60 °C. The suspension was allowed to cool before passing through a filter with a grade of 413 (particle retention of 5 μm) to recover the supernatant.

5.2.2 Zeta potential measurements

Mineral samples were pulverized in a Planetary Monomill, Pulverisette 6 (Fritsch, Germany). The D_{50} obtained was 2.3 µm for dolomite, monazite and bastnäsite. A solution of 1×10^{-3} M NaCl was used as the indifferent background electrolyte and the dolomite supernatant was used as a medium. Prior to addition of the mineral samples, the solutions of NaCl, supernatant and collector were pH adjusted using hydrochloric acid and potassium hydroxide. For the measurements with supernatant then collector, the minerals were first conditioned with the supernatant for a certain amount of time (0, 30, 60, 120 and 240 s) prior to addition of the collector. For every measurement, the 100 mg/L mineral suspension was kept mixed to ensure that the particles were suspended. Zeta potential measurements were then taken using a NanoBrook 90Plus Zeta Particle Size Analyzer (Brookhaven Instruments, USA).

5.2.3 Microflotation

Microflotation tests were conducted using a modified Hallimond tube (Figure 5.1). The flotation cell volume is approximately 170 mL. The cell, made of glass, has three parts – the lower part has a silicate frit at the bottom; the extensor part connects the lower part and the upper part, and the upper part is where the floated fractions can be collected.

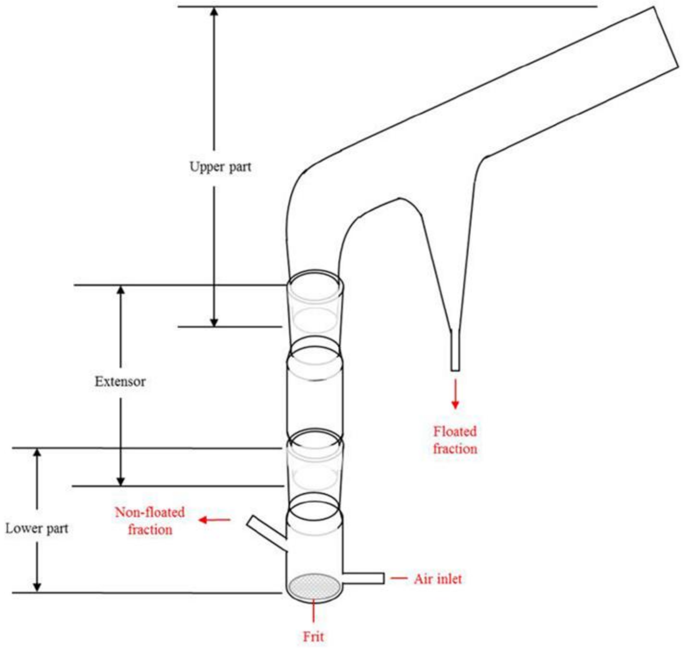

Figure 5.1 – Schematic diagram of the modified Hallimond tube.

One (1) gram of mineral sample, with a particle size range -106+38 μm, was placed in a beaker with 30 mL distilled water (adjusted to desired pH) and a magnetic stirring bar ensured that the mineral particles remained in suspension. The pH of the suspension was adjusted prior to addition of the collector, and was maintained during the 5-minute conditioning. For the tests with dolomite supernatant, the minerals were first exposed to the supernatant for 2 minutes (adjusted to desired pH), before the collector was added. The suspension was then transferred to the cell and was next added with 140 mL of pH adjusted water. Air was introduced through the cell at a flowrate of 40 mL/min. Flotation was conducted for 1 minute. The floated and non-floated fractions were collected, filtered, dried and weighed in order to calculate the recovery.

5.2.4 X-ray photoelectron spectroscopy (XPS)

The surfaces of dolomite, monazite and bastnäsite, in the presence and absence of supernatant, were studied using a Thermo Scientific K-Alpha Monochromatic X-ray Photoelectron Spectrometer (Thermo Fisher Scientific Inc., USA) equipped with an Al Kα X-ray source (1486.6 eV, 0.834 nm), ultrahigh vacuum chamber (10^{-9} Torr) and microfocused monochromator. Elemental survey scans from 0 to 1350 eV and high resolution scans were performed in the experiments, using a pass energy of 1 and 0.1 eV, respectively. The analyses were conducted using a spot size of 400 μm. An electron charge gun was employed to avoid surface charge effects. Prior to the experiments, the samples were kept in a desiccator (with silica gels) and degassed for 2 hours in a vacuum oven at room temperature. The results (binding energies) were calibrated using the C 1s peak for C–C at 284.8 eV, and fitted using the software Thermo Advantage 4.60 (Thermo Fisher Scientific Inc., USA).

5.2.5 Density Functional Theory (DFT) simulations

All DFT-based calculations were performed using Dmol3 package implemented in the Material Studio 2016 software. Through DFT simulations, geometric crystal parameters and total energy of dolomite and monazite bulk, their free surfaces considering their most stable cleavage plane, model benzohydroxamic acid collector, and adsorbed collector and species from dolomite supernatant onto mineral surfaces were calculated.

The generalized gradient approximation (GGA) with PBEsol exchange correlation functional was used to describe the exchange correlation interactions. Through calculations, the double numerical plus polarization (DNP) basis set and the calculation was done considering Spin-unrestricted. The self-consistent field (SCF) convergence was fixed to 2 ×

10^{-6} and convergence criteria set for the energy, maximum force and maximum displacement were set to 2 × 10^{-5} Ha, 0.05 Ha/Å, and 0.002 Å, respectively. No special treatment of core electrons was considered and all the electrons were included in the calculations. Also, smearing was set to 5 × 10^{-3} through all calculations. In this condition, the calculation was performed by use of various orbitals for different spins. Besides, the initial value for the number of unpaired electrons for each atom was taken from the formal spin introduced for each atom. In this situation, the starting value can be subsequently optimized throughout the calculations. For minerals bulk calculations, the Brillouin zone was sampled using a (2×2×2) Monkhorst-Pack k-point mesh. The most stable cleavage planes for dolomite and monazite were taken for calculations. In this regard, the cleavage plane (104) for dolomite and (100) for monazite, which both agree with the literature values [5.9, 5.19, 5.20], were used.

The mineral slabs were constructed by (1×2) dolomite (104) and monazite (100) surface supercells with 40 Å vacuum spacing to prevent interaction between image slabs. Special attention was paid to the importance of doing flotation in aqueous environment. Therefore, all the simulations were performed in the presence of conductor-like screening model (COSMO) as an implicit solvation model in which the solute molecules form a cavity within the dielectric continuum of permittivity equal to 78.54. During adsorption calculations of either collector or supernatant species on the mineral surfaces, the atoms at the top layer were allowed to undergo relaxation and the rest of atoms in sub-layers were constrained. This is because only the top layer mineral surface atoms have interactions with benzohydroxamic acid collector and other species through adsorption. The adsorption energy of either collector or precipitated species on the mineral surfaces was calculated based on the following definition [5.18]:

$$E_{\text{ads}} = E_{(\text{slab + collector or precipitated species})} - E_{(\text{slab})} - E_{(\text{collector or precipitated species})} \tag{5.1}$$

Where $E_{(\text{slab + collector or precipitated species})}$ is total energy after adsorption of either collector or precipitated species on the mineral surface, $E_{(\text{slab})}$ represents the energy of relaxed bare mineral slab and $E_{(\text{collector or precipitated species})}$ is the energy of collector or precipitated species after optimization.

In the cases that collector interacted with precipitated species on the mineral surfaces, the interaction energy was calculated as following:

$$E_{\text{ads}} = E_{(\text{slab + collector + precipitated species})} - E_{(\text{slab})} - E_{(\text{collector})} - E_{(\text{precipitated species})} \tag{5.2}$$

5.3 Results

5.3.1 Sample characterization

Mineral samples were characterized by X-ray Diffraction using Bruker D8 Discovery X-Ray Diffractometer (Cobalt source: Co Kα, λ=1.79 Å). Figure 5.2 presents the diffractograms of dolomite, bastnäsite and monazite. It was also labeled by the peaks of the reference patterns (a) dolomite reference pattern (JPDF reference number: 01-081-8229) [5.21]; (b) bastnäsite reference pattern (JPDF reference number: 00-011-0340) [5.22]; (c) monazite reference pattern (JPDF reference number: 00-046-1295) [5.23]. While a calcite peak was observed for monazite, no other significant peaks were observed for dolomite and bastnäsite, indicating that the latter have no major contaminants.

Further analyses were conducted to identify the elements present in the minerals using Inductively Coupled Plasma Optical Emission Spectrometry (ICP-OES). Samples of 0.1 g prepared in a crucible with borate flux were microwaved up to 950 °C. The fused products were digested at 95 °C for 2 hours using aqua regia and was analyzed using Thermo Scientific 6000 Series Spectrometer (Thermo Fisher Scientific Inc., USA). The chemical composition of the minerals is presented in Table 5.1.

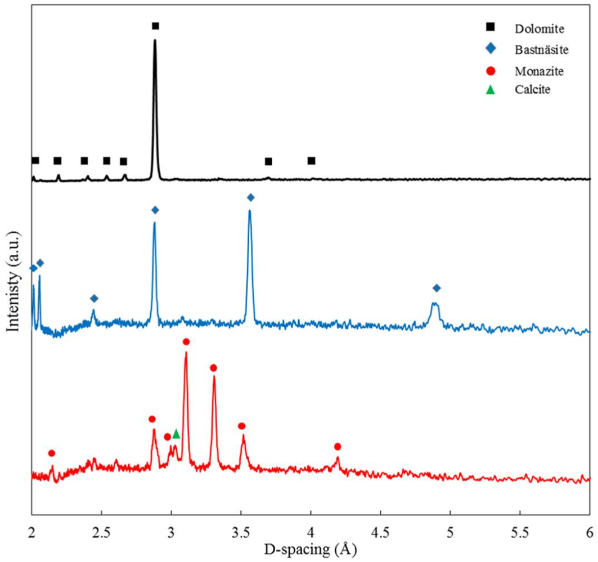

Figure 5.2 – X-ray powder diffraction patterns of dolomite, bastnäsite and monazite.

The conductivity of the distilled water was measured to be 5 µS/cm, while the dolomite supernatant was 90 µS/cm. The difference indicates that the supernatant should contain significantly more ions than the distilled water. The amounts of Ca^{2+} and Mg^{2+} ions in the supernatant, which were 8.07 ppm and 3.54 ppm, respectively, were analyzed using Varian AA240FS Fast Sequential Atomic Absorption Spectrometer (Agilent Technologies, USA). Distilled water was used as a blank for these measurements.

Table 5.1 – Chemical composition (wt %) of dolomite, monazite and bastnäsite samples.

Dolomite	**Ca**	**Mg**	**Fe**	**S**	**Mn**	**Na**	**K**	**Ti**	**Cu**	**Zn**	**Mo**
	21.71	12.74	0.37	0.21	0.06	0.05	0.04	0.03	0.02	0.02	0.01
Monazite	**P**	**Ce**	**Nd**	**La**	**Ca**	**Si**	**Pb**	**Zr**	**Fe**	**Al**	**As**
	10.24	8.00	5.41	4.64	0.75	0.51	0.49	0.46	0.12	0.10	0.10
Bastnäsite	**Ce**	**La**	**Nd**	**As**	**P**	**Ti**	**Fe**	**Ca**	**Al**	**Pb**	**Cu**
	13.55	13.44	8.08	0.69	0.53	0.40	0.25	0.21	0.18	0.09	0.06

5.3.2 Zeta potential measurements

The zeta potential of the minerals in the presence of 1 × 10^{-3} M NaCl (supporting electrolyte) was measured as a function of pH. As can be seen in Figure 5.3, the isoelectric point (IEP) of the 3 minerals occur around pH 7. The IEP of dolomite can be found in between pH 6 and 7, monazite at around pH 7, and bastnäsite in between pH 7 and 8. These values agree with those presented in the literature for dolomite [5.24, 5.25], monazite [5.26–5.28], and bastnäsite [5.28–5.30], respectively.

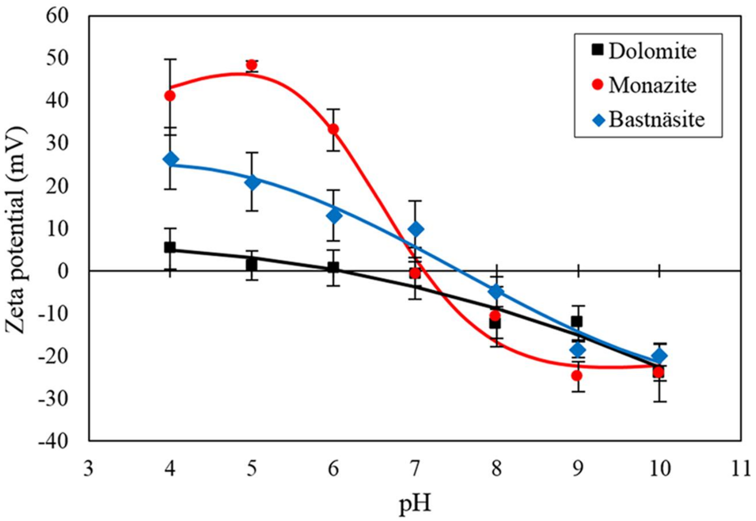

Figure 5.3 – Zeta potential curves of dolomite, monazite, and bastnäsite in the presence of 1 ×10^{-3} M NaCl as a function of pH.

The zeta potentials of the minerals at pH 5, 7, and 9 after conditioning with dolomite supernatant for 0, 30, 60, 120 and 240 s then added with benzohydroxamate were also measured. The results are presented in Figure 5.4, where the error bars represent 95% confidence interval. The changes of the zeta potential values as conditioning time increases do not seem to be significant, particularly those of dolomite and bastnäsite. To be able to determine if the changes are statistically significant, a paired *t*-test was conducted using GraphPad Software, Inc (California, USA). When dolomite is added with the collector after conditioning with supernatant, the zeta potential change after 60 and/or 120 s conditioning has been shown to be significant. However, for pH 7 and 9, after 240 s conditioning, the zeta potential seemed to resemble that of its original state (0 s). Monazite's zeta potential was not affected at pH 7, but has changed remarkably at pH 5, and at pH 9 (only after 120 s). Bastnäsite has been affected appreciably by the supernatant at pH 5, 7 and 9; however, at pH 7, the change in zeta potential after 240 s conditioning, is not statistically significant. In general, after 240 s conditioning:

a) at pH 5, the three minerals have been affected by the supernatant;
b) at pH 7, the change of minerals' zeta potential (compared to the initial zeta potential values) is not statistically significant; and,
c) at pH 9, both monazite and bastnäsite have been influenced by the supernatant, but not dolomite.

RE minerals (monazite and bastnäsite) have been observed to be mostly affected by the supernatant at pH 9 and literature reported that hydroxamic acid is found to be effective in RE mineral flotation between pH 8 and 9 [5.29, 5.31, 5.32]. Due to these behavior, further zeta potential measurements were conducted at pH 9 in the presence of only dolomite supernatant (Sup) and only benzohydroxamic acid (BHA). In Figure 5.5, the comparison of the measurements for NaCl, supernatant, benzohydroxamic acid (collector), and collector after supernatant conditioning, is presented. The zeta potential with and without collector is similar for dolomite, but has changed for monazite and bastnäsite. This suggests that benzohydroxamic acid had adsorbed significantly onto the latter but not the former. In the presence of the supernatant, the zeta potential of the minerals (with or without collector) became less negative. It should be noted that dissolution test was conducted for dolomite in the conditioning time investigated. The result showed that the decrease in the zeta potential of dolomite with the supernatant is indeed due to dissolved mineral species from supernatant and not due to the dissolution of dolomite itself.

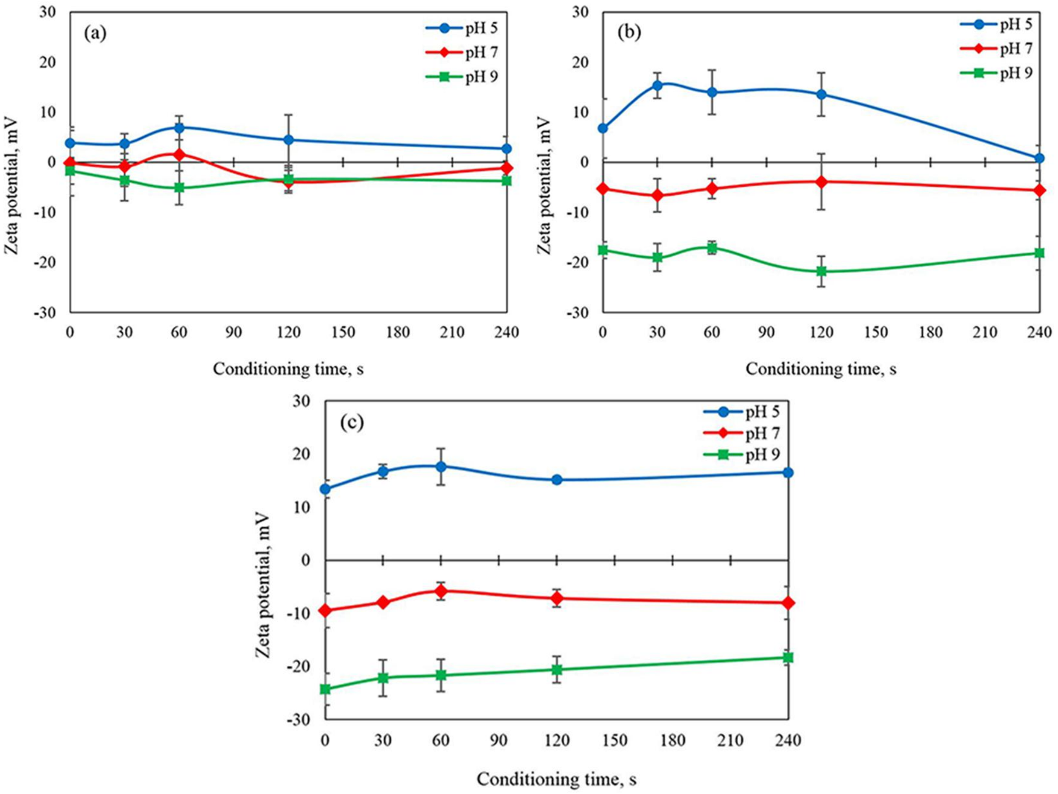

Figure 5.4 – Zeta potential curves of: (a) dolomite, (b) monazite, and (c) bastnäsite in the presence of benzohydroxamate collector as a function of conditioning time.

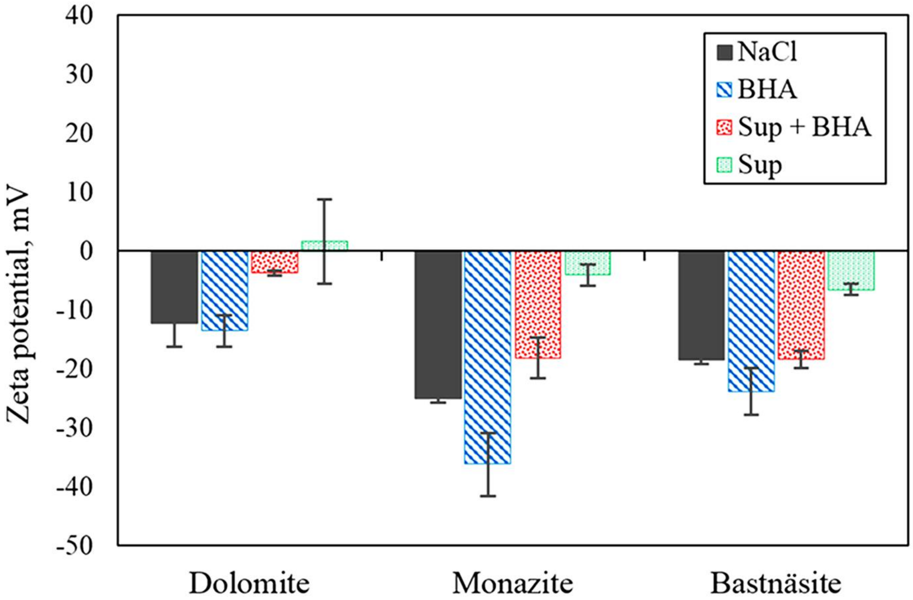

Figure 5.5 – Zeta potential values of dolomite, monazite, and bastnäsite in the presence of 1 $\times 10^{-3}$ M NaCl, benzohydroxamic acid (BHA), supernatant – benzohydroxamic acid (BHA) and only supernatant at pH 9.

5.3.3 Microflotation

The floatability of the dolomite, monazite, and bastnäsite in distilled water and in dolomite supernatant was measured by conducting microflotation tests. The results are presented with error bars representing 95% confidence interval. In Figure 5.6, the results showed that the floatability of dolomite in distilled water and supernatant are 14.5 ± 0.3 % and 15.2 ± 1.9 %, respectively. This indicates that the presence of supernatant does not affect the floatability of dolomite when floated with benzohydroxamic acid collector. However, the floatability of monazite and bastnäsite in distilled water, which are 61.3 ± 0.7 % and 74.6 ± 3.2 %, reduced to 28.6 ± 5.1 % and 14.0 ± 7.9 %, respectively, when floated in the presence of dolomite supernatant. This suggests that the dolomite supernatant has an impact on the adsorption of the collector onto monazite's and bastnäsite's surface. This corresponds well with the results of zeta potential measurements, which indicated a decrease in the collector adsorption in the presence of dolomite supernatant.

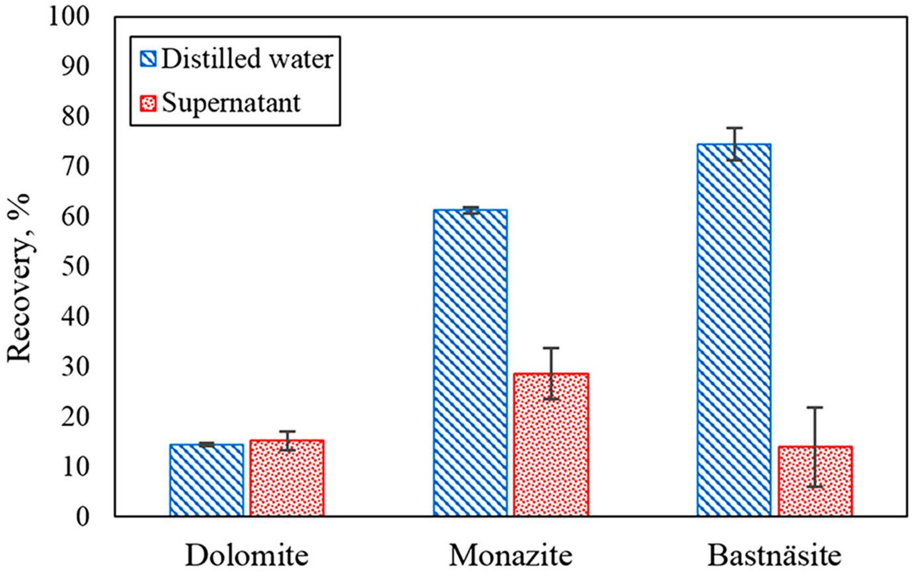

Figure 5.6 – Microflotation results of dolomite, monazite, and bastnäsite using benzohydroxamic acid (BHA) collector in distilled and dolomite supernatant at pH 9.

5.3.4 Speciation diagrams

Speciation diagrams were plotted using HySS2009 software (Protonic software) [5.33] and Spana (Java edition of Medusa) [5.34]. These programs are based on the algorithms by [5.35] and [5.36], respectively.

Speciation of dolomite supernatant is presented in Figure 5.7. The total concentration of Ca and Mg ions used in the calculation is 200 μM and 150 μM, respectively. The calculations were conducted assuming that the system is open to the atmosphere where $p\mathrm{CO_2}$ is $10^{-3.5}$ atm at 1 atm, 25 °C. Species containing Ca ions and species containing Mg ions are presented in separate figures for easier analysis. The results showed that the dolomite species in solution will precipitate forming $Mg(OH)_2$ and $Ca(OH)_2$ dominantly at pH 10 and 11, respectively. At pH lower than these, it will mostly occur as Ca and Mg ions; Mg-carbonate precipitate will also be formed and will be dominant at pH between 6 and 10. Minor amount of $CaCO_3$ will also precipitate at alkaline pH. The speciation was presented to simulate what species could be present in the solution and/or at the surface of the minerals at equilibrium condition. It does not necessarily reflect the actual system during the experimentation.

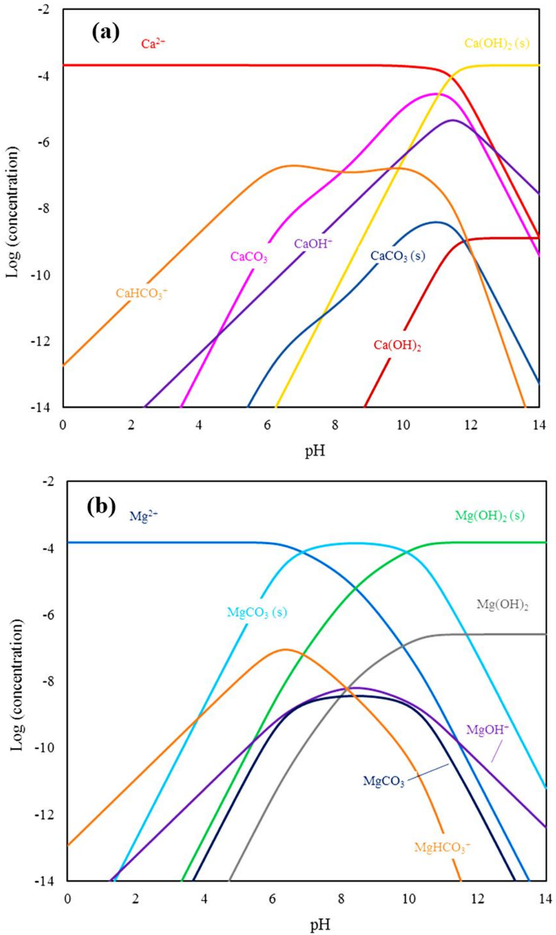

Figure 5.7 – Speciation diagram of dolomite species in solution: (a) species containing Ca ions; and, (b) species containing Mg ions. Total concentration: $[Ca^{2+}]_{TOT}$ = 200 μM, $[Mg^{2+}]_{TOT}$ = 150 μM, $p\mathrm{CO_2} = 10^{-3.5}$ atm at 1 atm and T = 25 °C.

5.3.5 X-ray Photoelectron Spectroscopy (XPS)

The samples were also analyzed with XPS to identify the actual species that might have precipitated at the mineral surfaces. XPS spectra of dolomite, monazite and bastnäsite are presented in Figure 5.8, Figure 5.9 and Figure 5.10, respectively. The analysis of results is presented in the following sections.

5.3.5.1 XPS spectra for dolomite

Different spectra (C 1s, O 1s, Ca 2p, and Mg 1s) for dolomite were presented in Figure 5.8a - Figure 5.8d. The C 1s spectra (Figure 5.8a) showed contaminants such as adventitious C–C, C–O–C and O–C=O with peaks at around 284.78, 286.38 and 287.88 eV [5.37–5.40], respectively. The C 1s peak at 289.55 eV [5.41, 5.42]; O 1s peak at 531.40 eV [5.41, 5.42]; Ca 2p peak at 346.98 eV [5.41, 5.42]; and Mg 1s peak at 1303.53 eV [5.43, 5.44]; confirm the presence of dolomite. The slight increase in the intensity and the shift of the Ca 2p peak from 346.98 eV to 346.88 eV after exposing the sample to dolomite supernatant, could be due to the formation of amorphous carbonate and/or magnesian calcite at the surface [5.45]. As shown in Figure 5.8c, besides the doublets for dolomite (Ca $2p_{3/2}$ at around 346.98 eV) [5.41, 5.42], the Ca 2p spectra also required the fitting of a doublet at higher energy (Ca $2p_{3/2}$ at around 347.87 eV), which could be assigned to $Ca(OH)_2$ [5.46] and/or $>CaOH^0$ [5.47]. The peak at around 532.98 eV of the O 1s spectra (Figure 5.8b) also indicated the presence of $Ca(OH)_2$ (Lee et al., 2014), $>CaOH^0$ [5.37, 5.47] and/or $MgCO_3$ [5.43, 5.48, 5.49]. $Ca(OH)_2$ might not be the best candidate for these peaks since they have been observed at a lower BE than that of the carbonates [5.50–5.52]. Meanwhile, $>CaOH^0$ (a surface hydrolysis product) could be present due to the hydration of the surface–Ca^+ as observed by Stipp and Hochella [5.47]. In the presence of the supernatant, both Ca 2p and O 1s spectra show that the contribution of the $Ca(OH)_2$ / $>CaOH^0$ and/or $MgCO_3$ peaks seem to decrease. However, the Mg KL4 Auger contribution at 350.93 eV [5.44] in the Ca 2p spectra (Figure 5.8c) and the secondary peak (1305.53 eV) assigned to $MgCO_3$ in the Mg 1s spectra (Figure 5.8d) have increased in the presence of the supernatant. This suggests that the decrease of the $Ca(OH)_2$ / $>CaOH^0$ and/or $MgCO_3$ assigned peaks is mostly due to the relative decrease of these Ca species at the surface compared to $MgCO_3$.

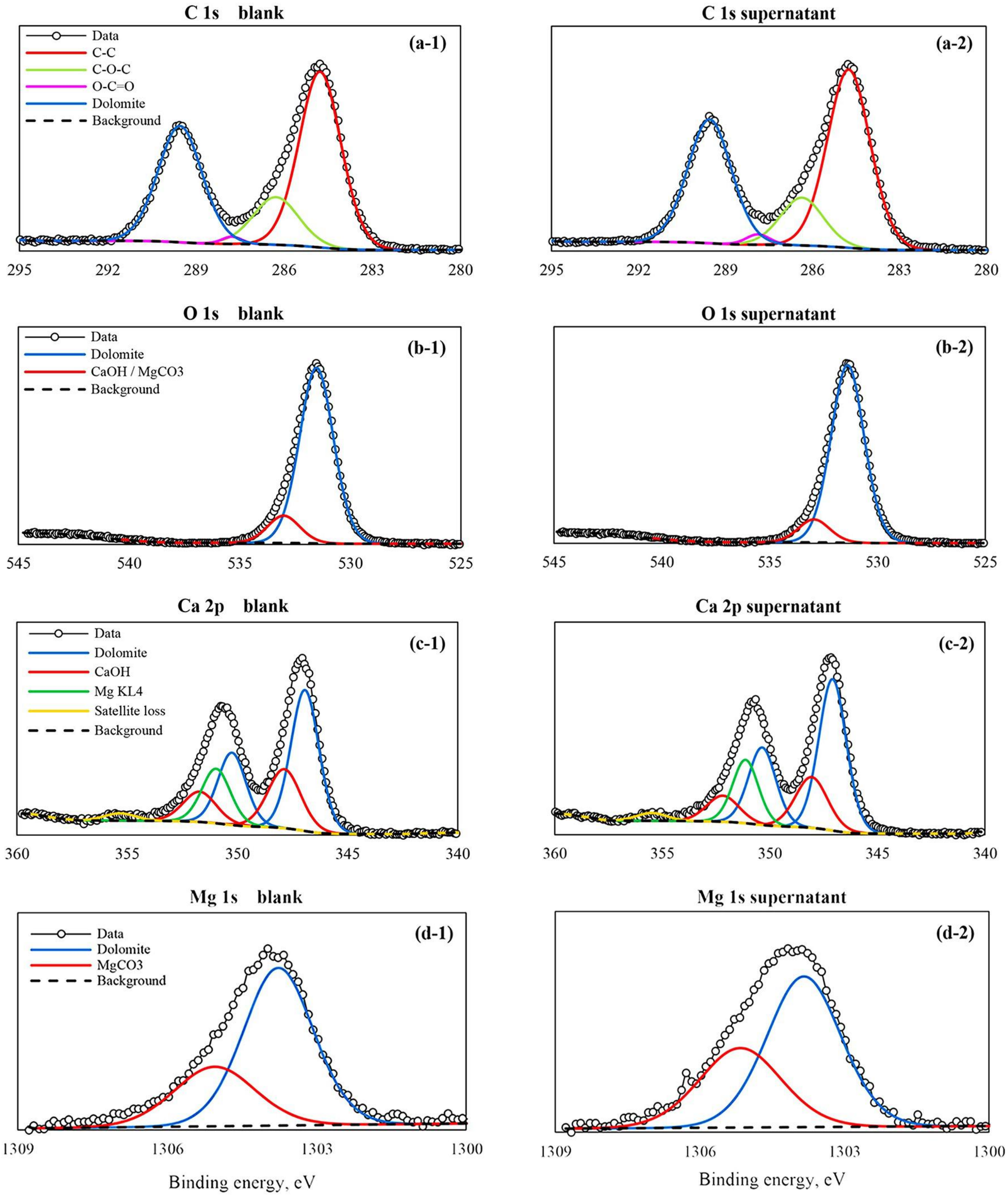

Figure 5.8 – XPS spectra of dolomite without (a-1, b-1, c-1, d-1) and with supernatant (a-2, b-2, c-2, d-2) considering C 1s, O 1s, Ca 2p and Mg 1s scans, respectively.

5.3.5.2 XPS spectra for monazite

The C 1s XPS spectra (Figure 5.9a) for the monazite sample presented peaks assigned to contaminants: adventitious C–C and C–O–C [5.37–5.40] at around 284.88 and 286.07 eV, respectively. The presence of the peak at around 288.48 eV could be assigned to O–C=O or to metal carbonates [5.40]. The existence of peak at around 532.48 eV in the O 1s spectra confirmed the occurrence of carbonate [5.37, 5.53], which could be due to calcite, a minor contaminant in the monazite sample (as presented in the XRD patterns). Apart from this peak, the O 1s spectra (Figure 5.9b) required another two peaks to fit the data: the lower BE, assigned to monazite [5.54–5.56], at around 530.97 eV; and the third peak at around 533.58 eV, close to the values referenced for $MgCO_3$ [5.43, 5.48, 5.49]. Although the $MgCO_3$ peak can be neglected in the fitting of the blank sample, by increasing the contribution from the C–O peak, it is necessary for a proper fitting of the spectra after contact of the sample with supernatant. The indication of the increase of the presence of $MgCO_3$ could also be confirmed by the Mg KL4 Auger line (at around 351.06 eV) required for fitting the Ca 2p spectra (Figure 5.9c) after exposing the monazite samples to dolomite supernatant. The fitting of the Ca 2p spectra also required a single peak at BE around 344.54 eV, which might be due to a Zr $3p_{1/2}$ line (Zr being present in monazite sample as a minor contaminant); and a doublet at higher BE (Ca $2p_{3/2}$ at around 347.03 eV) which could be assigned to carbonates [5.41, 5.42, 5.47, 5.50, 5.57, 5.58].

5.3.5.3 XPS spectra for bastnäsite

The bastnäsite C 1s XPS spectra (Figure 5.10a) required the fitting of peaks for multiple species. Adventitious C–C, C–O–C and O–C=O was assigned to the peaks fitted at 284.81, 286.13 and 287.24 eV [5.37–5.40], respectively. The bastnäsite peak was observed at around 289.72 eV [5.59], whereas a peak with higher binding energy, at around 291.78 eV, could indicate the presence of $>CO_3H^0$ (a surface complex) [5.47]. The contribution of the carbonate (bastnäsite), O–C=O and $>CO_3H^0$ (a surface complex) to the spectra increased after conditioning the sample with supernatant.

The peak at around 531.40 eV in the O 1s spectra (Figure 5.10b-1) confirmed the presence of carbonates (which could be assigned to bastnäsite) [5.59]; this peak and the peak at around 532.98 eV could also be assigned to C–O from calcium carbonate polymorphs [5.37]. In the presence of dolomite supernatant (Figure 5.10b-2), the shift of the peak at around 532.98 eV (assigned to calcium carbonate) to 533.28 eV, indicate the appearance of >CaOH^0 (a surface complex) [5.37, 5.47] and/or MgCO$_3$ [5.49] at the surface of the minerals. The Ca 2p spectra (Figure 5.10c), which required the fitting of doublets for bastnäsite (Ca2p$_{3/2}$ at around 346.47 eV) [5.59] and doublets at a higher binding energy (Ca2p$_{3/2}$ at around 349.28 eV), which might be assigned to >CaOH^0 [5.47]; validated the above finding. No Mg KL4 Auger line was necessary to achieve a good fitting of the Ca 2p spectra, which suggests the absence of Mg species.

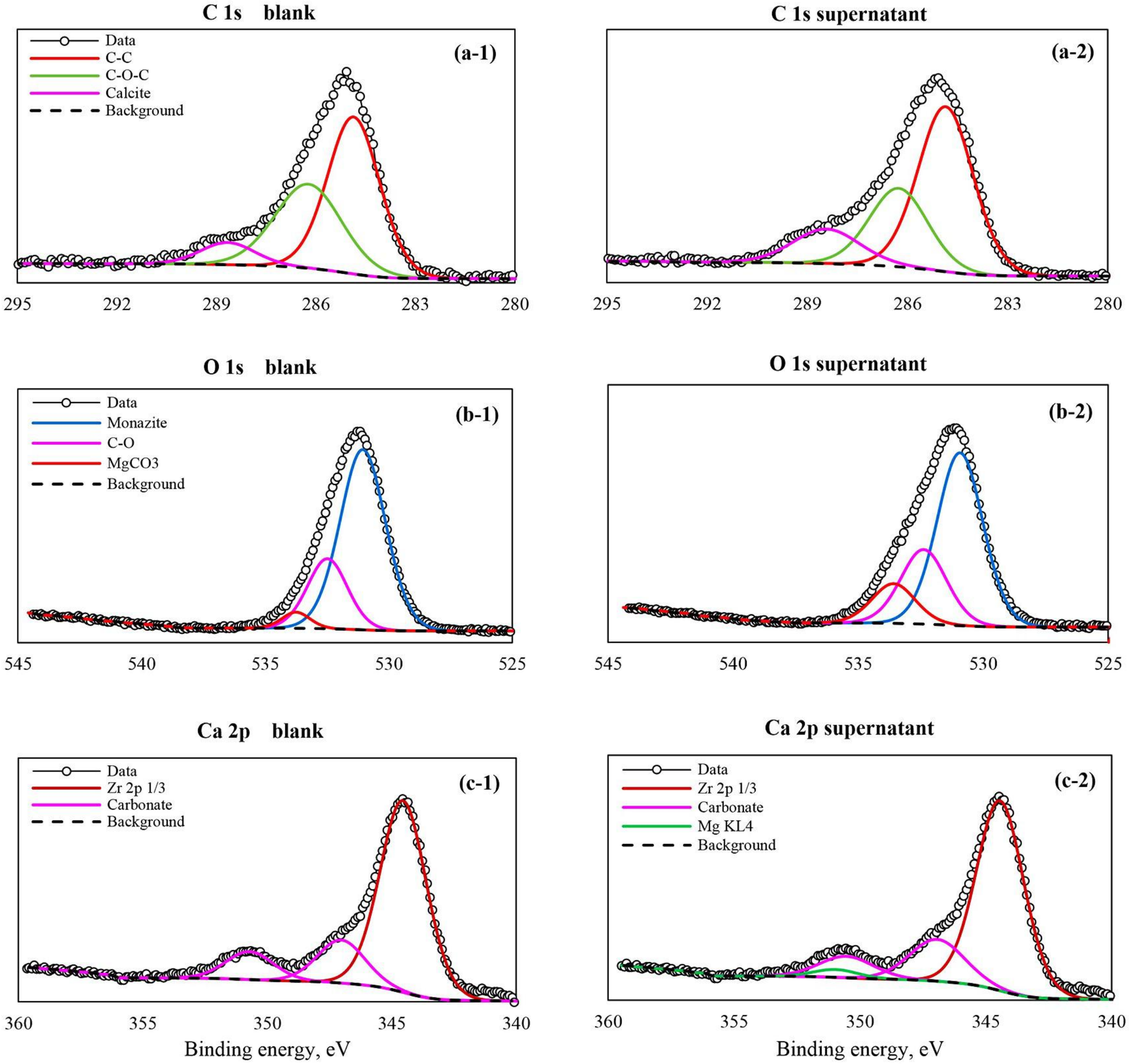

Figure 5.9 – XPS spectra of monazite without (a-1, b-1, c-1) and with supernatant (a-2, b-2, c-2) considering C 1s, O 1s, and Ca 2p scans, respectively.

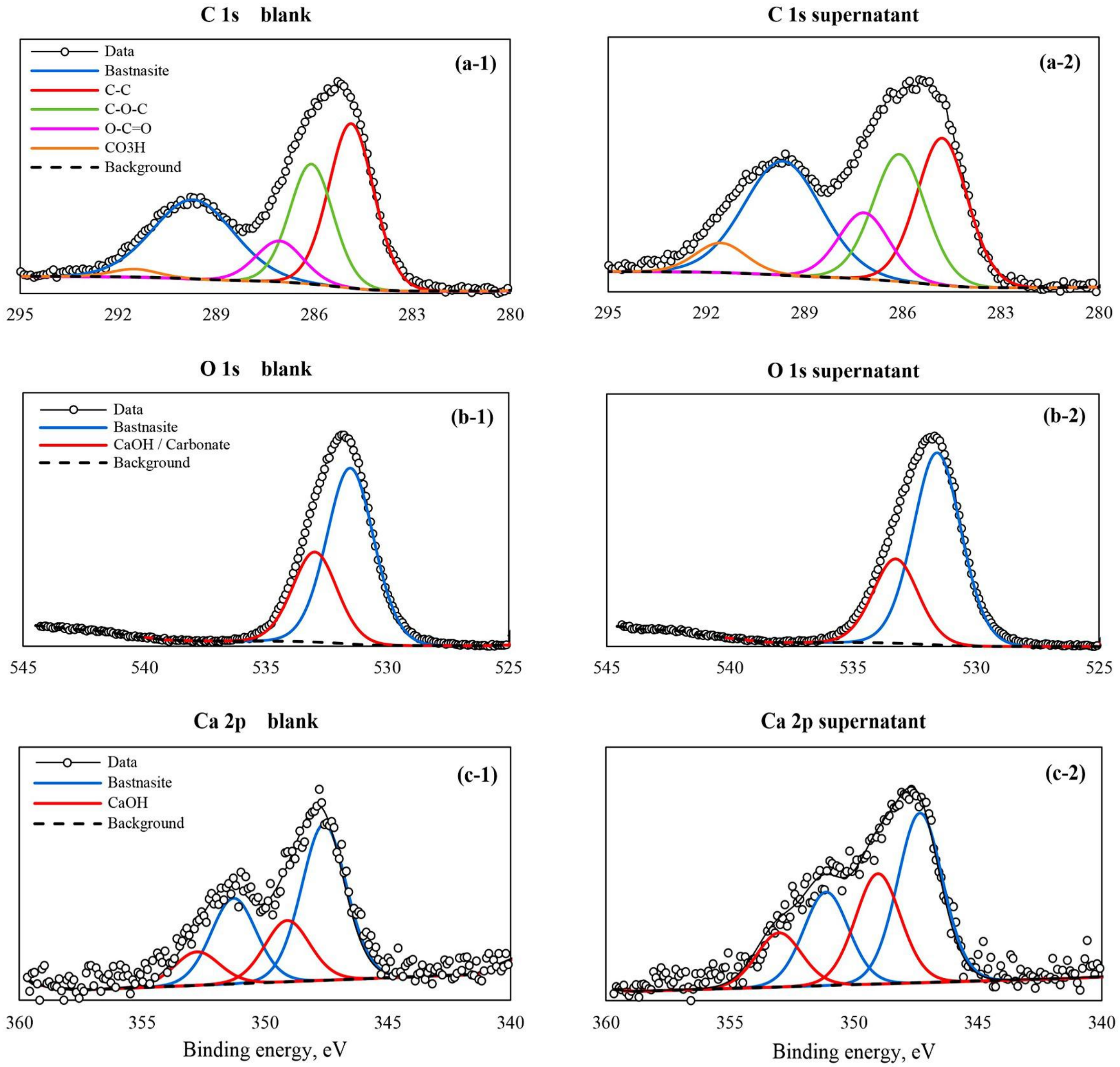

Figure 5.10 – XPS spectra of bastnäsite without (a-1, b-1, c-1) and with supernatant (a-2, b-2, c-2) considering C 1s, O 1s, and Ca 2p scans, respectively.

5.3.6 DFT calculations

This section contains the DFT calculations simulating the interaction of benzohydroxamic acid on the RE minerals and dolomite surfaces, as well as in the presence of dolomite supernatant. As the behavior of both monazite and bastnäsite were the same through flotation studies, it was decided to use only monazite for DFT simulation to economize simulation cost. Dolomite as a gangue carbonatite mineral was also considered to compare with monazite results.

5.3.6.1 Optimized structure of the collector

The structure and reactivity of the collector should be properly studied to discover the nature of its interaction with mineral surfaces. Therefore, it was firstly decided to optimize the structure of benzohydroxamic acid collector by DFT simulation. Benzohydroxamic acid collector is dissociated in an aqueous environment at pH above 8.8 (its pKa is 8.8) [5.60]. Since the experiments were conducted at pH 9 (pH>pKa), the geometry and electronic properties of ionic form of benzohydroxamic acid was considered in the simulation. The geometry of ionic form of the collector after optimization is shown in Figure 5.11a. The lengths of the bonds N–O and C=O are 1.269 and 1.231 Å, respectively. The simulated O–N–H, C–N–H, C–N–O, O=C–N, C–C–N, and O=C–C bond angles were obtained to be 117.6°, 119.8°, 122.5°, 119°, 115.8°, and 125.2°, respectively. Likewise, the Highest Occupied Molecular Orbital (HOMO) of benzohydroxamic acid collector is presented in Figure 5.11b. It can be seen that the collector's transferable charge is located on its polar head bearing the functional group RC(O)N(OH). In this regard, the average charge of O on both C=O and N–O amounts to -0.41e based on the Mulliken charge analysis, indicating that these two O can be considered as active part in the polar head of collector. This means that the N–O and C=O groups of the collector polar head can be involved in collector-mineral interactions. Through adsorption, electrons from the negatively charged ions can be shared with mineral surfaces through covalent bonding. This can take place through donating valence electrons from benzohydroxamic ions High Occupied Molecular Orbital (HOMO) to Lowest Unoccupied Molecular Orbital (LUMO) on the mineral surfaces [5.61]. The charges of O on each of C=O and N–O contribute for -0.35e and -0.47e respectively indicating that oxygen atom in N–O has a stronger coordination ability with the metal ions as compared to the carbonyl O.

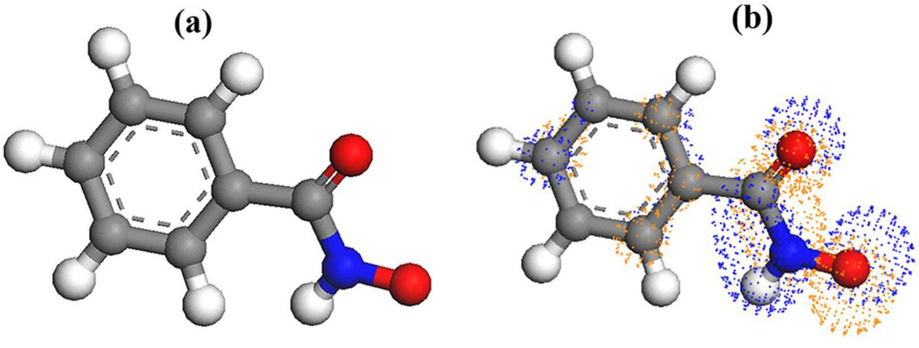

Figure 5.11 – DFT optimized structure of (a) benzohydroxamic acid ionic form, and (b) Highest occupied molecular orbitals (HOMO) of this anionic collector (N ≡ Blue, O ≡ Red, C ≡ Gray, H ≡ White).

5.3.6.2 Optimized structure of the crystal and slab of the minerals

The ideal structure of dolomite and monazite crystal are provided in Figure 5.12 and 5.13 respectively. After converging the unit cell of these two minerals, their corresponding dimensions are a=6.89, b=7.05, and c=6.68 Å for monazite; and a=b=4.92 Å and c=16.56 Å for dolomite. These results are in agreement with previously reported values derived from X-ray diffraction (for monazite: a=6.79, b=7.02, and c=6.46 Å, & for dolomite: a=b=4.81 Å and c=16.01 Å) and the literature values from DFT simulations (for dolomite: a=b=4.92 Å, c=16.63 Å) [5.19, 5.20, 5.62]. As seen in Figure 5.12, dolomite bulk structure consists of CO_3^{2-} layers sandwiched between Ca^{2+} and Mg^{2+} layers [5.19, 5.20]. The monazite crystal structure belongs to a monoclinic space group with P21/n settings in which the RE atoms are surrounded by nine-coordinated oxygen atoms. In the monazite structure, phosphorus atoms are only bound to oxygen atoms. The structures formed are polyhedral for RE - oxygen atoms coordination and tetrahedral for phosphate – oxygen structure yielding polyhedron – tetrahedron chains in the two RE(PO_4) structures [5.9, 5.62].

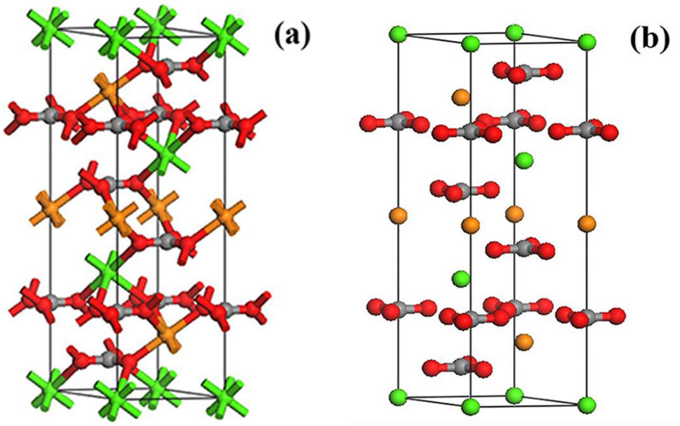

Figure 5.12 – Structure of dolomite crystal (Ca ≡ Green, O ≡ Red, C ≡ Gray, Mg ≡ Orange).

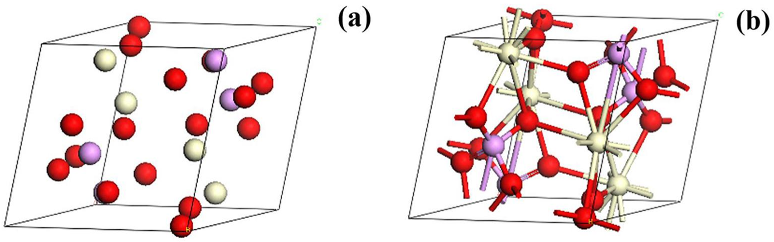

Figure 5.13 – Structure of monazite crystal (Ce ≡ Beige, O ≡ Red, P ≡ Purple).

For surface calculation, the (104) surface was used for dolomite since this slab is known to be the most stable surface of carbonatite minerals such as dolomite and calcite [5.20]. This surface was built by cleaving the optimized dolomite bulk structure through the (104) plane (as seen in Figure 5.12). In the case of monazite, the (100) plane was selected as this plane is more likely to occur [5.9]. Figures 5.14 and 5.15 illustrate dolomite and monazite slabs from different views.

Ca and Mg on the surface of dolomite, and Ce on the monazite surface can be considered as the main active centers for interaction with the anionic collector [5.63]. The site density of Ca–O and Mg–O on face (104) dolomite slab was calculated to be 2.55 nm^{-2} for each metal type (which agrees with the reported value of Wolthers *et al.* [5.64]) and Ce–O on face (100) monazite was 3.82 nm^{-2} based on optimized slab structure. Hence, the site density of Ce on the monazite surface is higher than that of each of Mg and Ca on the dolomite surface, but is less than their sum; suggesting that site density of metal cation on dolomite surface is higher than monazite.

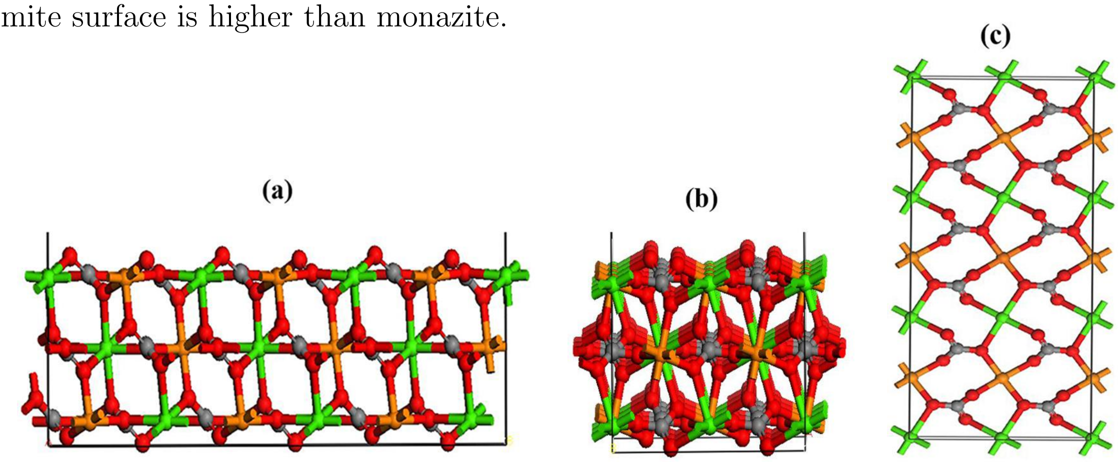

Figure 5.14 – Structure of dolomite slab (104) from (a) front, (b) side, and (c) top views (Ca ≡ Green, O ≡ Red, C ≡ Gray, Mg ≡ Orange).

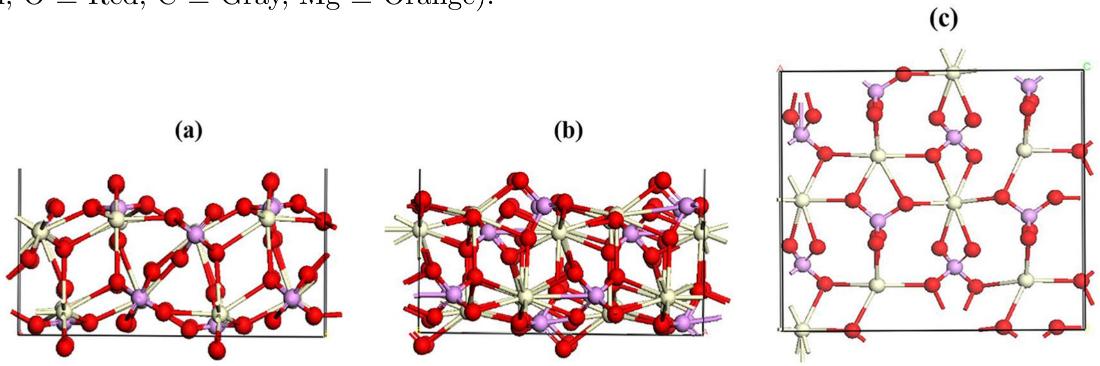

Figure 5.15 – Structure of monazite slab (100) from (a) front, (b) side, and (c) top views (Ce ≡ Beige, O ≡ Red, P ≡ Purple).

5.3.6.3 Adsorption of various supernatant species on monazite surface

Speciation diagram (Figure 5.7) shows that various species such as $Ca(OH)_2$, $Mg(OH)_2$, $CaCO_3$, and $MgCO_3$ could precipitate out of dolomite supernatant, as well as possibly adsorbing onto the surface of the minerals. Although the XPS results (Section 5.3.5) could identify only the presence of calcium and magnesium carbonates, the interaction of the hydroxide precipitates with monazite surface was also investigated and is provided in Figure 5.16.

As presented in Figure 5.16a and b, either $MgCO_3$ or $CaCO_3$ solvated ion pairs could interact on the monazite surface through covalent bonding between their O tethered in carbonate and Ce on the monazite surface. These ion pairs can be viewed as the precursors to their precipitate analog depending on the prevailing pH (Figure 5.7). The bond lengths were 2.7 and 2.76 Å for $MgCO_3$ and $CaCO_3$, respectively. As can be observed, Mg and Ca from these carbonate species are exposed at the interface, exposing these new metals centers, instead of a Ce atom located on the monazite surface. The interaction energy of $MgCO_3$ and $CaCO_3$ on the monazite surface was calculated to be -112.1 kJ/mol and -121.2 kJ/mol respectively. As presented in Figure 5.16c, $Ca(OH)_2$ is adsorbed on the surface through formation of two covalent bonds between Ca and O with surface O and Ce atoms, respectively. The lengths of Ca–O and O–Ce bonds are 2.07 and 2.51 Å, respectively. The second hydroxide group of $Ca(OH)_2$ did not participate to surface covalent bonding, but its hydrogen was involved in hydrogen bonding with oxygen atom on the surface with a bond length of 1.88 Å. The interaction energy of $Ca(OH)_2$ through adsorption is calculated to be -145.3 kJ/mol.

In addition to these species, Ca^{2+} present in supernatant could also adsorb onto the monazite surface. At pH 9, James and Healy [5.65] indicated that metal cation (such as Ca^{2+}) would preferentially adsorb electrostatically onto a negative surface. XPS results indicated the presence of Ca ion as a surface complex, $>CaOH^0$, due to the hydrated mineral surface. As such, adsorption of Ca^{2+} on the monazite (100) surface was also simulated. This cation was located at different initial positions on monazite (100) surface in order to locate its likeliest adsorption conformation. It was found that Ca^{2+} can only have one optimal configuration on the monazite surface (Figure 5.16d). In this most stable configuration, calcium cation adsorbed through strong covalent bonds with three O atoms and one P atom on the mineral surface. The interaction energy of this adsorption is calculated to be -534.6 kJ/mol, revealing a highly favourable interaction.

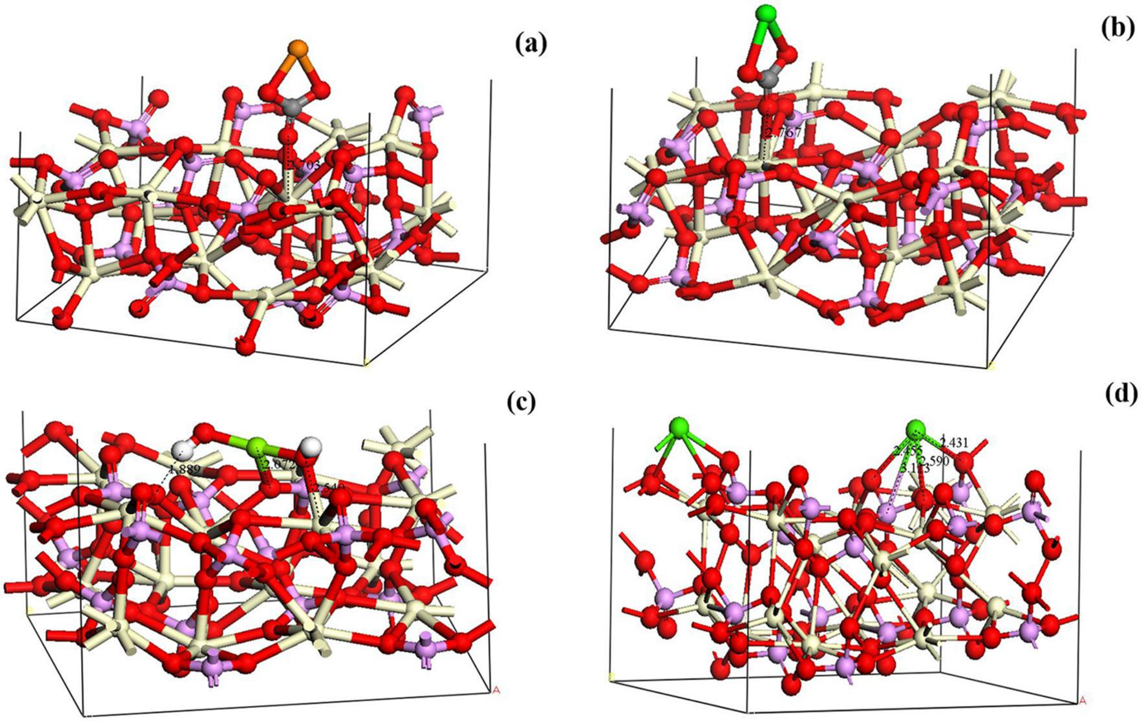

Figure 5.16 – Interaction of (a) $MgCO_3$, (b) $CaCO_3$, (c) $Ca(OH)_2$ and (d) Ca^{2+} ions on the monazite surface (100) (Ce ≡ Beige, O ≡ Red, P ≡ Purple, C ≡ Gray, Mg ≡ Orange, Ca ≡ Green, H ≡ White).

At pH 9, all these adsorbed species on the monazite (100) surface can act as active centers to interact with benzohydroxamic acid collector and even OH^-, a potential determining ion. At this pH, excess OH^- contributes to the negative charge on the monazite surface. Since the surface of monazite may be modified after precipitation of supernatant species, adsorption of OH^- may also be affected. For this reason, the interaction energy of $OH^-$with bare monazite (100) surface and with adsorbed supernatant species on the monazite (100) surface was calculated and provided in Table 5.2. These results indicate that monazite surface may adsorb strongly hydroxide ions on bare monazite surface.

Table 5.2 – Hydroxide adsorption energy on the monazite (100) surface active centers with and without precipitated supernatant species.

Ion	Interaction energy (kJ/mol) of OH^- with active centers on monazite (100) surface				
	Ce atoms on bare monazite (100) surface	Adsorbed supernatant species on the monazite (100) surface			
		$MgCO_3$	$CaCO_3$	$Ca(OH)_2$	Ca^{2+}
OH^-	-120.3	-71.6	-74.3	-71.4	-83.3

5.3.6.4 Collector – mineral interactions

In order to understand the behavior of monazite and dolomite flotation with supernatant and with distilled water, the interaction between benzohydroxamic acid collector and their surfaces was studied by DFT simulation. Figure 5.17 and 5.18 illustrate the detail of interaction of conjugate base of benzohydroxamic acid with bare monazite and dolomite surfaces, respectively.

As discussed earlier, the polar collector head has high potential to interact with the mineral surfaces on account of the HOMOs transferable charges located in the N–O and C=O groups (Figure 5.11). As presented in Figure 5.17a, either C=O or N–O group interact with Ce atoms on monazite surface through covalent bonding. The O–Ce distances between N–O and C=O groups and surface Ce atoms are *ca.* 2.38 and 2.42 Å, respectively. Figure 5.17b presents another possible configuration of collector interaction on the monazite surfaces. In this configuration, the O–Ce distances between N–O and C=O groups and surface Ce atoms are 2.43 and 2.5 Å, respectively. Such collector – mineral bond lengths are close to the Ce–O bond length average in the monazite slab (100) structure (2.55 Å). The two active functional groups can interact with Ce either through bidentate (Figure 5.17a) or bridged binding (Figure 5.17b) conformations. The N–C=O and C–N–O angles of adsorbed collector on the monazite surface are 117.3° and 114.2° for the collector configuration shown in Figure 5.17a; and 117.2° and 121.7° for that of Figure 5.17b. These angles are close to the equilibrium N–C=O and C–N–O angles of the free benzohydroxamic acid collector (119.0° and 122.5°), indicating some degree of stability of the interaction. Also, the corresponding interaction energies are calculated to be -385.5 and -330.3 kJ/mol for Figure 5.17 cases a and b, respectively. The bidentate configuration (Figure 5.17a) is more favourable than the bridged binding conformation (Figure 5.17b) for the collector – monazite interaction on account of bond length, interaction energy, and N–C=O and C–N–O angles.

The same information was obtained for the case of collector – dolomite interaction. The configuration of collector on the (104) dolomite slab is shown in Figure 5.18. This simulation was repeated several times to confirm this configuration. As seen, the interaction between N–O functional group and Ca atoms on the surface occurred via monodentate binding conformation. In this collector – dolomite interaction, it appears that the C=O group in collector and Mg atoms on the surface are less active than the N–O group and Ca atoms. This contrast in affinities can be ascribed to Ca higher ionic radius and lesser electronegativity as compared to Mg, enabling the former to be easily approached by the collector via N–O group.

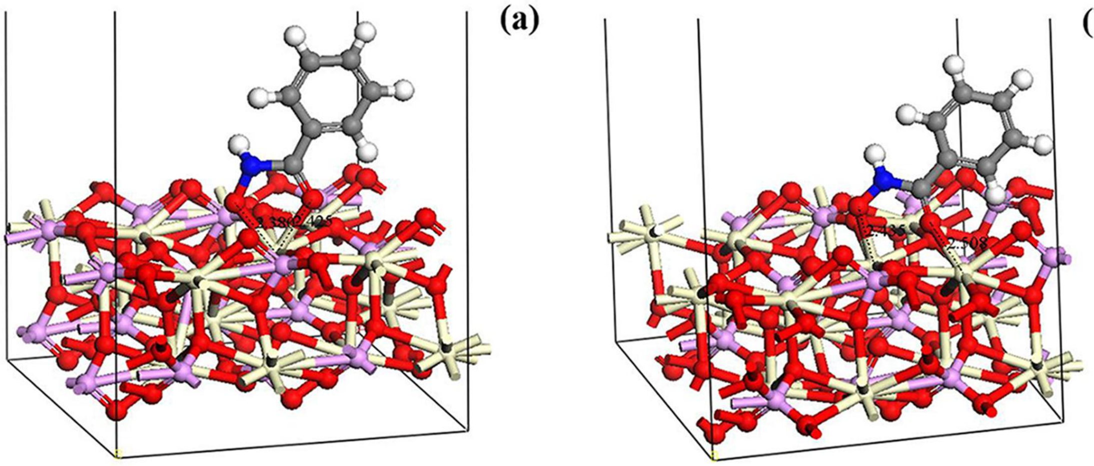

Figure 5.17 – Two possible conformations of benzohydroxamic acid collector through adsorption on monazite surface (100) (Ce ≡ Beige, O ≡ Red, P ≡ Purple, C ≡ Gray, N ≡ Blue, H ≡ White).

The interaction energy of dolomite – benzohydroxamic acid, -184.8 kJ/mol, is significantly lower than the monazite-collector interaction energy. As seen in Figure 5.18, bond lengths of O–Ca and distance between O–Mg are around 2.67 and 2.82 Å, respectively, and are both larger as compared with those involved in monazite – collector interactions. These distances are slightly exceeding than Ca–O and Mg–O distances (2.4 and 2.2 Å, respectively) on the dolomite surface structure, and confirm the chemical nature of interaction between dolomite and benzohydroxamic collector. These all indicate that the interaction of benzohydroxamic acid with monazite should be stronger than dolomite.

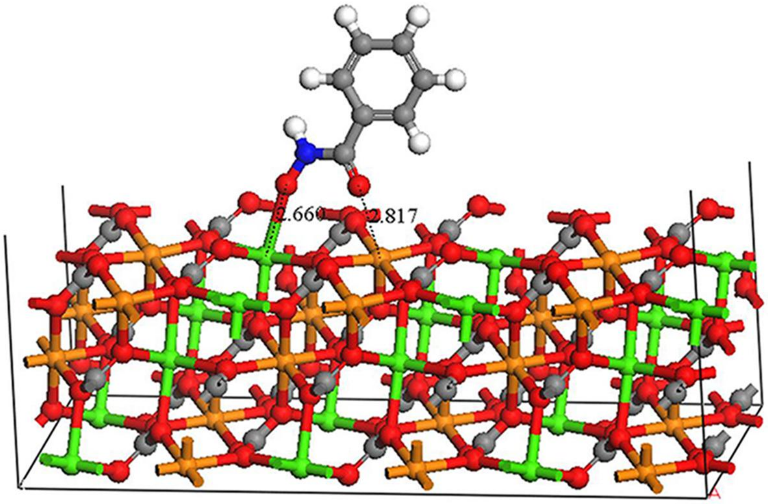

Figure 5.18 – Possible conformation of benzohydroxamic acid collector through adsorption on dolomite surface (104) (Ca ≡ Green, O ≡ Red, C ≡ Gray, Mg ≡ Orange, N ≡ Blue, H ≡ White).

As discussed in the Section 5.3.6.3, the ion pair precursor to the neo-formed precipitates could turn into new collector adsorption sites on the monazite surface. Adsorption of benzohydroxamic acid (ionic form) over pre-adsorbed $Ca(OH)_2$, $CaCO_3$ and $MgCO_3$ species on the monazite surface was studied and shown in Figure 5.19. The collector N–O group can interact with Mg and Ca atoms from the pre-adsorbed ion pair. Table 5.3 gives the interaction energies between the collector and adsorbed $Ca(OH)_2$, $CaCO_3$, $MgCO_3$ ion pairs as well as Ca^{2+}. It is evident that the collector interaction energies have significantly decreased once the monazite surface had pre-adsorbed collector-interacting Mg and Ca bearing inorganic species coming from the dolomite supernatant.

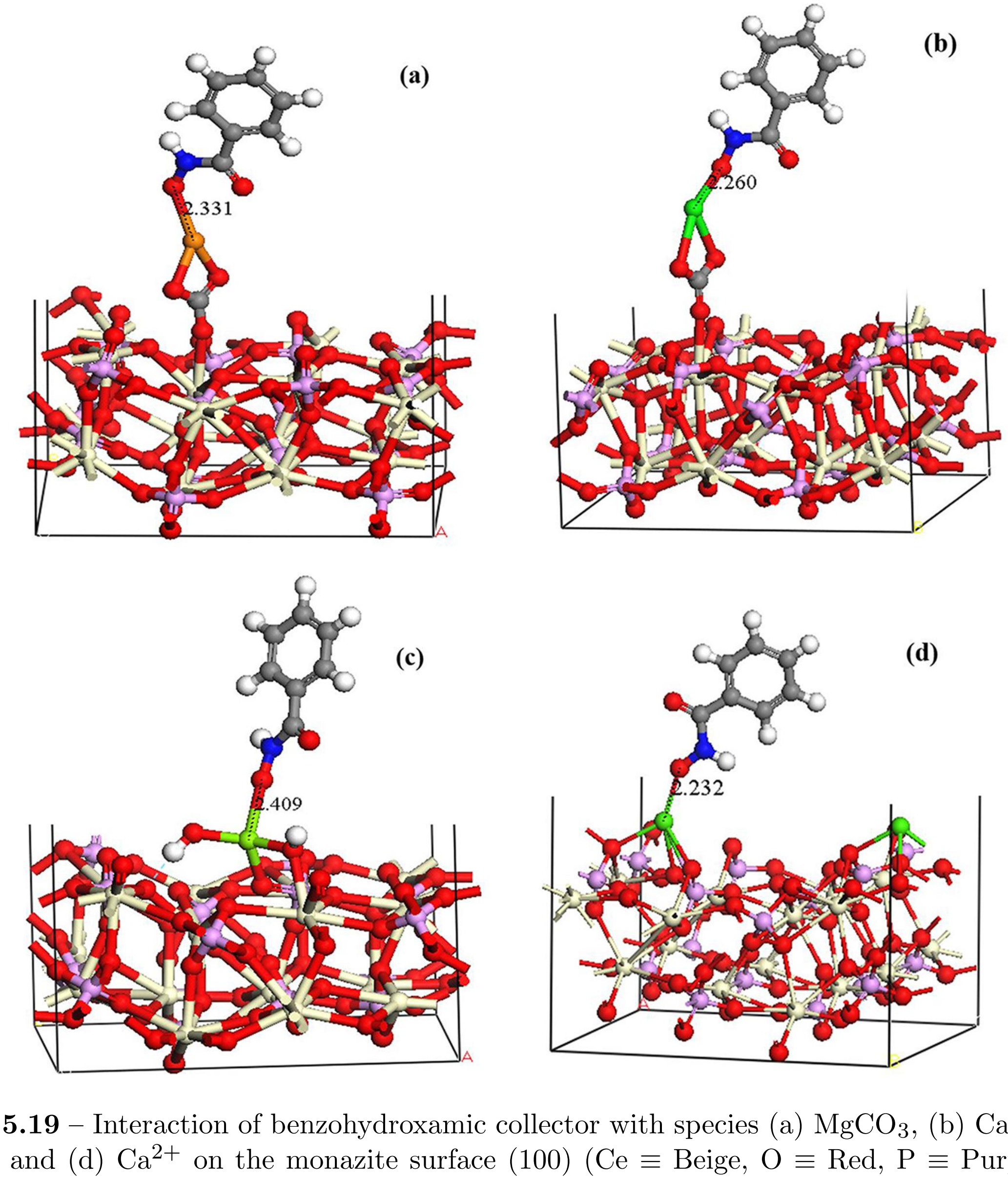

Figure 5.19 – Interaction of benzohydroxamic collector with species (a) $MgCO_3$, (b) $CaCO_3$, (c) $CaOH_2$, and (d) Ca^{2+} on the monazite surface (100) (Ce ≡ Beige, O ≡ Red, P ≡ Purple, C ≡ Gray, Mg ≡ Orange, Ca ≡ Green, N ≡ Blue, H ≡ White).

Table 5.3 – Adsorption energy of benzohydroxamate collector on dolomite (104) surface and monazite (100) surface active centers with and without precipitated supernatant species.

Component	Interaction energy (kJ/mol)					
	On dolomite (104) surface	On bare monazite (100) surface	Adsorbed supernatant species on the monazite (100) surface			
			$MgCO_3$	$CaCO_3$	$Ca(OH)_2$	Ca^{2+}
Collector	-184.4	-385.5 -330.3	-190.2	-187.7	-177.4	-200.4

5.3.6.5 Complexation of collector with solvated species in bulk solution

A fraction of the collector concentration may be lost and diverted at the expense of homogeneous complexation in bulk solution involving ligand collector and dolomite supernatant species such as Ca^{2+}, Mg^{2+}, $CaOH^+$ and $MgOH^+$. To study such possibility, the complexation affinity of benzohydroxamic acid collector with the solvated forms of these species was examined. Thus, the first hydration layers of Ca^{2+}, Mg^{2+}, $CaOH^+$ and $MgOH^+$ were accounted explicitly for the H_2O molecules. For this purpose, COSMO was applied to consider the effect of the higher hydration shells on the number of water molecules which directly interact with these species in the first hydration layer. For all the cases, the most stable structures considering their relaxation energy were $CaOH(H_2O)_7^+$, $Ca(H_2O)_8^{2+}$, $MgOH(H_2O)_7^+$, and $Mg(H_2O)_8^{2+}$, which are shown in Figure 5.20a-1, b-1, c-1 and d-1, respectively. As seen, $Ca^{2+}$and Mg^{2+} are solvated by eight water molecules in its first hydration shell. The square antiprismatic structures for both solvated $Ca^{2+}$and Mg^{2+} have an average Ca–O and Mg–O bonds length equal to 2.4 Å. On the other hand, $CaOH^+$ and $MgOH^+$ are solvated by seven water molecules in the most stable situation. In all cases, addition of new water molecules did not change $CaOH(H_2O)_7^+$, $Ca(H_2O)_8^{2+}$, $MgOH(H_2O)_7^+$, and $Mg(H_2O)_8^{2+}$ led to an extra solvent molecule located in the 2nd hydration shell, only allowing H bonding interactions with the 1st hydration shell water molecules. In the next step, the interaction and complex structure of benzohydroxamic acid anions with these solvated species in aqueous environment considering COSMO were simulated. The corresponding collector – $CaOH(H_2O)_7^+$, collector – $Ca(H_2O)_8^{2+}$, collector – $MgOH(H_2O)_7^+$, and collector – $Mg(H_2O)_8^{2+}$ structures are illustrated in Figure 5.20a-2, b-2, c-2 and d-2, respectively. Benzohydroxamic acid is indeed capable of strong interactions with these solvated species through covalent bonds which involve both O atoms belonging to collector N–O and C=O groups. These groups located at the collector polar head led to formation new bidentate covalent bond with the inorganic solvated species after these latter have lost two water molecules from their first hydration shell. The interaction energy of benzohydroxamic collector with $CaOH(H_2O)_7^+$, $Ca(H_2O)_8^{2+}$, $MgOH(H_2O)_7^+$, and $Mg(H_2O)_8^{2+}$ are summarized in Table 5.4.

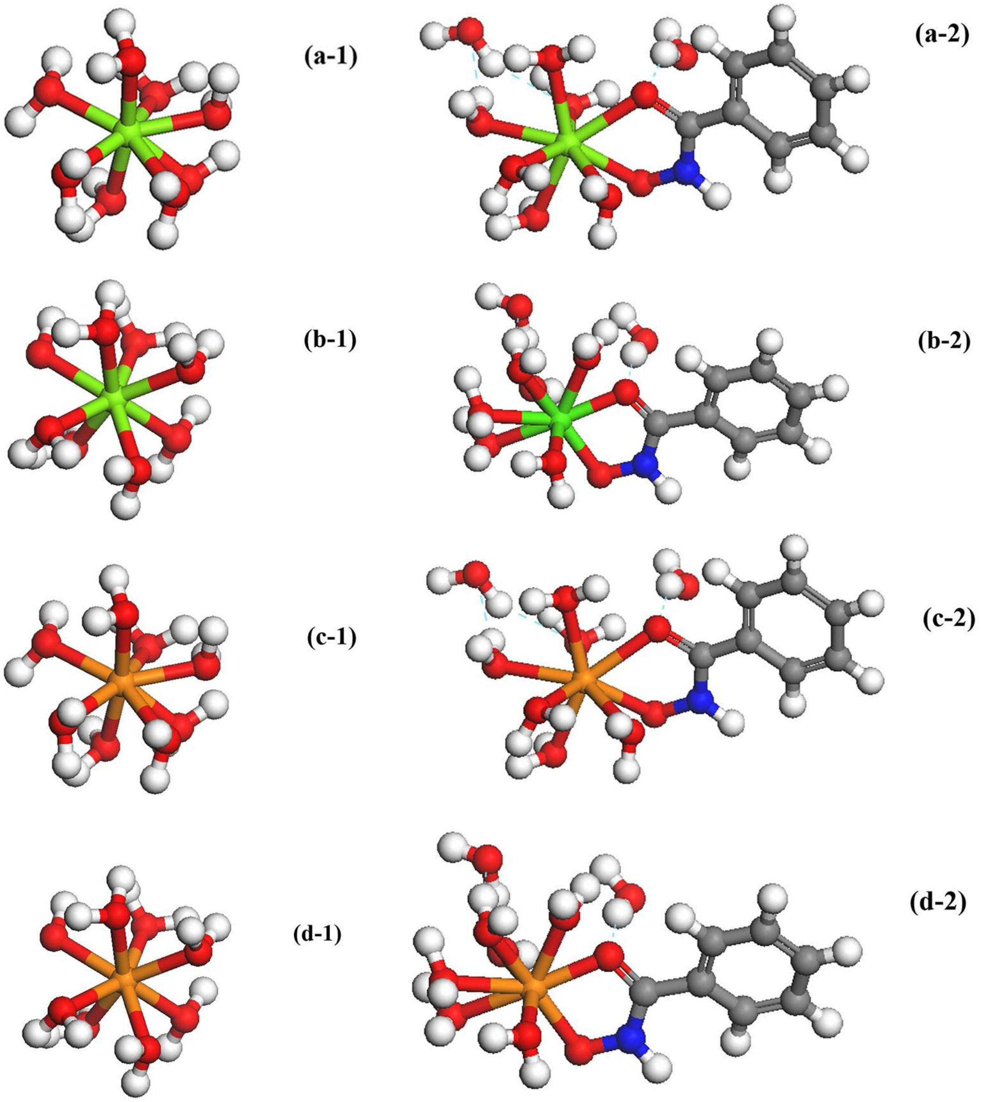

Figure 5.20 – Optimized structures of solvated dolomite supernatant species of (a-1) $CaOH(H_2O)_7^+$, (b-1) $Ca(H_2O)_8^{2+}$, (c-1) $MgOH(H_2O)_7^+$, (d-1) $Mg(H_2O)_8^{2+}$ in bulk solution and of benzohydroxamic collector with solvated species of (a-2) $CaOH(H_2O)_7^+$, (b-2) $Ca(H_2O)_8^{2+}$, (c-2) $MgOH(H_2O)_7^+$, (d-2) $Mg(H_2O)_8^{2+}$ (O ≡ Red, C ≡ Gray, Mg ≡ Orange, H ≡ White, Ca ≡ Green, N ≡ Blue).

Table 5.4 – Interaction energies (kJ/mol) for complexation between benzohydroxamic collector and dolomite supernatant species.

Ligand	Dolomite supernatant species in solution			
	$Ca(H_2O)_8^{2+}$	$MgOH(H_2O)_7^{+}$	$CaOH(H_2O)_7^{+}$	$MgOH(H_2O)_7^{+}$
Benzohydroxamic acid	-168.8	-155.4	-161.3	-147.4

The DFT simulation results suggest that complexation of the dolomite supernatant species is favourable and might be responsible for the loss of collector ligands in bulk solution. Depletion of free collector is tantamount to reduction of the number of collector adsorption events on the target minerals and thus, possibly a reduction in flotation recoveries.

5.4 Discussion

The presence of dolomite supernatant affected the surface properties of dolomite, monazite, and bastnäsite as shown by zeta potential and microflotation results. This could have been driven by the minerals' solubility and surface reactions, such as surface precipitation which was predicted by the speciation diagrams and was verified by XPS analyses.

At pH 5, the 3 minerals have the highest solubility, so the apparent effect of the dolomite supernatant on the zeta potential of these minerals at this pH condition may only be due to the relative increase in the ionic strength of the solution attributed to the solubility of the minerals. Meanwhile, at pH 7, the minerals are less soluble, and the species present in the supernatant are less likely to precipitate; thus, insignificant changes in the zeta potential values were observed. At pH 9, the effect is more evident because metals precipitate at this pH, forming hydroxides and carbonates which could adsorb onto the surface of the minerals. Since the dissolved mineral species are foreign to bastnäsite and monazite, they are the most affected by the precipitates.

Further zeta potential tests were conducted at pH 9 with only the supporting electrolyte (1×10^{-3} M NaCl), only collector and only supernatant (Figure 5.5). The changes in zeta potential of the minerals before and after addition of collectors indicate the selectivity of benzohydroxamic acid collector with the RE minerals over dolomite. DFT calculations agree that benzohydroxamate–RE mineral (monazite) interaction is more favoured than benzohydroxamate–dolomite interaction. This result is expected as this type of collector forms more stable complexes with RE elements than with those found in dolomite [5.4]. In the presence of the dissolved species from dolomite, there was an apparent decrease in the adsorption of the collector because a decrease in the absolute value of the zeta potential was observed. For the RE minerals, one of the reasons for this is the precipitation of different species from dolomite supernatant at the surface. The speciation diagrams (Figure 5.7) showed that $Ca(OH)_2$, $Mg(OH)_2$, $CaCO_3$ and $MgCO_3$ could precipitate out of dolomite supernatant; XPS results (Figure 5.8 - 5.10) indicated the presence of carbonate precipitate at the surface of the minerals. At pH 9, these species have either positive zeta potential or lesser negative zeta potential compared to bastnäsite and monazite as seen from the data previously presented [5.66–5.69]. Apart from these precipitated species, DFT simulations showed that these Ca^{2+} ions could also interact with the negatively charged RE mineral surface by electrostatic force (initially), followed by a strong covalent force. XPS results (Figure 5.8 - 5.10) also indicated the presence of this species, in hydroxylated form, which may be due to hydrated mineral surface [5.47]. This agrees with the work of Ananthapadmanabhan and Somasundaran [5.70], which shows that Ca^{2+} could adsorb at the mineral – water interface between pH 4 - 10. This positively charged ion could be lowering the overall zeta potential of the minerals. The presence of supernatant could have also affected the interaction of OH^-, a potential determining ion, with the surface of the minerals. DFT simulation reveals that OH^- interact favourably with Ce atoms on the surface of monazite compared to precipitated species at the surface of the minerals (see Table 5.2). This means that when species precipitate at the surface of the minerals, OH^- ions (which makes the surface more negative) will have less affinity to the surface, leading to a lesser negative surface. For dolomite, the decrease was not anticipated because the species that could precipitate at its surface and the species at the surface at this pH condition are expected to be the same. However, dissolved species could actually reprecipitate as another species (such as amorphous carbonates and/or magnesian calcite), altering the dolomite surface composition. Furthermore, it should be noted that addition of dolomite supernatant increases the available Ca^{2+}, Mg^{2+} and CO_3^{2-} in the solution; considering Le Chatelier's principle, an increase of reactant will disturb the system and will push the reaction forward to obtain equilibrium state. This means that further addition of reactants could form more $Ca(OH)_2$, $Mg(OH)_2$, $CaCO_3$ and $MgCO_3$ precipitates as products. As previously mentioned, these species have either positive zeta potential or lesser negative zeta potential compared to dolomite [5.66–5.69], again, causing the overall decrease in zeta potential.

Flotation tests were conducted to confirm the effect of dolomite supernatant as presented by the zeta potential measurements. Figure 5.6 shows that dolomite recovery is not affected even with the presence of dolomite supernatant. This indicates that the change in the zeta potential of dolomite (see Figure 5.5) in the presence of dolomite supernatant and collector (labeled as Sup + BHA) is mostly due to the lesser negative zeta potential of the precipitated species, and not because of a reduction of collector adsorption. Bastnäsite and monazite's recovery, however, was greatly affected by the presence of the dissolved dolomite species. Based on the XPS results, species could precipitate/adsorb at the surface of the minerals; these precipitated/adsorbed species could hinder collector adsorption on the mineral's surface. Since collector – monazite interaction is stronger than collector – dolomite and collector – adsorbed species interaction, as presented by DFT simulations, the presence of the supernatant species caused a decrease in the RE minerals' recovery. Another reason for this behavior could be the loss of available collector (for the minerals' surface) through the complexation of the collector with the solvated dolomite (ionic) species such as Ca^{2+}, Mg^{2+}, $CaOH^+$ and $MgOH^+$ in the solution as evidenced by DFT simulations.

Interestingly, while flotation results (Figure 5.6) show that bastnäsite's floatability was more affected compared to monazite's in the presence of the dissolved dolomite species, zeta potential measurements (Figure 5.5) present otherwise. Upon addition of dolomite supernatant, monazite surface could behave like carbonate mineral due to species precipitation. As revealed by surface characterization, monazite's surface could have $MgCO_3$ and more $CaCO_3$ after conditioning with the supernatant. Since monazite is a phosphate mineral, modification to a carbonate-like surface has greatly affected the surface properties, as observed in the zeta potential results. Ce at the surface could also react with carbonate ions as shown in Equations 5.3 - 5.5 [5.71], forming Ce-carbonate complexes making its surface similar to bastnäsite. However, adsorption of positively charged supernatant species is higher with more negatively charged monazite (as can be seen from XPS results), causing its surface to be less negative than bastnäsite. The lesser negative monazite surface will have lower electrostatic repulsion with the anionic collector; this has led the monazite to adsorb more of the collector, then float more than bastnäsite.

$$Ce^{3+} + CO_3^{2-} \rightleftharpoons CeCO_3^{+} \qquad \log K_1 = 7.56 \qquad (5.3)$$

$$Ce^{3+} + 2\ CO_3^{2-} \rightleftharpoons Ce(CO_3)_2^{-} \qquad \log K_2 = 12.19 \qquad (5.4)$$

$$Ce^{3+} + HCO_3^{-} \rightleftharpoons CeHCO_3^{2+} \qquad \log K_3 = 2.42 \qquad (5.5)$$

5.5 Conclusions

The presence of dolomite supernatant has been shown to be detrimental to the flotation of RE minerals. The adsorbed ions or precipitated species at the surface of RE minerals could act as new sites for collector adsorption. In this case, interaction of these species with collector is less favourable than mineral surface – collector interaction, causing a decrease in the minerals' recovery. Another important discovery in this study is the possible loss of collector in the solution due to complexation with ionic species from dolomite supernatant. Although benzohydroxamate is considered to be one of the best collectors for RE minerals due to its selectivity, these findings confirm that this characteristic is not enough to achieve a good RE mineral flotation. Even under proper flotation conditions (such as pH and collector concentration), the presence of dissolved mineral species from the gangue could counteract the efficacy of the collector. These discoveries suggest that measures should be taken to minimize the aging of the minerals or the adsorption of precipitates/ions at the surface of the minerals prior to collector addition. In the mill, one way to do it is to add the collector during grinding. By doing so, collector could have more chance to adsorb at the surface before it even gets lost in the solution, through reactions with the dolomite species (from dissolution and precipitation). Also, complexing agent could be added before collector addition to eliminate the ions that could adsorb at the surface or even prevent these ions from surface/bulk precipitation. Lastly, dissipating the precipitated species adsorbed at the minerals' surface could be done by adding dispersants. Further tests investigating these proposed measures are necessary to understand how to reverse the effects of the dolomite supernatant in RE mineral flotation.

References

[5.1] Gupta, C. and Krishnamurthy, N. Extractive metallurgy of rare earths. *International Materials Reviews*, 37(5):52, 1992.

[5.2] Jordens, A., Cheng, Y. P., and Waters, K. E. A review of the beneficiation of rare earth element bearing minerals. *Minerals Engineering*, 41:97–114, 2013.

[5.3] Zhang, J. and Edwards, C. A review of rare earth mineral processing technology. In *44th Annual Meeting of The Canadian Mineral Processors*, volume 79, Ottawa, Canada, 2012.

[5.4] Fuerstenau, M. Chelating agents as flotation collectors. In Miller, J., Young, C., Kellar, J., and Free, M., Editors, *Innovations in Natural Resource Processing: Proceedings of the Jan. D. Miller Symposium*. Society for Mining, Metallurgy, and Exploration, Incorporated, 2005.

[5.5] Pradip, P. and Fuerstenau, D. The adsorption of hydroxamate on semi-soluble minerals. Part I: Adsorption on barite, calcite and bastnaesite. *Colloids and Surfaces*, 8(2):103–119, 1983.

[5.6] Zhang, X., Du, H., Wang, X., and Miller, J. D. Surface chemistry considerations in the flotation of rare-earth and other semisoluble salt minerals. *Minerals and Metallurgical Processing*, 30(1):24–37, 2013.

[5.7] Yuehua, H., Chi, R., and Xu, Z. Solution chemistry study of salt-type mineral flotation systems: Role of inorganic dispersants. *Industrial and Engineering Chemistry Research*, 42(8):1641–1647, 2003.

[5.8] Fuerstenau, D., Pradip, P., and Herrera-Urbina, R. The surface chemistry of bastnaesite, barite and calcite in aqueous carbonate solutions. *Colloids and Surfaces*, 68(1–2):95–102, 1992.

[5.9] Zhang, W., Honaker, R. Q., and Groppo, J. G. Flotation of monazite in the presence of calcite part I: Calcium ion effects on the adsorption of hydroxamic acid. *Minerals Engineering*, 100:40–48, 2017.

[5.10] Amankonah, J. O. and Somasundaran, P. Effects of dissolved mineral species on the electrokinetic behavior of calcite and apatite. *Colloids and Surfaces*, 15:335–353, 1985.

[5.11] Hu, Y. and Xu, Z. Interactions of amphoteric amino phosphoric acids with calcium-containing minerals and selective flotation. *International Journal of Mineral Processing*, 72(1–4):87–94, 2003.

[5.12] Li, D., Yin, W.-z., Xue, J.-w., Yao, J., Fu, Y.-f., and Liu, Q. Solution chemistry of carbonate minerals and its effects on the flotation of hematite with sodium oleate. *International Journal of Minerals, Metallurgy, and Materials*, 24(7):736–744, 2017.

[5.13] Van Cappellen, P., Charlet, L., Stumm, W., and Wersin, P. A surface complexation model of the carbonate mineral-aqueous solution interface. *Geochimica et Cosmochimica Acta*, 57(15):3505–3518, 1993.

[5.14] Ordoñez-Regil, E., Drot, R., and Simoni, E. Surface complexation modeling of uranium(VI) sorbed onto lanthanum monophosphate. *Journal of Colloid and Interface Science*, 263(2):391–399, 2003.

[5.15] Luo, N., Wei, D., Shen, Y., Han, C., and Zhang, C. Elimination of the adverse effect of calcium ion on the flotation separation of magnesite from dolomite. *Minerals*, 7(8):150, 2017.

[5.16] Fuerstenau, D. and Pradip, P. Zeta potentials in the flotation of oxide and silicate minerals. *Advances in Colloid and Interface Science*, 114–115:9–26, 2005.

[5.17] Wills, B. A. and Finch, J. A. Froth Flotation. In Finch, J. A. and Wills, B. A., Editors, *Wills' Mineral Processing Technology*, pages 265–380. Butterworth-Heinemann, Boston, 8th edition, 2016.

[5.18] Rai, B. *Molecular modeling for the design of novel performance chemicals and materials.* CRC Press, New York, 2012.

[5.19] Ataman, E., Andersson, M. P., Ceccato, M., Bovet, N., and Stipp, S. L. S. Functional group adsorption on calcite: I. Oxygen containing and nonpolar organic molecules. *The Journal of Physical Chemistry C*, 120(30):16586–16596, 2016.

[5.20] Ataman, E., Andersson, M. P., Ceccato, M., Bovet, N., and Stipp, S. L. S. Functional group adsorption on calcite: II. Nitrogen and sulfur containing organic molecules. *The Journal of Physical Chemistry C*, 120(30):16597–16607, 2016.

[5.21] Zucchini, A., Comodi, P., Katerinopoulou, A., Balic-Zunic, T., McCammon, C., and Frondini, F. Order–disorder–reorder process in thermally treated dolomite samples: a combined powder and single-crystal X-ray diffraction study. *Physics and Chemistry of Minerals*, 39(4):319–328, 2012.

[5.22] Donnay, G. and Donnay, J. The crystallography of bastnaesite, parisite, roentgenite, and synchisite. *American Mineralogist*, 38(11-1):932–963, 1953.

[5.23] Bermanec, V., Tibljaš, D., Gessner, M., and Kniewald, G. Monazite in hydrothermal veins from Alinci, Yugoslavia. *Mineralogy and Petrology*, 38(2):139–150, 1988.

[5.24] Gallios, G. P. and Matis, K. A. Flotation of salt-type minerals. In Mavros, P. and Matis, K. A., Editors, *Innovations in Flotation Technology*, pages 357–382. Springer Netherlands, Dordrecht, 1992.

[5.25] Predali, J. J. and Cases, J. M. Zeta potential of magnesian carbonates in inorganic electrolytes. *Journal of Colloid and Interface Science*, 45(3):449–458, 1973.

[5.26] Cheng, T. W. Point of zero charge of monazite and xenotime. *Minerals Engineering*, 13(1):105–109, 2000.

[5.27] Harada, T., Owada, S., Takiuchi, T., and Kurita, M. A flotation study for effective separation of the heavy mineral sands. In *XVIII International Mineral Processing Congress*, volume 4, page 10, 1993.

[5.28] Houot, R., Cuif, J.-P., Mottot, Y., and Samana, J.-C. Recovery of rare earth mineral, with emphasis on flotation process. In *International Conference on Rare Earth Minerals and Minerals for Electronic Uses*, volume 70-72, pages 301–324. Trans Tech Publications, 1991.

[5.29] Jordens, A., Marion, C., Kuzmina, O., and Waters, K. E. Surface chemistry considerations in the flotation of bastnäsite. *Minerals Engineering*, 66-68:119–129, 2014.

[5.30] Luo, J. and Chen, X. Research into the recovery of high-grade rare-earth concentrate from Baotou Complex Iron Ores, China. *Mineral Processing and Extractive Metallurgy*, pages 663–675, 1984.

[5.31] Cheng, T. W., Holtham, P. N., and Tran, T. Froth flotation of monazite and xenotime. *Minerals Engineering*, 6(4):341–351, 1993.

[5.32] Pradip and Fuerstenau, D. Alkyl hydroxamates as collectors for the flotation of bastnaesite rare-earth ores. *Rare Earths: Extraction, Preparation and Applications*, pages 57–70, 1989.

[5.33] Gans, P. Hyperquad Simulation and Speciation (HySS). [Computer Program], Protonic software, Leeds, England, 2009.

[5.34] Puigdomenech, I. Spana Speciation Software. [Computer Program], Royal Institute of Technology, Stockholm, Sweden, 2015.

[5.35] Alderighi, L., Gans, P., Ienco, A., Peters, D., Sabatini, A., and Vacca, A. Hyperquad simulation and speciation (HySS): a utility program for the investigation of equilibria involving soluble and partially soluble species. *Coordination Chemistry Reviews*, 184(1):311–318, 1999.

[5.36] Eriksson, G. An algorithm for the computation of aqueous multi-component, multiphase equilibria. *Analytica Chimica Acta*, 112(4):375–383, 1979.

[5.37] Chu, D. H., Vinoba, M., Bhagiyalakshmi, M., Baek, I. H., Nam, S. C., Yoon, Y., Kim, S. H., and Jeong, S. K. CO_2 mineralization into different polymorphs of $CaCO_3$ using an aqueous-CO_2 system. *RSC Advances*, 3(44):21722–21729, 2013.

[5.38] Liu, S., Huang, B., Chai, L., Liu, Y., Zeng, G., Wang, X., Zeng, W., Shang, M., Deng, J., and Zhou, Z. Enhancement of As (v) adsorption from aqueous solution by a magnetic chitosan/biochar composite. *RSC Advances*, 7(18):10891–10900, 2017.

[5.39] Salvi, A. M., Langerame, F., Macchia, A., Sammartino, M. P., and Tabasso, M. L. XPS characterization of (copper-based) coloured stains formed on limestone surfaces of outdoor Roman monuments. *Chemistry Central Journal*, 6(2):S10, 2012.

[5.40] Thermo Scientific XPS. Carbon - Nonmetals. http://xpssimplified.com/elements/carbon.php, 2017. Accessed Feb. 08, 2017.

[5.41] Gopinath, C. S., Hegde, S. G., Ramaswamy, A. V., and Mahapatra, S. Photoemission studies of polymorphic $CaCO_3$ materials. *Materials Research Bulletin*, 37(7):1323–1332, 2002.

[5.42] Hu, X., Joshi, P., Mukhopadhyay, S. M., and Higgins, S. R. X-ray photoelectron spectroscopic studies of dolomite surfaces exposed to undersaturated and supersaturated aqueous solutions. *Geochimica et Cosmochimica Acta*, 70(13):3342–3350, 2006.

[5.43] Süzer, Ş. and Erten, H. N. Photoelectron spectroscopy: A tool in sorption studies. *Turkish Journal of Chemistry*, 21(4):409–414, 1997.

[5.44] Thermo Scientific XPS. Magnesium - Alkaline Earth Metals. http://xpssimplified.com/elements/magnesium.php, 2017. Accessed Feb. 08, 2017.

[5.45] Hosseini, T., Selomulya, C., Haque, N., and Zhang, L. Investigating the effect of the Mg^{2+}/Ca^{2+} molar ratio on the carbonate speciation during the mild mineral carbonation process at atmospheric pressure. *Energy & Fuels*, 29(11):7483–7496, 2015.

[5.46] Lee, B.-S., Lin, Y.-C., Chen, S.-F., Chen, S.-Y., and Chang, C.-C. Influence of calcium hydroxide dressing and acid etching on the push-out bond strengths of three luting resins to root canal dentin. *Clinical Oral Investigations*, 18(2):489–498, 2014.

[5.47] Stipp, S. L. and Hochella, M. F. Structure and bonding environments at the calcite surface as observed with X-ray photoelectron spectroscopy (XPS) and low energy electron diffraction (LEED). *Geochimica et Cosmochimica Acta*, 55(6):1723–1736, 1991.

[5.48] Forsgren, J., Frykstrand, S., Grandfield, K., Mihranyan, A., and Strømme, M. A template-free, ultra-adsorbing, high surface area carbonate nanostructure. *PLOS ONE*, 8(7), 2013.

[5.49] Rheinheimer, V., Unluer, C., Liu, J., Ruan, S., Pan, J., and Monteiro, P. XPS study on the stability and transformation of hydrate and carbonate phases within MgO systems. *Materials*, 10(1):75, 2017.

[5.50] Cizaire, L., Martin, J. M., Le Mogne, T., and Gresser, E. Chemical analysis of overbased calcium sulfonate detergents by coupling XPS, ToF-SIMS, XANES, and EFTEM. *Colloids and Surfaces A: Physicochemical and Engineering Aspects*, 238(1):151–158, 2004.

[5.51] Gu, W., Bousfield, D. W., and Tripp, C. P. Formation of calcium carbonate particles by direct contact of $Ca(OH)_2$ powders with supercritical CO_2. *Journal of Materials Chemistry*, 16(32):3312–3317, 2006.

[5.52] Sugama, T., Kukacka, L. E., Carciello, N., and Hocker, N. J. Study of interactions at water-soluble polymer/$Ca(OH)_2$ or gibbsite interfaces by XPS. *Cement and Concrete Research*, 19(6):857–867, 1989.

[5.53] Thermo Scientific XPS. Oxygen - Nonmetals. http://xpssimplified.com/elements/oxygen.php, 2017. Accessed Feb. 08, 2017.

[5.54] Bêche, E., Charvin, P., Perarnau, D., Abanades, S., and Flamant, G. Ce 3d XPS investigation of cerium oxides and mixed cerium oxide ($Ce_xTi_yO_z$). *Surface and Interface Analysis*, 40(3-4):264–267, 2008.

[5.55] Ivanova, O. P., Vasilyev, L. A., Naumkin, A. V., and Kantsel, V. V. XPS studies of natural monazite and relative compounds under ion bombardment. *Applied Surface Science*, 72(4):307–312, 1993.

[5.56] Lai, H., Bao, A., Yang, Y., Tao, Y., and Yang, H. Selective synthesis and luminescence property of monazite- and hexagonal-type $LaPO_4$: Eu nanocrystals. *CrystEngComm*, 11(6):1109–1113, 2009.

[5.57] Baer, D. R. and Moulder, J. F. High Resolution XPS Spectrum of Calcite ($CaCO_3$). *Surface Science Spectra*, 2(1):1–7, 1993.

[5.58] Ni, M. and Ratner, B. D. Differentiation of calcium carbonate polymorphs by surface analysis techniques – An XPS and TOF-SIMS study. *Surface and Interface Analysis*, 40(10):1356–1361, 2008.

[5.59] Cui, J., Hope, G. A., and Buckley, A. N. Spectroscopic investigation of the interaction of hydroxamate with bastnaesite (cerium) and rare earth oxides. *Minerals Engineering*, 36:91–99, 2012.

[5.60] Bonnitcha, P. D., Kim, B. J., Hocking, R. K., Clegg, J. K., Turner, P., Neville, S. M., and Hambley, T. W. Cobalt complexes with tripodal ligands: implications for the design of drug chaperones. *Dalton Transactions*, 41(37):11293–11304, 2012.

[5.61] Albright, T. A., Burdett, J. K., and Whangbo, M.-H. *Orbital Interactions in Chemistry.* John Wiley & Sons, New Jersey, 2013.

[5.62] Ni, Y., Hughes, J. M., and Mariano, A. N. Crystal chemistry of the monazite and xenotime structures. *American Mineralogist*, 80(1-2):21–26, 1995.

[5.63] Fuerstenau, M., Jameson, G. J., and Yoon, R.-H. *Froth flotation: A century of innovation.* Society for Mining, Metallurgy, and Exploration, Littleton, Colorado, 2007.

[5.64] Wolthers, M., Charlet, L., and Van Cappellen, P. The surface chemistry of divalent metal carbonate minerals; a critical assessment of surface charge and potential data using the charge distribution multi-site ion complexation model. *American Journal of Science*, 308(8):905–941, 2008.

[5.65] James, R. O. and Healy, T. W. Adsorption of hydrolyzable metal ions at the oxide-water interface. III. A thermodynamic model of adsorption. *Journal of Colloid and Interface Science*, 40(1):65–81, 1972.

[5.66] Chibowski, E., Hotysz, L., and Szcześ, A. Time dependent changes in zeta potential of freshly precipitated calcium carbonate. *Colloids and Surfaces A: Physicochemical and Engineering Aspects*, 222(1):41–54, 2003.

[5.67] Kilic, S., Toprak, G., and Ozdemir, E. Stability of $CaCO_3$ in $Ca(OH)_2$ solution. *International Journal of Mineral Processing*, 147:1–9, 2016.

[5.68] Parks, G. A. The isoelectric points of solid oxides, solid hydroxides, and aqueous hydroxo complex systems. *Chemical Reviews*, 65(2):177–198, 1965.

[5.69] Škvarla, J. and Kmet, S. Non-equilibrium electrokinetic properties of magnesite and dolomite determined by the laser-Doppler electrophoretic light scattering (ELS) technique. A solids concentration effect. *Colloids and Surfaces A: Physicochemical and Engineering Aspects*, 111(1):153–157, 1996.

[5.70] Ananthapadmanabhan, K. P. and Somasundaran, P. Surface precipitation of inorganics and surfactants and its role in adsorption and flotation. *Colloids and Surfaces*, 13:151–167, 1985.

[5.71] Herrera-Urbina, R., Pradip, P., and Fuerstenau, D. Electrophoretic mobility and computations of solid-aqueous solution equilibria for the bastnaesite-H_2O system. *Minerals and Metallurgical Processing*, 30(1):18–23, 2013.

Chapter 6

The effect of dissolved mineral species on mineral – sodium oleate interaction

Previous chapters indicated that more efficient separation could be achieved with the use of benzohydroxamate (Chapter 3) and sodium oleate (Chapter 4). In Chapter 5, the effect of dissolved mineral species on the flotation of dolomite, monazite and bastnäsite in the presence of benzohydroxamate was presented. In this chapter, the effect of dissolved mineral species in the presence of sodium oleate will be presented.

Abstract

Common RE minerals, such as bastnäsite and monazite, may be formed in deposits associated with carbonate gangue such as calcite and dolomite. Sodium oleate is a widely used collector for the flotation of both RE and gangue minerals, which might, therefore, be an inefficient process due to the lack of selectivity of this collector. Since these minerals are also sparingly soluble in solution, they could release their constituent ions into the solution, which could affect the floatability of other minerals. In this study, the interactions of sodium oleate with bastnäsite and monazite in the presence of dissolved dolomite species have been investigated. Microflotation tests were carried out to explore the effects of these dissolved species on the floatability of the RE minerals. Zeta potential measurements and XPS characterization were carried out to understand how the species affect the collector adsorption. To complement these characterizations, DFT simulations were conducted to investigate the collector – mineral and collector – adsorbed species (on the mineral surface) interactions. The results showed that collector – dolomite interaction energy is greater than that of collector – adsorbed species, but lower than collector – monazite interaction energy, explaining the decrease in the minerals' recovery upon exposure to the dissolved mineral

species. It also showed that oleate ion (Ol^-) have the strongest interaction with the minerals compared to other oleate species such as acid soap (HOl_2^-) and oleate dimer (Ol_2^{2-}). The behavior (strength and selectivity) of sodium oleate towards RE minerals and dolomite, as compared to other RE mineral collectors (such as aromatic hydroxamate), is attributed mainly to the collector's and the minerals' structure. The long hydrocarbon chain of sodium oleate which imparts hydrophobic characteristic to the minerals, makes it stronger collector than benzohydroxamate. Moreover, sodium oleate (with linear structure), unlike the aromatic hydroxamate, can approach the mineral easier due to lesser steric hindrance effect and higher reactivity of O involved in the interaction, making it less selective. In addition, it can interact easily with dolomite due to the presence of more exposed active sites than RE minerals.

6.1 Introduction

Sodium oleate, an oxyhydryl collector, is a widely used industrial collector [6.1] especially for non-sulphide minerals [6.2]. It floats a variety of non-sulphide minerals such as Ca-, Ba-, and Mg-containing minerals, non-ferrous carbonates, the soluble salts of alkali and alkaline earth metals [6.2] and even rare earth (RE) minerals [6.3]. Main RE minerals, such as bastnäsite and monazite, usually occur associated with carbonate gangue such as calcite and dolomite. Since this is the case, RE flotation using only sodium oleate is inefficient due to the non-selectivity of the collector [6.4]. In addition, the carbonate gangue and RE minerals are sparingly soluble in water [6.5], which means that constituent ions from the minerals could be dissolved in the solution. Although RE minerals are usually associated with semi-soluble carbonate minerals, surprisingly the effect of the dissolved mineral species on RE minerals has barely been investigated in the open literature. These ions are reported to possibly interact with the RE mineral surface affecting their flotation behavior [Chapter 5; 6.6]. In this regard, the possible interaction of sodium oleate with mineral surfaces has been studied to understand interfacial interactions [6.7, 6.8]. Although this is a widely-studied collector, there are relatively few investigations involving RE minerals, more work has been conducted on calcite and other gangue minerals. Interaction of sodium oleate with calcite and other gangue minerals have been studied extensively. Somasundaran and Ananthapadmanabhan [6.9] have presented the formation of various oleic acid species in solution and its possible correlation to flotation performance. They highlighted the possible role of acid soap (HOl_2^-) in the increase in flotation of hematite in the alkaline pH range. They also mentioned that neutral oleic acid (HOl) could adsorb through hydrogen bonding with surface hydroxyl groups or co-adsorption between the ionic species. Others reported similar findings where mineral's maximum recovery occur at pH between 7 and 9 in the presence of oleate [6.10, 6.11]. They attributed the high recovery to the maximum activity of oleate caused by the presence of acid soap complex in this pH region. Maximum recovery of RE minerals in the presence of sodium oleate were also found to occur at this pH range [6.12, 6.13], but the interaction of these complexes with RE minerals are barely discuss comprehensively.

Typical methodologies to understand the mechanism of the adsorption of the collector onto the RE minerals involving dissolved mineral species (in the solution) can be through surface characterization (*e.g.,* FTIR and XPS) and electrokinetic tests (*e.g.,* zeta potential measurements). However, some of the results could have discrepancies since these measurements are seldom conducted in situ. In this regard, atomically-resolved computer simulations such as Density Functional Theory (DFT) simulations could strengthen the inferences from these experimental results. DFT simulations could contribute further understandings of the mineral flotation behavior in the presence of supernatant that cannot be directly achieved by experiments. It has been reported that molecular modelling study has been helpful in understanding mineral – reagent interactions [6.14–6.17], because it can provide valuable information even without detailed experimental testing [6.18]. With regards to oleate adsorption on mineral surfaces, several molecular modelling studies have already been presented in the literature [6.17, 6.18]. However, their computer simulation was conducted solely with oleate (Ol^-) and not the other possible oleate species that could also be present in the solution such as oleate dimer (Ol_2^{2-}) and acid soap (HOl_2^-) [6.10].

Therefore, an integrated experimental and DFT simulation study was conducted not only with oleate but also with the consideration of other oleate species (*e.g.,* acid soap and oleate dimer) in order to make this study more comprehensive. In this work, the effects of dissolved ions from dolomite on the flotation of RE minerals, bastnäsite and monazite, were investigated through microflotation tests. These were rationalized with the help of zeta potential measurements, XPS analyses and DFT simulations.

6.2 Materials and methods

6.2.1 Materials

African Rare Earths (Pty.) Ltd. (South Africa) provided the bastnäsite. Monazite (Eureka Farm 99, Namibia) and dolomite (Sterling Hill Mine, New Jersey) were purchased from Mineralogical Research Company (USA) and Boreal Science (Canada), respectively. X-ray diffraction (XRD) analysis and inductively coupled plasma - optical emission spectroscopy (ICP-OES) for mineral and elemental analysis, respectively, indicated that the dolomite and bastnäsite are relatively pure, while monazite sample has minor calcite contamination (see Chapter 5). The elemental analysis is also presented in Table 6.1 for reference (from Chapter 5).

The sodium chloride (supporting electrolyte), the hydrochloric acid and potassium hydroxide (pH modifiers) and the sodium oleate (NaOl) collector were obtained from Fisher Scientific (Canada). The dolomite supernatant was obtained by conditioning 75 g of dolomite in 1500 mL deionised water for 8 hours at 60 °C. The suspension was allowed to cool before passing through a filter with a grade of 413 (particle retention of 5 µm) to recover the supernatant. The measured conductivities of the deionised water and supernatant were found to be 5 µS and 90 µS, respectively. The amounts of Ca^{2+} and Mg^{2+} in the supernatant were analyzed using Varian AA240FS Fast Sequential Atomic Absorption Spectrometer (Agilent Technologies, USA) and observed to be 8.07 ppm and 3.54 ppm, respectively. Deionised water was used as the blank for this measurement. It must be noted that these Ca and Mg contents are lower than typical tap water concentrations.

Table 6.1 – Chemical composition (wt %) of dolomite, monazite and bastnäsite samples.

Dolomite	**Ca**	**Mg**	**Fe**	**S**	**Mn**	**Na**	**K**	**Ti**	**Cu**	**Zn**	**Mo**
	21.71	12.74	0.37	0.21	0.06	0.05	0.04	0.03	0.02	0.02	0.01
Monazite	**P**	**Ce**	**Nd**	**La**	**Ca**	**Si**	**Pb**	**Zr**	**Fe**	**Al**	**As**
	10.24	8.00	5.41	4.64	0.75	0.51	0.49	0.46	0.12	0.10	0.10
Bastnäsite	**Ce**	**La**	**Nd**	**As**	**P**	**Ti**	**Fe**	**Ca**	**Al**	**Pb**	**Cu**
	13.55	13.44	8.08	0.69	0.53	0.40	0.25	0.21	0.18	0.09	0.06

6.2.2 Zeta potential measurements

The mineral samples used for zeta potential measurements (dolomite, monazite and bastnäsite) have a D_{50} of 2.3 µm. The minerals are placed in a pre-adjusted solution of 1×10^{-3} M NaCl (indifferent electrolyte) or dolomite supernatant. The solution pH was adjusted using dilute concentrations of HCl and KOH. For the measurements with the collector, the minerals were first conditioned with supernatant for 0, 30, 60, 120 and 240 s, then with the collector for another 240 s. The 100 mg/L mineral suspension was mixed prior to the measurement to ensure particle dispersion. Zeta potential measurements were then taken using a NanoBrook 90Plus Zeta Particle Size Analyzer (Brookhaven Instruments, USA).

6.2.3 Flotation

A modified Hallimond tube, as presented and described previously (Chapter 5), was used for the microflotation tests. One gram (1 g) of -106+38 μm mineral sample was placed in a 50-mL beaker containing 30 mL deionised water or dolomite supernatant (pre-adjusted to desired pH). The suspension was conditioned for 2 minutes with dolomite supernatant then 5 minutes with 3.3×10^{-5} M (or 10 mg/L) sodium oleate collector, while keeping the pH constant. The mineral particles were kept suspended by employing a magnetic stirrer. The suspension was then added to the cell and further completed up to 170 cm^3 with pH-adjusted deionised water. Air was introduced at a flowrate of 40 mL/min and the flotation test was conducted for 1 minute.

6.2.4 X-ray Photoelectron Spectroscopy (XPS)

The surface of dolomite, monazite and bastnäsite, in the presence and absence of supernatant, were studied using a Thermo Scientific K-Alpha Monochromatic X-ray Photoelectron Spectrometer (Thermo Fisher Scientific Inc., USA) equipped with an Al Kα X-ray source (1486.6 eV, 0.834 nm), ultrahigh vacuum chamber (10^{-9} Torr) and microfocused monochromator. Elemental survey scans from 0 to 1350 eV and high resolution scans were performed in the experiments, using a pass energy of 1 and 0.1 eV, respectively. The analyses were conducted using a spot size of 400 μm. An electron charge gun was employed to avoid surface charge effects. Prior to the experiments, the samples were kept in a desiccator (with silica gels) and degassed for 2 hours in a vacuum oven at room temperature. The results (binding energies) were calibrated using the C 1s peak for C–C at 284.8 eV, and the peak reconstructions performed using the software Thermo Advantage 4.60 (Thermo Fisher Scientific Inc., USA).

6.2.5 Density Functional Theory (DFT) simulations

All DFT-based calculations were performed using Dmol3 package implemented in the Material Studio 2016 software. Through DFT simulations, geometric crystal parameters and total energy of dolomite and monazite bulk, their free surfaces considering their most stable cleavage plane, model benzohydroxamic acid collector, and adsorbed collector and species from dolomite supernatant onto mineral surfaces were calculated.

The generalized gradient approximation (GGA) with PBEsol exchange correlation functional was used to describe the exchange correlation interactions. Through calculations, the double numerical plus polarization (DNP) basis set and the calculation was done considering Spin-unrestricted. The self-consistent field (SCF) convergence was fixed to 2 × 10^{-6} and convergence criteria set for the energy, maximum force and maximum displacement were set to 2 × 10^{-5} Ha, 0.05 Ha/Å, and 0.002 Å, respectively. It is worth mentioning that the simulation results with fixed SCF value in 1 × 10^{-6} were the same with simulations with SCF value equals to 2 × 10^{-6}. No special treatment of core electrons was considered and all the electrons were included in the calculations. Also, smearing was set to 5 × 10^{-3} through all calculations. In this condition, the calculation was performed by use of various orbitals for different spins. Besides, the initial value for the number of unpaired electrons for each atom was taken from the formal spin introduced for each atom. In this situation, the starting value can be subsequently optimized throughout the calculations. For minerals bulk calculations, the Brillouin zone was sampled using a (2×2×2) Monkhorst-Pack *k*-point mesh. This mesh value has been selected after a systematic simulation studies using finer values. It was found the simulation results with *k*-point mesh (2×2×2) are highly close to results with finer values, with lesser simulation time. The most stable cleavage planes for dolomite and monazite were taken for calculations. In this regard, the cleavage plane (104) for dolomite and (100) for monazite, which both agree with the literature values [6.6, 6.19, 6.20], were used.

The mineral slabs were constructed by (1×2) dolomite (104) and monazite (100) surface supercells with 40 Å vacuum spacing to prevent interaction between image slabs. Special attention was paid to the importance of doing flotation in aqueous environment. Therefore, all the simulations were performed in the presence of conductor-like screening model (COSMO) as an implicit solvation model in which the solute molecules form a cavity within the dielectric continuum of permittivity equal to 78.54. During adsorption calculations of either collector or supernatant species on the mineral surfaces, the atoms at the top layer were allowed to undergo relaxation and the rest of atoms in sub-layers were constrained. This is because only the top layer mineral surface atoms have interactions with benzohydroxamic acid collector and other species through adsorption. The adsorption energy of either collector or precipitated species on the mineral surfaces was calculated based on the following definition [6.16]:

$$E_{\text{ads}} = E_{(\text{slab + collector or precipitated species})} - E_{(\text{slab})} - E_{(\text{collector or precipitated species})} \tag{6.1}$$

Where $E_{(\text{slab + collector or precipitated species})}$ is total energy after adsorption of either collector or precipitated species on the mineral surface, $E_{(\text{slab})}$ represents the energy of relaxed bare mineral slab and $E_{(\text{collector or precipitated species})}$ is the energy of collector or precipitated species after optimization.

In the cases that collector interacted with precipitated species on the mineral surfaces, the interaction energy was calculated as following:

$$E_{\text{ads}} = E_{(\text{slab + collector + precipitated species})} - E_{(\text{slab})} - E_{(\text{collector})} - E_{(\text{precipitated species})} \tag{6.2}$$

6.3 Results

6.3.1 Zeta potential

Dolomite, monazite and bastnäsite were conditioned with dolomite supernatant for 0, 30, 60, 120 and 240 s. The zeta potential was then measured in the presence of sodium oleate and was presented in Figure 6.1. The changes in the zeta potential as a function of conditioning time could not be absolutely determined as either significant or insignificant based solely on the figure presented. Thus, a paired *t*-test on the set of zeta potential values (with 0 s as the baseline) was conducted using GraphPad Software, Inc. (California, USA). The results (see Appendix G) showed that at 240 s conditioning, the changes in the zeta potential of dolomite and bastnäsite are statistically significant at all the pH investigated; while monazite's zeta potential changes are only statistically significant at pH 7 and 9. Although the changes in the zeta potential of bastnäsite are considerable after 240 s, lesser conditioning time did not appear to influence its surface.

In Figure 6.1, it can be seen that the zeta potential is greatly influenced by the presence of the supernatant at pH 7 and 9. Since previous studies have shown that maximum recovery of RE minerals in the presence of oleate occurred at pH close to 7 [6.12, 6.13], further zeta potential measurements were conducted at this pH value. The measurements at pH 7, presented in Figure 6.2, showed that dolomite has a negative zeta potential (-10 mV); monazite has slightly negative potential (-0.6 mV); while bastnäsite has a positive zeta potential (9.8 mV). The measurements with NaOl collector (-29 mV, -25 mV, and -35 mV, respectively) suggest that collector was adsorbed at the surface of each mineral. It can also be seen that the presence of dolomite supernatant has caused the zeta potential of the minerals to become less negative (Figure 6.2). This behavior is similar to that observed in the previous study (see Chapter 5) at pH 9. When the minerals conditioned with supernatant were put in contact with the collector, their zeta potential values became more negative than only with the presence of supernatant (but not as negative as only with the presence of NaOl), indicating that the collector could still adsorb onto the minerals' surface.

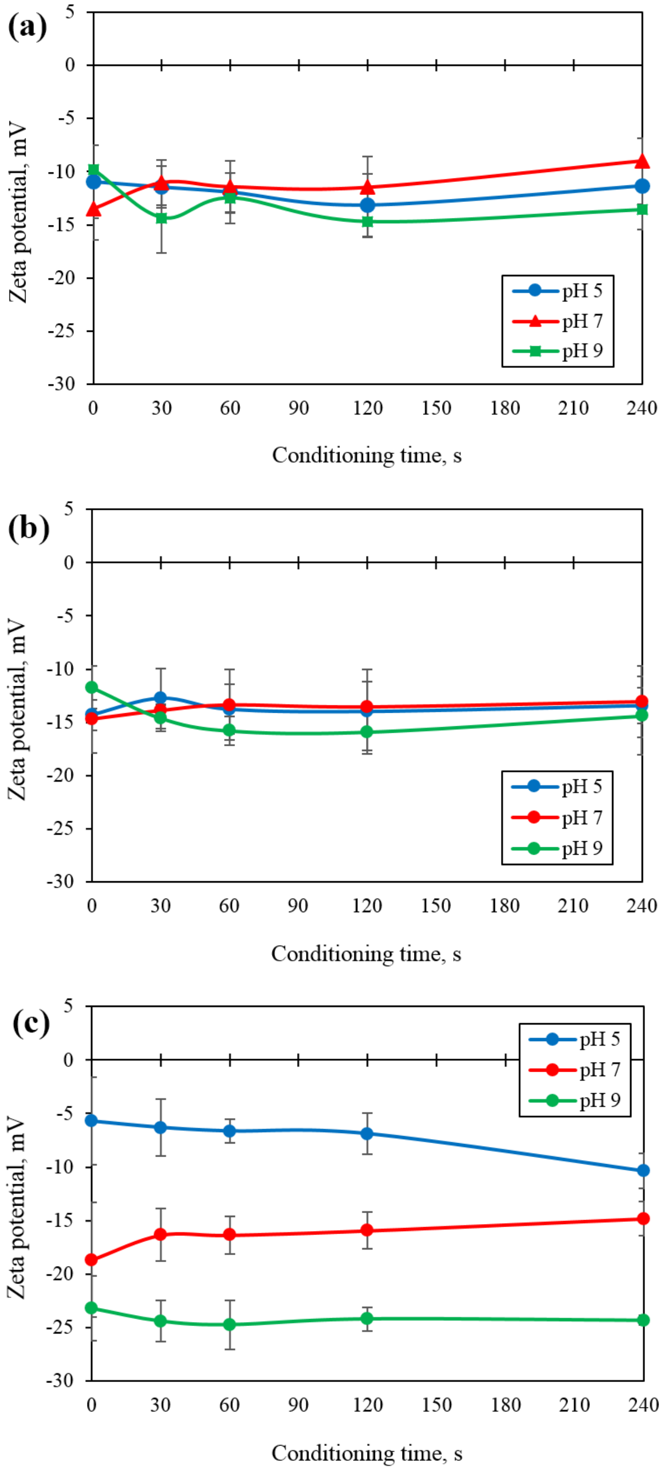

Figure 6.1 – Zeta potential curves of (a) dolomite, (b) monazite, and (c) bastnäsite in the presence of 3.3 × 10^{-5} M NaOl as a function of conditioning time.

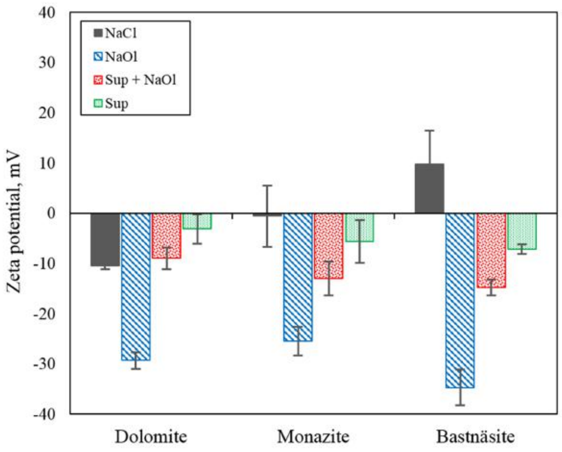

Figure 6.2 – Zeta potential of dolomite, monazite, and bastnäsite in the presence of 1 × 10^{-3} M NaCl (background electrolyte), with 3.3 × 10^{-5} M NaOl, with supernatant and NaOl, and with only supernatant at pH 7.

6.3.2 Microflotation

The effect of dolomite supernatant on the floatability of dolomite, monazite, and bastnäsite was also studied through microflotation tests. In Figure 6.3, the recovery of the minerals with and without dolomite supernatant was presented, where the error bars represent 95% confidence interval. The recovery of dolomite conditioned with the collector in deionised water and in dolomite supernatant is 69% and 66%, respectively. The presence of the supernatant does not seem to affect dolomite's floatability in the presence of NaOl collector, which is similar with the result presented in the presence of benzohydroxamate at pH 9 (see Chapter 5). However, the presence of dolomite supernatant has clearly influenced the floatability of the other minerals, reducing the recovery of monazite and bastnäsite from 98% and 99% to 57% and 51%, respectively (see Figure 6.3).

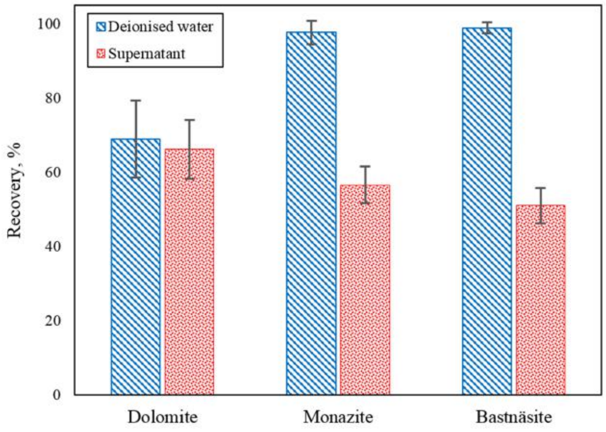

Figure 6.3 – Microflotation results of dolomite, monazite, and bastnäsite using 3.3 × 10^{-5} M NaOl in deionised water and dolomite supernatant at pH 7.

6.3.3 Speciation

Since dolomite supernatant was used, it is important to understand its speciation in the solution. In this regard, the following equilibria for dolomite – water – CO_2 system were considered:

$$\mathrm{MgCO_{3(s)} \rightleftharpoons MgCO_{3(aq)}} \qquad \mathrm{pK_1 = 4.51} \tag{6.3}$$

$$\mathrm{MgCO_{3(aq)} \rightleftharpoons Mg^{2+} + CO_3^{2-}} \qquad \mathrm{pK_2 = 3.40} \tag{6.4}$$

$$\mathrm{CO_3^{2-} + H_2O \rightleftharpoons HCO_3^- + OH^-} \qquad \mathrm{pK_3 = 3.67} \tag{6.5}$$

$$\mathrm{HCO_3^- + H_2O \rightleftharpoons H_2CO_3 + OH^-} \qquad \mathrm{pK_4 = 7.62} \tag{6.6}$$

$$\mathrm{H_2CO_3 \rightleftharpoons CO_2(g) + H_2O} \qquad \mathrm{pK_5 = -1.43} \tag{6.7}$$

$$\mathrm{Mg^{2+} + HCO_3^- \rightleftharpoons MgHCO_3^+} \qquad \mathrm{pK_6 = -1.16} \tag{6.8}$$

$$\mathrm{MgHCO_3^+ \rightleftharpoons H^+ + MgCO_{3(aq)}} \qquad \mathrm{pK_7 = 8.09} \tag{6.9}$$

$$\mathrm{Mg^{2+} + OH^- \rightleftharpoons MgOH^+} \qquad \mathrm{pK_8 = -2.57} \tag{6.10}$$

$$\mathrm{MgOH^+ + OH^- \rightleftharpoons Mg(OH)_{2(s)}} \qquad \mathrm{pK_9 = -8.48} \tag{6.11}$$

$$\mathrm{MgOH^+ + OH^- \rightleftharpoons Mg(OH)_{2(aq)}} \qquad \mathrm{pK_{10} = -5.81} \tag{6.12}$$

$$\mathrm{Mg(OH)_{2(aq)} \rightleftharpoons Mg(OH)_{2(s)}} \qquad \mathrm{pK_{11} = -2.67} \tag{6.13}$$

$$\mathrm{CaMg(CO_3)_2 \rightleftharpoons Ca^{2+} + Mg^{2+} + 2\,CO_3^{2-}} \qquad \mathrm{pK_{12} = 19.35} \tag{6.14}$$

$$\mathrm{Ca^{2+} + HCO_3^- \rightleftharpoons CaHCO3^+} \qquad \mathrm{pK_{13} = -0.87} \tag{6.15}$$

$$\mathrm{CaHCO_3^+ \rightleftharpoons CaCO_{3(aq)} + H^+} \qquad \mathrm{pK_{14} = 7.99} \tag{6.16}$$

$$\mathrm{Ca^{2+} + OH^- \rightleftharpoons CaOH^+} \qquad \mathrm{pK_{15} = -1.30} \tag{6.17}$$

$$\mathrm{CaOH^+ + OH^- \rightleftharpoons Ca(OH)_{2(aq)}} \qquad \mathrm{pK_{16} = 1.30} \tag{6.18}$$

$$\mathrm{Ca(OH)_{2(aq)} \rightleftharpoons Ca(OH)_{2(s)}} \qquad \mathrm{pK_{17} = -5.10} \tag{6.19}$$

The above constants are based on the Gibbs free energy of formation of the species at standard conditions (25 °C and 1 atm) [6.21]. The speciation diagram of dolomite supernatant (Figure 6.4) was plotted using HySS2009 software (Protonic software) [6.22], considering the presented equilibrium equations. The total concentration of Ca and Mg ions used in the calculation is 2×10^{-4} M and 1.5×10^{-4} M, respectively. The calculations were conducted assuming the system to be in equilibrium and open to the atmosphere where $p\mathrm{CO_2}$ is $10^{-3.5}$ atm at 1 atm, 25 °C. Species containing Ca ions and species containing Mg ions are presented in separate figures for easier analysis. Figure 6.4 indicated that $MgCO_3$, $CaCO_3$, $Mg(OH)_2$ and $Ca(OH)_2$ precipitates could be present at pH 7. The species can be formed at the solution/surface interface or in the solution and then adsorbed at the surface [6.23].

The speciation diagram of oleate (Figures 6.5a and 6.5b) was also plotted using HySS2009 software (Protonic software) [6.22]. The speciation of oleate was based on the data provided by Somasundaran and Ananthapadmanabhan [6.9], where the reported pKs (conversion of liquid to aqueous) is 7.6 and acid dissociation constant (pKa) is 4.95. The presence of Ca and Mg ions led to the formation of Ca- and Mg-oleate precipitates.

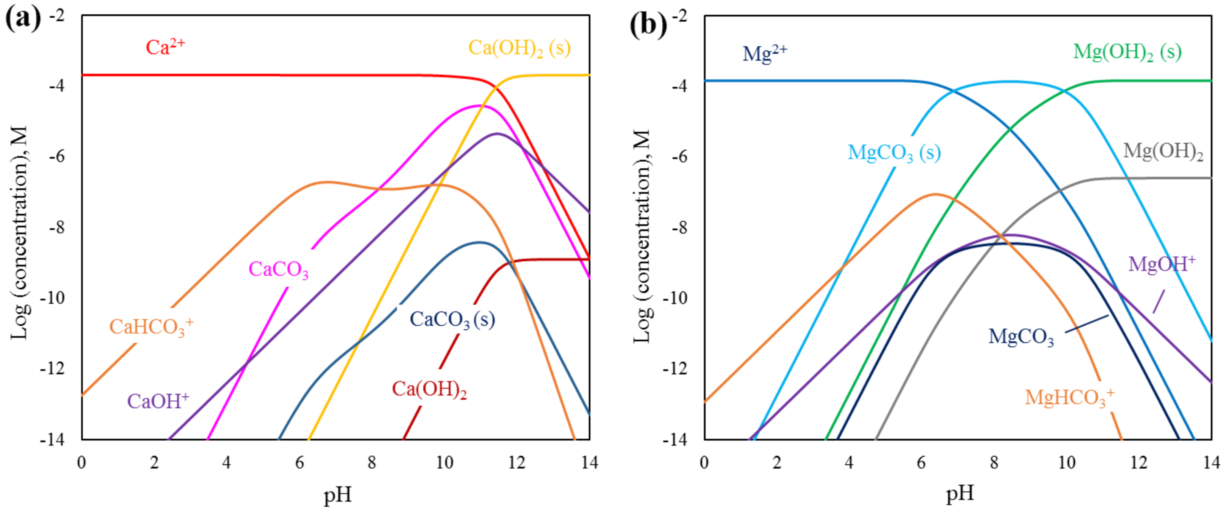

Figure 6.4 – Speciation diagram of dolomite species in solution: (a) species containing Ca ions; and, (b) species containing Mg ions. Total concentration: $[Ca^{2+}]_{TOT}$ = 200 μM, $[Mg^{2+}]_{TOT}$ = 150 μM, $p\mathrm{CO}_2 = 10^{-3.5}$ atm at 1 atm and T = 25 °C.

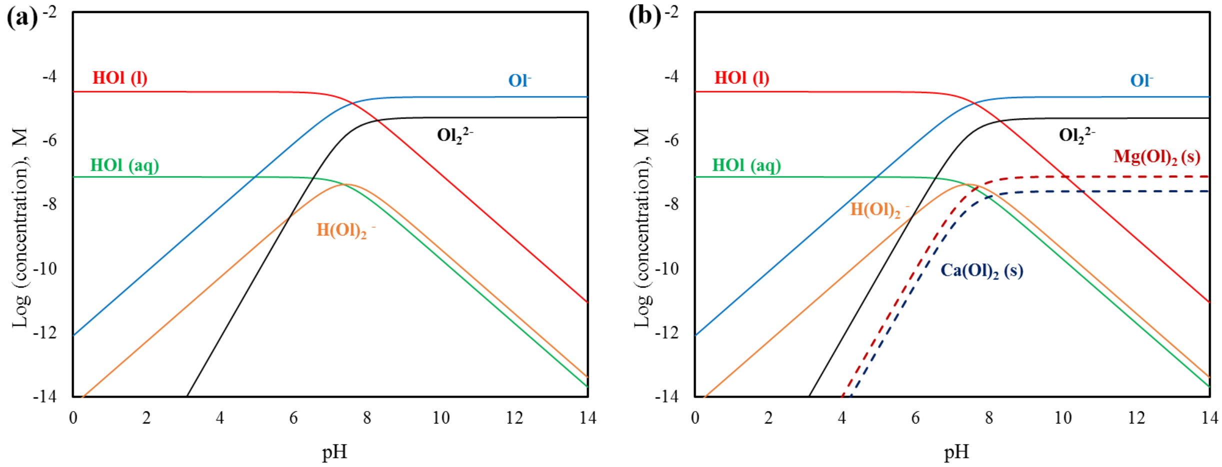

Figure 6.5 – Speciation diagram for oleate system (a) without and (b) with Ca and Mg ions. Total concentration: $[Ol^-]_{TOT} = 3.3 \times 10^{-5}$, $[Ca^{2+}]_{TOT}$ = 200 μM, $[Mg^{2+}]_{TOT}$ = 150 μM, $p\mathrm{CO}_2 = 10^{-3.5}$ atm at 1 atm and T = 25 °C.

6.3.4 X-ray Photoelectron Spectroscopy (XPS)

6.3.4.1 XPS spectra for dolomite

The presence of adventitious carbon contaminations on the minerals' surfaces in the form of C–C, C–O–C and O–C=O was observed on the C 1s XPS spectra (Figure 6.6a) with peaks at around 284.82, 286.58 and 288.08 eV [6.24–6.27], respectively. The C 1s peak fitted at around 289.59 eV [6.28, 6.29], and the O 1s (Figure 6.6b) peak at around 531.40 eV [6.28, 6.29] were assigned to dolomite. Another O 1s peak at around 532.95 eV could be attributed to the presence of $Ca(OH)_2$ [6.30], $>CaOH^0$ [6.24, 6.31] and/or $MgCO_3$ [6.32–6.34]. $Ca(OH)_2$ might not be the best candidate for this peak since it has been observed at a lower BE than that of the carbonates [6.35–6.37]. This is corroborated by the Ca 2p core spectra (Figure 6.6c) and Mg 1s core spectra (Figure 6.6d), which suggested the presence of: (1) $>CaOH^0$ due to fitting of a doublet with the Ca $2p_{3/2}$ line at around 347.98 eV (Stipp & Hochella, 1991); and (2) $MgCO_3$ due to the presence of Mg KL4 Auger contribution at 350.98 eV [6.38] and the presence of Mg 1s peak at 1305.33 eV (assigned to $MgCO_3$) [6.34, 6.38]. The XPS spectra have indicated that $>CaOH^0$ and $MgCO_3$ are more dominant at the surface of supernatant-conditioned dolomite.

The notation $>CaOH^0$ means a surface complex of Ca due to hydrated mineral surface, where > represents the mineral lattice, and Ca is a mineral cation. The presence of this surface complex was proposed by Somasundaran and Agar [6.39], and was later confirmed by Stipp and Hochella [6.31].

6.3.4.2 XPS spectra for monazite

Monazite is designated by the O 1s peak (Figure 6.7b) at around 530.95 eV [6.40–42]. The Ca 2p spectra (Figure 6.7c) required the fitting of a single peak at BE around 344.55 eV, possibly due to a Zr $3p_{1/2}$ line (since Zr is a minor contaminant of monazite). The C 1s XPS spectra (Figure 6.7a) presented peaks assigned to adventitious C–C, C–O–C and O–C=O [6.24–6.27] at around 284.88, 286.28 and 288.44 eV, respectively. The C 1s peak (288.44 eV) assigned to O–C=O could also overlap with the peak for carbonate [6.27]. The conditioning with supernatant (Figure 6.7a-2) seem to have increased the C–O–C and O–C=O / carbonate contribution to the spectra. This can also be observed in the O 1s spectra (Figure 6.7b): the contribution of the C–O peak (which could also be due to the occurrence of carbonates) [6.43] (532.51 eV) increased upon conditioning with the supernatant, along with the $MgCO_3$ peak (533.60 eV)[6.32–6.34]. The presence of carbonates (calcium and magnesium) was also indicated by the Ca 2p doublet (Figure 6.7c) at higher BE (at around 347.08 eV) [6.28, 6.29, 6.31, 6.35, 6.44, 6.45] and an Mg KL4 Auger line (at around 351.01 eV), respectively. The presence of carbonate species prior to conditioning with dolomite supernatant could be due to the presence of calcite as minor contaminant (as suggested by the XRD patterns and elemental assay).

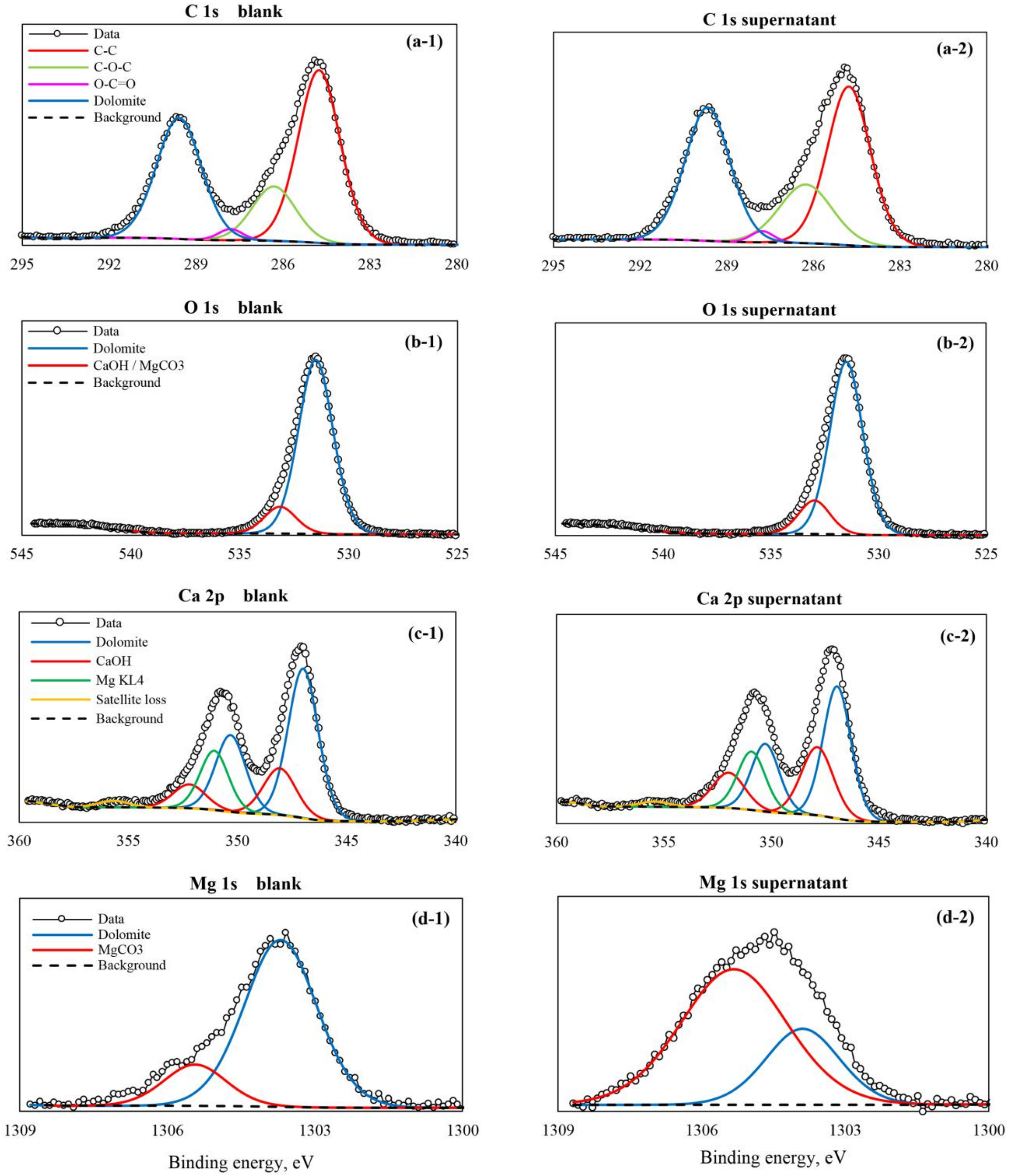

Figure 6.6 – C 1s, O 1s, Ca 2p and Mg 1s XPS spectra of dolomite without (a-1, b-1, c-1, d-1) and with supernatant (a-2, b-2, c-2, d-2), respectively.

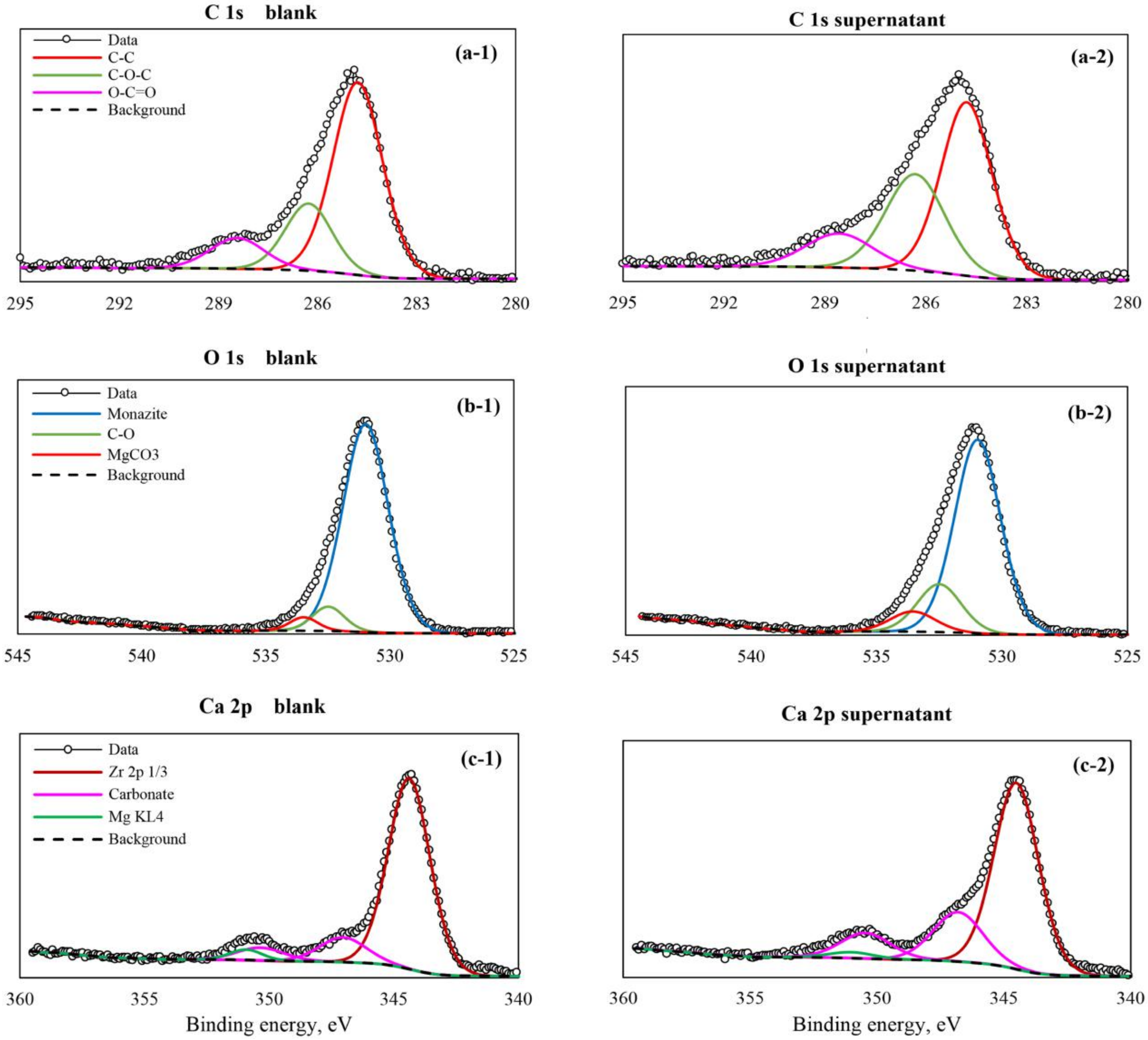

Figure 6.7 – C 1s, O 1s, Ca 2p and Mg 1s XPS spectra of monazite without (a-1, b-1, c-1, d-1) and with supernatant (a-2, b-2, c-2, d-2), respectively.

6.3.4.3 XPS spectra for bastnäsite

Adventitious C–C, C–O–C and O–C=O was assigned to the C 1s (Figure 6.8a) peaks fitted at 284.80, 286.10 and 287.21 eV [6.24–6.27], respectively. The O–C=O peak presented a lower binding energy than expected from previous data [6.24–6.27], which might suggest a contribution of C–O or C–OH [6.26]. The bastnäsite peak was observed at around 289.70 eV [6.46] whereas a peak with higher binding energy, at around 291.78 eV, could indicate the presence of $>CO_3H^0$ [6.31]. Like $>CaOH^0$, $>CO_3H^0$ is another surface complex formed by hydrolysis of surface-bound species (in this case CO_3^-) [6.47]. The contribution of the $>CO_3H^0$ peak to the spectra seems to increase after conditioning the sample with supernatant.

The O 1s spectra (Figure 6.8b-1) was fitted with peaks for carbonate (bastnäsite) at around 531.45 eV [6.46] and $>CaOH^0$ at around 532.92 eV [6.24, 6.31]. The contribution of the $>CaOH^0$ peak to the O 1s spectra increased after conditioning with supernatant. It can also be seen in the Ca 2p spectra (Figure 6.8c), the doublet assigned to $>CaOH^0$ (Ca $2p_{3/2}$ at around 349.18 eV) [6.31] also increased relative to the bastnäsite peak (Ca $2p_{3/2}$ at around 347.72 eV) [6.46].

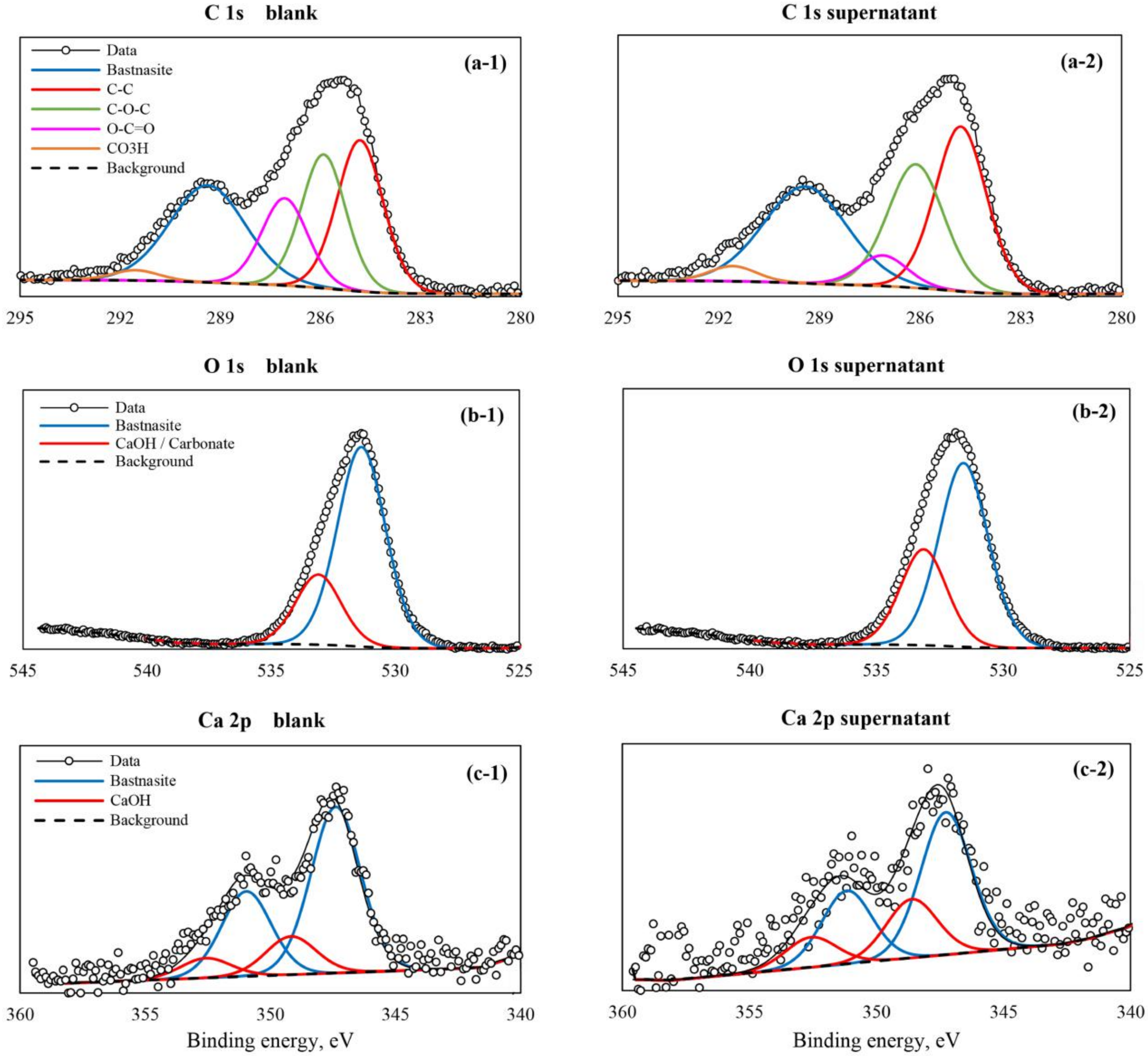

Figure 6.8 – C 1s, O 1s, Ca 2p and Mg 1s XPS spectra of bastnäsite without (a-1, b-1, c-1, d-1) and with supernatant (a-2, b-2, c-2, d-2), respectively.

6.3.5 DFT calculations

DFT simulations have been carried out to objectify the interaction of oleic acid collector species in aqueous phase on the RE minerals and dolomite surfaces, as well as RE minerals in the presence of dolomite supernatant. As the behaviors of both monazite and bastnäsite were comparable through flotation studies, it was decided, for the sake of brevity, to use only monazite for DFT simulation. Dolomite as a carbonatite gangue mineral was also considered for comparisons with monazite results.

The solution chemistry of oleic acid in aqueous phase reveals that this collector dissociates in three main species including, oleate ions Ol^{-}, oleate dimer $(\mathrm{Ol})_2^{2-}$, and acid soap $\mathrm{H(Ol)}_2^{-}$ [6.10]. Thus, their electronic properties and interaction with mineral surfaces will be discussed first. Among these species, the focus will be on oleate ion as it is the most abundant form at the pH investigated (Figure 6.5).

6.3.5.1 Optimised structure of oleate ion, oleate dimer and acid soap

The structure of oleate ion was first optimized by DFT simulations to understand its reactivity and the nature of its interaction with mineral surfaces. Oleic acid is dissociated into an ionic form in aqueous solutions at $\mathrm{pH} > 5$ [6.48]. The geometry of ionic form of the collector after optimization is shown in Figure 6.9a with C–O and C=O bond length of 1.28 Å, and O=C–C bond angle of 120.14°. Likewise, the Highest Occupied Molecular Orbitals (HOMOs) and the Lowest Unoccupied Molecular Orbitals (LUMOs) of oleate ion are shown in Figures 6.9b and 6.9c, respectively. These HOMOs and LUMOs in oleate ion polar head are responsible for the collector interaction with the minerals surfaces through exchange of electrons with HOMOs and LUMOs on the minerals' surfaces. In this regard, the oleate ion can transfer its HOMO electrons to LUMOs of metal atoms on the mineral surfaces to form covalent bond. Conversely, if the metal atoms can transfer some of their electrons to the oleate ion LUMOs back-donation covalent bond may also be formed increasing interaction between collector and mineral surfaces [6.49]. As seen in Figure 6.9a-c, oleate ion has the potential for both donating and accepting electrons through bond formation via either HOMOs or LUMOs in its structure.

The collector's transferable charges are mostly located on its polar head bearing the functional group (carboxyl functional group), Figure 6.9. In addition, the polar head has an ability to accept electrons attributed to its LUMOs. In this regard, the average charge of O atom on both C=O and C–O functional groups amounts to -0.50e based on the Mulliken charge analysis. This indicates that the two O atoms are active centers in the collector polar head to enable the two functional groups to be involved in collector – mineral interactions. Through adsorption, electrons from the negatively charged ions can be shared with mineral surfaces through covalent bonding. The charges of O on each of C=O and C–O contribute for -0.41e and -0.58e, respectively, indicating that oxygen atom in C–O has a stronger coordination ability with the metal ions as compared to the carbonyl O.

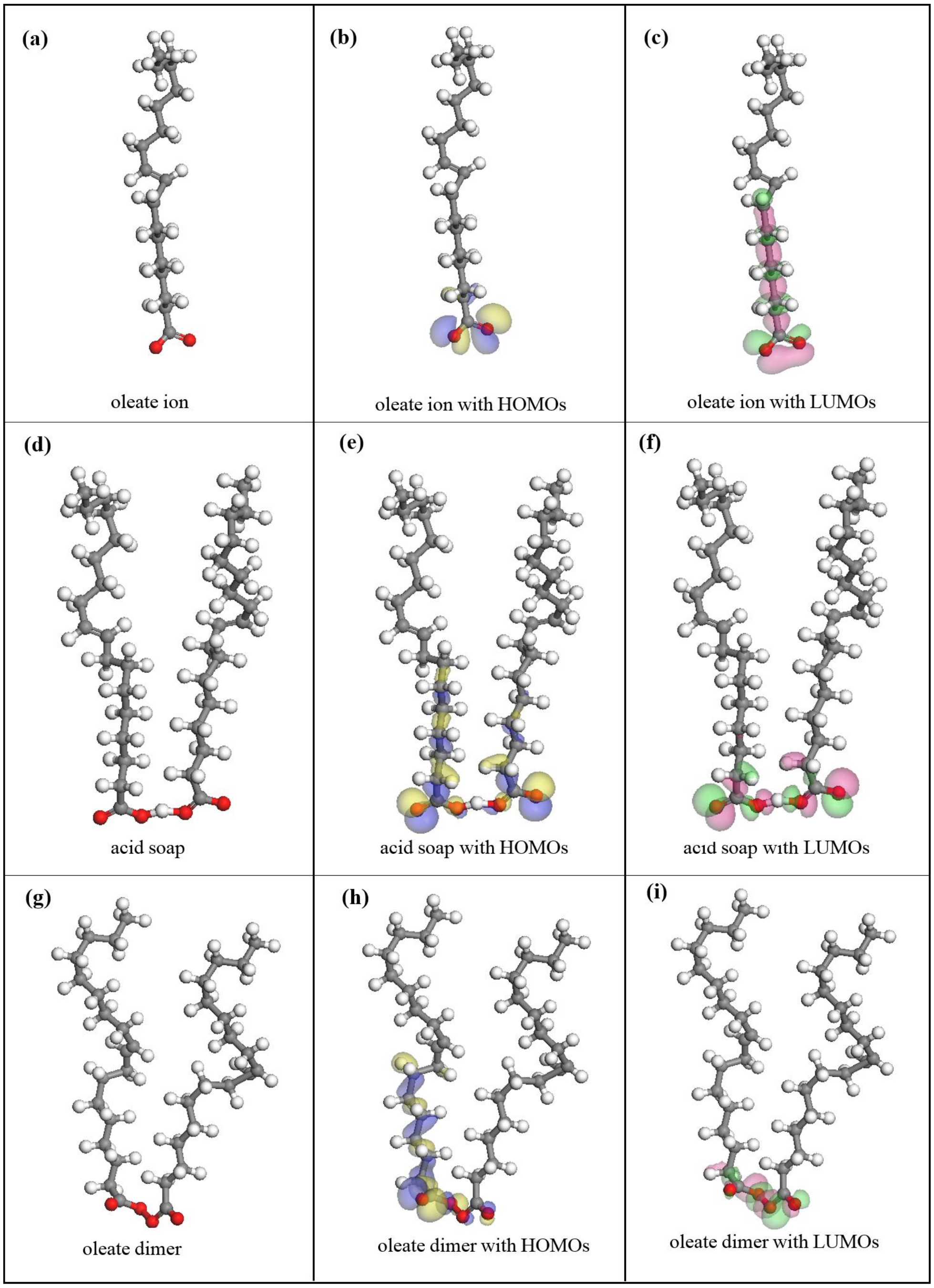
(a) oleate ion
(b) oleate ion with HOMOs
(c) oleate ion with LUMOs
(d) acid soap
(e) acid soap with HOMOs
(f) acid soap with LUMOs
(g) oleate dimer
(h) oleate dimer with HOMOs
(i) oleate dimer with LUMOs

Figure 6.9 – DFT optimized structures for the different oleic acid species in aqueous solution and their corresponding structures with HOMOs and LUMOs (O ≡ Red, C ≡ Gray, H ≡ White).

The optimized structures of acid soap $H(Ol)_2^-$ and oleate dimer $(Ol)_2^{2-}$ were also calculated through DFT simulations (Figure 6.9). A higher distribution of LUMOs and HOMOs is found for $H(Ol)_2^-$. This latter species exhibits higher activity as compared with the oleate dimer. This higher activity can be captured from a Mulliken charge analysis: oxygen atoms in acid soap polar head (C=O and C–O functional groups) are -0.37e, -0.50e, -0.49e, and -0.36e (average= -0.43e), from left to right, respectively (Figure 9d); while for oleate dimer oxygen these charges (Figure 6.9g) were -0.40e, -0.22e, -0.23e, and -0.40e (average= -0.31e), from left to right, respectively (Figure 6.9g). The average negative charge of oxygen atoms in C=O and C–O groups of oleate ions (-0.5e) exceeds that of either acid soap or oleate dimer suggesting the following order of interaction strength: oleate ions $Ol^- >$ acid soap $H(Ol)_2^- >$ oleate dimer $(Ol)_2^{2-}$.

6.3.5.2 Collector – mineral surface interactions

Case of oleate ion on monazite and dolomite surface

Figures 6.10a and 6.10b illustrate the geometrical details of the interaction of oleate ion with bare monazite and dolomite surfaces, respectively. Either C=O or C–O group interacts with Ce atoms on monazite surface through covalent bonding (Figure 6.10a). This type of bonding can be confirmed by the interaction energy, bond lengths and Mulliken charge analysis. The collector – monazite interaction energy amounts to -422.2 kJ/mol (as seen in Table 6.4) is large enough favoring chemical type of interaction. Moreover, the O–Ce distances between C–O and C=O groups and surface Ce atoms are *ca.* 2.24 and 2.23 Å, respectively. These collector – mineral bond lengths are close to the Ce–O bond length average in the monazite slab (100) structure (2.55 Å). The two active functional groups can interact with Ce through bridged binding conformations (Figure 6.10a). The O–C=O angle of adsorbed collector on the monazite surface is 121.55° for the configuration shown in Figure 6.10a. This angle is close to the equilibrium O–C=O angle in the free oleate ion (120.14°) suggesting some degree of stability of the adsorbed species.

The interaction between C–O and C=O functional groups and Ca atoms on the dolomite surface (Figure 6.10b) occurs via bidentate binding conformation. The interaction energy amounts only to -352.2 kJ/mol (as seen in Table 6.4) and the O–Ca bond lengths are around 2.46 and 2.71 Å for C–O and C=O groups, respectively (Figure 6.10b), which indicates less activity of C=O. This conformation between collector and Ca on the surface were obtained from several repetitions; and in any of these simulations, Mg atoms were not approached by collector. These suggest that the C=O group in the collector and the Mg atoms on the surface are less active than the C–O group and Ca atoms. This difference in affinities is ascribed to the larger ionic radius (and lesser electronegativity) of Ca with respect to Mg. In addition, O atom in C–O group carries more negative charge as compared to C=O group, causing the former to be more reactive. The O–Ca bond lengths are around 2.46 and 2.71 Å for C–O and C=O groups, respectively (Figure 6.10b). Both O–Ca bond lengths are larger as compared with those involved in the monazite – collector interactions. Furthermore, these distances are slightly greater than those of Ca–O and Mg–O (2.4 and 2.2 Å, respectively) on the dolomite surface structure, and confirm the chemical nature of the interaction between dolomite and oleate ion. In addition, the calculated O–C=O angle of adsorbed collector on the dolomite surface is 120.76°, which is again close to the angle of the free collector. These computed properties all concur to an interaction of oleate ion and dolomite of a chemical nature though to a with lesser strength than for monazite.

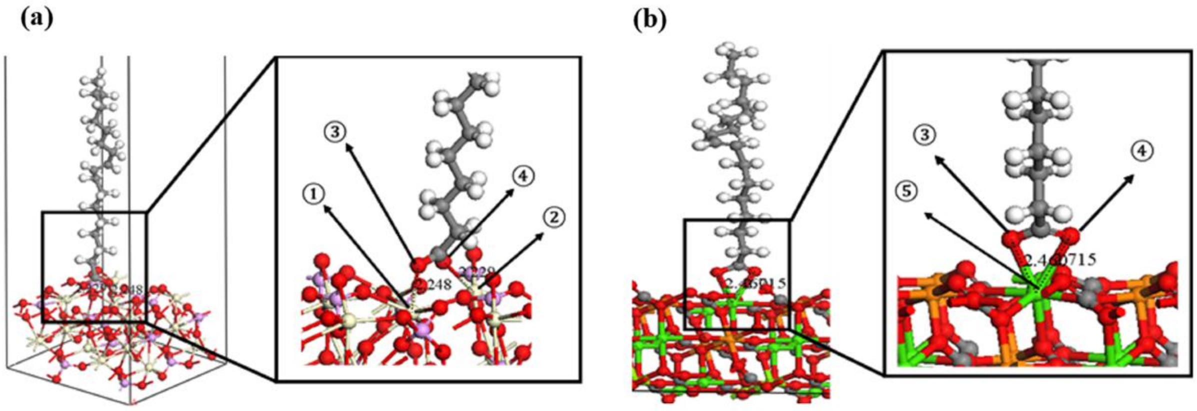

Figure 6.10 – Interaction of oleate ion onto (a) monazite surface (100) and (b) dolomite surface (104) (Ce ≡ Beige, O ≡ Red, P ≡ Purple, C ≡ Gray, Mg ≡ Orange, Ca ≡ Green, H ≡ White).

Table 6.2 – Mulliken charge analysis of monazite and dolomite surface atoms before and after collector adsorption.

Mineral	Figure number	Mulliken atomic charge (e)									
		(1)* Ce (in Ce–O)		(2)* Ce (in Ce=O)		(3)* –O– (from collector)		(4)* =O (from collector)		(5)* Ca (in dolomite)	
		Before	After	Before	After	Before	After	Before	After	Before	After
Monazite	6.10a	1.23	1.24	1.23	1.2	-0.58	-0.45	-0.41	-0.46	n.a.	n.a.
Dolomite	6.10b	n.a.	n.a.	n.a.	n.a.	-0.58	-0.56	-0.41	-0.5	1.5	1.58

*(1), (2), (3), (4) and (5) refer to marked atoms in Figure 6.10.

Mulliken charge analysis (Table 6.2) quantifies the importance of electron transfer between collector and minerals surface lattice atoms in terms of shared electrons involving

HOMOs and LUMOs to give rise to covalent bonds. The C–O group oxygen atoms give up more electron charge when the oleate collector has adsorbed onto monazite than dolomite. This is coherent with the relatively more negative interaction energy between collector and monazite than dolomite (see also Table 6.4).

Cases of oleate dimer and acid soap on monazite and dolomite surfaces

As seen in Figure 6.5, oleate dimer, $(\mathrm{Ol})_2^{2-}$, and acid soap, $\mathrm{H(Ol)}_2^-$, could also form in aqueous solution at pH around 7, and could likewise be adsorbed on the mineral surfaces. These three species differ from each other considering their polarity, surface activity and solubility; they are therefore expected to behave differently for the same mineral surfaces [6.10]. The interaction energies, the average lengths of covalent bond formed, the configuration of both oleate dimer and acid soap on the mineral have been quantified through DFT simulations.

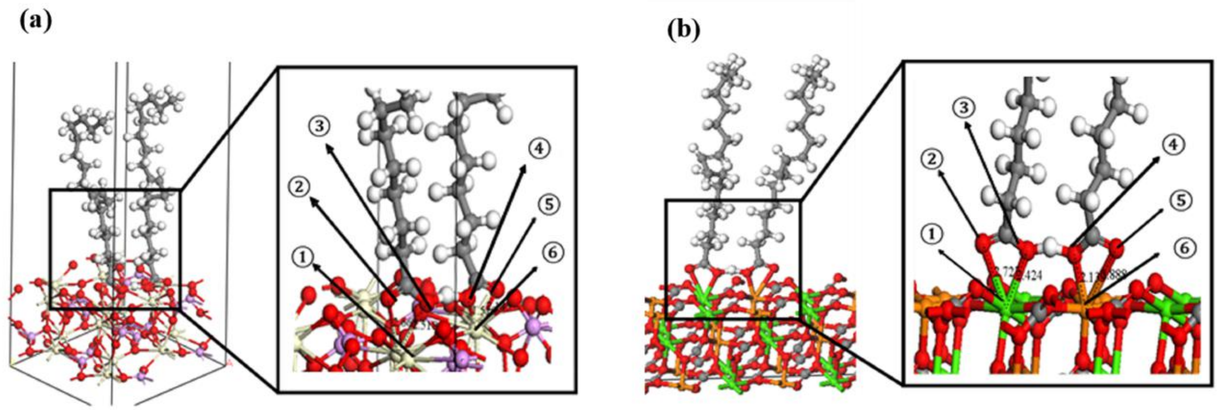

Figure 6.11 – Interaction of acid soap onto (a) monazite surface (100) and (b) dolomite surface (104) (Ce ≡ Beige, O ≡ Red, P ≡ Purple, C ≡ Gray, Mg ≡ Orange, Ca ≡ Green, H ≡ White).

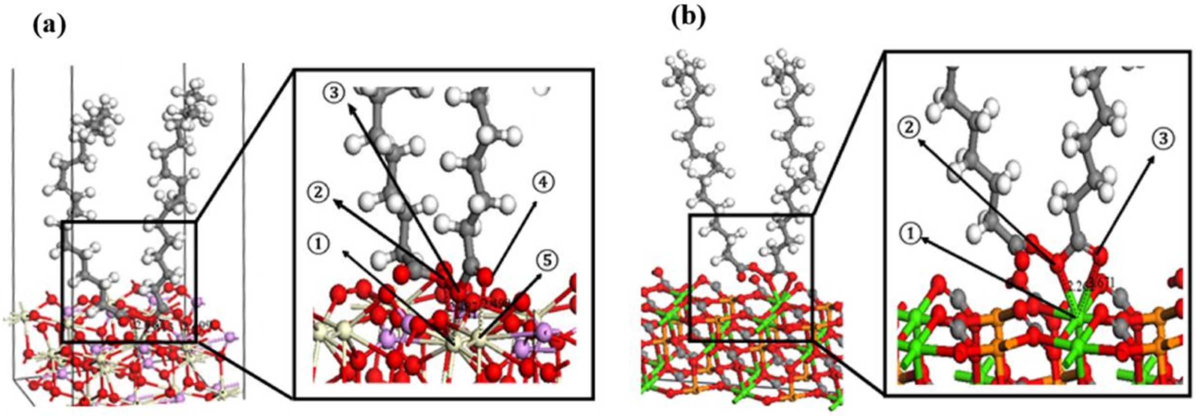

Figure 6.12 – Interaction of oleate dimer onto (a) monazite surface (100) and (b) dolomite surface (104) (Ce ≡ Beige, O ≡ Red, P ≡ Purple, C ≡ Gray, Mg ≡ Orange, Ca ≡ Green, H ≡ White).

Mulliken charge analysis of mineral surfaces after and before interaction with oleate dimer and acid soap (Table 6.3) suggests that the interaction should be chemisorption. Moreover, as seen in Table 6.4, bond lengths are relatively close to bond lengths between atoms in mineral structure (around 2 Å) which indicates formation of covalent bonding between oleate collector species and mineral surfaces. In Figure 6.11, it can be observed that all oxygen atoms in C=O and C–O groups in acid soap interact with the metal atoms both on dolomite or monazite surfaces. This is unlike the behavior of the oleate dimer shown (Figure 6.12). Three (respectively, two) out of four oxygen atoms of oleate dimer polar heads in the case of monazite (respectively, dolomite) have formed covalent bonding.

Table 6.3 – Mulliken charge analysis of monazite and dolomite surface atoms before and after adsorption acid soap and oleate dimer.

Interaction System	Figure number	Mulliken atomic charge (e)									
		(1)*/(6)* Metal atoms		(2)* (O in C=O)		(3)* (O in C–O)		(4)* (O in C=O)		(5)* (O in C–O)	
		Before	After	Before	After	Before	After	Before	After	Before	After
Monazite-acid soap	6.11a	1.23	1.25/1.24	-0.37	-0.4	-0.5	-0.43	-0.36	-0.4	-0.49	-0.44
Monazite-oleate dimer	6.12a	1.23	1.24	-0.23	-0.25	-0.4	-0.35	-0.22	-0.26	-0.4	-0.37
Dolomite-acid soap	6.11b	1.5	1.54	-0.37	-0.4	-0.5	-0.45	-0.36	-0.4	-0.49	-0.46
Dolomite-oleate dimer	6.12b	1.5	1.57	-0.23	-0.24	-0.4	-0.38	-0.22	-0.23	-0.4	-0.36

*(1), (2), (3), (4), (5) and (6) refer to marked atoms in Figures 6.11 and 6.12.

Table 6.4 – Adsorption energies and average formed covalent bond lengths of oleate ion, acid soap and oleate dimer during interaction with dolomite (104) and monazite (100) surface.

	Monazite (100) surface			Dolomite (104) surface		
	Oleate ion	Acid soap	Oleate dimer	Oleate ion	Acid soap	Oleate dimer
Interaction energy (kJ/mol)	-422.2	-391.2	-342.1	-358.2	-332.2	-311.4
Ave. length of formed covalent bonds (Å)	2.23	2.21	2.46	2.58	2.54	2.96

6.3.5.3 Adsorption of supernatant species on monazite surface

The speciation of dolomite in solution shows that various species such as $MgCO_3$, $CaCO_3$, $Mg(OH)_2$ and $Ca(OH)_2$ ion pairs or solid precipitates could precipitate out of dolomite supernatant and adsorb onto the surface of the minerals (see Section 6.3.3). Although the XPS results (Section 6.3.4) could identify only the presence of calcium and magnesium carbonates on the surface of monazite, the interaction of the hydroxide precipitates with the mineral surface was also investigated (Figures 5 - 7). The interaction of these species with the mineral surfaces has been discussed in previous work (see Chapter 5). The result from previous work showed that the precipitated species interact with the surface of the minerals through covalent bonding. The Ca and Mg atoms of $CaCO_3$ and $MgCO_3$, respectively, became exposed at the interface instead of Ce atom from monazite. $Ca(OH)_2$ interact with monazite covalently (through its Ca and O atoms); while Ca^{2+} ions adsorb at the surface initially through electrostatic interaction, followed by a strong covalent bond. Based on the calculated interaction energy, the adsorption of Ca^{2+} ions at the surface presented the most favourable scenario. It must be noted that the above findings are from the author's previous work and was mentioned to avoid describing the mechanism again. The authors refer the readers to the previous work (Chapter 5) for more details. It should also be noted that hydrated Ca^{2+} could form $CaOH^+$ before adsorption on the mineral's surface [6.6]. In this work, Ca^{2+} adsorption on mineral's surface was the one presented since the simulation using COSMO has already considered the presence of solvation layer.

The influence of adsorption of any species on the mineral surfaces' chemical reactivity was studied through comparison of the Mulliken charge analysis. Table 6.5 summarizes the results for the participating atoms (both from monazite and from supernatant species) before and after supernatant species adsorption. The results show occurrence of electron transfer between the atoms during species adsorption. The results (Table 6.2) suggest that the metals (Ca and Mg from the adsorbed species; and Ce at the monazite surface), which are active centers for collector adsorption [6.4], could be less reactive to collector species as seen from the decrease in the Mulliken charge after supernatant species adsorption.

Speciation of oleate (Figure 6.5) showed that the concentration of Ol^- was higher than the others at the studied conditions. Also, the interaction energy of oleate ions (Table 6.4) with the mineral surfaces was found to be the most negative, hence the strongest. Therefore, the interactions of oleate ions with adsorbed Ca^{2+}, $Ca(OH)_2$, $CaCO_3$ and $MgCO_3$ species on the monazite surface were prioritized and studied as shown in Figure 14. In this figure, it can be seen that the collector's C–O and C=O groups interact with the Mg and Ca atoms from the adsorbed species through bidentate conformation. It has been mentioned earlier that the metals (Ca or Mg) from the neutral ion pairs or solid precipitates could turn into new collector adsorption sites on the monazite surface. Table 6.6 summarizes the interaction energies between sodium oleate and adsorbed $Ca(OH)_2$, $CaCO_3$, $MgCO_3$ species and Ca^{2+} ions. The interaction energies with monazite decreased in the presence of pre-adsorbed Mg and Ca bearing species from dolomite supernatant. Monazite-collector interaction with pre-adsorbed species is less favourable than in the case of bare monazite.

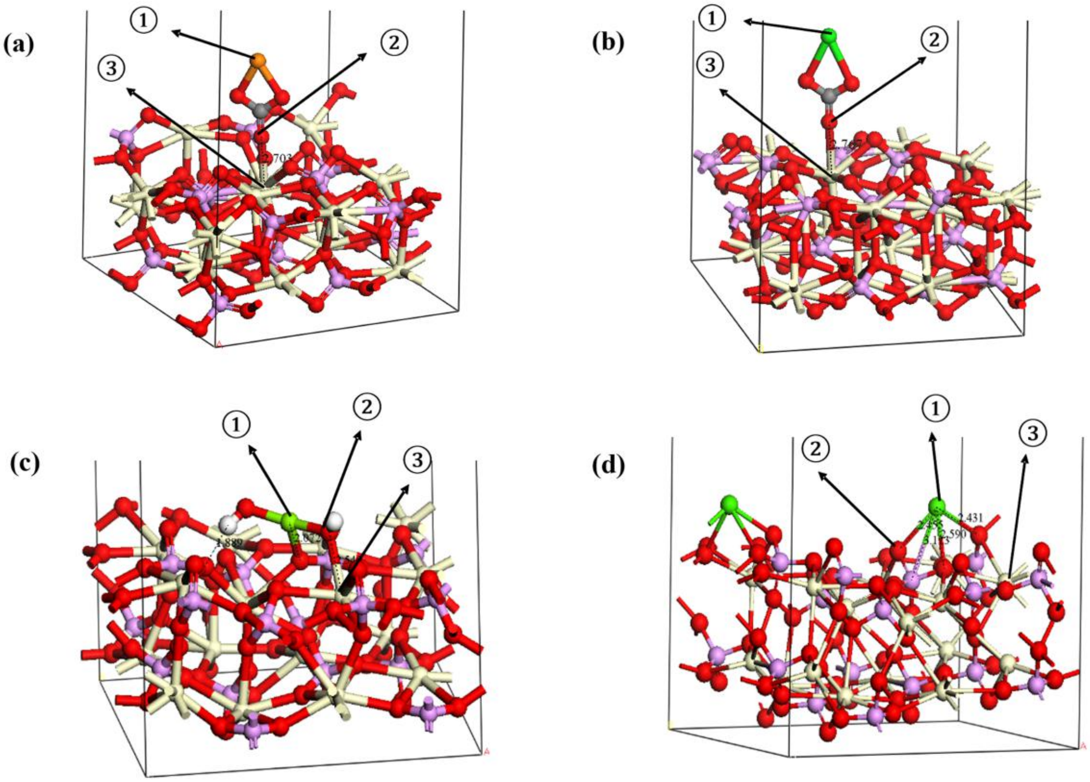

Figure 6.13 – Interaction of (a) $MgCO_3$, (b) $CaCO_3$, (c) $Ca(OH)_2$ and (d) Ca^{2+} ions on the monazite surface (100) (Ce ≡ Beige, O ≡ Red, P ≡ Purple, C ≡ Gray, Mg ≡ Orange, Ca ≡ Green, H ≡ White).

Table 6.5 – Mulliken charge analysis of monazite and dolomite surface atoms before and after supernatant adsorption.

Adsorbed species	Figure number	Mulliken atomic charge (e)					
		(1)* Metal from supernatant species (Ca/Mg)		(2)* O in O–Ce		(3)* Ce from monazite	
		Before	After	Before	After	Before	After
MgCO_3	6.13a	1.86	1.36	-0.71	-0.41	1.23	1.15
CaCO_3	6.13b	1.72	1.65	-0.67	-0.41	1.23	1.14
Ca$(OH)_2$	6.13c	2	1.45	-1.2	-0.92	1.23	1.16
Ca^{2+}	6.13d	2	1.43	-0.67	-0.79	1.23	1.20

*(1), (2) and (3) refer to marked atoms in Figure 6.13.

For further understanding of the interaction between collector and supernatant species at the monazite surface, Mulliken charge analysis was also considered. As presented in Table 6.5, electron transfer occurred between all atoms of the mineral surface, adsorbed supernatant species and collector polar head. This analysis shows that atoms on the minerals surface were still involved in collector interaction since their charges have been changed, even though the mineral surface was covered with new species. It was also found that sharing of electrons between collector – mineral (Table 6.5) occurred more than collector – adsorbed supernatant (Table 6.7). This finding is deduced from: (1) comparison between changes on electron charges of O in C–O and C=O groups (collector polar head) and (2) comparison between changes on electron charges of all metal atoms involved in covalent bond with either C–O or C=O groups (collector polar head).

Table 6.6 – Adsorption energy of oleic acid on dolomite (104) surface and monazite (100) surface active centers with and without precipitated supernatant species.

Component	Interaction energy (kJ/mol)					
	On dolomite (104) surface	On bare monazite (100) surface	Adsorbed supernatant species on the monazite (100) surface			
			$MgCO_3$	$CaCO_3$	$Ca(OH)_2$	Ca^{2+}
Collector	-358.2	-422.2	-326.5	-335.1	-320.2	-356.4

Table 6.7 – Mulliken charge analysis of monazite with adsorbed supernatant species before and after collector adsorption.

Adsorbed species	Figure number	Mulliken atomic charge (e)									
		(1)* Ca/Mg from adsorbed species		(2)* O (in Ce-O)		(3)* Ce from monazite		(4)* –O– from collector		(5)* =O from collector	
		Before	After	Before	After	Before	After	Before	After	Before	After
$\mathbf{Mg}CO_3$	6.14a	1.36	1.4	-0.56	-0.67	1.23	1.15	-0.58	-0.56	-0.41	-0.56
$\mathbf{Ca}CO_3$	6.14b	1.65	1.63	-0.41	-0.48	1.23	1.14	-0.58	-0.55	-0.41	-0.56
$\mathbf{Ca}(OH)_2$	6.14c	1.45	1.37	-0.89	-0.91	1.23	1.16	-0.58	-0.57	-0.41	-0.43
Ca^{2+}	6.14d	1.43	1.56	-0.79	-0.78	1.23	1.06	-0.58	-0.56	-0.41	-0.57

*(1), (2), (3), (4) and (5) refer to marked atoms in Figure 6.14.

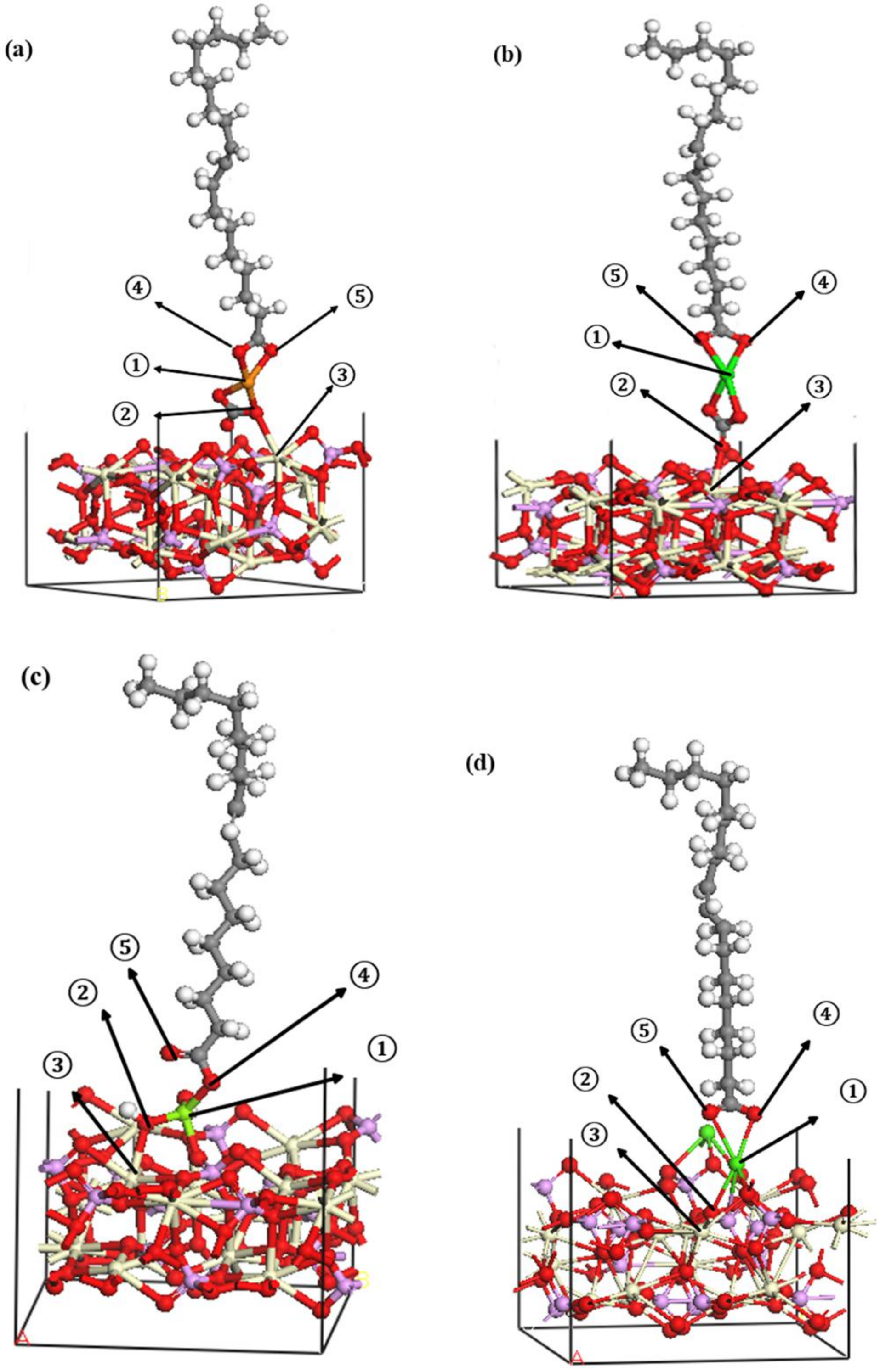

Figure 6.14 – Interaction of (a) $MgCO_3$, (b) $CaCO_3$, (c) $Ca(OH)_2$ and (d) Ca^{2+} ions on the monazite surface (100) (Ce ≡ Beige, O ≡ Red, P ≡ Purple, C ≡ Gray, Mg ≡ Orange, Ca ≡ Green, H ≡ White).

6.4 Discussion

The effect of dolomite supernatant on the flotation of dolomite, monazite and bastnäsite with sodium oleate at pH 7 was investigated. Possible species from dolomite supernatant that can be formed/precipitate in the solution or at the solution/mineral interface are $MgCO_3$, $CaCO_3$, $Mg(OH)_2$ and $Ca(OH)_2$ based from the equilibrium equations (6.3) – (6.19) and speciation diagram of dolomite supernatant (Section 6.3.3). However, among these, only the carbonate precipitates were observed at surface of the minerals through XPS analyses. The deviation could be attributed to the conditioning time used in this experiment, which could be shorter than the time needed for the hydroxides to precipitate. Other species found at the surface of the minerals through XPS analyses are $>CaOH^0$ (dolomite) and $>CO_3H^0$ (bastnäsite). These are expected as carbonate minerals when exposed to water tend to form these surface sites [6.50].

6.4.1 The interaction of the mineral surface with oleate ion, acid soap and oleate dimer

Before interpreting the effect of the supernatant on the mineral surface, the interaction of the different oleate species in the solution will be discussed first. Since, oleate can dissociate in the solution into oleate ion, Ol^-, acid soap, $H(Ol)_2^-$, and oleate dimer, $(Ol)_2^{2-}$, [6.10], these three species were investigated through DFT simulation. The calculations showed that all the C–O and C=O groups of the oleate ion and acid soap are involved in the interaction with the mineral surface through covalent bonding (see Section 6.3.5.2). However, for the oleate dimer, only 3 out of 4 O atoms are engaged in the collector – monazite interaction (Figure 12a); while, only 2 O atoms are involved in the collector – dolomite interaction (Figure 6.12b). This kind of configuration may indicate that acid soap interacts more strongly with the mineral surfaces compared with oleate dimer. This can also be confirmed through comparison between interaction energies and the average lengths of formed covalent bonds during mineral – collector species interactions (Table 6.4). Since shorter average bond lengths reflect stronger interaction, it can be validated that the interaction of acid soap is more favorable than oleate dimer with both monazite and dolomite. Other studies also suggested that acid soap is more stable and surface active than the dimer because of the absence of charge repulsion [6.9]. An assessment between the oleate ion (monomer) and the dimer was not made by these authors due to the contrasting influence of the size and the charge. In this study, considering the HOMOs and LUMOs, no direct comparison between oleate ion and the dimer can also be made. However, it confirms that acid soap should interact more with the minerals than with the dimer, as well as than oleate ion. Though it suggests that acid soap should be more reactive than oleate ion, contrary to what was proposed in the literature [6.9], Mulliken charge of the O atom in C–O (which is involved in the collector – mineral interaction), suggests that oleate ion (Table 6.2) has stronger interaction with the minerals than acid soap (Table 6.3). Also, on the basis of calculated interaction energies provided in Table 6.4, it can be observed that the strength of the interaction on the mineral surfaces is greater (indicated by more negative interaction energy) for oleate ions Ol^- than acid soap $H(Ol)_2^-$; and acid soap is greater than oleate dimer $(Ol)_2^{2-}$.

6.4.2 The effect of dolomite supernatant on the zeta potential of the minerals

When the minerals are conditioned with only the NaOl, the zeta potential of the minerals became greatly negative (Figure 6.2), suggesting that the dissociated forms of the collector have strong interaction with the bare mineral surface. The adsorption of negatively charged oleate species at the surface of negatively charged dolomite surface, confirms the chemisorbing characteristic of the collector at this pH condition [6.7]. In addition, DFT simulations (Table 6.4) showed that the bond lengths of O–Ca interacting with the C–O and C=O groups of the collector are slightly exceeding the bond lengths of Ca–O and Mg–O on dolomite surface, indicating that the interaction of dolomite and the collector is chemical by nature. The results of Mulliken charge analysis also confirmed the chemical nature of collector – mineral interaction by presenting that electron sharing (charge exchanges) occurs between atoms of collector and mineral (Table 2 - 3). Electrostatic forces also appeared to have an important role in the adsorption of the collector due to the differences between the zeta potential before (presence of NaCl) and after conditioning with NaOl; it can be observed that the interaction with sodium oleate is stronger for bastnäsite, followed by monazite and then dolomite. This correlates well with the zeta potential of bare mineral surface: bastnäsite is 9.8 eV > monazite is -0.6 eV > dolomite is -10.4 eV, and in agreement with calculated interaction energies demonstrated in Table 6.4.

Zeta potential measurements (Figure 6.1) showed that conditioning with dolomite supernatant in the presence of NaOl collector significantly affects the minerals (particularly the RE minerals) at basic pH. This is expected as the cations (from dolomite supernatant) start to form precipitates at these pH conditions [6.23]. Since the effect of dolomite supernatant was already investigated at pH 9 (Chapter 5), the authors decided to investigate further the consequences of the dissolved mineral species at pH 7. Also, previous studies have shown that maximum recovery of RE minerals in the presence of oleate occurred close to this pH [6.12, 6.13]. Additional zeta potential measurements were conducted with the minerals in the presence of only 1×10^{-3} M NaCl, and only supernatant (Figure 6.2). When the negatively-charged dolomite was exposed to the supernatant, zeta potential became less negative. This could be due to the adsorption of positively-charged species such as Ca^{2+} or $CaOH^{+}$ as suggested by speciation diagram (Figure 6.4) and as confirmed by XPS analyses (Figures 6.6 - 6.8). However, when monazite and bastnäsite were pulped with the supernatant, the zeta potential reduced significantly (see Figure 6.2). At pH 7, the zeta potential of the main precipitated species $MgCO_3$, is slightly negative [6.51]; moreover, HCO_3^- species from the supernatant could also make the surface of the bastnäsite negative and monazite more negative [6.23]. These negatively charged species ($MgCO_3$ and HCO_3^-) could interact more with the positively charged surface of bastnäsite than with the slightly negative monazite and negatively charged dolomite, as can be seen from the zeta potential values (Figure 6.2). This was also supported by the XPS results, which show that the increase in the amount of $>CO_3H^0$ can be observed at the surface of bastnäsite after conditioning with the supernatant (Section 6.3.4.3).

6.4.3 The effect of dolomite supernatant on minerals' flotation

The minerals' zeta potential (Figure 6.2) agreed with the flotation results (Figure 6.3), which showed that the RE minerals have higher floatability than dolomite in deionised water. It seems that both electrostatic forces and chemical interactions between collector and minerals were more promoted in the case of RE minerals resulting in higher flotation recoveries (Figure 6.3). Although oleate is a strong collector, and is known to be nonselective, the DFT simulations still show that this collector has stronger interaction with monazite than dolomite (Table 6.4). By comparing the changes in the atomic charge by Mulliken analyses (see Table 6.2), it can be seen that the O in C–O (which has more coordinating ability than O in C=O) participated more in the monazite – collector interaction than in the dolomite – collector interaction. Compared to previous finding with benzohydroxamate collector (Chapter **??**), the presence of dolomite supernatant also had detrimental effect to monazite and bastnäsite flotation with sodium oleate, (considered to be) a strong collector. In the presence of dissolved mineral species, it can be observed that bastnäsite is more affected than monazite, while monazite is more affected than dolomite (Figure 6.3). As mentioned previously, electrostatic interaction might play an important role in the adsorption of negatively charged precipitate and ionic species onto the surface of the minerals. Since bastnäsite is positively charged and monazite is less negative than dolomite (see Figure

6.2), these RE minerals have more affinity to these species, making their surface adsorb more of these species than that of dolomite. In addition, the floatability of bastnäsite and monazite is expected to be more affected, since the precipitated species – collector interaction is less favourable than bare mineral – collector interaction, as suggested by the calculated interaction energies (Table 6.6). Dolomite might have some species precipitated at its surface as well, which would explain why dolomite recovery was also slightly affected. Another reason for the decrease in flotation recovery could be the formation of Ca- and Mg-oleate precipitate (Figure 6.5) in the solution. The precipitation of these species could have led to a decrease in the available oleate for mineral interaction, thus a decrease in recovery.

6.4.4 Sodium oleate compared with benzohydroxamate

Based from these results, oleate can be considered stronger collector than typical RE mineral collector, benzohydroxamate (an aromatic hydroxamate). As seen from the calculated interaction energies (Table 6.3) and by the results from the previous work (see Table 6.8 from Chapter 5), mineral – oleate interaction energies are more negative (hence, stronger) than mineral – benzohydroxamate interaction energies. This is highly influenced by the chain length of sodium oleate, since the length of the hydrophobic radical influences the level of hydrophobicity that the collector provides to the mineral [6.2]. Increasing the chain length of the collector makes it a stronger collector but less selective [6.2]. The difference between the interaction energies of dolomite and monazite are also observed to be smaller (Table 6.3) with sodium oleate than benzohydroxamate (see Table 6.8), indicating that benzohydroxamate is a more selective collector than sodium oleate. The degree of selectivity can be explained by the polarity of the O in N–O (benzohydroxamate) and C–O (oleate) groups, which are involved in the collector – mineral interactions. Since N is more electronegative than C, O in N–O will have lesser negative charge (-0.48e) (Chapter 5) than O in C–O (-0.58e) (see Section 6.3.5.1). The lesser negative charge of O in N–O makes it more selective for interaction with metals than O in C–O. Interestingly, the calculated interaction energies show that there was only a slight difference between monazite – benzohydroxamate and monazite – oleate interaction, while a significant difference was observed between dolomite – benzohydroxamate and dolomite – oleate interactions. This observation can be attributed to the surface structure of the minerals and the collector. The Ce atoms at the monazite surface are more reactive than the Ca and Mg atoms at the dolomite surface, however the combined site densities of Ca and Mg are greater than that of Ce. Moreover, because of the aromatic chain of the benzohydroxamate, it will have more steric hindrance effect than oleate which has a linear chain. It means that oleate can approach the mineral surfaces more easily than benzohydroxamate. Since more reactive oleate can interact easier with more exposed active centers of dolomite, then the difference in interaction energy between monazite – benzohydroxamate and monazite – oleate could be significantly less compared to the difference between dolomite – benzohydroxamate and dolomite – oleate.

Table 6.8 – Adsorption energy of benzohydroxamate collector on dolomite (104) surface and monazite (100) surface active centers with and without precipitated supernatant species.

Component	Interaction energy (kJ/mol)					
	On dolomite (104) surface	On bare monazite (100) surface	Adsorbed supernatant species on the monazite (100) surface			
			$MgCO_3$	$CaCO_3$	$Ca(OH)_2$	Ca^{2+}
Collector	-184.4	-385.5 -330.3	-190.2	-187.7	-177.4	-200.4

6.5 Conclusions

Sodium oleate is a popular collector for RE minerals, and though it is known to also have strong affinity to carbonate minerals such as dolomite; the presence of dolomite supernatant still showed to have decreased the floatability of RE minerals. It was found that at pH 7, the dissolved and precipitated dolomite species such as hydrated Ca^{2+}, $CaCO_3$ and $MgCO_3$ might adsorb at the surface of the minerals. The adsorbed species – collector interaction is slightly lesser than dolomite – collector interaction, and dolomite – collector is lesser than monazite – collector interaction, reflecting the decrease in the mineral's recovery in the presence of dolomite supernatant. Moreover, thermodynamic calculations indicated that precipitation of oleate as Ca-oleate and Mg-oleate could occur at pH 7, which could also be a reason for a decrease in recovery.

When compared to aromatic hydroxamate collectors, the strength and non-selectivity of sodium oleate collector could be mostly attributed to its structure and the gangue's structure. The oleate's strength as a collector is mostly attributed to its long hydrocarbon chain, which what imparts hydrophobic characteristic to the mineral. The low selectivity is attributed to oleate's lower steric hindrance effect and has higher reactive O atom involved in the interaction. The dolomite's structure, which present more exposed active sites to the collector than those of RE minerals also influences the ease at which the collector approaches the mineral's surface-active sites.

DFT simulations of the oleate ion, acid soap and dimer have also been presented in this work. Although the importance of acid soap in the flotation has been emphasized in the literature, in this work, the simulations indicated that oleate ion is the most important species due to its strong interaction with the mineral surface. It could be proposed that oleate ion adsorbed onto the mineral surface through a strong covalent interaction. Due to the lack of charge repulsion from undissociated oleate (HOl), it could adsorb to the initially adsorbed oleate ion through hydrogen bonding, forming an acid soap at the mineral surface. Further investigations by DFT simulations must be conducted to understand the mechanism of formation/adsorption of the acid soap on the mineral surface.

References

[6.1] Bulatovic, S. M. Collectors. In Bulatovic, S. M., Editor, *Handbook of Flotation Reagents*, pages 5–40. Elsevier, Amsterdam, 2007.

[6.2] Wills, B. A. and Finch, J. A. Froth Flotation. In Finch, J. A. and Wills, B. A., Editors, *Wills' Mineral Processing Technology*, pages 265–380. Butterworth-Heinemann, Boston, 8th edition, 2016.

[6.3] Jordens, A., Cheng, Y. P., and Waters, K. E. A review of the beneficiation of rare earth element bearing minerals. *Minerals Engineering*, 41:97–114, 2013.

[6.4] Fuerstenau, M., Jameson, G. J., and Yoon, R.-H. *Froth flotation: A century of innovation.* Society for Mining, Metallurgy, and Exploration, Littleton, Colorado, 2007.

[6.5] Zhang, X., Du, H., Wang, X., and Miller, J. D. Surface chemistry considerations in the flotation of rare-earth and other semisoluble salt minerals. *Minerals and Metallurgical Processing*, 30(1):24–37, 2013.

[6.6] Zhang, W., Honaker, R. Q., and Groppo, J. G. Flotation of monazite in the presence of calcite part I: Calcium ion effects on the adsorption of hydroxamic acid. *Minerals Engineering*, 100:40–48, 2017.

[6.7] Fuerstenau, M. and Miller, J. D. The role of the hydrocarbon chain in anionic flotation of calcite. *Transactions of AIME*, 238(2):153–160, 1967.

[6.8] Predali, J. Flotation of carbonates with salts of fatty acids: role of pH and the alkyl chain. *Transactions of the Institution of Mining and Metallurgy*, 78:C140–C147, 1969.

[6.9] Somasundaran, P. and Ananthapadmanabhan, K. Solution chemistry of surfactants and the role of it in adsorption and froth flotation in mineral-water systems. *Solution Chemistry of Surfactants*, 2:17–38, 1979.

[6.10] Kulkarni, R. D. and Somasundaran, P. Flotation chemistry of hematite/oleate system. *Colloids and Surfaces*, 1(3):387–405, 1980.

[6.11] Pugh, R. and Stenius, P. Solution chemistry studies and flotation behaviour of apatite, calcite and fluorite minerals with sodium oleate collector. *International Journal of Mineral Processing*, 15(3):193–218, 1985.

[6.12] Dixit, S. and Biswas, A. pH-dependence of the flotation and adsorption properties of some beach sand minerals. *Transactions of the Society of Mining Engineers of AIME*, 244(2):173–178, 1969.

[6.13] Gerdel, M. and Smith, R. The role of lignin sulfonate in flotation of bastnasite from barite. In Bautista, R. and Wong, M., Editors, *Rare Earths, Extraction, Preparation and Applications*. The Minerals, Metals and Materials Society, 1988.

[6.14] Pradip, Rai, B., Rao, T. K., Krishnamurthy, S., Vetrivel, R., Mielczarski, J., and Cases, J. M. Molecular modeling of interactions of diphosphonic acid based surfactants with calcium minerals. *Langmuir*, 18(3):932–940, 2002.

[6.15] Pradip and Rai, B. Molecular modeling and rational design of flotation reagents. *International Journal of Mineral Processing*, 72(1–4):95–110, 2003.

[6.16] Rai, B. *Molecular Modeling for the Design of Novel Performance Chemicals and Materials*. CRC Press, New York, 2012.

[6.17] Rai, B. and Pradip. Design of highly selective industrial performance chemicals: a molecular modelling approach. *Molecular Simulation*, 34(10-15):1209–1214, 2008.

[6.18] Rath, S. S., Sinha, N., Sahoo, H., Das, B., and Mishra, B. K. Molecular modeling studies of oleate adsorption on iron oxides. *Applied Surface Science*, 295:115–122, 2014.

[6.19] Ataman, E., Andersson, M. P., Ceccato, M., Bovet, N., and Stipp, S. L. S. Functional group adsorption on calcite: I. Oxygen containing and nonpolar organic molecules. *The Journal of Physical Chemistry C*, 120(30):16586–16596, 2016.

[6.20] Ataman, E., Andersson, M. P., Ceccato, M., Bovet, N., and Stipp, S. L. S. Functional group adsorption on calcite: II. Nitrogen and sulfur containing organic molecules. *The Journal of Physical Chemistry C*, 120(30):16597–16607, 2016.

[6.21] Predali, J. and Cases, J. M. Zeta potential of magnesian carbonates in inorganic electrolytes. *Journal of Colloid and Interface Science*, 45(3):449–458, 1973.

[6.22] Gans, P. Hyperquad Simulation and Speciation (HySS). [Computer Program], Protonic software, Leeds, England, 2009.

[6.23] Chen, G. and Tao, D. Effect of solution chemistry on flotability of magnesite and dolomite. *International Journal of Mineral Processing*, 74(1–4):343–357, 2004.

[6.24] Chu, D. H., Vinoba, M., Bhagiyalakshmi, M., Baek, I. H., Nam, S. C., Yoon, Y., Kim, S. H., and Jeong, S. K. CO_2 mineralization into different polymorphs of $CaCO_3$ using an aqueous-CO_2 system. *RSC Advances*, 3(44):21722–21729, 2013.

[6.25] Liu, S., Huang, B., Chai, L., Liu, Y., Zeng, G., Wang, X., Zeng, W., Shang, M., Deng, J., and Zhou, Z. Enhancement of As (v) adsorption from aqueous solution by a magnetic chitosan/biochar composite. *RSC Advances*, 7(18):10891–10900, 2017.

[6.26] Salvi, A. M., Langerame, F., Macchia, A., Sammartino, M. P., and Tabasso, M. L. XPS characterization of (copper-based) coloured stains formed on limestone surfaces of outdoor Roman monuments. *Chemistry Central Journal*, 6(2):S10, 2012.

[6.27] Thermo Scientific XPS. Carbon - Nonmetals. http://xpssimplified.com/elements/carbon.php, 2017. Accessed Feb. 08, 2017.

[6.28] Gopinath, C. S., Hegde, S. G., Ramaswamy, A. V., and Mahapatra, S. Photoemission studies of polymorphic $CaCO_3$ materials. *Materials Research Bulletin*, 37(7):1323–1332, 2002.

[6.29] Hu, X., Joshi, P., Mukhopadhyay, S. M., and Higgins, S. R. X-ray photoelectron spectroscopic studies of dolomite surfaces exposed to undersaturated and supersaturated aqueous solutions. *Geochimica et Cosmochimica Acta*, 70(13):3342–3350, 2006.

[6.30] Lee, B.-S., Lin, Y.-C., Chen, S.-F., Chen, S.-Y., and Chang, C.-C. Influence of calcium hydroxide dressing and acid etching on the push-out bond strengths of three luting resins to root canal dentin. *Clinical Oral Investigations*, 18(2):489–498, 2014.

[6.31] Stipp, S. L. and Hochella, M. F. Structure and bonding environments at the calcite surface as observed with X-ray photoelectron spectroscopy (XPS) and low energy electron diffraction (LEED). *Geochimica et Cosmochimica Acta*, 55(6):1723–1736, 1991.

[6.32] Forsgren, J., Frykstrand, S., Grandfield, K., Mihranyan, A., and Strømme, M. A template-free, ultra-adsorbing, high surface area carbonate nanostructure. *PLOS ONE*, 8(7), 2013.

[6.33] Rheinheimer, V., Unluer, C., Liu, J., Ruan, S., Pan, J., and Monteiro, P. XPS study on the stability and transformation of hydrate and carbonate phases within MgO systems. *Materials*, 10(1):75, 2017.

[6.34] Süzer, Ş. and Erten, H. N. Photoelectron spectroscopy: A tool in sorption studies. *Turkish Journal of Chemistry*, 21(4):409–414, 1997.

[6.35] Cizaire, L., Martin, J. M., Le Mogne, T., and Gresser, E. Chemical analysis of overbased calcium sulfonate detergents by coupling XPS, ToF-SIMS, XANES, and EFTEM. *Colloids and Surfaces A: Physicochemical and Engineering Aspects*, 238(1):151–158, 2004.

[6.36] Gu, W., Bousfield, D. W., and Tripp, C. P. Formation of calcium carbonate particles by direct contact of $Ca(OH)_2$ powders with supercritical CO_2. *Journal of Materials Chemistry*, 16(32):3312–3317, 2006.

[6.37] Sugama, T., Kukacka, L. E., Carciello, N., and Hocker, N. J. Study of interactions at water-soluble polymer/$Ca(OH)_2$ or gibbsite interfaces by XPS. *Cement and Concrete Research*, 19(6):857–867, 1989.

[6.38] Thermo Scientific XPS. Magnesium - Alkaline Earth Metals. http://xpssimplified.com/elements/magnesium.php, 2017. Accessed Feb. 08, 2017.

[6.39] Somasundaran, P. and Agar, G. E. The zero point of charge of calcite. *Journal of Colloid and Interface Science*, 24(4):433–440, 1967.

[6.40] Bêche, E., Charvin, P., Perarnau, D., Abanades, S., and Flamant, G. Ce 3d XPS investigation of cerium oxides and mixed cerium oxide ($Ce_xTi_yO_z$). *Surface and Interface Analysis*, 40(3-4):264–267, 2008.

[6.41] Ivanova, O. P., Vasilyev, L. A., Naumkin, A. V., and Kantsel, V. V. XPS studies of natural monazite and relative compounds under ion bombardment. *Applied Surface Science*, 72(4):307–312, 1993.

[6.42] Lai, H., Bao, A., Yang, Y., Tao, Y., and Yang, H. Selective synthesis and luminescence property of monazite- and hexagonal-type $LaPO_4$: Eu nanocrystals. *CrystEngComm*, 11(6):1109–1113, 2009.

[6.43] Thermo Scientific XPS. Oxygen - Nonmetals. http://xpssimplified.com/elements/oxygen.php, 2017. Accessed Feb. 08, 2017.

[6.44] Baer, D. R. and Moulder, J. F. High Resolution XPS Spectrum of Calcite ($CaCO_3$). *Surface Science Spectra*, 2(1):1–7, 1993.

[6.45] Ni, M. and Ratner, B. D. Differentiation of calcium carbonate polymorphs by surface analysis techniques – An XPS and TOF-SIMS study. *Surface and Interface Analysis*, 40(10):1356–1361, 2008.

[6.46] Cui, J., Hope, G. A., and Buckley, A. N. Spectroscopic investigation of the interaction of hydroxamate with bastnaesite (cerium) and rare earth oxides. *Minerals Engineering*, 36:91–99, 2012.

[6.47] Chibowski, E., Hotysz, L., and Szcześ, A. Time dependent changes in zeta potential of freshly precipitated calcium carbonate. *Colloids and Surfaces A: Physicochemical and Engineering Aspects*, 222(1):41–54, 2003.

[6.48] Bonnitcha, P. D., Kim, B. J., Hocking, R. K., Clegg, J. K., Turner, P., Neville, S. M., and Hambley, T. W. Cobalt complexes with tripodal ligands: implications for the design of drug chaperones. *Dalton Transactions*, 41(37):11293–11304, 2012.

[6.49] Albright, T. A., Burdett, J. K., and Whangbo, M.-H. *Orbital Interactions in Chemistry*. John Wiley & Sons, New Jersey, 2013.

[6.50] Van Cappellen, P., Charlet, L., Stumm, W., and Wersin, P. A surface complexation model of the carbonate mineral-aqueous solution interface. *Geochimica et Cosmochimica Acta*, 57(15):3505–3518, 1993.

[6.51] Škvarla, J. and Kmet, S. Non-equilibrium electrokinetic properties of magnesite and dolomite determined by the laser-Doppler electrophoretic light scattering (ELS) technique. A solids concentration effect. *Colloids and Surfaces A: Physicochemical and Engineering Aspects*, 111(1):153–157, 1996.

Chapter 7

Niobec rare earth ore flotation

The important findings from the fundamental studies presented in Chapters 3, 4, 5 and 6, as well as mineralogical studies, provided guidance in designing the tests concerning the Niobec RE ore. This chapter presents the separate processing of the fine (-20 μm) and coarse (+20 μm) fractions of Niobec RE ore. The work detailed in this chapter focuses on exploring the feasibility of using an specially designed column cell for the processing of the fine fraction.

Abstract

The RE minerals in Niobec RE ore are fine-grained, which requires fine grinding to achieve liberation. Due to this, flotation is the most appropriate beneficiation method for effective separation of RE minerals from the gangue. However, flotation with a conventional mechanical cell can be difficult for fine particles due to the low bubble-particle collision probability, which is a key component in achieving efficient flotation recovery. Because of this problem and the significant concentration of RE elements in the -20 μm particle size range, it was deemed practical to split the milled ore into -20 and +20 μm fractions for separate processing. The +20 μm ore fraction was further ground prior to bench-scale mechanical cell flotation. This does not only prevent overgrinding of the -20 μm particles but also achieve a more efficient grinding of the +20 μm particles. A column cell, which was inspired by the work of Maoming *et al.* [7.1], was specially designed to process the -20 μm ore fraction. The design involves the introduction of conventional and finer bubbles through a sparger and a cavitation tube, respectively. The results indicated that a significant recovery and enrichment of RE elements in the concentrate could be achieved in both the mechanical and column cell flotation. As this was just an exploratory investigation, further improvements in the column set-up should be evaluated.

7.1 Introduction

RE elements include yttrium and the lanthanoids [7.2], which can be further divided into light (La, Ce, Pr, Nd, Pm, Sm, Eu) and heavy (Y, Gd, Tb, Dy, Ho, Er, Tm, Yb, Lu) RE elements [7.3]. Due to their chemical properties, they have proven useful in high technology applications. Because of the emergence of high technology requiring RE elements [7.4], the demand for RE elements are expected to continue to increase in the future [7.5]. However, with the expected RE production and demand, RE elements such as La, Nd, Pr, Dy, and Tb, are highly to be in short supply by 2025 [7.6]. This shortage can only be avoided with constant development of new mines outside of China (main producer of RE elements). Among the Advanced Projects located in Canada is the Niobec RE project of Magris Resources Inc., which has been found to contain a significant resource of RE elements with 1058.6 million tonnes at 1.73% total RE oxide (TREO) [7.7, 7.8]. This corresponds to 18.3 million tonnes of TREO, which is almost half of China's RE elements reserve (∼43 million tonnes TREO) [7.9].

The Niobec RE ore deposit is a carbonatite complex located in St Honoré, Quebec. It is composed of a central carbonatite core, surrounded by mainly alkaline syenite, a feldspathoid-bearing syenite and syenitic foidites. The carbonatite core consists of concentric lenses of calcitites and dolomitites with compositions from calcitite, to dolomitite to ferro-carbonatite towards the core. The massive to brecciated ferro-carbonatite core contains the RE elements mineralization in the form of fluorocarbonates and monazite [7.10]. Based from the mineralogical analysis of the 12 drill core samples done recently, the crushed samples have a D_{50} of 15 - 34 μm for bastnäsite/synchisite (fluorocarbonate) and 10 - 25 μm for monazite (phosphate). The RE minerals liberation is found to be poor to moderate as most of the particles occur as complex particles (ternary and quaternary middlings) [7.11]. Because of the fine grain sizes of the RE minerals, the most suitable concentration method would be flotation. Flotation is a process that takes advantage of the differences in the surface properties of the minerals in solution, whether natural or modified by reagents. When bubbles are introduced into the system, hydrophobic particles can attach to the bubbles and be recovered as the bubble rises to the top (forming the froth) [7.12]. Thus, bubble-particle interaction is the important aspect of achieving an efficient flotation recovery, which could be divided into 3 processes: collision, attachment and detachment [7.13]. Due to low collision probability of fines to bubbles (attributed to its size relative to bubble size), fine particles are difficult to float [7.14]. It has been shown that making use of smaller bubbles is required to achieve a more efficient flotation of fines [7.14].

As described by Wills and Finch [7.12], there are several machines used in flotation, of which the most popular are mechanical, column and reactor/separator flotation machines (*e.g.,* Jameson cell). Mechanical machines have an impeller (mechanically driven) that mixes the slurry and disperses air as bubbles into the machine. Flotation columns are known to improve separation efficiency, especially for fine particles. Apart from this, some of the advantages it has over mechanical cells include low capital and operation cost, and less space requirement. In column cells, the air is introduced via a sparger, which can be installed either as an internal device or an external one. Internal spargers are not preferred to due possible wear and plugging of ore particles. The SlamJet® (internal jetting sparger) is an improved version of these internal spargers with the added wear protection, air flowrate control and shut-off mechanism. As for external spargers, CISA/Microcel™ mixes slurry (from the column) and air through an in-line contactor. This mechanism breaks the air into smaller bubbles at the same time mixes them with the particles. Another way of introducing air is by using a cavitation tube (CavTube™), in which fine bubbles are produced due to cavitation. This cavitation is a result of the pressure drop attributed to the special geometry of the tube. Another type of flotation machine is the reactor/separator. These machines differentiate the bubble-particle mixing region (reactor) and the bubble-particle aggregates separation (from the slurry) region (separator). The most popular of which is the Jameson cell which was developed by Mount Isa Mines Ltd and University of New Castle in Australia. It is often referred to as a column, however due to the mechanism of bubble-particle mixing and separation from the slurry, it was also considered a reactor/separator type machine. The mode of air introduction in Jameson cell is by plunging a jet of slurry through a downcomer. The high-pressure jet entrains the air in the atmosphere and the impact with the liquid shears the air into fine bubbles [7.12].

In this work, the concept of producing fine bubbles by pressure difference was utilized. The column design used in this work which is practical for lab-scale set-up was inspired by the work of Maoming *et al.* [7.1]. The design incorporates production of conventional bubbles and of finer bubbles with a typical sparger and cavitation, respectively. The design will be discussed in detail in the Materials and Methods section. The column was used to process the fine particles (-20 μm) Niobec ore, while the coarse particle fraction (+20 μm) was processed using a conventional flotation machine. Although conventional flotation was conducted, the work focused primarily on the feasibility of using the specially designed column cell in processing the fines.

7.2 Materials and methods

7.2.1 Materials

The sample used for this work was provided by Magris Resources Inc. (Canada). The as-received sample has a product size 80% passing approximately 918 µm. The chemical assay of the sample using different techniques. (1) X-ray Fluorescence (XRF) is a technique that measures intensity of emitted fluorescent X-ray radiation and wavelength [7.15]. (2) Inductively Coupled Plasma Optical Emission Spectroscopy (ICP-OES) determines the elemental composition through plasma and spectrometer. The emitted spectra are used to identify and quantify the elements in the sample [7.16]. (3) Neutron Activation Analysis (NAA) determines the elements present in the sample by excitation of the neutrons. The excitation will release gamma radiation that is characteristic of the element it is coming from [7.17]. As seen in Table 7.1, although XRF appears to be underestimating the RE assay, this technique is non-destructive and has the fastest turnaround time. Instead of considering all the RE elements, the total RE elements (TREE) reported in this work is the sum of Ce, La and Nd. The assay indicated that Ce, La, and Nd from the RE minerals has a TREE of around 2%, while the Ca, Mg, Fe and Al from the gangue was found to be around 13%, 2.5 - 7%, 10% and 0.2 - 0.3%, respectively. The goal of the flotation tests was to recover the TREE and improve the TREE grade in the concentrate.

Table 7.1 – Elemental assay (%) of Niobec ore.

Technique	Al	Ca	Ce	Fe	La	Mg	Nd	TREE
XRF	0.18	13.89	0.97	10.82	0.58	2.54	0.35	1.90
ICP-OES	0.27	13.59	0.97	10.11	0.71	7.07	0.53	2.21
NAA	0.28	13.13	1.30	9.54	0.72	7.19	0.43	2.45

The mineralogical study of the ore (see Appendix H) presented that the main RE minerals are monazite (Ce,La,Nd,Th)PO_4 and bastnäsite (Ce,La,Sm,Nd)$(CO_3)F$/synchisite Ca(Ce,La,Sm,Nd)$(CO_3)_2F$ with an average grade of 1.43% and 1.96%, respectively. The gangue minerals are mostly carbonates including dolomite (50%), calcite (13.2%), ankerite (13.7%) and siderite (0.21%). Grain size profile (see Figure H.1 in Appendix H) indicated that majority of monazite and bastnäsite/synchisite occur with a grain size of 13 and 14 µm, respectively. Bastnäsite/synchisite were also found to occur as free (30%), while monazite occur as a complex (23%). The rest of bastnäsite/synchisite and monazite are associated with silicates, carbonates or a combination of both.

The collectors, sodium oleate (NaOl) and Florrea 8920 (F8920, a modified aromatic hydroxamate), were obtained from Fisher Scientific (Canada) and Shenyang Florrea (China), respectively. The frother used, which was F150 (pine oil), was provided by Florrea (USA). Hydrochloric acid and potassium hydroxide (Fisher Scientific, Canada) were used as pH modifiers.

7.2.2 Elemental analysis

Estimation of elemental composition was conducted on loose powder samples using an energy dispersive X-ray Fluorescence (XRF) analyzer PANalytical Epsilon 1 (PANalytical Inc., Canada). The loose powder was placed into a sample holder and was place directly in the machine. The RE elements were analyzed at 12 kV and 286 μA conditions using an Al-50 filter. The Mg analysis is not accurate for loose powder samples, and only presented for semi-quantitative comparison between samples. The accuracy of the sample analysis for other metals vary between 10% (RE elements) and 25% (fore matrix element). But since it requires little sample preparation time and safe preparation method unlike inductively coupled plasma spectroscopy which involves extra steps such as HF acid digestion or fusion flux, this method is appropriate for faster and cheaper turnaround of results.

7.2.3 Comminution

Before the final wet grinding prior to flotation, the ∼300 kg as-received sample was riffled into 15 kg representative batches. Each batch was dry ground in a laboratory rod mill (29 cm × 60 cm, rotational speed of 46 rev/min) for 90 min. The rod mill discharge was riffled into 7.5 kg, and was then further ground dry in a 30 cm × 30 cm (diameter × length), 70 rev/min laboratory Bico ball mill (Bico, USA) for 30 min. The product size distribution was 80% passing 128 μm. Further grinding was conducted with these samples varying grinding time using a 500-g capacity ceramic ball mill.

7.2.4 Flotation

The processing of the ore was different for the fine (-20 μm) and the coarse (+20 μm) fractions. The process route for the 2 size fractions are summarized in Figure 7.1. These are further described in Sections 7.2.4.2 and 7.2.4.3.

7.2.4.1 Column cell design

The column cell, made of glass, has a diameter of 40 mm and a height of 840 mm from the bottom to overflow lip. Initially the tube with a geometry similar to a cavitation tube was attached to the cell to serve as the bubble producer, however due to the limitation of the pump, the tube did not facilitate cavitation. It was also possible that the narrowest diameter of the tube is not small enough to enable cavitation. It was found that the cavitation bubbles were produced in between the slurry flow controller and the pump, which could be attributed to the acceptable flowrate and tube size combination satisfying cavitation requirement. The cavitation tube was left installed since it was found that it aids in further bubble breakage as shown in Figure 7.3. In the figure, it can be seen that the bubble accelerates as it enters the narrow portion of the tube. This acceleration led to bubble breakage as it exits the narrow portion, producing finer bubbles.

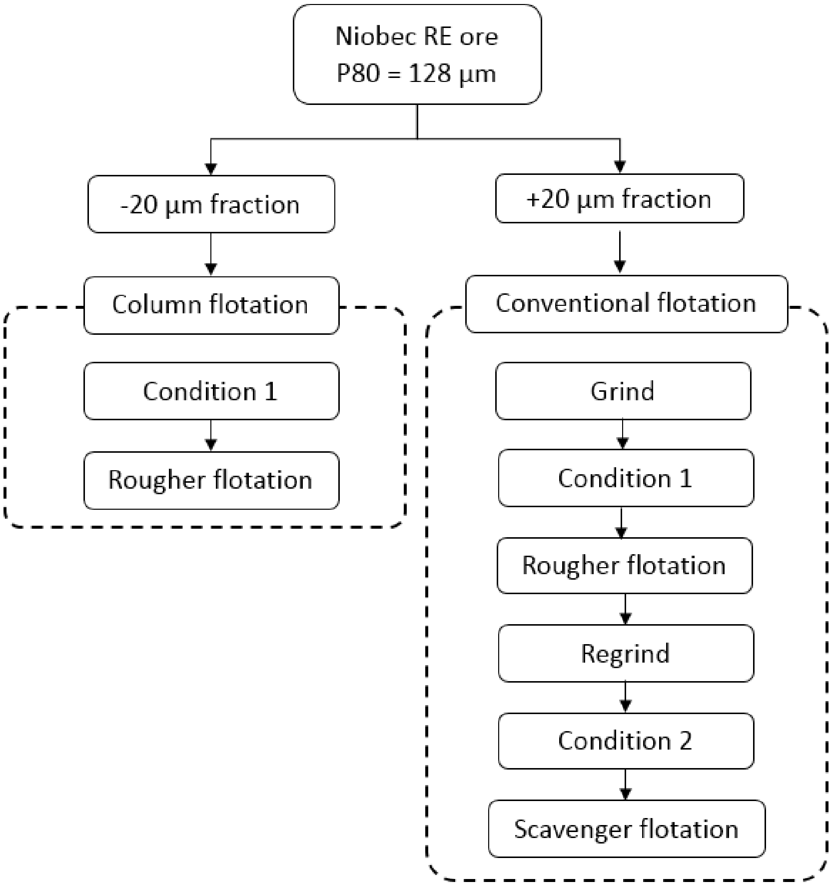

Figure 7.1 – Simple flow sheet of the flotation of Niobec RE ore.

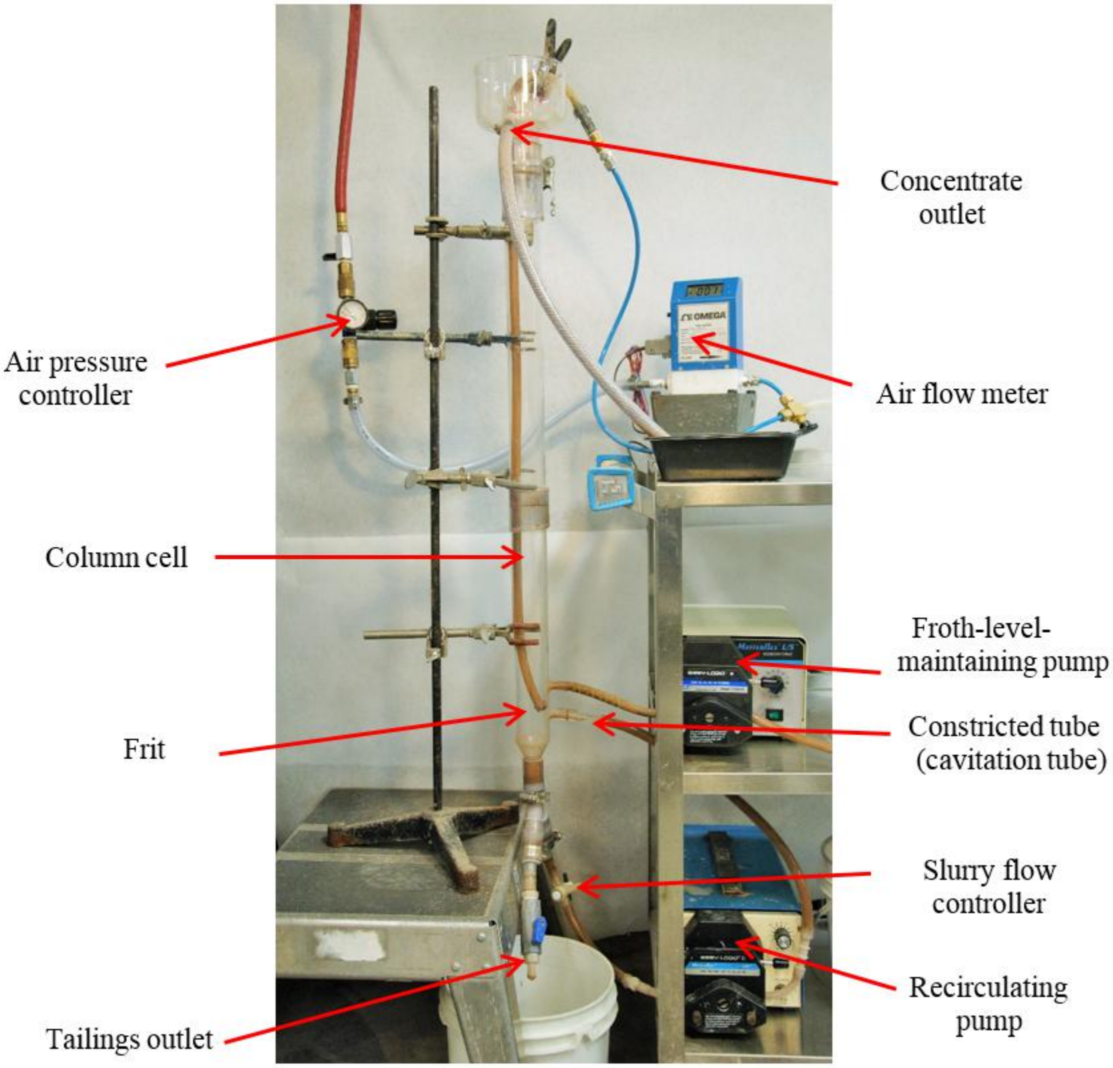

Figure 7.2 – Column flotation cell set-up.

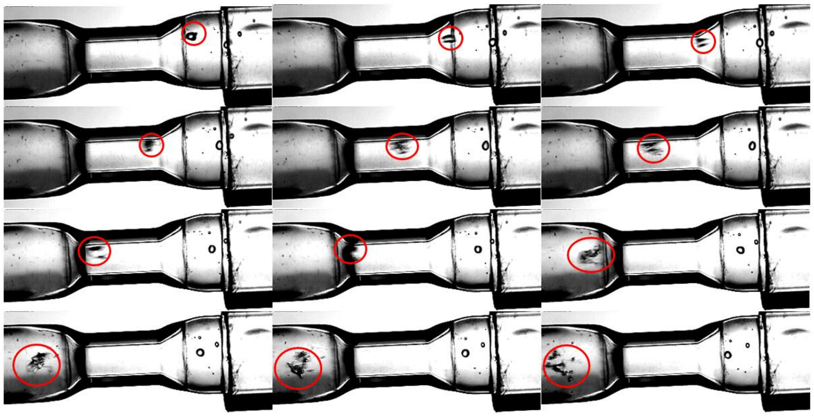

Figure 7.3 – Bubble breakage inside the "cavitation tube".

7.2.4.2 Column flotation

Flotation of the -20 μm fractions from the split ore was conducted using the bench-scale column flotation cell (see Figure 7.2). Twenty percent (20%) solids (by weight) slurry was prepared using 100 g samples with an experimental design considering the factors presented in Tables 7.2 and 7.3 for hydroxamate (F8920) and sodium oleate collectors, respectively. The slurry was poured into the cell and was topped up with tap water until 5 cm from the top of the overflow lip. The recirculating pump, which circulates the product at 300 mL/min, was used during this step to ensure mixing and to avoid settling. The air was introduced at a flow rate of 380 mL/min (equivalent to J_g of 0.5 cm·s^{-1}). The flotation was conducted for 30 min. The condition which gave the highest recovery was further studied by varying collector dosage, temperature, and further reagent addition. The concentrates and the tails were recovered, dried, and then analyzed for metal contents to obtain the grade and recovery.

A response surface methodology (RSM) was used in this part of the study to investigate the effects of the independent variables on the recovery and grade of RE elements. This method quantifies the relationship between the input parameters (controllable) and the obtained response through statistical and mathematical approaches in modeling and data analysis [7.18, 7.19]. The functional relationship between the independent variables (x) and the response variable (y) is usually described using the second-order model:

$$y = \beta_0 + \sum_{i=1}^{k} \beta_i x_i + \sum_{i=1}^{k} \beta_{ii} x_i^2 + \sum_{i=1}^{k} \sum_{j=1}^{i} \beta_{ij} x_i x_j + \varepsilon \tag{7.1}$$

where ε is a random error, and the β coefficients are determined using the least square method. RSM is based on these types of design of experiment matrices: (1) central composite design and (2) Box-Behnken design [7.18, 7.19].

Central composite design

For the modified aromatic hydroxamate, a central composite design was used (see Figure 7.4b). This approach, which determines the optimum conditions for the response, also helps to determine the most significant factor and the interaction between them [7.19–7.21]. A CCD is a 2^k full factorial with added central point and star points [7.22]. Because of the added central point and star points, CCD has five levels for each factor ($\pm\alpha$, ± 1, 0) [7.23]. With this method, additional points outside the range of usual conditions can be investigated. This is particularly useful when the upper and lower limit of each variable is not certain [7.19]. The coded and actual levels of the independent variables used in column cell flotation using F8920 (modified aromatic hydroxamate) are presented in Table 7.2.

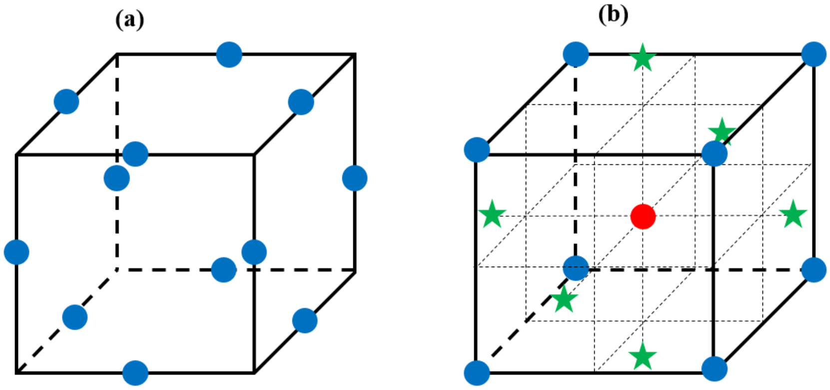

Figure 7.4 – Types of response surface designs: (a) Box-Behnken design (BBD) and (b) Central composite design (CCD).

Table 7.2 – Independent variables (and their levels) considered in central composite design for F8920 collector.

Factors	Symbol	Lowest -α (-2)	Low -1	Center 0	High +1	Highest +α (+2)
Collector dosage, g/t	x_1	250	500	750	1000	1250
Conditioning pH	x_2	7.5	8.0	8.5	9.0	9.5
Conditioning time, min	x_3	5.0	7.5	10.0	12.5	15.0

Box-Behnken design

For the column tests using sodium oleate collector, a Box-Behnken design (BBD) was employed (see Figure 7.4a). BBD is a three-level design which are constructed by combining 2^k factorial designs with incomplete block designs [7.19, 7.22]. Unlike CCD, BBD does not contain any points outside the upper and lower limits of each variable. This can be advantageous especially if these points are expensive or impossible to test [7.19]. In this work, apart from economic reasons, a BBD was used for the tests involving sodium oleate since the upper and lower limits of the variables have already been defined in Chapter 4. The coded and actual levels of the independent variables used in column cell flotation test (in the presence of sodium oleate) are presented in Table 7.3.

Table 7.3 – Independent variables (and their levels) considered in Box-Behnken design for sodium oleate collector.

Factors	Symbol	Low -1	Center 0	High +1
Depressant dosage, g/t	x_1	0	180	360
Collector dosage, g/t	x_2	100	200	300
Conditioning pH	x_3	5.5	6.7	8.0

Statistical analysis

The data obtained from the design of experiments are analyzed using Minitab® Statistical Software 18 (Minitab Inc., USA). Analysis of Variance (ANOVA) was used to calculate the β coefficients of the second-order regression model. The significance of each variable on the response was determined through Fischer (F) test and p-values at 95% confidence level. The F-test also indicated the significance of the model.

7.2.4.3 Bench-scale mechanical cell flotation

The mechanical cell used in this test was a laboratory Denver cell, which simulates the conventional industrial mechanical cell set-up. The cell has a mechanical impeller (1200 rev/min) which agitates the pulp and disperses air as bubbles into the pulp. The +20 μm fraction was prepared at 60% solids slurry and was further ground to P80 = 45 μm using a 500-g capacity ball mill. The slurry was transferred to 1.2-L cell and water was added to obtain approximately 30% solids. The slurry was heated to around 50 °C; pH was maintained at 8.7 prior to addition of the flotation reagents (dispersant or collector). If dispersant (*i.e.,* sodium silicate) was added, this would have been added prior to the collector. The slurry was conditioned for 10 minutes after each addition. The frother (30 ppm) was added last and was conditioned for 1 min, before the introduction of air at a flow rate of 3 L/min. Rougher concentrates were collected at 5, 15 and 30 min. The tailing was reground at 60% solids for 15 min to obtain a P80 of 38 μm. The reground rougher tails became the scavenger feed, pH was maintained at 8.7 and conditioned at around 50 °C for 10 min with 500 g/t F8920. The slurry was again added with frother (30 ppm) and was conditioned for 1 minute prior to addition of air at the same flow rate. The rougher concentrates, scavenger concentrates, and tails were recovered, dried and analyzed for grade and recovery.

7.3 Results

7.3.1 Particle size analysis and elemental distribution

Since the liberation of bastnäsite (47.4%) and monazite (26.8%) is still poor even when ground to P80 of 150 µm (see Appendix H), the feed (F80 = 1180 µm) was reduced to give a P80 of 128 µm, suitable for pre-flotation wet grinding. To prepare the ore for bench-scale flotation, different grinding times were investigated to obtain the desired P80. The pre-ground ore, which contains 30% finer than 20 µm, was further ground at 5 min, 10 min, 15 min, 30min, 45 min, 60 min and 80 min. Figure 7.5 presents the mass distribution of the particles at each size range. These particle size ranges were analyzed using XRF and the metal grades are presented in Figures 7.6a and 7.6b. It can be observed that La, Ce and Nd grade (see Figure 7.6a) in the -20 µm fraction significantly decreased with increased grinding time. There was also a slight decrease in the La, Ce and Nd grades in the +20 µm fraction with increased grinding time. The grinding also augmented Ca, Fe, and Mg grades both in the +20 and -20 µm fractions (see Figure 7.6b). It was expected that RE elements would concentrate more in the fine fractions, while the elements from gangue (except Mg) concentrate in the coarser fractions.

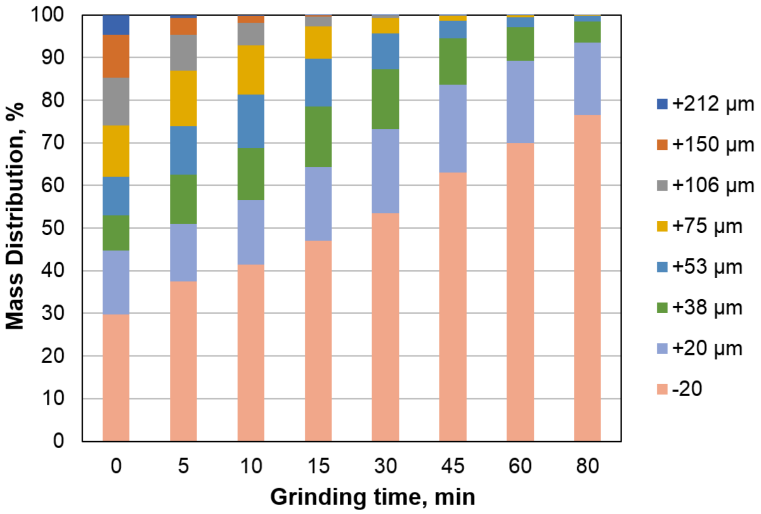

Figure 7.5 – Particle analysis of –300 µm samples ground at different times.

As the ore sample is ground further, the amount of RE elements that can be found in the -20 µm fraction increases, as evidenced by the grade – recovery curve shown in Figure 7.7a. Initially, 70% of each of the total RE elements present in the ore, while only around 25% of the total Ca, total Mg, and total Fe report to -20 µm fraction. As the grinding time is increased, the amount of Ca, Mg, and Fe that reports to this fine fraction increased significantly as well.

Due to these observations, it was decided to focus on the pre-ground ore and analyze the sample as-is without further grinding. The elemental analysis of the size-by-size fractions are presented in Figure 7.8. The elemental distribution showed that indeed most of the RE elements can be found in the -20 µm fraction, while the rest of the size fractions have similar RE elements distributions. This led to the next important step which was to split the ore samples into +20 µm and -20 µm fractions. Further grinding of the +20 µm samples was conducted and the particle size distribution was analyzed (see Figure 7.9). When the initial -20 µm particles are not considered in the size analysis of -300 µm samples, the particle size distribution profiles for the -300 µm and -300+20 µm samples are different at shorter grinding time and relatively similar at longer grinding times (Figure 7.10a). In Figure 7.10b, it can be seen that the relative amount of the ore that was ground to -20 µm is greater with the +20 µm fractions of the split samples compared to unsplit samples.

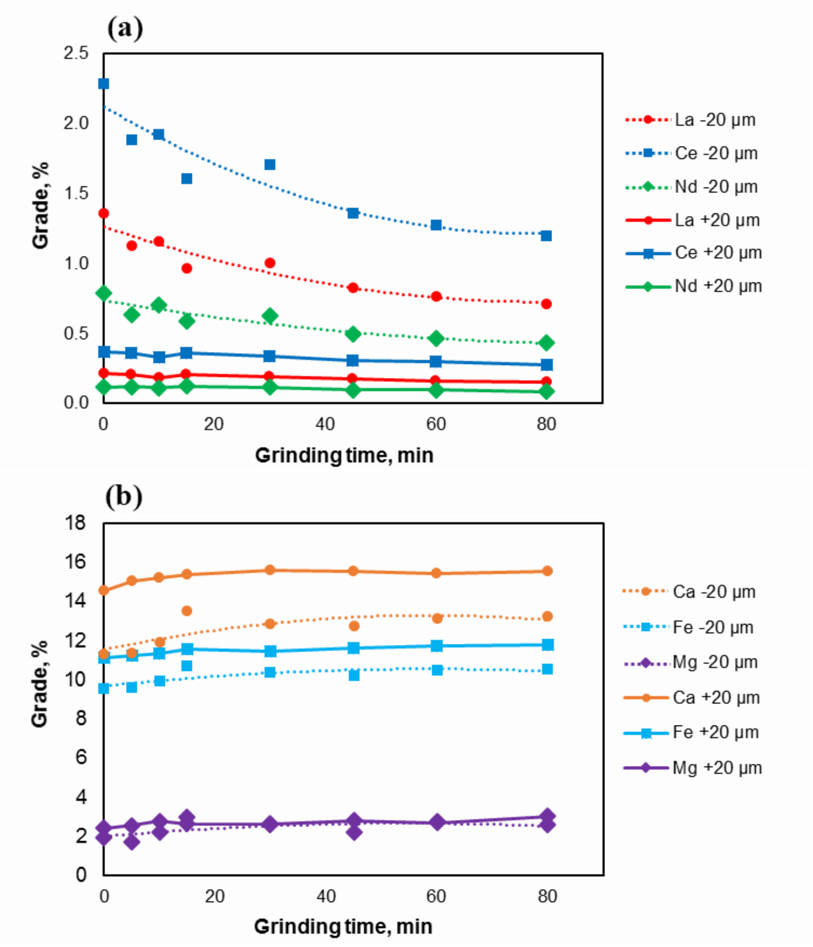

Figure 7.6 – Grade of (a) RE elements and (b) gangue elements as a function of grinding time.

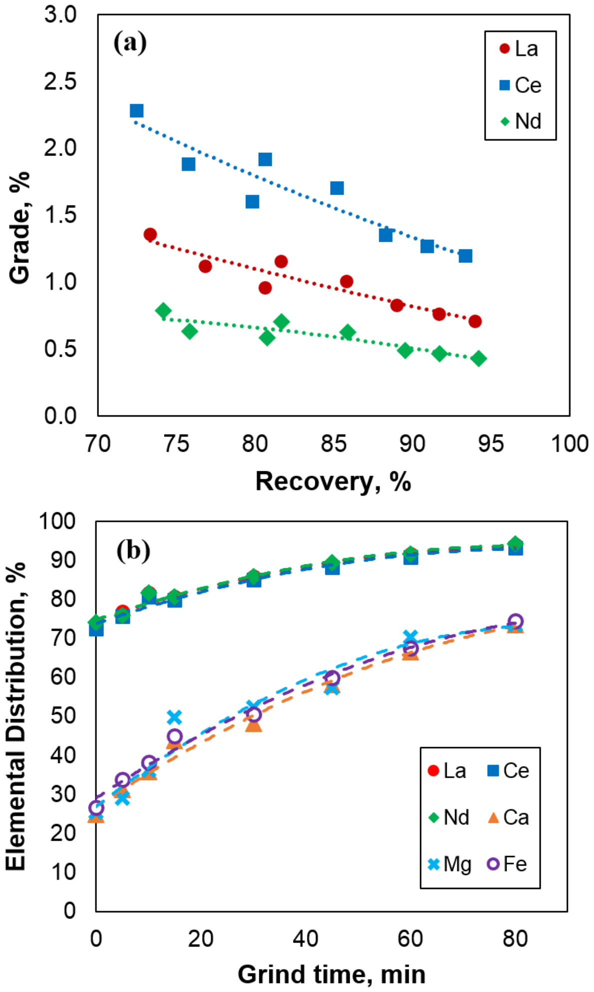

Figure 7.7 – (a) Grade and recovery curve of RE elements; and, (b) elemental distribution of RE elements and gangue elements in the in the –20 µm fractions as influenced by grinding time.

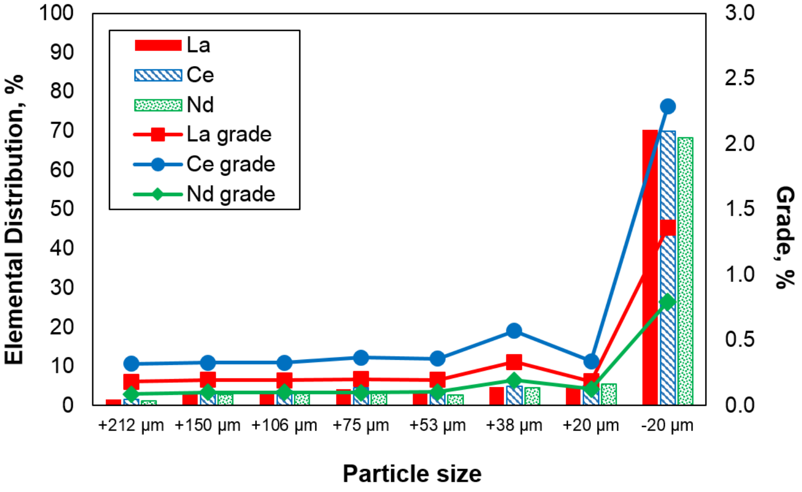

Figure 7.8 – Grade and elemental distribution of the pre-ground sample (not subjected to further grinding).

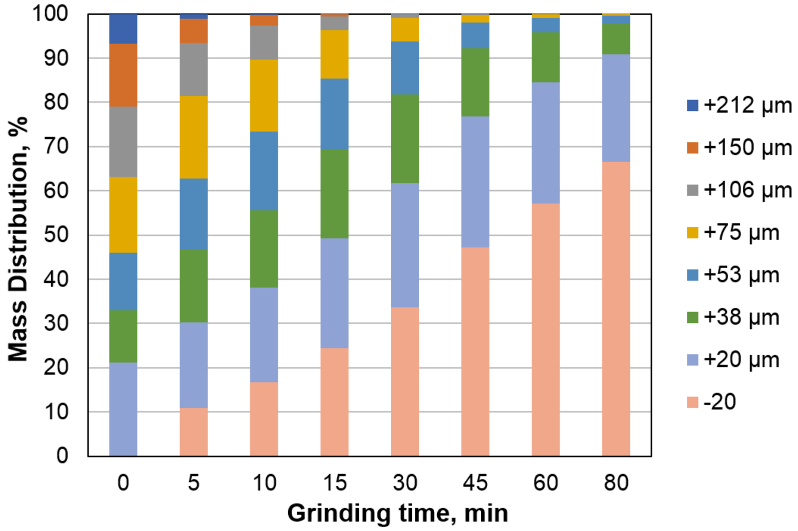

Figure 7.9 – Particle analysis of -300+20 µm samples ground at different times.

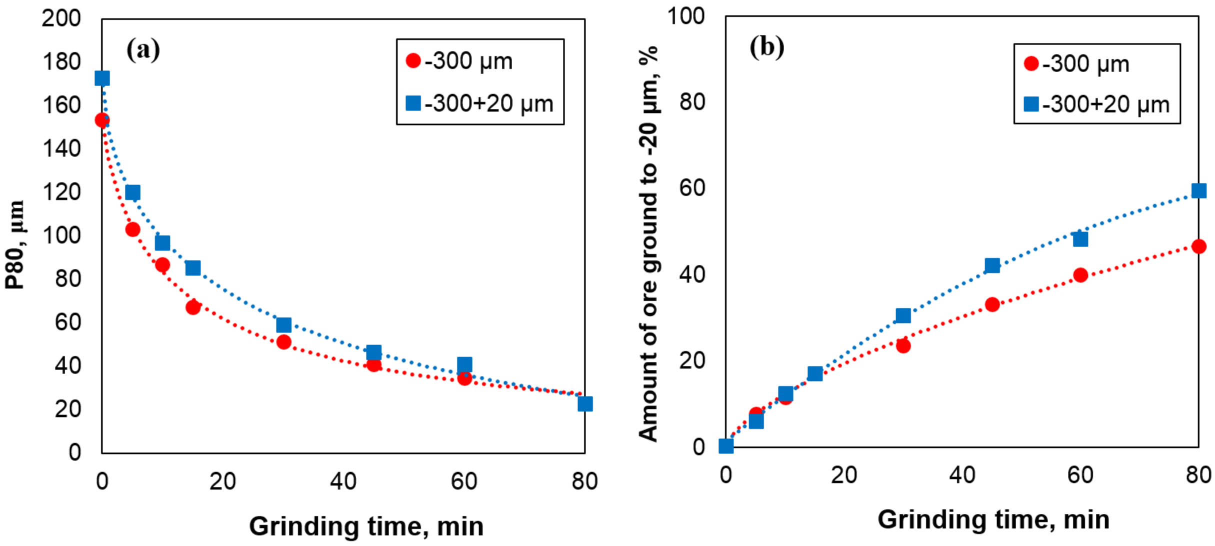

Figure 7.10 – (a) Relative P80 of the -300 µm and -300+20 µm samples; and, (b) amount of ore ground to -20 µm as a function of grinding time.

7.3.2 Column cell flotation

7.3.2.1 Sodium oleate

A response surface method design of experiment (Box-Benhken) was used in testing carboxymethylcellulose (CMC) - sodium oleate reagent scheme for the flotation of RE minerals from the ore. Previous flotation studies (Chapter 4) involving pure RE minerals and pure dolomite indicated that certain dosage combination of sodium oleate and CMC could yield to an effective separation of RE minerals from dolomite. Upon testing specific ranges of depressant dosage (x_1), collector dosage (x_2), and pH conditions (x_3) (Table 7.3), the grade (y_1) and recovery (y_2) response (see Table 7.4), which was analyzed through Minitab® Statistical Software 18, yielded the following regression models:

$$\begin{aligned}\text{Grade: } y_1 &= 6.36 + 0.20x_1 - 0.15x_2 + 0.12x_3 + 0.85x_1^2 + 0.08x_2^2 - 0.04x_3^2 \\ &\quad - 0.43x_1x_2 + 0.15x_1x_3 + 0.06x_2x_3\end{aligned} \tag{7.2}$$

$$\begin{aligned}\text{Recovery: } y_2 &= 43.42 - 25.36x_1 + 8.33x_2 + 2.13x_3 + 3.36x_1^2 - 5.49x_2^2 - 2.60x_3^2 \\ &\quad - 1.67x_1x_2 - 7.78x_1x_3 - 2.23x_2x_3\end{aligned} \tag{7.3}$$

The response surface regression of grade (y_1) reported an R^2 of 76%, while the response surface regression of recovery (y_2) has an R^2 of 90%. The R^2 of the grade regression y_1 is below the accepted R^2 (80% [7.24, 7.25]) as such only the variance of the recovery regression y_2 was analyzed (presented in Table 7.5). The unsatisfactory R^2 of the grade regression (y_1) may be due to the fact that a small change in concentrate mass (*e.g.,* due to gangue entrainment), greatly affects the grade, while recovery may remain unchanged. The Model F-value of 6.90 implies the model (y_2) is significant. P-values less than 0.05 indicate model terms are significant. In this case, depressant dosage (x_1) and collector dosage (x_2) are the significant model terms. The Lack of Fit F-value of 1.29 implies the Lack of Fit is not significant relative to the pure error (Table 7.5); non-significant lack of fit is preferred since it indicates a good model fit.

The Analysis of Variance (ANOVA) indicated that recovery is mostly affected by depressant dosage (x_1) and collector dosage (x_2). Figure 7.11b indicates that pH does not have significant effect on recovery especially at higher depressant dosage. Figure 7.11c confirmed that pH is an non-significant factor since recovery do not change significantly with pH at a wide range of depressant dosage. In the contour plot (Figure 7.11a), it can be seen that higher recovery could be achieved at high sodium oleate dosage and low depressant dosage. Although high recovery of RE elements is possible, the enrichment of the RE elements in the concentrate is still around 1 (Table 7.4), indicating that the process is not efficient. Although the conditions considered in these tests are based on previous pure mineral studies which is expected to yield an efficient separation between the RE minerals and dolomite, the results in the bench-scale tests did not present similar efficiency.

Table 7.4 – Column flotation results using sodium oleate (NaOl).

Run number	pH	Collector dosage, g/t	Depressant dosage, g/t	Feed Grade	Mass pull, %	TREE Grade, %	Recovery, %			Enrichment ratio
							Ca	Fe	TREE	
1	5	300	180	5.201	35.39	5.97	31.61	32.72	38.46	1.15
2	5	200	360	5.201	27.00	5.53	24.49	25.35	29.79	1.06
3	6.5	100	0	5.201	60.79	5.12	61.98	54.86	56.65	0.98
4	6.5	200	180	5.20	50.59	5.54	45.08	45.43	50.32	1.07
5	6.5	300	360	5.20	23.94	5.20	19.18	20.08	22.60	1.04
6	5	200	0	5.20	66.86	5.39	65.41	61.23	67.09	1.04
7	6.5	200	180	5.20	20.44	7.19	17.55	18.04	26.82	1.38
8	6.5	300	0	5.20	75.53	5.70	75.91	72.44	74.51	1.10
9	8	300	180	5.20	42.75	6.53	39.23	39.65	51.03	1.26
10	8	200	360	5.20	5.33	5.86	4.85	4.92	5.71	1.13
11	6.5	100	360	5.45	10.01	6.35	9.42	9.48	11.43	1.16
12	6.5	200	180	5.45	40.21	6.33	35.55	35.89	46.73	1.16
13	6.5	200	180	5.45	40.57	6.33	35.6	36.62	47.17	1.16
14	8	100	180	5.45	29.86	6.73	26.35	26.87	36.66	1.23
15	6.5	200	180	5.45	39.25	6.42	35.27	35.83	46.08	1.18
16	8	200	0	5.45	72.37	5.10	75.47	71.02	74.14	0.93
17	5	100	180	5.45	13.36	6.40	10.02	10.86	15.18	1.17

Table 7.5 – Analysis of Variance for regression model y_2 for the tests with sodium oleate collector.

Source	DF	Adj SS	Adj MS	F-Value	P-Value
Model	9	6207.16	689.68	6.90	0.009
Linear	3	5735.75	1911.92	19.12	0.001
x_1: depressant dosage	1	5143.87	5143.87	51.45	0.000
x_2: collector dosage	1	555.61	555.61	5.56	0.051
x_3: conditioning pH	1	36.27	36.27	0.36	0.566
Square	3	198.05	66.02	0.66	0.602
$x_1 * x_1$	1	47.60	47.60	0.48	0.512
$x_2 * x_2$	1	126.84	126.84	1.27	0.297
$x_3 * x_3$	1	28.50	28.50	0.29	0.610
2-Way Interaction	3	273.35	91.12	0.91	0.483
$x_1 * x_2$	1	11.22	11.22	0.11	0.747
$x_1 * x_3$	1	242.31	242.31	2.42	0.163
$x_2 * x_3$	1	19.83	19.83	0.20	0.670
Error	7	699.87	99.98		
Lack-of-Fit	3	344.73	114.91	1.29	0.391
Pure Error	4	355.15	88.79		
Total	16	6907.03			

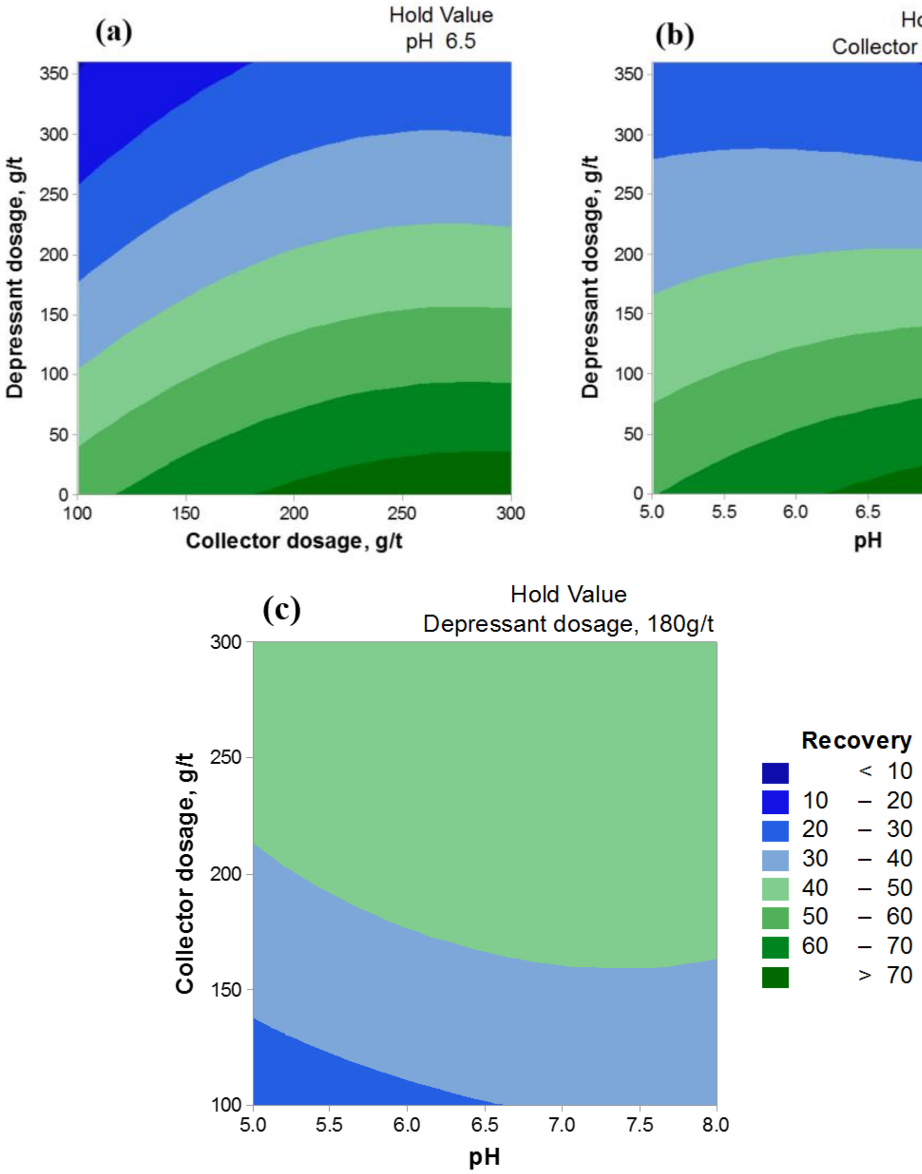

Figure 7.11 – Contour plot of recovery in the presence of sodium oleate: (a) depressant dosage vs collector dosage, (b) depressant dosage vs pH, and (c) collector dosage and pH.

7.3.2.2 Aromatic hydroxamate

A response surface method design of experiment (central composite design) was also used to investigate the effect of hydroxamate dosage (x_1), conditioning pH (x_2) and conditioning time (x_3) on the grade (y_3) and recovery (y_4) of RE elements. In this design, collector dosage of 250 - 1250 g/t, conditioning pH of 7.5 - 9.5, and conditioning time of 5 - 15 min was considered. The grade and recovery response of each test was presented in Table 7.4. They were analyzed through Minitab® Statistical Software 18, which yielded the following regression models:

$$\text{Grade: } y_3 = 8.71 - 0.16x_1 - 0.53x_2 + 0.44x_3 - 0.98x_1^2 - 0.20x_2^2 + 0.27x_3^2 + 3.07x_1x_2 - 0.04x_1x_3 - 0.62x_2x_3 \tag{7.4}$$

$$\text{Recovery: } y_4 = 42.10 + 23.10x_1 - 12.89x_2 + 1.11x_3 - 8.64x_1^2 - 7.32x_2^2 - 4.12x_3^2 + 3.27x_1x_2 + 9.42x_1x_3 + 7.99x_2x_3 \tag{7.5}$$

Table 7.6 – Column flotation results using F8920.

Run number	Collector dosage, g/t	Conditioning time, min	pH	Feed Grade	Mass pull, %	TREE Grade, %	Recovery, %			Enrichment ratio
							Ca	Fe	TREE	
1	750	10	8.5	4.85	23.45	8.98	18.59	21.89	43.21	1.85
2	1250	10	8.5	4.85	36.32	7.93	31.72	34.38	58.96	1.64
3	500	7.5	8	4.85	20.05	8.89	15.46	18.55	36.77	1.83
4	750	10	8.5	4.68	35.04	7.41	27.15	29.65	51.79	1.58
5	250	10	8.5	4.68	12.39	7.42	9.62	10.90	18.31	1.58
6	1000	12.5	8	4.68	38.84	7.54	33.86	36.84	60.34	1.61
7	500	12.5	8	4.68	14.95	9.55	12.24	14.23	30.49	2.04
8	1000	12.5	9	4.68	22.5	9.10	20.19	23.21	48.41	1.94
9	750	10	7.5	4.68	27.19	9.49	20.04	24.99	51.48	2.03
10	750	10	9.5	4.68	22.91	7.16	19.02	20.03	30.9	1.53
11	1000	7.5	8	4.68	45.77	6.60	36.75	39.71	60.77	1.41
12	750	10	8.5	4.68	25.27	8.36	21.21	23.89	45.11	1.79
13	750	10	8.5	4.83	21.22	8.93	16.59	20.08	39.55	1.85
14	750	10	9.5	4.83	11.29	7.88	9.11	10.97	18.73	1.63
15	750	15	8.5	4.83	22.07	9.18	16.76	20.49	41.87	1.90
16	750	5	8.5	4.83	21.15	9.20	16.86	20.35	40.24	1.91
17	750	10	8.5	4.83	19.63	9.30	14.89	18.72	37.79	1.93
18	750	5	8.5	4.83	19.57	8.02	13.38	17.05	32.41	1.66
19	500	12.5	9	4.83	6.80	8.36	4.84	6.43	11.72	1.73
20	500	7.5	9	4.83	8.23	7.99	6.26	7.95	13.58	1.66
21	250	10	8.5	4.83	4.32	8.00	3.17	4.18	7.26	1.66
22	1250	10	8.5	4.96	30.84	7.77	22.91	28.39	48.09	1.57
23	750	10	7.5	4.96	18.86	9.69	12.87	17.37	36.8	1.96
24	1000	7.5	9	4.96	20.59	9.09	15.31	17.59	37.28	1.83
25	750	15	8.5	4.96	18.63	9.69	12.79	16.59	36.16	1.96
26	750	10	8.5	4.96	17.83	9.46	12.64	16.66	33.74	1.91

The obtained response surface regression of grade (y_3) reported an R^2 of 59%, while the response surface regression of recovery (y_4) yielded an R^2 of 85%. Again, the unsatisfactory R^2 of the grade regression (y_3) may be due to the fact that a small change in concentrate mass greatly affects the grade, while recovery may remain unchanged. Because of this, only the regression model of recovery (y_4) and contour plots of recovery (see Figure 7.12) were presented. The Analysis of Variance of the recovery regression (y_4) was presented in Table 7.5. The Model F-value of 10.40 implies the model (y_4) is significant. P-values less than 0.05 indicate model terms are significant. In this case, collector dosage (x_1) and conditioning pH (x_2) are the significant model terms. The Lack of Fit F-value of 0.90 implies the Lack of Fit is not significant relative to the pure error (Table 7.5). Non-significant lack of fit is preferred since it indicates a good model fit.

Table 7.7 – Analysis of Variance for regression model y_4 for the tests with F8920.

Source	DF	Adj SS	Adj MS	F-Value	P-Value
Model	9	4511.88	501.32	10.4	0.000
Linear	3	4206.25	1402.08	29.09	0.000
x_1: collector dosage	1	3202.14	3202.14	66.43	0.000
x_2: conditioning pH	1	996.69	996.69	20.68	0.000
x_3: conditioning time	1	7.42	7.42	0.15	0.700
Square	3	224.04	74.68	1.55	0.240
$x_1 * x_1$	1	180.14	180.14	3.74	0.071
$x_2 * x_2$	1	129.25	129.25	2.68	0.121
$x_3 * x_3$	1	41.01	41.01	0.85	0.370
2-Way Interaction	3	81.59	27.2	0.56	0.646
$x_1 * x_2$	1	5.35	5.35	0.11	0.743
$x_1 * x_3$	1	44.36	44.36	0.92	0.352
$x_2 * x_3$	1	31.88	31.88	0.66	0.428
Error	16	771.24	48.2		
Lack-of-Fit	5	223.52	44.7	0.90	0.516
Pure Error	11	547.72	49.79		
Total	25	5283.12			

The contour plot (Figure 7.12a) indicated that conditioning time did not affect the recovery significantly especially at low collector dosage as evidenced by the horizontal contour lines. Figure 7.12b validated this by showing that a wide range of conditioning time yields similar recovery values. The collector dosage - conditioning pH contour plot (Figure 7.12c) shows that the maximum recovery can be obtained at pH values below 9 and at high collector dosage. Considering the regression (y_4), a condition which could yield reasonable recovery were estimated (Table 7.8). Due to limited time and resources, only one condition was investigated further. Confirmation test revealed that a recovery of 52% could be obtained, which has a 15% deviation from the expected recovery. This value is acceptable since it is reflected within the R^2 of the regression.

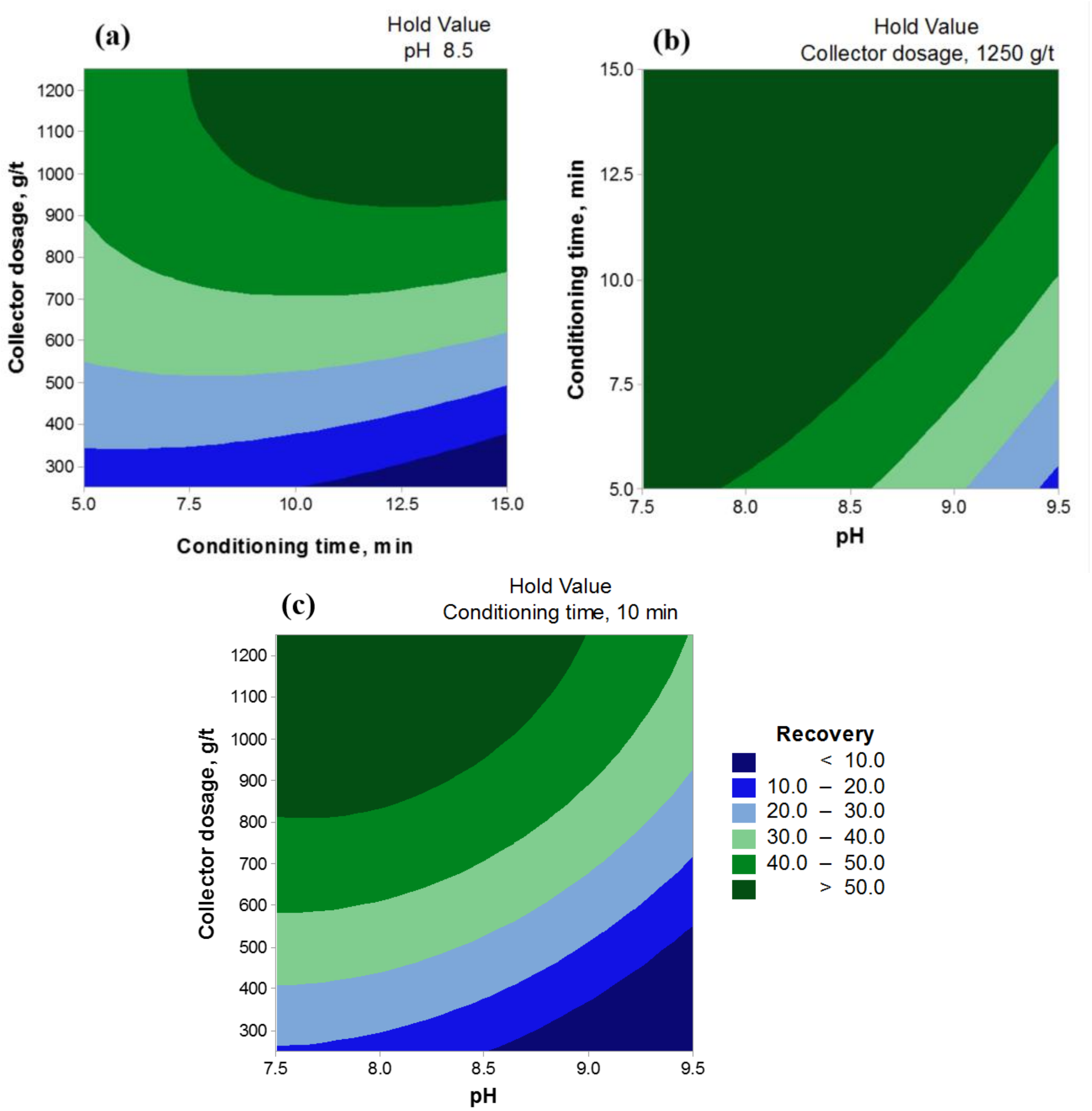

Figure 7.12 – Contour plot of the recovery in the presence of F8920: (a) collector dosage vs conditioning time, (b) conditioning time vs pH, and (c) collector dosage and pH.

Table 7.8 – Estimated conditions that will yield maximum recovery.

pH	Collector dosage, g/t	Conditioning time, min	Expected recovery, %	Actual recovery, %	Error, %
8.7	1250	10	61.3	52	15.2

Some of the factors, which were suggested in the literature, that could affect (improve) flotation performance were temperature and addition of modifiers [7.26, 7.27]. An investigation using pure bastnäsite mineral at different temperatures were conducted with laboratory grade benzohydroxamate collector. The result showed that an increase in temperature could improve the recovery of bastnäsite at the same time increase the selectivity between the RE minerals and dolomite (Figure 7.13). The condition in which highest recovery of bastnäsite was obtained was tested with actual ore. It can be seen in Figure 7.14a, that the increase in temperature has improved the grade but has reduced the recovery. This result does not agree with that of pure mineral flotation. This could be due to the fact that pure mineral flotation were conducted under controlled environment, while ore flotation could be affected by other factors such as mineral association, mineral competition for reagent, and entrainment. Further explanation was provided in the Discussion section.

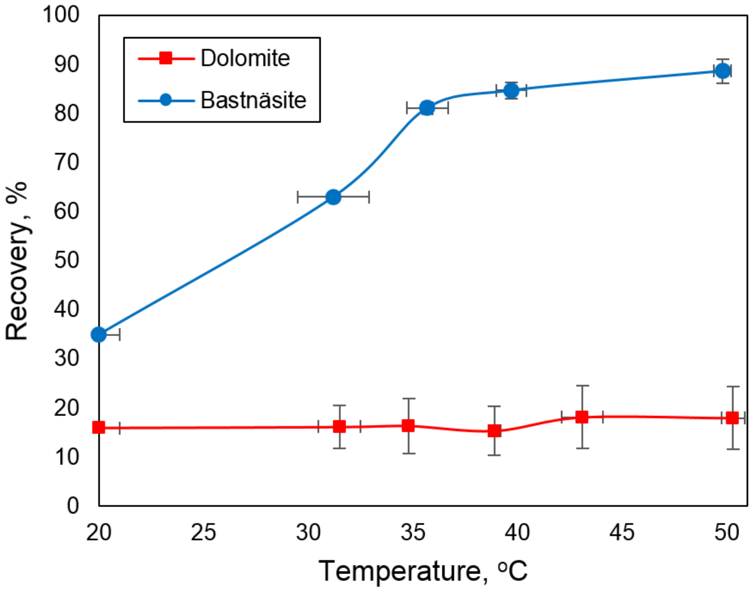

Figure 7.13 – Pure bastnäsite and pure dolomite recovery as a function of temperature in the presence of laboratory grade benzohydroxamate (5000 g/t) at pH 9.

Figure 7.14b showed that the frother dosage highly affects the grade and recovery of the RE elements. Higher frother dosage yielded a higher recovery but has reduced the RE grade. The same behavior was observed when collector dosage was increased (Figure 7.14c). For the test using EDTA, a chelating agent, the addition did not affect the grade, but has decrease the recovery. It also appears that addition of sodium silicate which is a dolomite depressant [7.28] affected the recovery but not the grade.

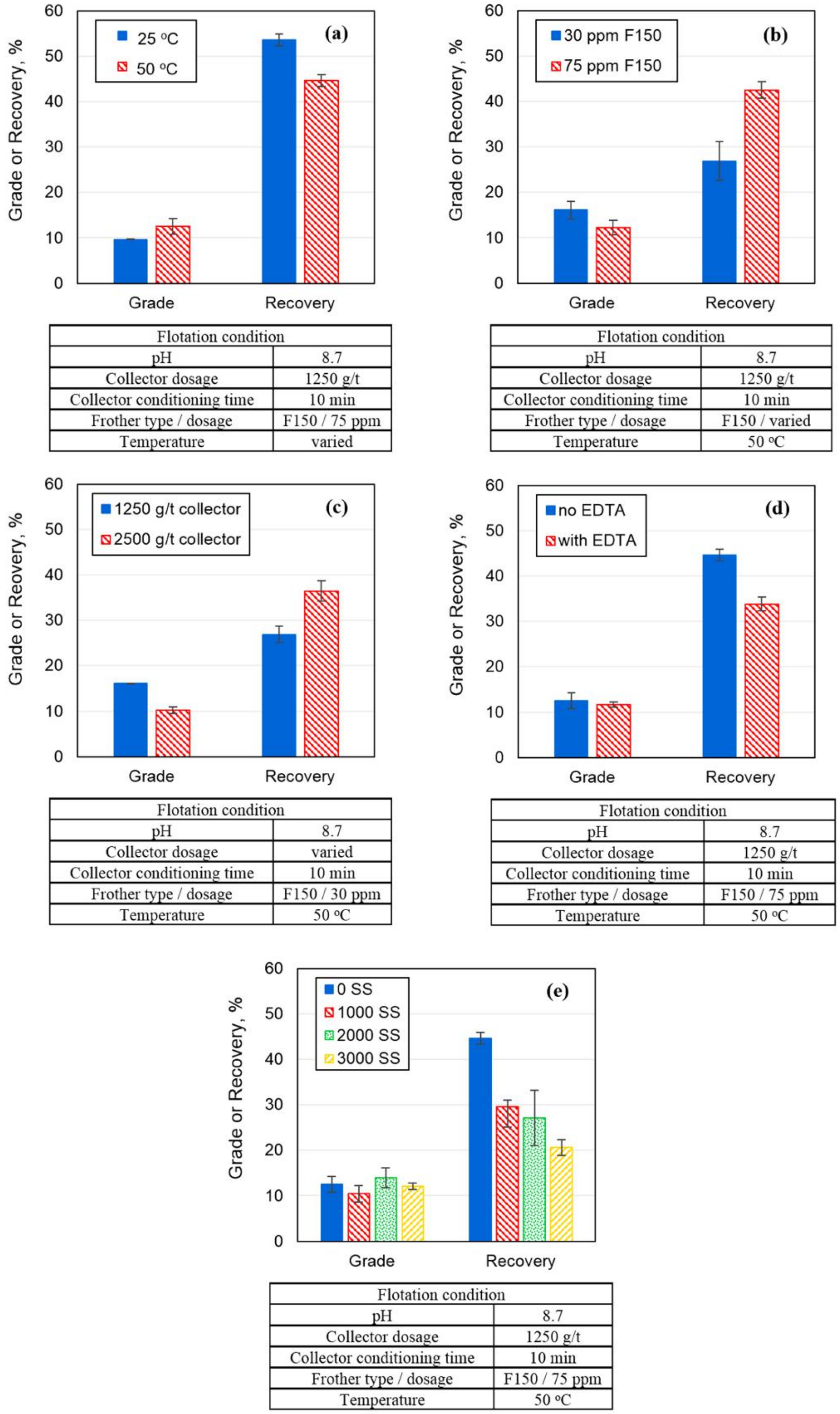

Flotation condition	
pH	8.7
Collector dosage	1250 g/t
Collector conditioning time	10 min
Frother type / dosage	F150 / 75 ppm
Temperature	varied

Flotation condition	
pH	8.7
Collector dosage	1250 g/t
Collector conditioning time	10 min
Frother type / dosage	F150 / varied
Temperature	50 °C

Flotation condition	
pH	8.7
Collector dosage	varied
Collector conditioning time	10 min
Frother type / dosage	F150 / 30 ppm
Temperature	50 °C

Flotation condition	
pH	8.7
Collector dosage	1250 g/t
Collector conditioning time	10 min
Frother type / dosage	F150 / 75 ppm
Temperature	50 °C

Flotation condition	
pH	8.7
Collector dosage	1250 g/t
Collector conditioning time	10 min
Frother type / dosage	F150 / 75 ppm
Temperature	50 °C

Figure 7.14 – Further column flotation tests investigating (a) different temperatures, (b) frother concentration, (c) higher collector dosage, (d) addition of EDTA, and (e) addition of Na silicate (SS).

7.3.3 Bench-scale mechanical cell flotation

Bench-scale flotation of the +20 μm fraction (initial TREE grade of ~0.7%) was conducted at around 50 °C with 1250 g/t of F8920 collector prepared with 1 F8920 : 0.24 NaOH ratio. This ratio was found to produce less froth than the 1:1 ratio as per manufacturer's instructor. Rougher – scavenger flotation scheme showed that around 3 - 7.3 enrichment ratio with 43 - 47% recovery could be achieved with a mass pull of 11 - 13%. Addition of sodium silicate has improved the recovery in the rougher phase but has decreased the RE grade. This is also observed in the enrichment ratio vs mass pull, where a decrease in the enrichment ratio and an improvement in the mass pull were observed.

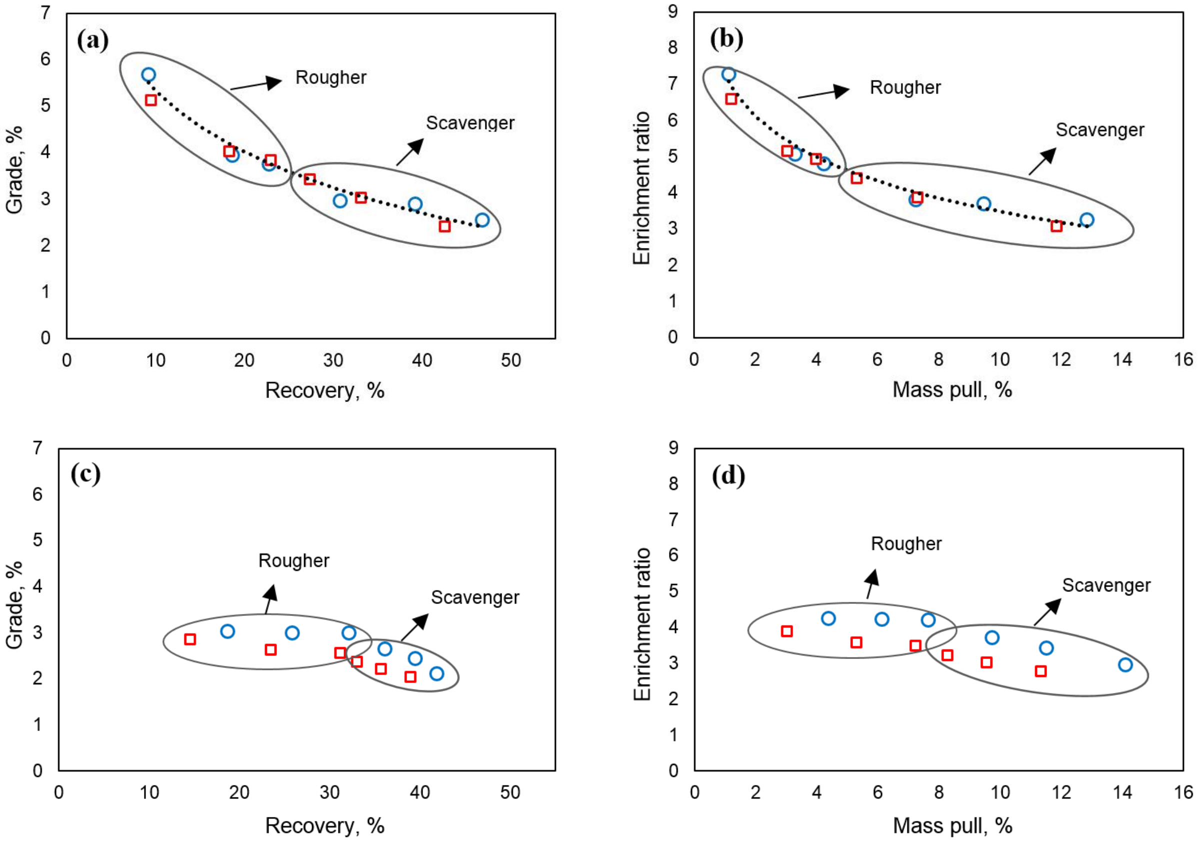

Figure 7.15 – Bench-scale flotation of +20 μm fraction in the presence of F8920 showing the (a) grade vs recovery curve and (b) enrichment ratio vs mass pull curve; and in the presence of sodium silicate – F8920 collector showing the (c) grade vs recovery curve and (d) enrichment ratio vs mass pull curve.

7.4 Discussion

Splitting the ore into -20 μm and +20 μm fractions was brought about by the observed concentration of RE elements in the -20 μm size range. Instead of grinding further the pre-ground ore (+20 and -20 μm) which could overgrind the already fine particles, grinding only the +20 μm did not only avoid this but has also improved the grinding efficiency as presented by the increase in the amount of ore ground from +20 to -20 μm. These observations pushed towards different flotation processing route for +20 and -20 μm fractions.

7.4.1 Column cell flotation

7.4.1.1 Column cell mechanism

Since fine particles (-20 μm) were shown to be difficult to float in a conventional flotation machine [7.12], several improvements were suggested and investigated. In this work, a column flotation cell, which was intended to float fine particles was set-up. The design was inspired by the work presented by Maoming *et al.* [7.1], which showed a great improvement in the flotation of fine phosphate ore. The design has incorporated the production of conventional bubble size through typical sparging mechanism (silica frit) and finer bubbles through cavitation. Initially, fine bubbles were thought to be originating from the "cavitation" tube, however, closer investigation through a hi-speed camera indicated that these bubbles were already present prior to entering the "cavitation" tube. Therefore, it can be deduced that the tube did not facilitate cavitation which could be attributed to the geometry and pump limitation. The formation of bubbles was found to be due to the decrease in the diameter of the pipe in between the recirculating outlet and the pump, caused by the small diameter of the 3-way valve in between these two. However, hi-speed camera showed that the "cavitation" tube could further break coarser bubbles into finer bubbles, as such, it was decided to keep the "cavitation" tube in the set-up.

The presence of cavitation bubbles at the mineral surface (see Figure 7.16a) through gas nucleation or adsorption [7.29] has been shown to increase the bubble – particle attachment, while decreasing detachment probability [7.1]. It has been proposed that as hydrophobic particles with attached nanobubbles (cavitation bubbles) approached each other (see Figure 7.16b), the nanobubbles could interact and coalesce resulting to capillary bridge between the two hydrophobic particles as shown in Figure 7.18 [7.30]. This could provide the particles with enough mass and effective size to attach to larger bubbles, hence facilitate flotation. It is also possible that the attachment of small bubbles to hydrophobic particles increased the particle – bubble collision probability since the effective size of the particle has been improved by the presence of the bubble. This bubble aggregates could rise to the froth layer carrying the attached hydrophobic particles with it. When a 2-phase system (liquid – air) was observed through a hi-speed camera, it showed that small bubbles could attach to bigger bubbles, indicating the mechanism of particle attachment and flotation (Figure 7.18). It is then proposed that fine particle – bubble aggregates could attach to bigger bubbles, which could then attach to an even bigger bubble. This double-attachment mechanism, which was shown in Figure 7.16c, suggests that hydrophobic particles with different sizes could float due to the variability of the bubble sizes and the adsorption of very fine bubbles on their surface, aiding in their adsorption to bigger bubbles.

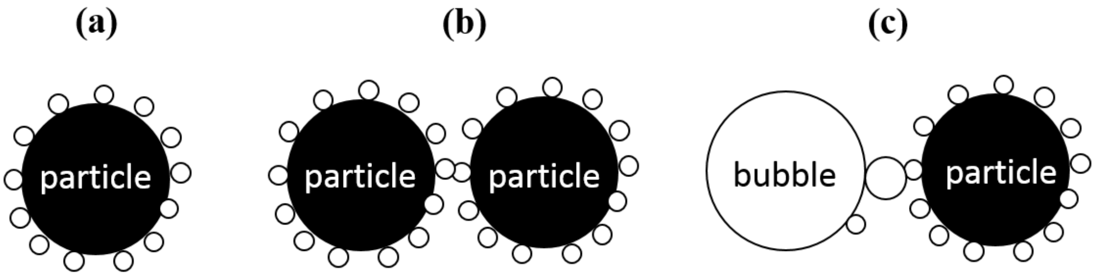

Figure 7.16 – Proposed mechanism: (a) adsorption or formation of fine bubbles on the particle surface; (b) particle aggregation; and, (c) double-attachment (solid circles = particles; hollow circles = bubbles).

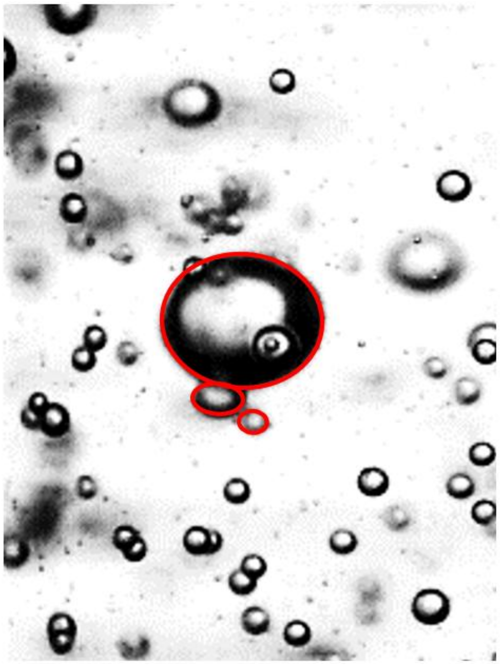

Figure 7.17 – Double-attachment mechanism under a hi-speed camera.

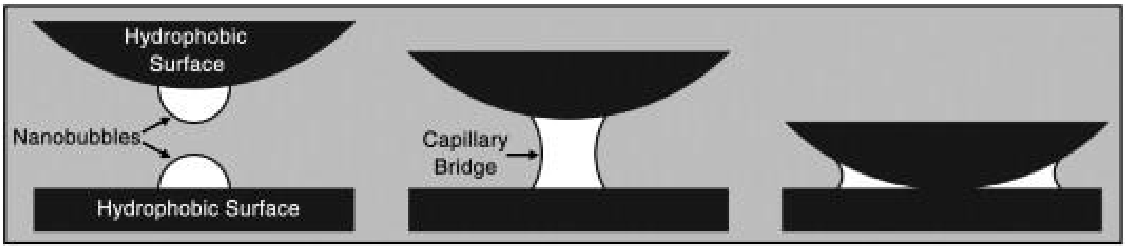

Figure 7.18 – Simplified mechanism of the nanobubble bridging capillary force between two hydrophobic surfaces with nanobubbles in aqueous solution [7.30]. Reprinted with permission from Elsevier.

7.4.1.2 Reagent scheme

Previous studies with pure minerals showed that carboxymethylcellulose (CMC) – sodium oleate reagent combination has the potential to depress dolomite and still recover RE minerals (see Chapter 4). However, the specific pH ranges, depressant dosage and collector dosage that were investigated in the bench-scale column flotation did not show significant enrichment of RE elements in the concentrate. This could be due to the fact that pure mineral studies, where the test conditions are based from, failed to consider the effect of the dissolved ions from the minerals and the competition of minerals for reagent. In addition, the effect of frother dosage, which was not investigated in this work, could have affected the mineral – bubble aggregation. Beside the low selectivity of the collector, it could be presumed that liberation and association of RE minerals must be highly affecting the enrichment of the RE elements in the concentrate.

A modified aromatic hydroxamate collector (F8920), another collector which was found to be more selective than sodium oleate, was also investigated. At ambient temperature, it was estimated that a good recovery can be achieved at pH around 8.7 and a collector dosage of 1250 g/t. Since previous studies suggested that an elevated temperature could improve RE elements recovery [7.26, 7.27], it has also been tested in this work. Pure bastnäsite microflotation studies indicated that an increase in recovery could be achieved at higher temperature. However, in the bench-scale column flotation tests, a decrease in recovery was observed. Again, this could be due to the fact that pure mineral studies do not take into account the possible association of RE minerals with the gangue and the competition of minerals for reagent. It is possible that during ore flotation, where several minerals are present, an increase in temperature would favor the RE mineral - reagent than gangue - reagent interaction, making the reagent adsorbed more on the RE mineral-rich middling particles than on the gangue-rich middling particles, consequently reducing the recovery of gangue-rich middling particles (with associated RE minerals). It was also observed that the froth quality was different when the slurry was conditioned at elevated temperature. Previous work suggested that temperature could affect the froth [7.31]. It was found that at elevated temperatures, water recovery (hence, particle entrainment) is lower [7.31] which could be due to lower average number of hydrogen bonding per water molecule [7.32]. The effect of frother dosage was also investigated; since frother controls froth stability and affects particle entrainment, it could influence grade and recovery as well [7.12]. The result indicated that a balance between collector dosage and frother dosage is important especially for collectors such as F8920 which has a frothing capability. Since the modified aromatic hydroxamate collector, F8920, has a frothing ability, increasing the collector dosage (Figure 7.14c) has similar effect as that of increasing frother dosage (Figure 7.14b). Further addition of collector in the slurry, would also increase the amount adsorbed at the surface of RE-bearing minerals. However, it could also become detrimental to the RE element grade, indicating that the collector was able to adsorb to gangue mineral too, rendering them hydrophobic. It is also possible that some of the RE minerals being floated are locked with other gangue minerals, as such recovering more RE elements will float gangue as well, reducing the grade. For the test using EDTA, a chelating agent, the addition did not affect the grade, but decreased the recovery. This result was not expected as this reagent is anticipated to improve the recovery by replacing the collector that might interact with the cations [7.33]. However, due to the nature of minerals in the ore, in which valuable minerals could be locked with the gangue minerals, it could also be that the chelating agent could have reacted with the gangue cations on the locked particle surface preventing collector adsorption, hence, reducing RE elements recovery as well. This behavior was also observed when the slurry was conditioned with sodium silicate. Sodium silicate, a gangue depressant [7.28, 7.34], could also have interacted with a middling particle consequently depressing a RE-bearing mineral as it depresses the gangue.

7.4.2 Bench-scale mechanical cell

Since the use of bench-scale mechanical cell (Denver cell) has been long-established and the main focus of the work was to explore the possibility of column flotation in RE ore processing, the design of the mechanical cell will not be discussed in this work. The purpose of doing the conventional flotation was to determine the flotation performance (in terms of grade and recovery) of the +20 μm ore fraction in the presence of F8920 collector. A number of tests with 1 F8920 : 1 NaOH ratio (as per manufacturer's instruction) were conducted, however significant production of froth was observed. When it was conducted with the reagent prepared with 1 F8920 : 0.24 NaOH ratio, the produced froth was less than that of the 1:1 ratio. Using the latter ratio, bench-scale mechanical flotation in the presence and absence of sodium silicate was conducted at around 50 °C. While, column cell flotation indicated that sodium silicate did not affect the grade but has reduced the recovery, this was not the case in the conventional mechanical flotation. The presence of sodium silicate in the bench-scale mechanical cell flotation tests reduced the grade but improved the recovery. Since sodium silicate could prevent slime (fine particles) coating onto the surface of minerals, it could also improve collector adsorption, hence, floatability of the valuable minerals [7.34]. However, as floatability of valuable minerals is improved, flotation of those locked with the gangue could have reduced the grade as well. For the tests without the presence of sodium silicate, although significant enrichment was obtained in the first rougher concentrate (see Figure 7.15b), the recovery (see Figure 7.15a) was observed to be sufficiently low. This could be due to the initial flotation of the fines (produced by grinding) which may be rich with RE minerals. Further flotation increased the recovery, but has gradually reduced the grade; which could be attributed to the flotation of middling particles.

It was observed that even though the initial grades (TREE) of the +20 μm (∼0.7%) and -20 μm (∼5%) were considerably different, the column cell final concentrates yielded comparable enrichment, but relatively higher recovery than those of the conventional flotation cell. Since the bench-scale mechanical flotation tests were not optimised, no valid conclusion can be drawn from this comparison except that column flotation cell could significantly enrich and recover RE elements (RE minerals) in the rougher concentrate.

7.5 Conclusions

Since the RE elements are found concentrated in the -20 μm fraction, it was practical to split the ore processing of the -20 and +20 μm fractions. Further grinding of only the coarse fraction could prevent overgrinding of the fine fraction and improve grinding efficiency. The specially design column cell was shown to have a potential to recover the RE minerals in the -20 μm fraction and enrich RE elements in the concentrate. A grade of equal or greater than 10% (as analyzed by XRF) with a recovery of around 50% could be achieved in just one step of flotation, which is not common in a typical RE processing where several flotation stages (cleaning and scavenging stages) are required. It was also found that processing of +20 μm ore in a bench-scale mechanical cell could also yield a satisfactory grade and recovery, which can be further processed in another mechanical cell flotation stage or in the specially designed column cell. Since the column set-up parameters are not investigated in detail, thus not optimized, further improvements could be evaluated. It is suggested to improve the cavitation and increase the cavitation volume by installing several cavitation tubes. Jameson cell, which has a similar mechanism, could also be explored in the processing of the ore.

References

[7.1] Maoming, F., Daniel, T., Honaker, R., and Zhenfu, L. Nanobubble generation and its applications in froth flotation (part III): specially designed laboratory scale column flotation of phosphate. *Mining Science and Technology (China)*, 20(3):317–338, 2010.

[7.2] Henderson, P. General geochemical properties and abundances of the rare earth elements. In Henderson, P., Editor, *Developments in Geochemistry*, volume 2, pages 1–32. Elsevier, 1984.

[7.3] Gupta, C. and Krishnamurthy, N. Extractive metallurgy of rare earths. *International Materials Reviews*, 37(5):52, 1992.

[7.4] Clark II, W. W. and Cooke, G. *Emerging Green Industrial Revolution Technologies*, pages 173–190. Butterworth-Heinemann, Boston, 2015.

[7.5] Matamec. Matamec Management Discussion and Analysis. Report, 2017.

[7.6] Castilloux, R. Rare Earth Market Outlook: Supply, Demand, and Pricing from 2016 through 2025. Report, 2016.

[7.7] Canadian Rare Earth Elements Network. Submission to the House of Commons Standing Committee on Finance Pre-Budget Consultations 2014. Report, 2014.

[7.8] Hatch, G. TMR Advanced Rare-Earth Projects Index. Report, Technology Metals Research, 2015.

[7.9] Chen, Z. Global rare earth resources and scenarios of future rare earth industry. *Journal of Rare Earths*, 29(1):1–6, 2011.

[7.10] Grenier, L. and Tremblay, J.-F. IAMGOLD NI 43-101 Technical report: Surface diamond drilling exploration program for rare earth elements (Niobec mine property). Report, 2013.

[7.11] SGS. The mineralogical characteristics of twenty-two drill core samples from a REE carbonatite deposit, adjacent to the Niobec Mine, Quebec. Report, 2012.

[7.12] Wills, B. A. and Finch, J. A. Froth Flotation. In Finch, J. A. and Wills, B. A., Editors, *Wills' Mineral Processing Technology*, pages 265–380. Butterworth-Heinemann, Boston, 8th edition, 2016.

[7.13] Nguyen, A. V. and Evans, G. M. Attachment interaction between air bubbles and particles in froth flotation. *Experimental Thermal and Fluid Science*, 28(5):381–385, 2004.

[7.14] Matis, K. A., Gallios, G. P., and Kydros, K. A. Separation of fines by flotation techniques. *Separations Technology*, 3(2):76–90, 1993.

[7.15] Lucideon. X-Ray Fluorescence Spectrometry (XRF Analysis). https://www.lucideon.com/testing-characterization/techniques/x-ray-fluorescence-spectrometry-xrf, 2018.

[7.16] Lucideon. Inductively Coupled Plasma Optical Emission Spectroscopy (ICP-OES Analysis). https://www.lucideon.com/testing-characterization/techniques/inductively-coupled-plasma-optical-emission-spectroscopy-icp-oes, 2018.

[7.17] NMI3. For chemical analysis: Neutron Activation Analysis. https://nmi3.eu/neutron-research/techniques-for-/chemical-analysis.html, 2012.

[7.18] Raissi, S. Developing new processes and optimizing performance using response surface methodology. *World Academy of Science, Engineering and Technology*, 49:1039–1042, 2009.

[7.19] Montgomery, D. C. *Design and Analysis of Experiments*. John Wiley & Sons, New York, 2017.

[7.20] Kökkılıç, O., Langlois, R., and Waters, K. E. A design of experiments investigation into dry separation using a Knelson Concentrator. *Minerals Engineering*, 72:73–86, 2015.

[7.21] Zhou, M., Kökkılıç, O., Langlois, R., and Waters, K. E. Size-by-size analysis of dry gravity separation using a 3-in. Knelson Concentrator. *Minerals Engineering*, 91:42–54, 2016.

[7.22] Cavazzuti, M. Design of experiments. In *Optimization Methods*, pages 13–42. Springer-Verlag Berlin Heidelberg, New York, 2013.

[7.23] Dean, A., Voss, D., and Draguljić, D. Response surface methodology. In *Design and Analysis of Experiments*, pages 565–614. Springer International Publishing, Cham, 2017.

[7.24] Azizi, D., Shafaei, S. Z., Noaparast, M., and Abdollahi, H. Modeling and optimization of low-grade Mn bearing ore leaching using response surface methodology and central composite rotatable design. *Transactions of Nonferrous Metals Society of China*, 22(9):2295–2305, 2012.

[7.25] Joglekar, A. M., May, A. T., Graf, E., and Saguy, I. Product excellence through experimental design. In Saguy, I. S. and Graf, E., Editors, *Food Product and Development: From Concept to the Marketplace*, pages 211–230. Aspen Publishers, New York, 1987.

[7.26] Jordens, A., Cheng, Y. P., and Waters, K. E. A review of the beneficiation of rare earth element bearing minerals. *Minerals Engineering*, 41:97–114, 2013.

[7.27] Pradip, P. and Fuerstenau, D. W. Design and development of novel flotation reagents for the beneficiation of Mountain Pass rare-earth ore. *Minerals and Metallurgical Processing*, 30(1):1–9, 2013.

[7.28] Azizi, D. and Larachi, F. Surface interactions and flotation behavior of calcite, dolomite and ankerite with alkyl hydroxamic acid bearing collector and sodium silicate. *Colloids and Surfaces A: Physicochemical and Engineering Aspects*, 537:126–138, 2018.

[7.29] Zhou, Z., Xu, Z., and Finch, J. On the role of cavitation in particle collection during flotation - a critical review. *Minerals Engineering*, 7(9):1073–1084, 1994.

[7.30] Hampton, M. A. and Nguyen, A. V. Nanobubbles and the nanobubble bridging capillary force. *Advances in Colloid and Interface Science*, 154(1):30–55, 2010.

[7.31] O'Connor, C. T. and Mills, P. J. T. The effect of temperature on the pulp and froth phases in the flotation of pyrite. *Minerals Engineering*, 3(6):615–624, 1990.

[7.32] Rastogi, A., Ghosh, A. K., and Suresh, S. J. Hydrogen bond interactions between water molecules in bulk liquid, near electrode surfaces and around ions. In *Thermodynamics - Physical Chemistry of Aqueous Systems*. InTech, Rijeka, 2011.

[7.33] Lelis, D. F., Leão, V. A., and Lima, R. M. F. Effect of EDTA on quartz and hematite flotation with starch/amine in an aqueous solution containing Mn^{2+} ions. *REM-International Engineering Journal*, 69(4):479–485, 2016.

[7.34] Park, C.-H. and Jeon, H.-S. The effect of sodium silicate as ph modifier and depressant in the froth flotation of molybdenite ores. *Materials Transactions*, 51(7):1367–1369, 2010.

Chapter 8

Conclusions, contributions to original knowledge and future work

This chapter presents the main conclusions from this dissertation, the contributions to original knowledge and the proposed future work that could contribute further to the improvement of the research area.

8.1 Conclusions

The main objective of the research was to recover the RE minerals from Niobec RE ore using froth flotation. The reagent scheme used for the process was designed based from understanding the mineralogy of the ore and the flotation behavior of pure RE minerals (monazite and bastnäsite) and the main gangue (dolomite).

The mineralogical study of the ore revealed that monazite (Ce,La,Nd,Th)PO_4 and bastnäsite (Ce,La,Sm,Nd)(CO_3)F/synchisite Ca(Ce,La,Sm,Nd)$(CO_3)_2$F are the main RE minerals with an average grade of 1.43% and 1.96%, respectively; and dolomite, $CaMg(CO_3)_2$, is the main gangue with an average grade of 50%. The fine grain sizes of the RE minerals in Niobec RE ore made them difficult to be recovered through magnetic and gravity processes; and made flotation to be the most applicable beneficiation process for the separation. However, the literature review revealed that the available information regarding RE mineral flotation is very limited, as such fundamental studies are necessary to provide information that will guide the researchers in the processing of the ore.

- Fundamental investigations of the readily available RE minerals (*i.e.,* monazite and bastnäsite) and gangue (*i.e.,* dolomite) were conducted through single-mineral microflotation, electrophoretic studies and surface characterizations. The variation in flotation behavior of the pure RE minerals (monazite and bastnäsite) and main gangue (dolomite) in different pH conditions in the presence of different collectors (benzohydroxamate, sodium oleate and organic phosphoric acid) were due to disparity in the mineral's solubility and collector's speciation in solution. Zeta potential measurements, attenuated total reflectance Fourier-transform (ATR-FTIR) spectroscopy and thermodynamic calculations (chemical speciation) proved to be useful in understanding the possible mineral-collector interaction.

- It was shown that sodium oleate and organic phosphoric acid have low selectivity due to their strong collecting ability with dolomite. Investigation of various dolomite depressants (*e.g.,* sodium carbonate, citric acid, starch, carboxymethylcelluose, lignosulfonate and F-100) revealed that the polymeric type depressants have superior depressing ability than others. Among them, carboxymethylcellulose was found to perform the best in depressing dolomite in the presence of either sodium oleate or organic phosphoric acid at the pH values investigated.
- Dissolved minerals from dolomite presented detrimental effect on the flotation recovery of monazite and bastnäsite in the presence of benzohydroxamate or sodium oleate. Thermodynamic calculations (chemical speciation) and X-ray photoelectron spectroscopy (XPS) showed that species such as $CaOH^+$ (from hydrated Ca^{2+}), $MgCO_3$ /$CaCO_3$ or HCO_3^- could be adsorbed or precipitated at the mineral surface, providing new sites for collector adsorption. The metal cations (Ca^{2+} and Mg^{2+}) in the solution from dolomite dissolution could also take up some collectors through formation of metal-collector precipitates.
- Comparison of the strength between different mineral-collector interactions were also made possible by molecular modeling. Density functional theory (DFT) based simulations were also able to identify possible configurations of the collector when adsorbed at the surface of the minerals.

It has been demonstrated that the knowledge of the surface chemistry of the minerals, the adsorption behavior of the collectors and the mineral-reagent interactions contributed to a better understanding of the flotation behavior of the pure minerals, which were found useful in the processing of Niobec RE ore. The following main conclusions were drawn from the processing of the Niobec RE ore:

- The observed concentration of the RE elements in the fine size fraction (-20 μm) marked the turning point of the research, leading to a decision to process the coarse (+20 μm) and fine (-20 μm) ore particles into two separate processing routes. The process of splitting the ore into two fractions was found to improve the grinding efficiency of the coarse fraction and avoided overgrinding of the initially present fine (-20 μm) particles.

- Flotation of the fine (-20 μm) fraction using a specially designed cavitation column cell proved to be effective in enriching the RE element grade in the concentrate. Although the column cell set-up used in this work was not fully optimized, it has been shown to yield satisfactory enrichment ratio and recovery even with only one roughing stage. The fine bubbles can attach to conventional bubbles (as seen through hi-speed camera), enabling fine particles to be recovered.

8.2 Contributions to original knowledge

This is the first work to present a more detailed flotation behavior of monazite, bastnäsite and dolomite in the presence of benzohydroxamate and organic phosphoric acid (Flotinor 1682), both of which are relatively new RE collectors. Proposed adsorption mechanisms of Flotinor 1682 (an organic phosphoric acid) were also presented in this work. It was suggested that the second dissociation product of Flotinor 1682, $ROPO_3^{2-}$, is the main active species in the flotation of the minerals.

This work also presents the first scientific investigation of the depressing capability of dolomite depressants such as sodium carbonate, citric acid, starch, carboxymethylcellulose, lignosulfonate and F-100 (biopolymer) in the presence of organic phosphoric acid collector. It was shown that although depressants could work with other collectors such as sodium oleate, it might not work with the same efficiency as in the presence of organic phosphoric acid collector.

Investigations on the effect of dissolved dolomite species on the flotation behavior of monazite, bastnäsite and dolomite in the presence of sodium oleate and benzohydroxamate were also detailed in this work. Most of the investigations regarding the effect of cations on the flotation of minerals were conducted using synthetic solution. In this work, dissolved species were obtained from dolomite since it comprises most of the ore (50%). The adsorption mechanism of the different species that could adsorb at the mineral's surface is predicted through molecular modeling.

Through molecular modeling, the collector configurations when adsorbed at the surface of the minerals was predicted. This work also presented that benzohydroxamate and sodium oleate could be lost in solution through the formation of metal-benzohydroxamate complexes and/or metal-oleate precipitates. Acid soap, $H(OOCR)_2^-$, was proposed by other researchers to have an important role in mineral's flotation; however, through the molecular simulations, it was found that the oleate ion, $RCOO^-$, is the one that interacts stronger with the minerals.

This work is also the first one to explore the possibility of processing the fine and coarse RE ore separately. The feasibility of using cavitation column flotation cell for the fine ore fraction was also considered in this work. It was presented that significant enrichment and recovery of the RE elements can be achieved even with only one stage of rougher flotation, which was typically obtained through several stages of cleaning or scavenging.

8.3 Recommendations for future work

Although the work has demonstrated detailed investigations of the flotation behavior of the pure minerals and presented work on the flotation of Niobec RE ore, there are still several aspects that could be considered. The following are some future directions for the extension of the research.

- Investigation of the surface chemistry and flotation behavior of other minerals present in Niobec RE ore including synchisite (RE mineral), and gangue such as ankerite, calcite, and barite.
- Evaluation of the adsorption behavior (*e.g.,* adsorption kinetics and adsorption isotherm) of the collectors on the mineral surface through UV-Vis spectroscopy for benzohydroxamate and sodium oleate. Since Flotinor 1682 (organic phosphoric acid) cannot be detected through UV-Vis spectroscopy, other technique such as titration, calorimetry or other applicable method could be suggested.
- Other flotation system uses mixture of collectors, as such, it would also be interesting to explore the synergistic effect of mixed collectors on the flotation of the RE minerals and gangue.
- The optimisation of the specially designed column flotation cell is also highly encouraged to improve the flotation efficiency not only from the chemical aspect, but also from the physical aspect of the process.
- A more thorough design of experiment and reagent scheme (collectors, frothers, depressants) optimisation is required to achieve a more efficient RE minerals separation in terms of grade, recovery and selectivity.

Appendix A

Exploratory investigation of different rare earth mineral collectors

Minerals Engineering 116 (2018) 101–106

Contents lists available at ScienceDirect

Minerals Engineering

journal homepage: www.elsevier.com/locate/mineng

Flotation studies of monazite and dolomite

E.R.L. Espiritu, K.E. Waters *

Department of Mining and Materials Engineering, McGill University, 3610 University Street, Montreal, Quebec H3A 0C5, Canada

ARTICLE INFO

Article history:
Received 12 February 2016
Revised 7 February 2017
Accepted 21 February 2017
Available online 10 March 2017

Keywords:
Rare earth elements
Rare earth minerals
Flotation
Zeta potential
Monazite
Dolomite
Benzohydroxamic acid
Sodium oleate
Organic phosphoric acid
Phosphoric acid ester

ABSTRACT

Rare earth elements (REE) are key components of many emerging green technologies. This leads to an increase in demand for REE, hence to the development of new deposits, such as the Niobec carbonatite rare earth deposit in Quebec, Canada. One of the valuable minerals in this deposit is monazite, one of the primary sources of REE. Although there has already been previous research investigating monazite flotation, most of these are focused on monazite from heavy mineral deposits. Since minerals from different deposits may behave differently, it is important to investigate the flotation behavior of monazite from carbonatites as well. This work investigates the surface properties of monazite from carbonatite deposit through zeta potential analyses. Electrophoretic zeta potential measurements were conducted to identify the interaction of monazite and dolomite, a gangue mineral commonly associated with carbonatites, with different collectors (namely sodium oleate, organic phosphoric acid and benzohydroxamic acid). Floatability of the minerals were analyzed through microflotation tests, to obtain the potential conditions for effective separation. Zeta potential measurements of monazite and dolomite showed that the isoelectric point (IEP) for both minerals occur at a pH of approximately 5. Sodium oleate, benzohydroxamic acid and Flotinor 1682 (organic phosphoric acid) have been shown to adsorb on to monazite at pH 7. The results suggest that benzohydroxamic acid can be selective at neutral pH condition, sodium oleate can be potentially used in reverse flotation of monazite in acidic condition and Flotinor 1682 (organic phosphoric acid) can be a potential collector for monazite. However, the use of reagents such as activators and depressants is suggested to achieve a more selective separation.

1. Introduction

The rare earth elements (REE) consist of yttrium (Y) and the lanthanides, which can be further divided into light REE (La to Eu) and heavy REE (Gd to Lu, and Y) (Gupta and Krishnamurthy, 1992). Due to their unique chemical properties, they are regarded as essential components of emerging green technologies such as wind turbines, hybrid vehicles and storage batteries (Kara et al., 2010). This leads to an increase in demand for REE, hence the development of new deposits, such as the Niobec rare earth deposit in Quebec, Canada. This rare earth deposit, which is adjacent to their existing Niobium mine, is a carbonatite complex containing monazite as one of the valuable minerals.

Monazite ($REPO_4$), a RE phosphate, is one of the primary sources of light REE (Kamitani, 1991). The most significant sources of this mineral are heavy mineral sands (Gupta and Krishnamurthy, 1992). Monazite is usually beneficiated from heavy mineral sands using gravity, magnetic and electrostatic separation (Bulatovic, 2010). When the mineral grains are too fine for these methods, a more suitable beneficiation method such as flotation is employed (Bulatovic, 2010). Research studies have shown that flotation of monazite from heavy mineral sand deposit is possible using collectors such as: fatty acids; amines; sulfonates; and hydroxamates (Abeidu, 1972; Cheng et al., 1993; Cuthbertson, 1952; Houot et al., 1991; Pavez and Peres, 1993a, 1993b, 1994). Monazite can also occur as finely disseminated in carbonatites (Zaitsev et al., 1998); however, research work involving monazite from carbonatites are very limited (Chelgani et al., 2015; Jordens et al., 2013). The aim of this work is thus to examine the flotation behavior of monazite from this type of deposit.

In general, oxhydryl collectors (e.g., carboxylates, phosphoric acid esters and hydroxamates) have been the focus of rare earth mineral flotation studies due to their efficiency (Bulatovic, 2010; Zhang et al., 2013). These oxhydryl collectors have two oxygen atoms, which are responsible for bonding with metal cations. Carboxylates (e.g., fatty acids, oleates and tall oils) are the most widely used industrial collectors (Bulatovic, 2007b), however, they have poor selectivity towards rare earth minerals (REM) (Wills and Finch, 2016). Hydroxamates have caught the interest of many researchers due to their selectivity and efficiency. Various flotation

---

* Corresponding author.
E-mail addresses: eileen.espiritu@mail.mcgill.ca (E.R.L. Espiritu), kristian.waters@mcgill.ca (K.E. Waters).

http://dx.doi.org/10.1016/j.mineng.2017.02.010

studies demonstrated that this collector is more selective than carboxylates (Bulatovic, 2010; Houot et al., 1991; Pradip and Fuerstenau, 2013; Zhang et al., 2013), which is attributed to its formation of more stable chelates with rare earth cations than with alkaline earth cations (such as those found in the gangue minerals) (Fuerstenau, 2005). Another type of collector that has been investigated includes phosphoric acid esters (organic phosphoric acid). These have shown potential to be a REM collector (Ren et al., 2003). However, available literature with regards to the response of organic phosphoric acid with monazite is scarce (Chelgani et al., 2015). This study provides information on the flotation of monazite using this type of collector, in comparison to the conventional REM collectors – carboxylate and hydroxamate. Moreover, it will investigate the flotation response of dolomite (which is one of the major gangue minerals in the Niobec rare earth deposit), providing information on flotation conditions where separation from monazite are possible.

General classification of collector adsorption mechanisms is physisorption and chemisorption (Bulatovic, 2007a). If the adsorption involves forces such as electrostatic (coulombic forces) or hydrophobic bonding, it is considered physical adsorption; however, if it involves covalent bonding, then it is chemisorption (Somasundaran and Moudgil, 1987). Fuerstenau and Urbina (1988) summarized the reactions involved in the flotation of sparingly soluble minerals (e.g., rare earth minerals, barite, calcite, apatite, and dolomite). These include: physical adsorption of the collector ions in the double layer; chemisorption in the Stern plane; surface formation of a more insoluble compound; chemisorption on hydrolyzed metal sites; surface reaction, dissolution of mineral and precipitation of metal-collector salt; and, autoactivation through surface dissolution, cation hydrolysis and re-adsorption of hydrolyzed ion. In addition, possible reactions between the metal ion and collector ions can also occur as surface precipitation and bulk precipitation. Surface precipitation happens when the reagent interacts with the surface "through movement of metal atoms from their lattice sites" while bulk precipitation of the metal reagent salts occurs when the dissolved lattice ions forms an insoluble compound with the collector away from the surface of the mineral (Chander and Fuerstenau, 1975). The reactions between the metal cations and the collector can be used to understand what is happening in the flotation system and as a guide in the improvement of flotation performance.

In this study, the surface properties of monazite (from carbonatite) and dolomite in the presence of Flotinor 1682 (organic phosphoric acid) were investigated through zeta potential measurements and microflotation tests. These were compared to the minerals' behavior in the presence of conventional REM collectors such as sodium oleate (carboxylate) and benzohydroxamic acid (hydroxamate). For a good introduction to zeta potentials and for the relevance to mineral flotation, the reader is referred to Hunter (1981) and Fuerstenau and Pradip (2005), respectively.

2. Experimental

2.1. Materials

Monazite from Eureka Farm 99 (carbonatite deposit) in Namibia was purchased from the Mineralogical Research Company (U.S.A). Dolomite from Sterling Hill Mine in New Jersey, the gangue mineral investigated, was obtained from Ward's Science (U.S.A.).

Benzohydroxamic acid was purchased from Sigma-Aldrich (Canada), sodium oleate was obtained from Fischer Scientific Company (Canada) and Flotinor 1682 (organic phosphoric acid) was provided by Clariant (Canada). The frother (F150) was provided by Flottec (Canada).

The potassium chloride that was used as supporting electrolyte for zeta potential measurements was purchased from Sigma-Aldrich (Canada); while the hydrochloric acid and the potassium hydroxide that were used as pH modifiers, were purchased from Fisher Scientific (Canada).

2.2. Mineral purification

The purchased minerals were not pure, thus concentration steps (such as gravity and/or magnetic separation) were conducted prior to surface chemistry and flotation experiments. Since these methods are particle size dependent, mineral samples were first pulverized to 100% passing 212 μm and were divided into different size fractions (−212 + 150 μm, −150 + 106 μm, −106 + 75 μm, −75 + 53 μm, −53 + 38 μm and −38 μm). All these size classes were processed using a Mozley MKII Laboratory Separator (Mozley, U.K.) separately. The heavy fraction was then further purified using a Frantz Isodynamic Separator (Frantz, U.S.A.) with a gradual increase in applied current (corresponding to increasing magnetic field). Since different minerals have different susceptibility to magnetic field, concentration can then be achieved.

2.3. Zeta potential measurements

Purified mineral samples were first pulverized using a Planetary Monomill Pulverisette (Fritsch, Germany) to obtain a particle size smaller than 10 μm. Solution of 1×10^{-3} M KCl was used as supporting electrolyte. The solution was pH adjusted using hydrochloric acid and potassium hydroxide prior to addition of the mineral particles. The suspension was then ultrasonicated for 180 s to ensure particle dispersion. Zeta potential measurements were then undertaken using a NanoBrook 90Plus Zeta Particle Size Analyzer (Brookhaven Instruments, U.S.A.).

2.4. Microflotation experiments

Microflotation tests were carried out using a modified Partridge-Smith cell (Partridge and Smith, 1971). The flotation volume of the cell is approximately 60 mL. The cell, made out of glass, has a porous silicate frit at the bottom; and a launder that receives the froth at the top. A magnetic stirring bar was employed to ensure that the minerals remained in suspension.

Mineral samples within the particle size range of – 106 + 38 μm were suspended in 40 mL reverse osmosis water (adjusted to desired pH). The pH of the suspension was maintained prior to addition of the collector, and throughout the 5 min of conditioning. The suspension was transferred to the microflotation cell and a further 20 mL of pH adjusted water was added. Then, 3 drops of 10 mg/mL F150 frother was added before air at a flowrate of 40 mL/min was bubbled through the cell. Flotation was conducted for 1 min.

3. Results

3.1. Mineral characterization

X-ray diffraction analyses of the mineral samples were conducted using Bruker D8 Discovery X-Ray Diffractometer (Cobalt source). The diffractograms of the samples before and after purification are presented in Fig. 1. The quantity of the minerals in the sample were analyzed using the Rietveld method. The results indicated that each mineral contains around 94% monazite and 99% dolomite, respectively.

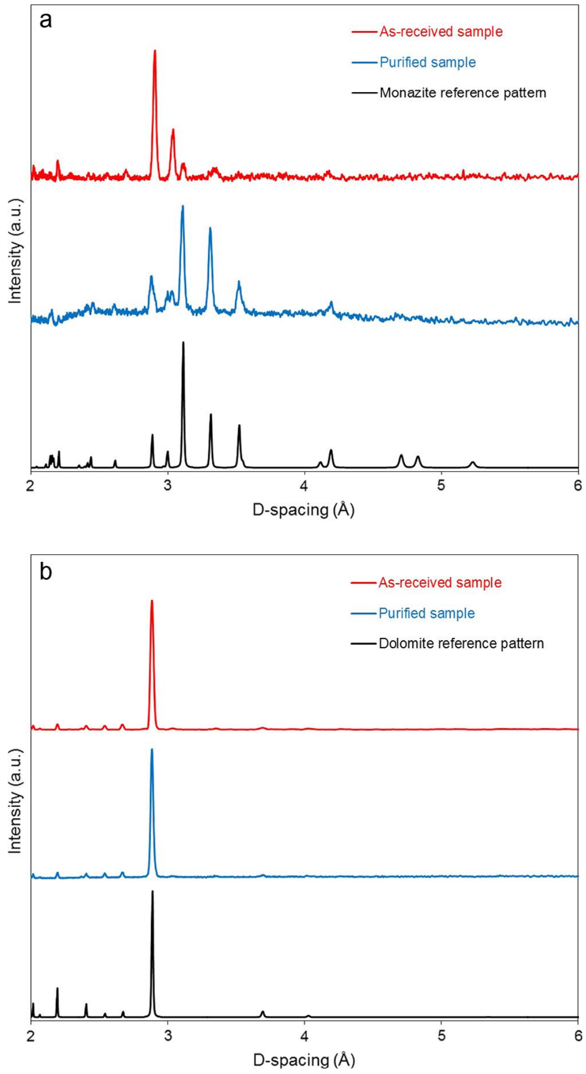

Fig. 1. X-ray powder diffraction patterns of monazite and dolomite (cobalt source). The figures represent: (top) monazite as-received sample; purified sample; and reference pattern (JPDF reference number: 00-046-1295) (Bermanec et al., 1988); (bottom) dolomite as-received sample, purified sample and reference pattern (JPDF reference number: 01-081-8229) (Zucchini et al., 2012).

3.2. Zeta potential

Zeta potential curves of monazite and dolomite with 1 x 10^{-3} M KCl supporting electrolyte are shown in Fig. 2. The isoelectric point of both minerals was determined to be at a pH of approximately 5. The zeta potential of the two minerals added with different collectors – sodium oleate, benzohydroxamic acid and Flotinor 1682 (organic phosphoric acid) were also measured as shown in Figs. 3 and 4. The changes in zeta potential values after addition of these collectors indicate collector adsorption at the surface of the minerals.

The zeta potential measurements of dolomite (Fig. 3) showed that the addition of benzohydroxamic acid has very little effect on the zeta potential of dolomite. However, the addition of sodium oleate has an appreciable effect at acidic pH; and the addition of Flotinor 1682 (organic phosphoric acid) significantly changed the

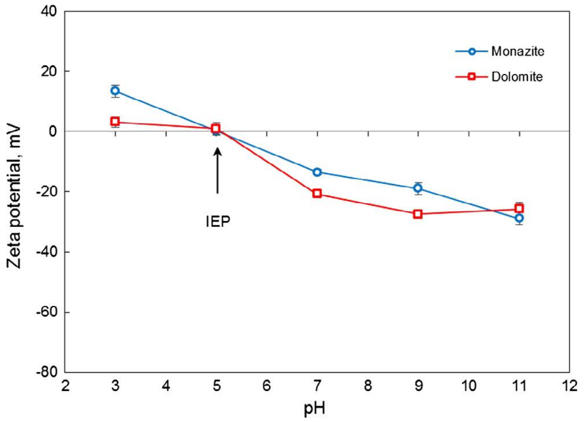

Fig. 2. Zeta potential curves of dolomite and monazite with 1×10^{-3} M KCl supporting electrolyte at different pH conditions. The error bars represent ± standard error (SE).

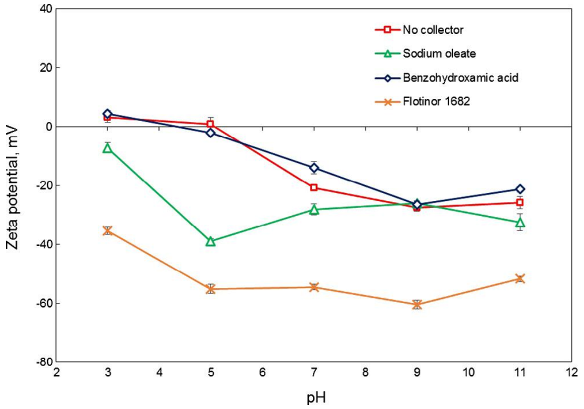

Fig. 3. Zeta potential curves of dolomite with different collectors – sodium oleate, benzohydroxamic acid and Flotinor 1682 (organic phosphoric acid). The error bars represent ± standard error (SE).

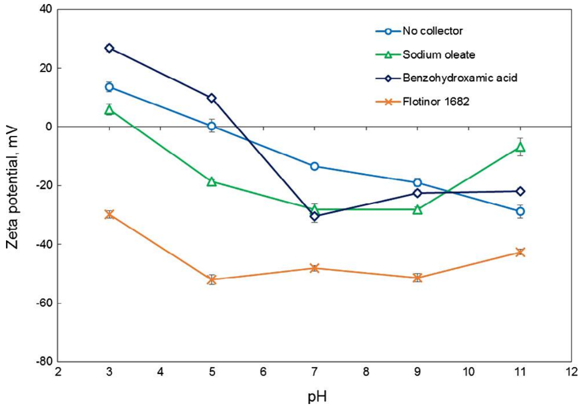

Fig. 4. Zeta potential curves of monazite with different collectors – sodium oleate, benzohydroxamic acid and Flotinor 1682 (organic phosphoric acid). The error bars represent ± standard error (SE).

zeta potential of dolomite to a more negative value across the entire pH range tested. As the changes in zeta potential indicates collector adsorption, these would imply that benzohydroxamic acid may not affect the floatability of dolomite; sodium oleate may be more effective in acidic conditions than in basic conditions; and Flotinor 1682 may float dolomite across the entire pH range tested.

Fig. 4 shows the zeta potential measurements of monazite with 1×10^{-3} M KCl, sodium oleate, benzohydroxamic acid and Flotinor 1682 (organic phosphoric acid). It can be seen that the three collectors were able to significantly change the zeta potential of monazite. In flotation, this would indicate that these collectors will be able to float monazite.

Among the three collectors, Flotinor 1682 (organic phosphoric acid) appeared to have the greatest effect on the zeta potential values of the two minerals. After addition of this collector to suspensions of monazite or dolomite, the resulting zeta potential values were comparable to one another. Although these indicated adsorption of the collector on the surface of the minerals, the small difference of the zeta potential values suggested a challenging separation between the two minerals if they were to coexist in a flotation system. With sodium oleate, the zeta potential values of monazite and dolomite have significant differences at acidic pH. This observation would suggest that at these pH conditions, sodium oleate has a certain degree of selectivity between monazite and dolomite.

3.3. Microflotation

Microflotation of monazite and dolomite was conducted using increasing dosages of collectors as presented in Figs. 5 and 6. The figures show that, in general, an increase in the collector dosage has led to an increase in recovery. However, this is not observed with dolomite when floated using benzohydroxamic acid. To compare the flotation behavior of monazite and dolomite, the following collector dosages were used: 138 mg/L benzohydroxamic acid, 1.5 mg/L sodium oleate, and 1.5 mg/L Flotinor 1682 (organic phosphoric acid). They were chosen because these dosages have yielded approximately the same recoveries of monazite.

The recovery of each mineral at different pH conditions is shown in Figs. 7–9. While flotation was conducted separately on monazite and dolomite, their recoveries are plotted side by side on one graph to compare their flotation behavior. The difference in their recovery can give an indication to the potential selectivity of the collector between these minerals.

Fig. 7 illustrates that 138 mg/L benzohydroxamic acid was able to float 3%, 37% and 11% monazite at pH 4, 7 and 10 respectively. The highest amount of monazite was floated at pH 7. This trend is consistent with the results of Pavez and Peres (1993b) using potassium octyl hydroxamate. At this pH and collector dosage, it can also be inferred from the difference in recovery that this collector would have good selectivity for monazite over dolomite.

In Fig. 8, the results of monazite and dolomite flotation using sodium oleate are presented. Although there appears to be a difference in recovery at pH 7, after conducting a T-test, these differences are not statistically significant. Thus, sodium oleate would not be selective at pH 7 and pH 10, but could be relatively selective at pH 4. Fig. 8 also shows that the recovery of dolomite decreases from pH 4 (40%), to 7 (16%) to 10 (8%). For monazite, the maximum floatability was achieved at pH 7. The amount of floated monazite was 6%, 32% and 10% at pH 4, 7 and 10, respectively, comparable to flotation with benzohydroxamic acid. Likewise, this trend is also consistent with the work of Cheng et al. (1993), Abeidu (1972) and Pavez and Peres (1993b) using sodium oleate.

The results of microflotation tests using Flotinor 1682 (organic phosphoric acid) are presented in Fig. 9. It can be observed that dolomite floats more readily than monazite at pH 4 and 7. Based on this data, dolomite floated in decreasing amounts from pH 4 (66%), pH 7 (60%) to pH 10 (8%). Meanwhile, the amount of floated monazite was 29%, 31% and 15% at pH 4, 7 and 10 respectively.

4. Discussion

The results have showed that dolomite flotation results with sodium oleate and Flotinor 1682 (organic phosphoric acid) follows a decreasing floatability trend with increasing pH. For dolomite flotation with sodium oleate, at pH values below the IEP, it has been suggested that the mechanism of adsorption of the collector is by hydrogen bonding between the oleic acid molecules (RCOOH) and the H_2CO_3 sites at the mineral surface (Predali, 1969); and the "physical coating of the oleic acid" to the mineral surface (Moudgil and Chanchani, 1983). In this pH range, the amount of oleic acid molecules that can interact with the mineral surface is dominant in the solution. This resulted in the high floatability of dolomite with sodium oleate at pH 4. On the other hand, at pH above the IEP, Fuerstenau and Miller (1967) suggested that the mechanism of adsorption is through chemisorption. They proposed that oleate ions reacts with the surface forming CO_3^{2-} ions and $Me(OOCR)_2$ at the surface (Me can be Ca^{2+} or Mg^{2+}). The $Me(OOCR)_2$ renders the mineral hydrophobic, thus the mineral will float. However, in this study, it is believed that the decrease in the floatability at pH above the IEP is due to the depletion of oleate. This depletion is attributed to the bulk precipitation of $Me(OOCR)_{2(s)}$ and $MeOHOOCR_{(s)}$ in the solution, thus reducing the amount of available oleate that will adsorb onto the dolomite surface.

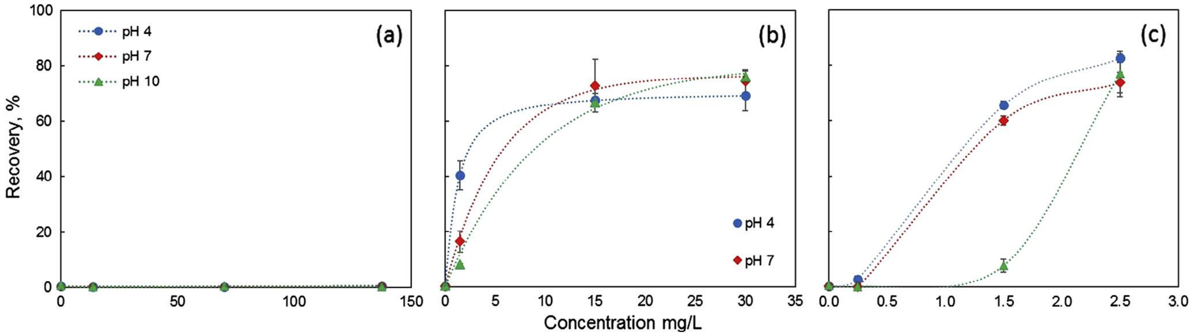

Fig. 5. Microflotation results of dolomite as a function of collector dosage: (a) benzohydroxamic acid; (b) sodium oleate; and (c) Flotinor 1682 (organic phosphoric acid). The error bars represent ± standard error (SE).

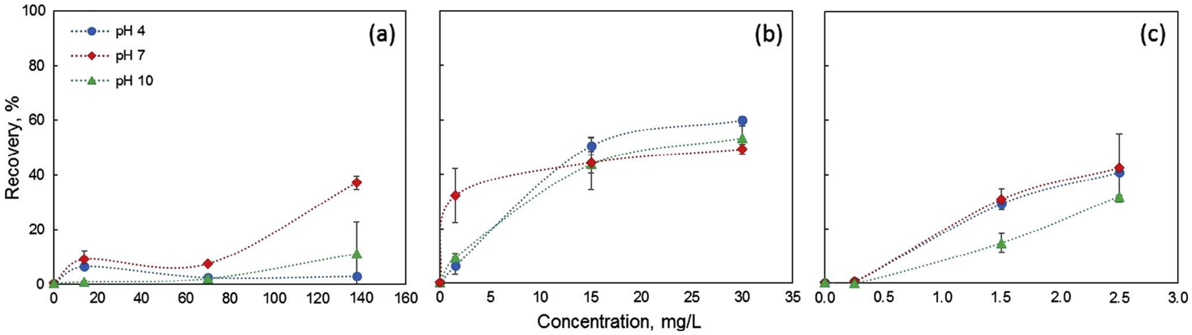

Fig. 6. Microflotation results of monazite as a function of collector dosage: (a) benzohydroxamic acid; (b) sodium oleate; and (c) Flotinor 1682 (organic phosphoric acid). The error bars represent ± standard error (SE).

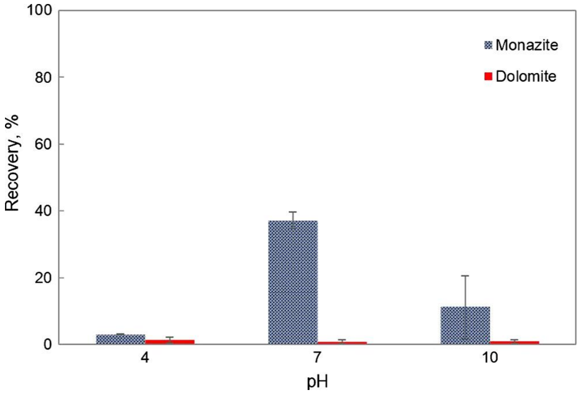

Fig. 7. Microflotation recovery of monazite and dolomite with benzohydroxamic acid as collector. The error bars represent ± standard error (SE).

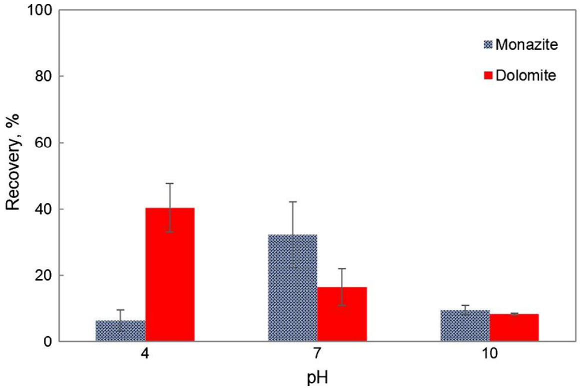

Fig. 8. Microflotation recovery of monazite and dolomite with sodium oleate as collector. The error bars represent ± standard error (SE).

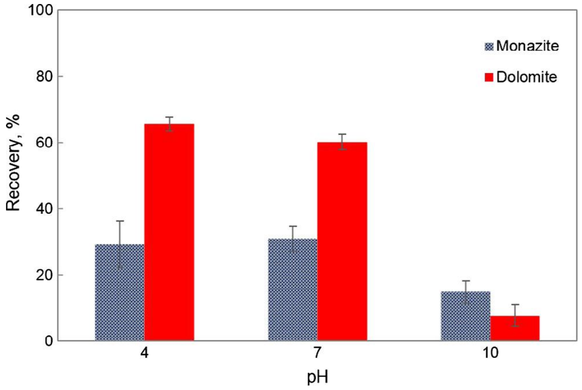

Fig. 9. Microflotation recovery of monazite and dolomite with Flotinor 1682 (organic phosphoric acid) as collector. The error bars represent ± standard error (SE).

The trend for dolomite flotation with Flotinor 1682 (organic phosphoric acid) can also be explained by the speciation of dolomite and the mechanism of collector adsorption. It was proposed that the mechanism of adsorption of this collector with calcium minerals involves the formation of coordinate bond between P═O and Ca^{2+} ions; covalent bond between P—O and Ca^{2+} ions; and the presence (weak) of hydrogen bonding between the collector and the mineral surface (Hu and Xu, 2003). Therefore, it can be inferred that the decrease in the dolomite floatability with increasing pH is due to the decrease in Ca^{2+} ions available for collector bonding.

Benzohydroxamic acid did not float dolomite, which is expected due to weak Ca-hydroxamate complex formation. Moreover, dolomite is a sparingly soluble mineral with a K_{sp} of $1 \times 10^{-19.35}$ (Chen and Tao, 2004). There may be too few Ca^{2+} ions available to react with benzohydroxamic acid and to provide a sufficient degree of hydrophobicity.

For monazite flotation, the three collectors appear to have achieved a good floatability at a pH at approximately 7. From the speciation diagram of monazite (Cheng et al., 1993), it can be observed that the flotation results correlates with the amount of $Ce(OH)^{2+}$ ions that can be formed when the mineral is in solution. This was also the finding of Cheng et al. (1993), where the floatability of monazite was related to the amount of $Ce(OH)^{2+}$ ions present in the solution. Pradip and Fuerstenau (1982) proposed that these species can be formed at the surface of the minerals; or they can be produce at the solution, adsorb back onto the mineral surface, both serving as collector adsorption sites. The results suggest that the three collectors might be operating under these mechanisms at certain pH conditions.

5. Conclusions

The surface chemistry of monazite and dolomite has been investigated through electrophoretic zeta potential measurements and microflotation tests with different collectors – benzohydroxamic acid, sodium oleate, and Flotinor 1682 (organic phosphoric acid). The IEPs of dolomite and monazite both occur at pH around 5. This suggests that well-chosen chemisorbing flotation reagents are necessary to separate this two minerals in a mixed flotation system. In this study, the zeta potential measurements after addition of collectors have indicated significant collector adsorption at certain pH conditions. These results corresponded well with the microflotation results. It was found that direct flotation of monazite can be achieved using benzohydroxamic acid at pH 7. Reverse flotation of monazite can also be possible using sodium oleate at pH 4; and Flotinor 1682 (organic phosphoric acid) at pH 4 and 7. However, it is suggested that depressants or activators are necessary to obtain a more effective separation.

The trends of dolomite and monazite floatability were explained by the speciation of these minerals in solution and the mechanism of collector adsorption. Both dolomite and monazite flotation behaviors were affected by their solubility. For dolomite, it was greatly affected by the solubility of metal cations – Ca^{2+} and Mg^{2+} ions; while for monazite, it was found to be correlated with the amount of RE-hydroxylated species that can be formed by dissolution, such as $Ce(OH)^{2+}$ ions, which provide adsorption sites for the collectors. Since, the minerals are slightly soluble, it is also worth investigating how each mineral will behave in a mixed flotation system, how the ions from each mineral will affect the flotation response of the individual minerals.

Acknowledgements

The authors would like to acknowledge Natural Sciences and Engineering Research Council of Canada (NSERC) and Niobec, a Magris Resources Company, for funding this research through the Collaborative Research and Development Program (CRDPJ 453164-13). The authors would also like to acknowledge McGill Engineering Doctoral Award.

References

Abeidu, A.M., 1972. The separation of monazite from zircon by flotation. J. Less Common Metals 29, 113–119.

Bermanec, V., Tibljaš, D., Gessner, M., Kniewald, G., 1988. Monazite in hydrothermal veins from Alinci, Yugoslavia. Mineral. Petrol. 38, 139–150.

Bulatovic, S.M., 2007a. Adsorption mechanism of flotation collectors. In: Bulatovic, S.M. (Ed.), Handbook of Flotation Reagents. Elsevier, Amsterdam, pp. 125–152.

Bulatovic, S.M., 2007b. Collectors. In: Bulatovic, S.M. (Ed.), Handbook of Flotation Reagents. Elsevier, Amsterdam, pp. 5–40.

Bulatovic, S.M., 2010. Flotation of REO minerals. In: Bulatovic, S.M. (Ed.), Handbook of Flotation Reagents: Chemistry, Theory and Practice. Elsevier, Amsterdam, pp. 151–173.

Chander, S., Fuerstenau, D.W., 1975. Electrochemical reaction control of contact angles on copper and synthetic chalcocite in aqueous potassium diethyldithiophosphate solutions. Int. J. Miner. Process. 2, 333–352.

Chelgani, S.C., Rudolph, M., Leistner, T., Gutzmer, J., Peuker, U.A., 2015. A review of rare earth minerals flotation: monazite and xenotime. Int. J. Min. Sci. Technol. 25, 877–883.

Chen, G., Tao, D., 2004. Effect of solution chemistry on flotability of magnesite and dolomite. Int. J. Miner. Process. 74, 343–357.

Cheng, T.-W., Holtham, P.N., Tran, T., 1993. Froth flotation of monazite and xenotime. Miner. Eng. 6, 341–351.

Cuthbertson, R.E., 1952. Froth flotation of monazite from heavy gravity minerals. Google Patents.

Fuerstenau, D.W., Pradip, P., 2005. Zeta potentials in the flotation of oxide and silicate minerals. Adv. Colloid Interface Sci. 114–115, 9–26.

Fuerstenau, D.W., Urbina, R.H., 1988. Flotation fundamentals. In: Somasundaran, P., Moudgil, B.M. (Eds.), Reagents in Mineral Technology. Marcel Dekker Inc., pp. 1–38.

Fuerstenau, M.C., 2005. Chelating agents as flotation collectors. In: Miller, J.D., Young, C., Kellar, J.J., Free, M.L. (Eds.), Innovations in Natural Resource Processing: Proceedings of the Jan. D. Miller Symposium. Society for Mining, Metallurgy, and Exploration, Incorporated.

Fuerstenau, M.C., Miller, J.D., 1967. The role of the hydrocarbon chain in anionic flotation of calcite. Trans. AIME 238, 153–160.

Gupta, C.K., Krishnamurthy, N., 1992. Extractive metallurgy of rare earths. Int. Mater. Rev. 37, 52.

Houot, R., Cuif, J.-P., Mottot, Y., Samana, J.-C., 1991. Recovery of rare earth mineral, with emphasis on flotation process. In: International Conference on Rare Earth Minerals and Minerals for Electronic Uses. Trans Tech Publications, HatYai, Thailand, pp. 301–324.

Hu, Y., Xu, Z., 2003. Interactions of amphoteric amino phosphoric acids with calcium-containing minerals and selective flotation. Int. J. Miner. Process. 72, 87–94.

Hunter, R.J., 1981. Zeta Potential in Colloid Science. Academic Press Inc., San Diego, CA.

Jordens, A., Cheng, Y.P., Waters, K.E., 2013. A review of the beneficiation of rare earth element bearing minerals. Miner. Eng. 41, 97–114.

Kamitani, M., 1991. Rare Earth Resources and the Problems. In: Siribumrungsukha, B., Arrykul, S., P. Sanguansai, Pungrassami, T., Sikong, L., Kooptarnond, K. (Eds.), International Conference on Rare Earth Minerals and Minerals for Electronic Uses. Trans Tech Publications, Hat Yai, Thailand, pp. 181–191.

Kara, H., Chapman, A., Crichton, T., Willis, P., Morley, N., 2010. Lanthanide resources and alternatives. Oakdene Hollins Research and Consulting.

Moudgil, B.M., Chanchani, R., 1983. Selective flotation of dolomite from apatite using sodium oleate as the collector, SME-AIME Annual Meeting.

Partridge, A., Smith, G., 1971. Small-sample flotation testing: a new cell. Trans. Inst. Min. Metall., Sect. C 80, C199.

Pavez, O., Peres, A.E.C., 1993a. Effect of sodium metasilicate and sodium sulphide on the floatability of monazite-zircon-rutile with oleate and hydroxamates. Miner. Eng. 6, 69–78.

Pavez, O., Peres, A.E.C., 1993b. Flotation of Monazite-Zircon-Rutile with Sodium Oleate and Hydroxamates. XVIII International Mineral Processing Congress, Sydney, pp. 1007–1012.

Pavez, O., Peres, A.E.C., 1994. Bench scale flotation of a Brazilian monazite ore. Miner. Eng. 7, 1561–1564.

Pradip, P., Fuerstenau, D.W., 1982. Adsorption of hydroxamate on semi-soluble minerals. Part I: Adsorption on barite, calcite and bastnaesite. Colloids Surf. 8, 103–119.

Pradip, P., Fuerstenau, D.W., 2013. Design and development of novel flotation reagents for the beneficiation of Mountain Pass rare-earth ore. Miner. Metall. Process 30, 1–9.

Predali, J., 1969. Flotation of carbonates with salts of fatty acids: role of pH and the alkyl chain. Trans. Inst. Min. Metall. 78, C140–C147.

Ren, J., Wang, W., Luo, J., Zhou, G., Tang, F., 2003. Progress of flotation reagents of rare earth minerals in China. J. Rare Earths 21, 1–8.

Somasundaran, P., Moudgil, B., 1987. Reagents in Mineral Technology. Taylor & Francis.

Wills, B.A., Finch, J.A., 2016. Froth flotation. In: Wills, B.A., Finch, J.A. (Eds.), Wills' Mineral Processing Technology. eighth ed. Butterworth-Heinemann, Oxford.

Zaitsev, A.N., Wall, F., Le Bas, M.J., 1998. REE-Sr-Ba minerals from the Khibina carbonatites, Kola Peninsula, Russia; their mineralogy, paragenesis and evolution. Mineral. Mag. 62, 225–250.

Zhang, X., Du, H., Wang, X., Miller, J.D., 2013. Surface chemistry considerations in the flotation of rare-earth and other semisoluble salt minerals. Miner. Metall. Process 30, 24–37.

Zucchini, A., Comodi, P., Katerinopoulou, A., Balic-Zunic, T., McCammon, C., Frondini, F., 2012. Order–disorder–reorder process in thermally treated dolomite samples: a combined powder and single-crystal X-ray diffraction study. Phys. Chem. Miner. 39, 319–328.

Appendix B

ATR-FTIR spectra of minerals conditioned with benzohydroxamate

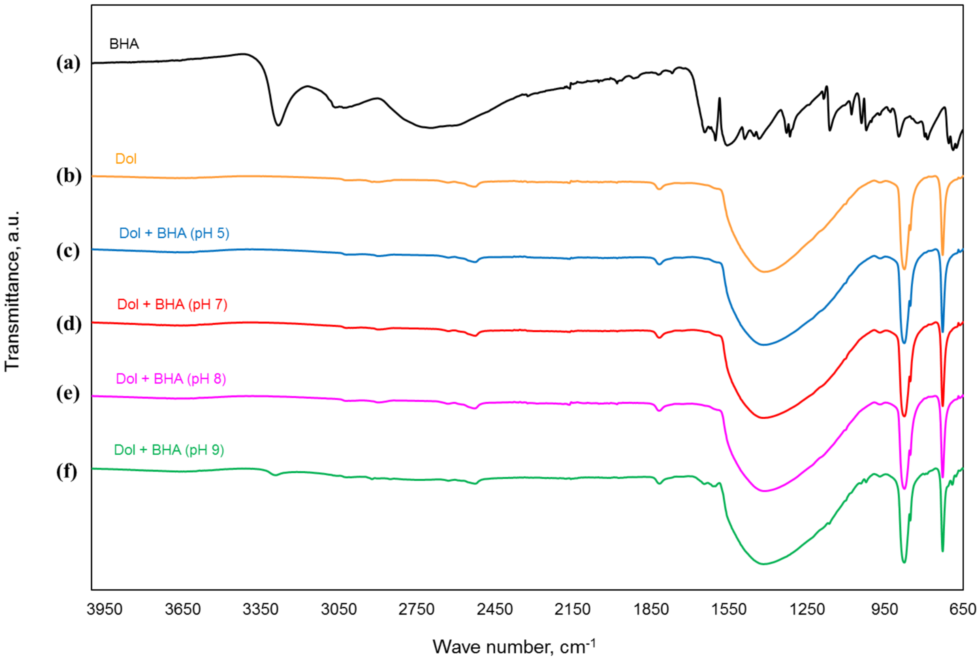

Figure B.1 – ATR-FTIR spectra of (a) BHA; (b) bare dolomite; dolomite conditioned with BHA at (c) pH 5; (d) pH 7; (e) pH 8 and (f) pH 9.

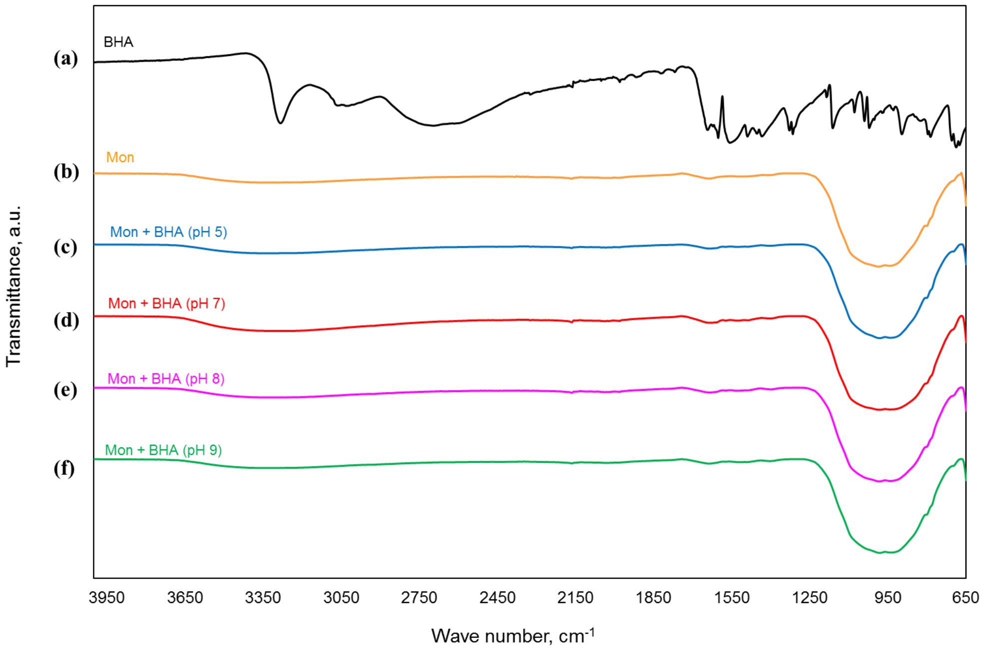

Figure B.2 – ATR-FTIR spectra of (a) BHA; (b) bare monazite; monazite conditioned with BHA at (c) pH 5; (d) pH 7; (e) pH 8 and (f) pH 9.

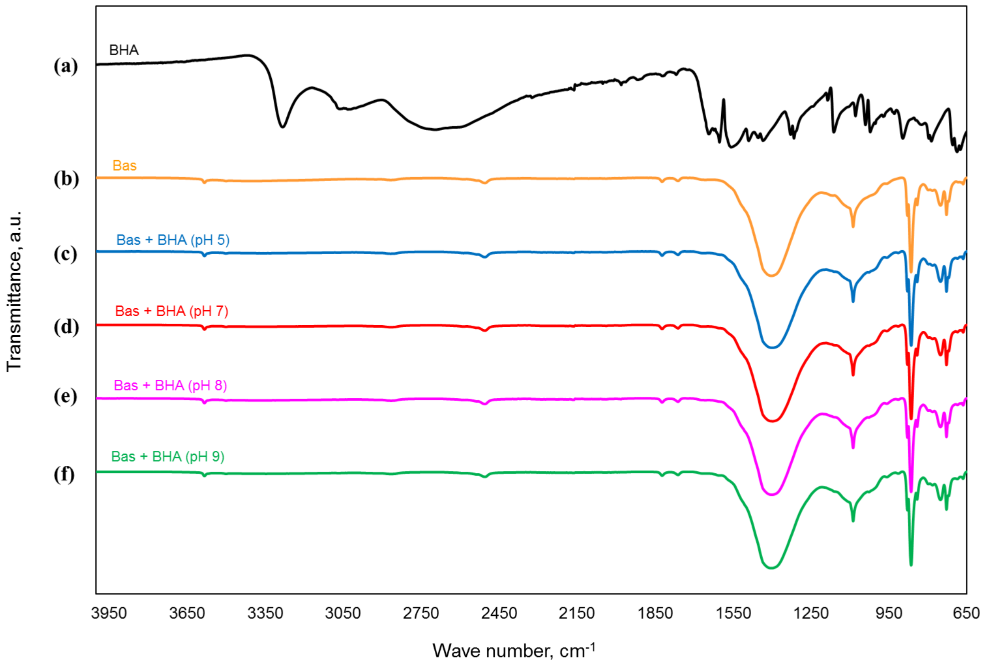

Figure B.3 – ATR-FTIR spectra of (a) BHA; (b) bare bastnäsite; bastnäsite conditioned with BHA at (c) pH 5; (d) pH 7; (e) pH 8 and (f) pH 9.

Appendix C

pKa determination of Flotinor 1682 by titration

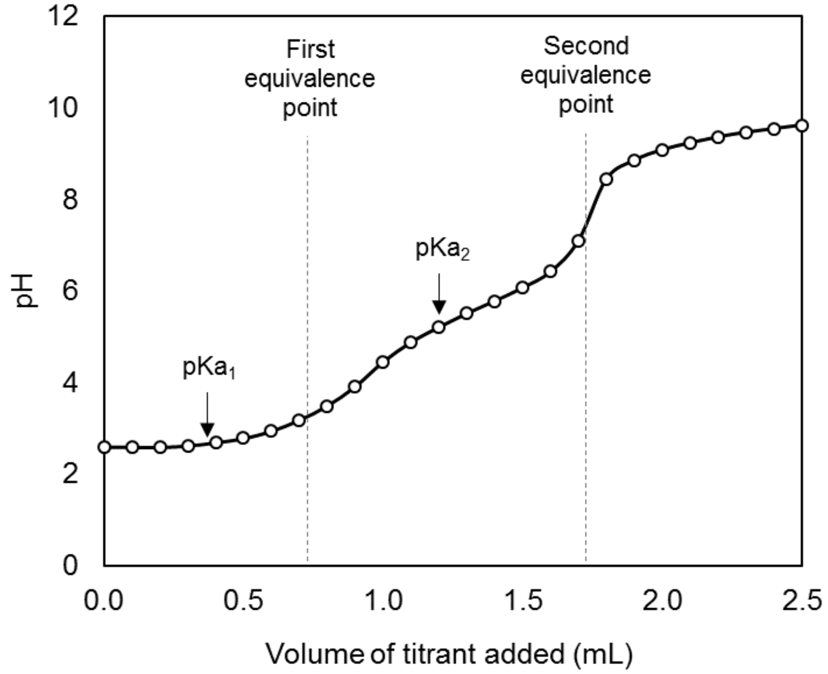

Figure C.1 – Titration curve of 50 mL 0.1 g/mL F1682 with 0.05 M NaOH.

Unlike benzohydroxamate and sodium oleate, the acid dissociation constants of Flotinor 1682 are unknown, as such these values were determined through titration. Fifty (50) mL of 0.1 g/L of the collector was placed in a beaker agitated using a magnetic stirrer. The initial pH of the solution was recorded, prior to the gradual addition of 0.05 M NaOH solution. The volume of NaOH added and the resulting collector pH were recorded. From the titration curve (pH versus volume of NaOH added), inflection points were obtained which is also known as the equivalence points. Half-way between volume = 0 and equivalence point 1, pKa_1 can be located, while half-way between equivalence point 1 and 2, pKa_2 can be found.

Appendix D

The effect of carbonate ions on the electrokinetic properties of the minerals

IMPC 2016: XXVIII International Mineral Processing Congress Proceedings - ISBN: 978-1-926872-29-2

THE EFFECT OF CARBONATE IONS ON THE ELECTROKINETIC PROPERTIES OF BASTNÄSITE, MONAZITE AND DOLOMITE

*E.R.L. Espiritu, G.R. da Silva and K.E. Waters

Department of Mining and Materials Engineering
McGill University
3610 University Street
Montreal, Quebec, Canada H3A 0C5
*(*Corresponding author: eileen.espiritu@mail.mcgill.ca)*

ABSTRACT

Rare earth (RE) elements are essential components of emerging green technologies. The increase in demand for these applications have driven the search and development of new rare earth deposits such as the Niobec project in Quebec, Canada. This deposit consists primarily of dolomite with significant amount of RE minerals bastnäsite and monazite, the primary sources of RE elements. Due to the minerals' fine liberation sizes, flotation is commonly used as a concentration method. To develop an efficient process, the electrokinetic properties of the minerals must be understood. In this study, the surface properties of bastnäsite, monazite (RE minerals) and dolomite (a common gangue mineral) were investigated by zeta potential measurements. These measurements are affected by various ions present in solution; for bastnäsite, monazite and dolomite, some of these ions are H^+, OH^-, PO_4^{3-} and CO_3^{2-}. Dolomite, being a sparingly soluble mineral and a primary component of the ore, may be the greatest contributor of these ions in solution in the form of CO_3^{2-} ions. Thus, different sources of CO_3^{2-} ions (from dolomite dissolution and from Na_2CO_3) were investigated. The research work aims at elucidating how these reagents may influence the minerals' surfaces. The results have shown that dolomite supernatant and sodium carbonate greatly affect the electrokinetic properties of each minerals. The addition of dolomite supernatant have resulted to relatively similar zeta potential of the minerals; while, sodium carbonate have affected them differently. These observations could be useful in efficient flotation of bastnäsite and/or monazite from bastnäsite-monazite-dolomite system.

KEYWORDS

Rare earth minerals, bastnäsite, monazite, dolomite, Zeta potential, sodium carbonate

INTRODUCTION

The increase in the demand for rare earth (RE) elements has driven the search and development of new deposits. Out of 53 rare earth projects in the world, 19 can be found in Canada (Hatch, 2015). These include the Niobec project of Magris Resources Company in Quebec. This deposit contains a significant amount of rare earth minerals (such as bastnäsite and monazite), with carbonates (such as dolomite) as the primary gangue minerals.

Bastnäsite ($REFCO_3$) is a RE fluorocarbonate mineral while monazite ($REPO_4$) is a RE phosphate mineral. Both minerals are typically beneficiated using flotation due to their fine liberation sizes (J. Zhang & Edwards, 2012; Jordens, Cheng, & Waters, 2013). However, these minerals are considered salt-type (X. Zhang, Du, Wang, & Miller, 2013) making the flotation system more complex. Salt-type minerals have relatively higher solubilities than most minerals but lower than salt minerals (e.g., halite and sylvite) (Yuehua, Chi, & Xu, 2003). Since this type of mineral is sparingly soluble in water, constituent ions that are being dissolved may influence other mineral surfaces. Thus, for efficient flotation process, surface chemistry of these minerals must be understood.

When minerals are submerged in a liquid, they may acquire a charge in various ways depending on their nature and the medium (Hunter, 1981; Lyklema, 1995; Shaw & Costello, 1993). Whatever the mechanism, the ions around the particle will reorient themselves in such a way that electroneutrality is maintained in the system (Lyklema, 1995). Adjacent to the surface, ions that are capable of specific adsorption can be found (Delgado, 2002). These ions have a chemical affinity to the surface, other than electrostatic interactions (Delgado, 2002; Lyklema, 1991). Chemical interactions may include Van der Waals, hydrogen bonding, π-electron exchange and complexation formation (Lyklema, 1991). Further from the surface, ions that only interact with the surface through electrostatic forces are located. Due to its weak interaction with the surface, these ions (also referred to as indifferent ions) are usually distributed over a certain distance around the solid (Delgado, 2002). The adsorption of ions onto the mineral surface (as a way to compensate to the acquired charge) causes unequal distribution of ions in the solution leading to the formation of electrical double layer (EDL). Accordingly, the distribution of the ions around the particle generates an electrostatic potential gradient as a function of distance (from the particle surface). The ions that are responsible for the surface charge and the surface potential are referred to as the potential determining ions (PDI) (Hunter, 1981). In most cases, constituent ions fall under the category of PDI (Lyklema, 1991).

In the estimation of the surface charge, one of the most widely studied electrokinetic phenomenon is electrophoresis. This phenomenon occurs when the particle moves due to an applied electric field (Hunter, 1981). When the particle moves, ions that are highly attracted to the surface will move with the particle; and some ions will remain in the bulk. An imaginary plane that divides these ions is known as the shear plane or slip plane. The mobility (electrophoretic mobility) of the particle measured at this plane, which indicates the measure of surface charge, is referred to as zeta potential (ζ) (Hunter, 1981). The pH at which there is no electrophoretic mobility due to a zero net charge is originally referred to as isoelectric point (IEP) (Leja, 1982). However, it should be noted that the proper definition of IEP is “the negative logarithm (base 10) of the concentration of the PDI at which the electrokinetic potential becomes zero” (Leja, 1982). For the details on EDL and zeta potential, the reader is referred to Lyklema (1995) and Hunter (1981).

Dolomite, monazite and bastnäsite, being sparingly soluble minerals, can release ions in the solution. However, dolomite (the primary component of the Niobec ore) may provide the greatest contribution to the PDI in the solution in the form of CO_3^- ions. This would imply that reagents that can contribute carbonate ions to the system may affect the system. Sodium carbonate is typically used as a depressant in the flotation of bastnäsite from calcite and barite in the presence of a carboxylate collector. It could then be a potential depressant in the flotation of bastnäsite and/or monazite from dolomite. In this study, the effect of carbonate ions (from Na_2CO_3 and dolomite dissolution) on the electrokinetic properties of dolomite, monazite and bastnäsite are investigated through zeta potential measurements. This study aims at elucidating how these reagents may influence the minerals' surfaces.

EXPERIMENTAL

Material

Bastnäsite was provided by African Rare Earths (Pty.) Ltd. (South Africa). Monazite from Eureka Farm 99 (Namibia) was purchased from Mineralogical Research Company (U.S.A). Dolomite from Sterling Hill Mine (New Jersey) was obtained from Ward's Science (U.S.A.).

The sodium chloride that was used as supporting electrolyte; the sodium carbonate that was used as a source of carbonate ions; and the hydrochloric acid and potassium hydroxide that were used as pH modifiers were obtained from Fisher Scientific (Canada).

The supernatant from dolomite dissolution was obtained by preparing 75 g of dolomite in 1500 mL deionized water. The suspension was aged for 8 hours with constant agitation at elevated temperature of 60°C. The supernatant was then recovered by filtration. Next, dilution was conducted to obtain a conductivity similar to that of 1×10^{-3} M Na_2CO_3. This ensures that the two solutions will have similar ionic strength to enable comparison of the zeta potential measurements.

Mineral Purification

The minerals were first purified with gravity and/or magnetic separation prior to zeta potential measurements. These methods are size dependent, thus efficient concentration process is achieved by dividing the minerals into different particle size fractions. Each fraction was processed using a Mozley MKII Laboratory Separator (Mozley, U.K.), a gravity separator. Then, the heavy fraction was further purified using a Frantz Isodynamic Separator (Frantz, U.S.A.), a magnetic separator.

Zeta Potential Measurements

To obtain a particle size smaller than 10 μm, purified mineral samples were pulverized in a Planetary Monomill, Pulverisette 6 (Fritsch, Germany). A solution of 1×10^{-3} M NaCl was used as the indifferent background electrolyte. For the source of carbonate ions, 1×10^{-3} M Na_2CO_3 and the dolomite supernatant were used. The solutions were pH adjusted using hydrochloric acid and potassium hydroxide prior to addition of the mineral particles. Prior to measurement, the 100 ppm suspension was mixed to ensure that the particles were kept in suspension. Zeta potential measurements were taken using a NanoBrook 90Plus Zeta Particle Size Analyzer (Brookhaven Instruments, U.S.A.).

RESULTS

Mineral Characterization

Mineral samples were characterized using Bruker D8 Discovery X-Ray Diffractometer (Cobalt source: Co κα, $\lambda = 1.79$ Å) to identify the purity of the samples. The diffractograms of dolomite, bastnäsite and monazite are presented in Figure 1. The figures represent: (a) dolomite sample and dolomite reference pattern (JPDF reference number: 01-081-8229) (Zucchini, Comodi, Katerinopoulou, Balic-Zunic, McCammon, & Frondini, 2002); (b) bastnäsite sample and bastnäsite reference pattern (JPDF reference number: 00-011-0340) (G. Donnay & J. Donnay, 1953); (c) monazite sample and monazite reference pattern (JPDF reference number: 00-046-1295) (Bermanec, Tibljaš, Gessner, & Kniewald, 1988). The peaks of the diffractograms corresponded with that of the reference patterns without the presence of any other significant peaks, indicating that the mineral samples were pure enough for zeta potential measurements.

Zeta Potential Measurements

The zeta potential of dolomite, bastnäsite and monazite minerals in the presence of 1 x 10^{-3} M NaCl, 1 x 10^{-3} M Na_2CO_3 and dolomite supernatant at different pH conditions were measured. The results are presented in Figure 2 - Figure 4, where the error bars represent 95% confidence interval

It was found that the IEP of dolomite using 1 x 10^{-3} M NaCl occurs at a pH of approximately 6 as shown in Figure 2. The use of sodium carbonate did not significantly affect the zeta potential at pH below 6; but did show an effect at pH values above 6, where the potential shifted to slightly positive values. The results also show that the addition of dolomite supernatant appeared to have the same effect as that of sodium carbonate, except at pH 6 and 7 where the zeta potential values are slightly negative.

In Figure 3, the results of the zeta potential measurements of bastnäsite are presented. It can be observed that the IEP of bastnäsite in the presence of 1 x 10^{-3} M NaCl occurs at a pH of approximately 8. The addition of sodium carbonate has resulted to a shift in the IEP from pH 7.5 to around pH 5.5. It can also be seen from the results that the zeta potential values of bastnäsite with dolomite supernatant are relatively constant throughout the whole pH range tested.

The zeta potential of monazite was presented in Figure 4. In the presence of sodium chloride, the IEP of monazite occurs at pH around 7; while the use of sodium carbonate has slightly shifted it to pH between 6 and 7. It can also be observed that the zeta potential values decreased until pH 7; while remained relatively constant at pH above 7, when sodium carbonate was used. The dolomite supernatant, however, seemed to have similar effect as on the bastnäsite, except at pH below 6 where the values have slightly increased.

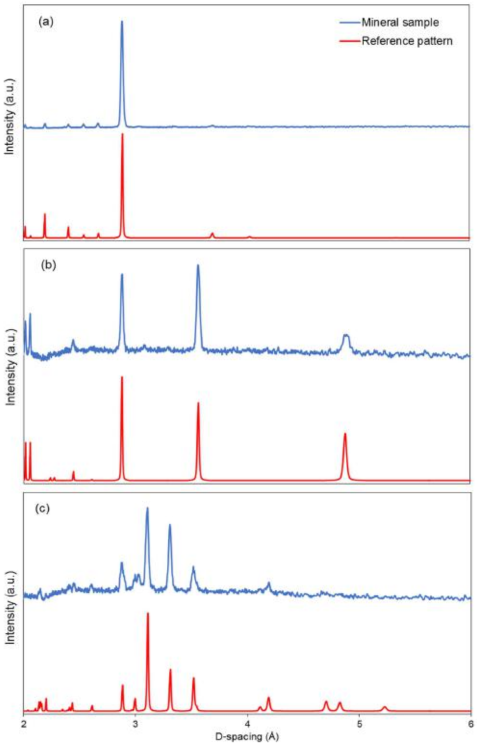

Figure 1 – X-ray powder diffraction patterns of (a) dolomite, (b) bastnäsite and (c) monazite

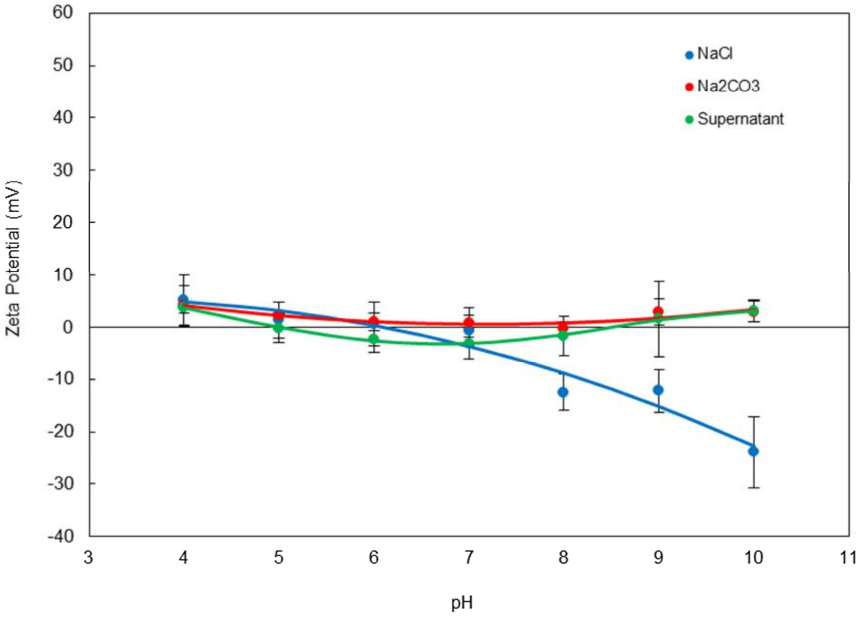

Figure 2 – Zeta potential curves of dolomite in the presence of 1 x 10^{-3} M NaCl, 1 x 10^{-3} M Na_2CO_3 and dolomite supernatant at different pH conditions

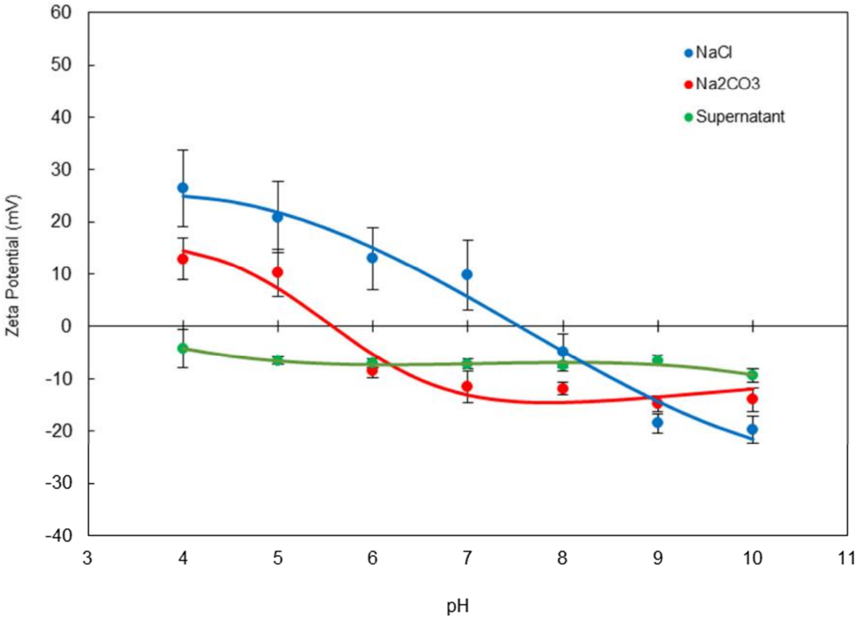

Figure 3 – Zeta potential curves of bastnäsite in the presence of 1 x 10^{-3} M NaCl, 1 x 10^{-3} M Na_2CO_3 and dolomite supernatant at different pH conditions

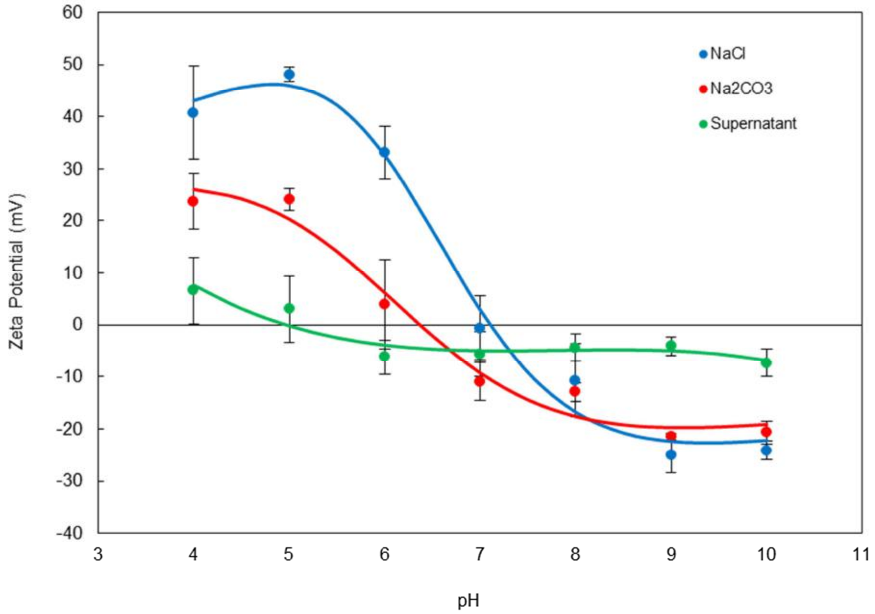

Figure 4 – Zeta potential curves of monazite in the presence of 1 x 10^{-3} M NaCl, 1 x 10^{-3} M Na_2CO_3 and dolomite supernatant at different pH conditions

DISCUSSION

The addition of sodium carbonate and dolomite supernatant has greatly affected the zeta potential of dolomite at basic pH conditions. At acidic pH conditions, dolomite would be soluble, indicating that constituent ions (such as carbonate ions) are present while obtaining the zeta potential measurements. This could explain why the addition of sodium carbonate and dolomite supernatant did not affect the system at these pH conditions. At basic pH conditions, the effects were more evident due to the presence of carbonate ions. These ions were able to change the zeta potential from negative to slightly positive values. This greatly indicates that CO_3^{2-} ions are potential determining ions of dolomite.

The presence of sodium carbonate had a pronounced effect on the zeta potential values of bastnäsite across the entire pH range tested. The addition of sodium carbonate to bastnäsite caused a significant shift in the IEP from pH 7.5 to 5.5 and a decrease in the magnitude of the zeta potential. The latter is consistent with the work done by Fuerstenau, Pradip and Herrera-Urbina (1992), where it was found that the addition of sodium carbonate could led to a sign reversal (from positive to negative) and a significant decrease in the zeta potential magnitude. Moreover, the decrease in the zeta potential with increasing pH is also similar to that found by Smith and Shonnard (1986). These changes in the zeta potential are attributed to the specific adsorption of the ions and also to adsorption of the carbonate ions on the mineral surface.

Since carbonate ions are not constituent ions of monazite, the addition of sodium carbonate did not significantly change its IEP; however, it did decrease the magnitude of the zeta potential. In terms of the behavior of the zeta potential, the addition of dolomite supernatant to monazite and to bastnäsite led to the same outcomes at alkaline pH. This suggests that the dolomite supernatant may have interacted in similar manner with monazite and bastnäsite. However, at acidic pH, the constituent ions from the minerals appeared to have an influence on the zeta potential.

Published by the Canadian Institute of Mining, Metallurgy and Petroleum

Appendix E

Speciation diagrams of the minerals

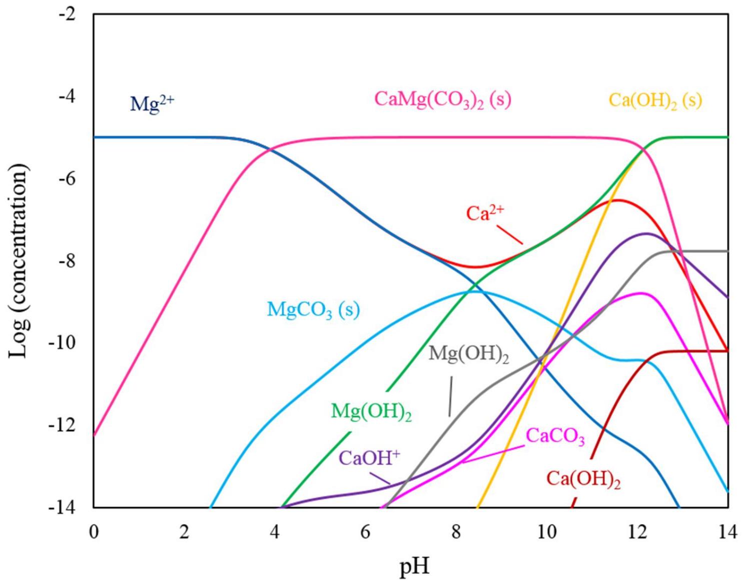

Figure E.1 – Speciation diagram of dolomite. Total concentration: $[Ca^{2+}]_{TOT}$ = $[Mg^{2+}]_{TOT}$ = 10 µM, $pCO_2 = 10^{-3.5}$ atm at 1 atm and T = 25 °C

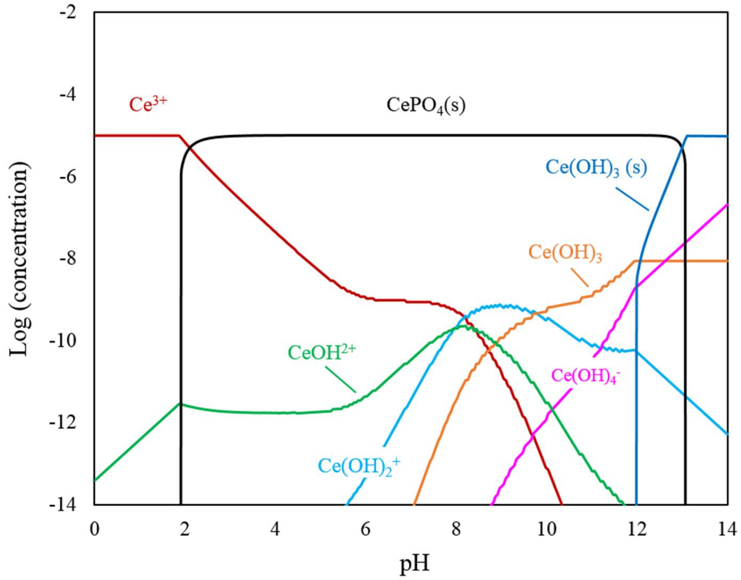

Figure E.2 – Speciation diagram of monazite. Total concentration: $[\mathrm{Ce}^{3+}]_{\mathrm{TOT}} = [\mathrm{PO}_4^{3-}]_{\mathrm{TOT}} =$ 10 µM, $p\mathrm{CO}_2 = 10^{-3.5}$ atm at 1 atm and T = 25 °C

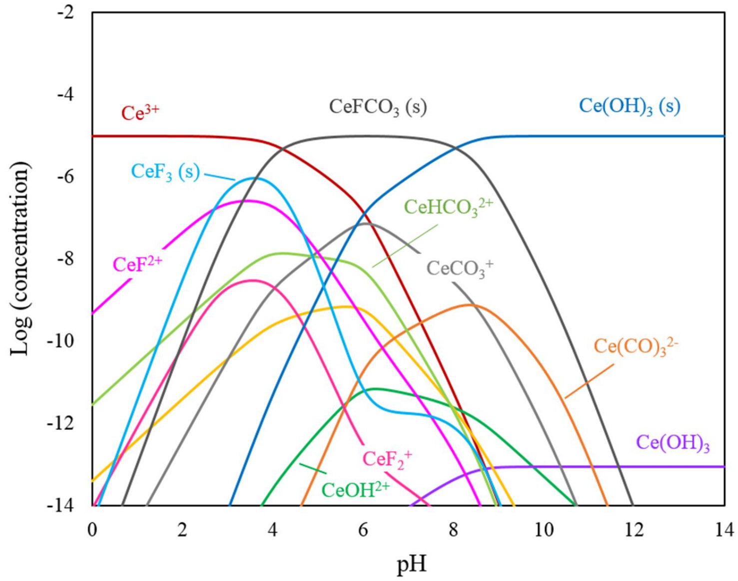

Figure E.3 – Speciation diagram of bastnäsite. Total concentration: $[\mathrm{Ce}^{3+}]_{\mathrm{TOT}} = [\mathrm{F}^{-}]_{\mathrm{TOT}} = 10$ µM, $p\mathrm{CO}_2 = 10^{-3.5}$ atm at 1 atm and T = 25 °C

Appendix F

Statistical *t*-test of the mineral's zeta potential: supernatant and benzohydroxamate

Table F.1 – Statistical *t*-test of the changes of zeta potential values of dolomite, monazite and bastnäsite as a function of supernatant conditioning time in the presence of benzohydroxamate

Mineral	pH	s	Ave	SD	95% CI	*p*-value	Statistically significant (Y/N)
DOLOMITE	pH 5	0	3.46	1.64	4.07	N/A	
		30	3.69	0.80	1.99	0.4878	N
		60	6.83	0.28	2.41	<0.0001	Y
		120	4.43	2.03	5.03	0.3552	N
		240	2.66	0.99	2.45	0.0297	Y
	pH 7	0	-0.21	2.64	6.55	N/A	
		30	-0.89	1.57	3.90	0.6639	N
		60	1.49	2.49	6.18	0.0608	N
		120	-4.02	0.96	2.38	0.0002	Y
		240	-1.17	0.16	1.37	0.0590	N
	pH 9	0	-1.77	1.06	2.64	N/A	
		30	-3.62	1.66	4.12	0.0560	N
		60	-5.09	1.36	3.38	0.0002	Y
		120	-3.43	0.93	2.31	0.0447	Y
		240	-3.75	0.16	0.39	0.0854	N
MONAZITE	pH 5	0	13.37	0.2	1.69	N/A	
		30	16.66	0.54	1.33	0.0178	Y
		60	17.62	2.52	3.43	0.0108	Y
		120	15.12	0.25	0.63	0.0584	N
		240	16.53	0.32	0.78	0.0032	Y
	pH 7	0	-9.52	1.3	3.22	N/A	
		30	-7.95	0.14	0.34	0.0081	Y
		60	-5.86	0.65	1.62	<0.0001	Y
		120	-7.19	0.65	1.63	0.0001	Y
		240	-8.04	1.25	3.12	0.1436	N
	pH 9	0	-24.27	1.2	2.98	N/A	
		30	-19.04	1.12	2.77	0.0671	N
		60	-17.11	0.51	1.27	0.6282	N
		120	-21.81	0.36	3.09	0.0019	Y
		240	-18.14	1.36	3.39	<0.0001	Y
BASTNÄSITE	pH 5	0	-9.52	1.3	3.22	N/A	
		30	-22.2	1.37	3.41	0.0593	N
		60	-21.7	1.23	3.05	0.0049	Y
		120	-20.62	1.01	2.5	0.0001	Y
		240	-18.36	0.59	1.47	<0.0001	Y
	pH 7	0	-9.52	1.3	3.22	N/A	
		30	-7.95	0.14	0.34	0.0081	Y
		60	-5.86	0.65	1.62	¡0.0001	Y
		120	-7.19	0.65	1.63	0.0001	Y
		240	-8.04	1.25	3.12	0.1436	N
	pH 9	0	-24.27	1.2	2.98	N/A	
		30	-22.2	1.37	3.41	0.0593	N
		60	-21.7	1.23	3.05	0.0049	Y
		120	-20.62	1.01	2.5	0.0001	Y
		240	-18.36	0.59	1.47	<0.0001	Y

Appendix G

Statistical *t*-test of the mineral's zeta potential: supernatant and sodium oleate

Table G.1 – Statistical *t*-test of the changes of zeta potential values of dolomite, monazite and bastnäsite as a function of supernatant conditioning time in the presence of sodium oleate

Mineral	pH	s	Ave	SD	95% CI	*p*-value	Statistically significant (Y/N)
DOLOMITE	pH 5	0	-10.94	1.38	3.42	N/A	
		30	-11.45	0.78	1.95	0.1629	N
		60	-11.94	0.74	1.84	0.0233	Y
		120	-13.17	1.19	2.95	<0.0001	Y
		240	-12.08	0.14	1.32	0.0039	Y
	pH 7	0	-13.48	1.2	2.98	N/A	
		30	-11.01	0.86	2.15	<0.0001	Y
		60	-11.41	0.99	2.47	<0.0001	Y
		120	-11.46	1.17	2.89	<0.0001	Y
		240	-8.97	0.86	2.14	<0.0001	Y
	pH 9	0	-9.78	0.04	0.32	N/A	
		30	-14.34	1.33	3.31	<0.0001	Y
		60	-12.47	0.96	2.37	<0.0001	Y
		120	-14.72	0.6	1.5	<0.0001	Y
		240	-13.59	0.75	1.86	<0.0001	Y
MONAZITE	pH 5	0	-14.29	0.57	1.43	N/A	
		30	-13.26	0.04	0.37	0.0769	N
		60	-13.78	0.94	2.33	0.6256	N
		120	-13.98	1.59	3.95	0.6252	N
		240	-13.45	0.67	1.67	0.1582	N
	pH 7	0	-14.73	1.28	3.18	N/A	
		30	-13.89	0.24	0.59	0.0557	N
		60	-13.35	1.33	3.31	0.0002	Y
		120	-13.54	0.96	2.39	0.0078	Y
		240	-13.03	1.35	3.36	0.0012	Y
	pH 9	0	-11.72	0.8	1.98	N/A	
		30	-14.59	0.48	1.2	0.016	Y
		60	-15.78	0.55	1.37	0.0008	Y
		120	-15.89	0.72	1.78	0.0003	Y
		240	-14.39	1.48	3.68	0.0094	Y
BASTNÄSITE	pH 5	0	-5.72	1.65	4.09	N/A	
		30	-6.3	1.06	2.64	0.2547	N
		60	-6.64	0.13	1.07	0.3479	N
		120	-6.89	0.78	1.95	0.4626	N
		240	-10.35	0.19	1.62	0.0019	Y
	pH 7	0	-18.66	2.16	5.37	N/A	
		30	-16.35	0.98	2.44	0.0003	Y
		60	-16.35	0.71	1.78	0.0005	Y
		120	-15.94	0.69	1.71	0.0009	Y
		240	-14.82	0.64	1.59	<0.0001	Y
	pH 9	0	-23.2	1.23	3.06	N/A	
		30	-24.4	0.78	1.93	0.0513	N
		60	-24.74	0.93	2.32	0.0357	Y
		120	-24.2	0.45	1.11	0.0496	Y
		240	-24.33	0.18	0.46	0.0148	Y

Appendix H

Mineralogy

H.1 Method

The samples used for Quantitative Evaluation of Materials by Scanning Electron Microscopy (QEMSCAN) was prepared at/by the Department of Mining, Metallurgical and Materials Engineering, Laval University. The mineralogy of the ore samples with a particle size range of -300+3 µm (P80 = 150 µm) was examined with QEMSCAN^{TM} (Quantitative Evaluation of Materials by Scanning Electron Microscopy) at the Advanced Mineralogy Facility at SGS Canada (Lakefield, Canada). The instrument is EVO 430 automated scanning electron microscope equipped with four light-element energy-dispersive X-ray spectrometers and employed with iDiscover software for image and data processing. The mode used for this project was Particle Mineral Analysis (PMA), while sample analysis was conducted using Specific Mineral Search (SMS) routine. The mode of operation presented as follows is directly quoted from the description provided by SGS Canada.

> *The PMA is a two-dimensional mapping analysis aimed at resolving liberation and locking characteristics of a generic set of particles, it provides a statistically robust population of mineral identifications based on X-ray chemistry of minerals. A pre-defined number of particles are mapped at a point spacing selected to spatially resolve and describe mineral textures and associations. This mode is often selected to characterize feed and concentrate products, as both gangue and value minerals report in statistically abundant quantities to be resolved.*
>
> *The SMS is a modified PMA analysis. However, in an SMS routine, a phase reports as a low-grade constituent and can be located by thresholding of the back-scattered electron intensity. Any accompanying phases of similar and higher brightness are also mapped. For example, this mode of measurement would be selected in ores of low sulphide grade, searching specifically for particles containing sulphide minerals.*

It should also be noted that due to nearly identical energy dispersive X-ray characteristics of magnetite and hematite, the two minerals are indistinguishable; as such, they will be referred singly as Fe-oxides in the following section.

H.2 Results

The mineralogical study of the ore presented that monazite (Ce,La,Nd,Th)PO_4 and bastnäsite (Ce,La,Sm,Nd)(CO_3)F/synchisite Ca(Ce,La,Sm,Nd)$(CO_3)_2$F are the main RE minerals with an average grade of 1.43% and 1.96%, respectively. The gangue minerals are mostly carbonates including dolomite (50%), calcite (13.2%), ankerite (13.7%) and siderite (0.21%).

The grain size profile of the minerals was presented in Figure H.1, while the modal grain size was presented in Table H.1 for easier data interpretation. Table H.1 showed that the modal grain size of all the minerals is less than 27 µm. Although the grain size profile presented that monazite and bastnäsite/synchisite could occur with a coarser grain size such as 66 µm and 113 µm, respectively, majority of these RE minerals occur with a grain size of 13 and 14 µm, respectively.

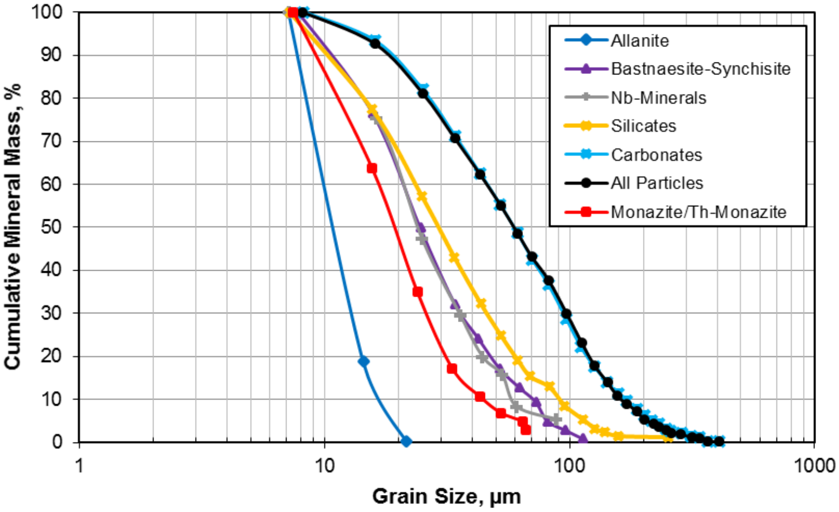

Figure H.1 – Grain size curve of the different minerals present in Niobec rare earth ore.

Bastnäsite/synchisite and monazite association were also investigated (see Tables H.2 and H.3). It was found that about 30% of bastnäsite/synchisite and 16.2% of monazite occurs as free particles (≥ 95% surface exposure) in the particle size range investigated. The amount of liberated (95% > surface exposure ≥ 80%) bastnäsite / synchisite (17.5%) and monazite (10.6%) are significantly lower than number of free particles. Bastnäsite/synchisite mostly occur as free (30%), while monazite occur as a complex (23%). The rest of bastnäsite/synchisite and monazite are associated with silicates, carbonates or a combination of both.

Table H.1 – Mass percentage and modal grain size of minerals present in Niobec ore.

Mineral	**Mineral mass, %**	**Modal grain size, µm**
Niobium-bearing		
Pyrochlore	0.12	11
Columbite	0.17	18
Rare earth		
Bastnäsite/Synchisite	**1.96**	**14**
Monazite/Th-Monazite	**1.43**	**13**
Allanite	0.13	7
Other RE	0.01	7
Oxides		
Fe-oxides	5.85	21
Ilmenite	0.07	7
Rutile	0.20	10
Other oxides	0.15	12
Carbonates		
Dolomite	**50.0**	**27**
Calcite	13.2	20
Ankerite	13.7	22
Siderite	0.21	7
Silicates		
Plagioclase	0.06	11
K-Feldspar	0.15	20
Quartz	0.92	14
Micas/Clays	1.15	10
Amphibole	0.75	9
Sphene	0.00	13
Chlorite	4.43	18
Other silicates	0.00	7
Sulphides		
Pyrite	2.86	25
Other sulphides	0.07	14
Others		
Zircon	0.03	6
Apatite	0.28	16
Barite	1.99	26
Rutile	0.13	8
Total	100	

Table H.2 – Bastnäsite/synchisite association.

Mineral Name	Amount, %
Free Bastnäsite/Synchisite	29.9
Liberated Bastnäsite/Synchisite	17.5
Bastnäsite/Synchisite: Nb-Minerals	0.01
Bastnäsite/Synchisite: Allanite	0.17
Bastnäsite/Synchisite: Monazite/Th-Monazite	0.83
Bastnäsite/Synchisite: Other REE	0.02
Bastnäsite/Synchisite: Fe-Oxides	0.08
Bastnäsite/Synchisite: Ti-Oxides	0.06
Bastnäsite/Synchisite: Silicates	13.5
Bastnäsite/Synchisite: Carbonates	10.8
Bastnäsite/Synchisite: Carbonates: Silicates	8.46
Bastnäsite/Synchisite: Apatites	0.01
Bastnäsite/Synchisite: Sulphides	0.33
Bastnäsite/Synchisite: Barite	0.40
Bastnäsite/Synchisite: Zircon	0.00
Bastnäsite/Synchisite: Other	0.00
Bastnäsite/Synchisite: Complex	18.0

Table H.3 – Monazite association.

Mineral Name	Amount, %
Free Monazite	16.2
Liberated Monazite	10.6
Monazite: Nb-Minerals	0.05
Monazite: Bastnäsite/Synchisite	1.33
Monazite: Allanite	0.05
Monazite: Other REE	0.03
Monazite: Fe-Oxides	0.06
Monazite: Ti-Oxides	0.04
Monazite: Silicates	18.7
Monazite: Carbonates	12.7
Monazite: Carbonates: Silicates	16.2
Monazite: Apatite	0.04
Monazite: Sulphides	0.30
Monazite: Barite	0.36
Monazite: Zircon	0.01
Monazite: Other	0.00
Monazite Complex	23.2